GROUNDWATER CONTAMINANT SOURCE IDENTIFICATION USING MESHFREE RADIAL POINT COLLOCATION METHOD AND PARTICLE SWARM INTELLIGENCE BASED SIMULATION-OPTIMIZATION APPROACH

By

LAISHRAM GUNESHWOR SINGH

(PHYS01201004009)

Bhabha Atomic Research Centre, Trombay, Mumbai

A thesis submitted to the

Board of Studies in Physical Sciences

In partial fulfillment of requirements

for the Degree of

DOCTOR OF PHILOSOPHY

of

HOMI BHABHA NATIONAL INSTITUTE

July 2017

Homi Bhabha National Institute

Recommendations of the Viva Voce Committee

As members of the Viva Voce Committee, we certify that we have read the dissertation prepared by **Laishram Guneshwor Singh** entitled "**Groundwater Contaminant Source Identification using Meshfree Radial Point Collocation Method and Particle Swarm Intelligence based Simulation-Optimization Approach**" and recommend that it may be accepted as fulfilling the thesis requirement for the award of Degree of Doctor of Philosophy.

Chairman –		**Date:** 12/7/2017
Guide / Convener – **Dr. A. Vinod Kumar**		**Date:** 12/7/17
Co-guide - **Prof. T.I. Eldho**		**Date:** 12/7/2017
Examiner – **Prof. Babu J. Alappat**		**Date:** 12/7/17
Member 1- **Dr. Y. S. Mayya**		**Date:** 12/7/17
Member 2- **Dr. D. Datta**		**Date:** 12/7/2017
Member 3- **Dr.(Smt.) B. K. Sapra**		**Date:** 12/7/2017

Final approval and acceptance of this thesis is contingent upon the candidate's submission of the final copies of the thesis to HBNI.

I/We hereby certify that I/we have read this thesis prepared under my/our direction and recommend that it may be accepted as fulfilling the thesis requirement.

Date: 12/7/2017

Place:

Co-guide **Guide**

STATEMENT BY AUTHOR

This dissertation has been submitted in partial fulfillment of requirements for an advanced degree at Homi Bhabha National Institute (HBNI) and is deposited in the Library to be made available to borrowers under rules of the HBNI.

Brief quotations from this dissertation are allowable without special permission, provided that accurate acknowledgement of source is made. Requests for permission for extended quotation from or reproduction of this manuscript in whole or in part may be granted by the Competent Authority of HBNI when in his or her judgment the proposed use of the material is in the interests of scholarship. In all other instances, however, permission must be obtained from the author.

Laishram Guneshwor Singh

Laishram Guneshwor Singh

DECLARATION

I, hereby declare that the investigation presented in the thesis has been carried out by me. The work is original and has not been submitted earlier as a whole or in part for a degree / diploma at this or any other Institution / University.

Laishram Guneshwor Singh

Laishram Guneshwor Singh

List of Publications arising from the thesis

Journal

1. "Coupled Groundwater Flow and Contaminant Transport Simulation in a confined Aquifer using Meshfree Radial Point Collocation method (RPCM)", L. Guneshwor S., T.I. Eldho and A. Vinodkumar , *Engineering Analysis with Boundary Elements*, 2016, Vol.66, pp.20-33

2. "Identification of Groundwater Contamination Sources using Meshfree RPCM simulation and Particle Swarm Optimization", L. Guneshwor S., T.I. Eldho and A. Vinodkumar, Paper is under review for publication in the journal "*Water Resources Management*"

Conferences

1. "Groundwater Flow Simulation in Confined Aquifers using Meshfree Radial Point Collocation Method (RPCM)", L. Guneshwor S., Dr. T.I. Eldho, and A. Vinod Kumar, HYDRO 2014 International, MANIT, Bhopal, India, December 18-20, 2014.

2. "Modeling contaminant transport in ground water using Meshfree methods", L. Guneshwor S., Dr. T.I. Eldho, and Dr. A. Vinod Kumar, 19th National Symposium on Environment (NSE), Kottayam, Kerala,India, December 11-13, 2014.

3. "Identification of Sources of Contamination in an Aquifer by a Simulation – Optimization Approach using Particle Swarm Optimization" L. Guneshwor S., T.I. Eldho, and A. Vinod Kumar, RSSD, BARC, HYDRO 2016 International, CWPRS, Pune, India, December 8-10, 2016.

Laishram Guneshwor Singh

Laishram Guneshwor Singh

DEDICATIONS

Dedicated to my mother

Late Smt. Laishram Ongbi Ibempishak Devi

May peace be with you

ACKNOWLEDGEMENTS

First and foremost, I would like to express my deepest sense of gratitude to my esteemed guides Dr A. Vinod Kumar, RSSD, BARC and Prof. T.I Eldho, Civil Engg., IIT Mumbai. I am very thankful to them for their continuous guidance, co-operation, constructive criticism and support in difficult situations and for sparing their valuable time. Their encouragement and systematic approach enabled me to carry out this research work successfully. They have provided me with the constant source of motivation to pursue this work.

I am thankful to all the members of the Doctoral Committee for their constructive criticisms, feedbacks and suggestions. I am grateful to Dr. Y.S. Mayya for his critical remarks and valuable suggestions which have been of immense help to me.

I am very grateful to Shri H. S. Kushwaha, ex-director, HS&EG, BARC for his inspiration and for permitting me to pursue this doctoral work. Without his help, this work would not have been possible. I am indebted to him for the help rendered by him. I am very thankful to Shri V. K. Sharma, ex-section head, SSS, HPD for his constant encouragement and motivation and for inspiring me to pursue this work.

I am grateful to our division head Dr. R. M. Tripathi and section head Shri Kapil Deo S. Singh for their cooperation and for allowing me to work unhindered despite all the office obligations. I express my sincere thanks to my colleagues Dr. S. Anand and Dr. Chinna Esakki for their constant help and cooperation throughout the course of this study. I am also thankful to my office colleagues Shri Pradeep Bhargava, Smt Chitra S., Smt. Arti Mhatre, Shri Tanmay Sarkar, Shri Jayant Krishan and Shri Praveen Kumar. I greatly appreciate the support and help rendered by them.

I will like to thank my fellow scholars from IIT, Smt. Alice Thomas, Kum. B. Swathi and Shri Kalpesh Patil for their constant support and help. The technical discussions and exchanges with them have been very fruitful and of immense help to me. I will also like to express my sincere thanks to Dr. (Smt.) Meenal Mategaonkar for sharing valuable insights on the meshfree methods. Her doctoral work has been of great help in carrying out this work.

I would like to take this opportunity to thank my spouse Smt. M. Bijaya Devi for the care, cooperation and understanding and for providing constant support all through the years. I am indebted to her for her sacrifices. I am thankful to my son Master. L. Lovinson and little daughter Meleisana for being patient and supportive during this work. Without the support and care of my family members, this thesis would not have been possible.

Table of Contents

Table of Contents

SYNOPSIS

Introduction

The remediation of a contaminated aquifer is a complex process which involves huge cost and time and requires proper planning to optimize the cost and effectiveness of the remediation. A very crucial aspect in the remediation process is to identify the locations and estimate the release magnitude of the unknown contaminant sources. Due to the complexity of groundwater transport process, models are required to identify the location and extent of contaminant plume. Groundwater contaminant transport modeling involves the solution of advection-dispersion-reaction (ADR) equation. Identification of the sources of contamination from the spatial and temporal measurements of contaminant concentrations in the aquifer is an inverse problem which requires solving the ADR equation backwards in time and an optimizer to minimize the error involved.

Grid or mesh based methods such as FDM or FEM are commonly used to model the groundwater flow and transport process in an aquifer. However, due to the difficulty and high computational costs of creating a mesh, meshfree methods have been recently developed. Meshfree methods require only a set of scattered nodes within and on the boundary to represent the modeling domain and no information are required on the connectivity of the nodes. Several meshfree methods have been developed in the last few decades (Liu and Gu, 2005). Meshfree Radial Point Collocation Method (RPCM) is a simple meshfree method (Kansa, 1990) based on the point collocation using Radial Basis Functions (RBF) as the interpolation function. In this study, meshfree RPCM is proposed for simulation of the groundwater flow and transport process.

A Simulation-Optimization (SO) approach is one of the effective techniques used for groundwater source identification. In this technique, the groundwater contaminant source identification problem is formulated as forward-time simulation in conjunction with an optimization model. Gorelick et al.(1983) are the first to apply simulation-optimization approach to groundwater contamination source identification using linear programming and regression as the optimizer. In recent times, many optimization tools based on artificial intelligence such as particle swarm optimization (PSO) has been evolved. In the present study, an attempt is made to develop groundwater contaminant source identification model with the SO approach using Meshfree RPCM as the simulation model and PSO as the optimizer. PSO offers advantages in terms of simplicity in implementation and easy integration with simulation models.

Within this context, the objectives of the present study are:

- Development of coupled groundwater flow and transport simulation models using meshfree radial point collocation methods (RPCM) for both confined and unconfined aquifer problems.

- Development of optimization model using Particle Swarm Optimization (PSO).
- Coupling of meshfree RPCM simulation model and PSO based optimization model to develop Simulation-Optimization (SO) models for groundwater contaminant source identification.
- Validation of the developed models with benchmark problems from published literature.
- Application of the developed SO model to hypothetical and field case studies and to cases with uncertainties in concentration data.

Groundwater Flow and Solute Transport Simulation

The governing equations describing the groundwater flow in a two dimensional inhomogeneous confined and unconfined aquifers can be written as (Bear, 1979):

$$\frac{\partial}{\partial x}\left[T_x\frac{\partial h}{\partial x}\right]+\frac{\partial}{\partial y}\left[T_y\frac{\partial h}{\partial y}\right]=S\frac{\partial h}{\partial t}+Q_w\delta(x-x_i)(y-y_i)-q \quad (1)$$

$$\frac{\partial}{\partial x}\left[K_x h\frac{\partial h}{\partial x}\right]+\frac{\partial}{\partial y}\left[K_y h\frac{\partial h}{\partial y}\right]=S_y\frac{\partial h}{\partial t}+Q_w\delta(x-x_i)(y-y_i)-q \quad (2)$$

Subject to the initial conditions: $h(x,y,0)=h_0(x,y)\ \forall\ x,y\in\Omega$ and the boundary conditions: $h(x,y,t)=h_1(x,y,t)\ \ \forall\ x,y\in\partial\Omega_1$; $T\partial h/\partial n=q_1(x,y,t)\ \ \forall\ x,y\in\partial\Omega_2$ or $Kh\partial h/\partial n=q_2(x,y,t)$ $\forall\ x,y\in\partial\Omega_2$. Here $h(x,y,t)$ is the piezometric head (m) which is the state variable; K_x, K_y are the hydraulic conductivities (m/d) in *x* & *y* directions; T_x, T_y are the transimissivities (m^2/d) in *x* & *y* directions; *S* is the storage coefficient; S_y is the specific yield and Q_w is the source or sink term (m^3/d/m^2). The flow region is represented by Ω while the boundary of the domain is denoted by $\partial\Omega$ ($\partial\Omega_1\cup\partial\Omega_2=\partial\Omega$). $\partial/\partial n$ denotes the normal derivative to the boundary. $h_0(x,y)$ is the initial head in the flow domain (m), $h_1(x,y,t)$ is the known head value of the boundary head (m) and $q(x,y,t)$ is the known inflow rate (m^3/d/m). Once the hydraulic head is computed, the seepage velocity V_x, V_y can be evaluated as: $V_x=-\frac{K_x}{\theta}\frac{\partial h}{\partial x}$; $V_y=-\frac{K_y}{\theta}\frac{\partial h}{\partial y}$ where θ is the porosity of the medium.

The governing equation for two dimensional solute transport of a single chemical constituent in groundwater is given by (Freeze and Cherry, 1979),

$$R\frac{\partial C}{\partial t}=\frac{\partial}{\partial x}\left(D_{xx}\frac{\partial C}{\partial x}\right)+\frac{\partial}{\partial y}\left(D_{yy}\frac{\partial C}{\partial y}\right)-\frac{\partial}{\partial x}(V_xC)-\frac{\partial}{\partial y}(V_yC)-\frac{c'w}{\theta b}-R\lambda C+\frac{q_wC}{\theta} \quad (3)$$

where, D_{xx} , D_{yy} are the components of dispersion coefficient tensor in *x* and *y* direction (m^2/day); $D_{xx}=\frac{\alpha_L V_x^2+\alpha_T V_y^2}{V^2}$; $D_{yy}=\frac{\alpha_L V_y^2+\alpha_T V_x^2}{V^2}$, α_L and α_T are the dispersivity in longitudinal (*x*) and

transverse (y) directions and $V^2 = V_x^2 + V_y^2$; C is the concentration of the dissolved species (kg/m^3); λ is the reaction rate constant (day^{-1}); w is the elemental recharge rate with solute concentration c' ; b is the aquifer thickness; $R = 1 + \rho_b K_d/\theta$ is the retardation factor, in which ρ_b is the media bulk density, K_d is the sorption coefficient and q_w is the volumetric pumping rate from a source. The initial condition is, $C(x, y, 0) = f(x, y, 0) \ \forall (x, y) \in \Omega$. The boundary conditions are of the form, $C(x, y, t) = g_1(x, y, t) \ \forall (x, y) \in \partial\Omega_1$ (Dirichlet boundary condition); $(D_{xx}\partial C/\partial x)n_x + \left(D_{yy}\partial C/\partial y\right)n_y = g_2(x, y, t) \ \forall (x, y) \in \partial\Omega_2$ (Neumann boundary condition). Here, Ω is the flow domain, $\partial\Omega(= \partial\Omega_1 \cup \partial\Omega_2)$ denotes the boundary of the modeling domain; f is a given function in Ω; g_1, g_2 are functions along the boundaries; and n_x, n_y are the components of the unit outer normal vector to the boundary. In this study, meshfree RPCM (Liu and Gu, 2005) has been used for solving the groundwater flow and transport equations. In this method, the interpolation of the unknown field variable is done by using radial basis functions (RBF) while discretization of the governing equations is achieved by point collocation.

Meshfree Radial Point Collocation Method (RPCM)

The unknown field variable is first approximated using trial or shape functions. A local support domain of a point x determines the nodes, in its neighborhood, to be used to approximate the function value at x. The approximation of a function $h(x)$ within a local support domain can be constructed as a linear combination of n radial basis functions as: $h(\boldsymbol{x}) = \sum_{i=1}^{n} a_i R_i(\boldsymbol{x}) = \boldsymbol{R}^T(\boldsymbol{x})\boldsymbol{a}$; where $R_i(\boldsymbol{x})$ is a radial basis function (RBF) such as a Multi-Quadrics or Gaussian RBF (Liu and Gu, 2005), n is the number of points in the support domain, a_i are unknown coefficients to be determined. The interpolation of the function at the k^{th} point has the following form:

$$h(x_k, y_k) = h_k = \sum_{i=1}^{n} a_i R_i(x_k, y_k) \qquad k = 1, \quad \dots, n \tag{4}$$

which yields n simultaneous linear algebraic equations with n unknowns. Solving the system of equations for the unknown coefficients a_i and substituting back these coefficients, the interpolation can be expressed as,

$$h(\boldsymbol{x}, \boldsymbol{t}) = \boldsymbol{\Phi}^{\boldsymbol{T}}(\boldsymbol{x})\boldsymbol{h_s}(t) \tag{5}$$

where $\boldsymbol{\Phi}^{\boldsymbol{T}}(\boldsymbol{x}) = \{\phi_1(x, y) \ \ \phi_2(x, y) \ \ \dots \ \ \phi_n(x, y)\}$ is known as the shape function and, $\boldsymbol{h_s} = \{h_1 h_2 \ \cdots h_n\}^T$ is the vector of nodal head values at the support domain nodes.

The discretization of the governing equation for groundwater flow and solute transport (eqns. 1, 2 and 3) is done by simple collocation at all the internal nodes. Thus by collocation at the point $\boldsymbol{x}_r(x_r, y_r)$, the governing equation (1), for a homogeneous and isotropic aquifer, is discretized as:

$$T_r\left[\frac{\partial^2 \boldsymbol{\Phi}^T}{\partial x^2}+\frac{\partial^2 \boldsymbol{\Phi}^T}{\partial y^2}\right]\boldsymbol{h}_s(t)=S_r\left(\frac{\partial h}{\partial t}\right)_r+Q_w\delta(\boldsymbol{x}_r-\boldsymbol{x}_i)-q_r \tag{6}$$

For time discretization, Cranck-Nicholson time stepping method is applied. Eqn. (6) is finally transformed as:

$$\begin{aligned}\left[S_r\boldsymbol{\phi}^{\boldsymbol{T}}-\theta\Delta t T_r\left(\frac{\partial^2 \boldsymbol{\phi}^{\boldsymbol{T}}}{\partial x^2}+\frac{\partial^2 \boldsymbol{\phi}^{\boldsymbol{T}}}{\partial y^2}\right)\right]\boldsymbol{h}_s^{t+\Delta t}\\ =S_r h_r^t+\Delta t(1-\theta)\left[\frac{\partial^2 \boldsymbol{\phi}^{\boldsymbol{T}}}{\partial x^2}+\frac{\partial^2 \boldsymbol{\phi}^{\boldsymbol{T}}}{\partial y^2}\right]\boldsymbol{h}_s^t-Q_w\delta(\boldsymbol{x}_r-\boldsymbol{x}_i)+q_r\end{aligned} \tag{7}$$

where $\theta = 0.5$. A similar discretization is performed for the solute transport equation which yields (after neglecting the source and reaction terms):

$$\begin{aligned}\left[R\boldsymbol{\Phi}^T-\theta\Delta t\left(D_{xx_r}\frac{\partial^2 \boldsymbol{\Phi}^T}{\partial x^2}+D_{yy_r}\frac{\partial^2 \boldsymbol{\Phi}^T}{\partial y^2}-V_{x_r}\frac{\partial \boldsymbol{\Phi}^T}{\partial x}-V_{y_r}\frac{\partial \boldsymbol{\Phi}^T}{\partial y}\right)\right]\boldsymbol{C}_s^{t+\Delta t}\\ =RC_r^t+(1-\theta)\Delta t\left[D_{xx_r}\frac{\partial^2 \boldsymbol{\Phi}^T}{\partial x^2}+D_{yy_r}\frac{\partial^2 \boldsymbol{\Phi}^T}{\partial y^2}-V_{x_r}\frac{\partial \boldsymbol{\Phi}^T}{\partial x}-V_{y_r}\frac{\partial \boldsymbol{\Phi}^T}{\partial y}\right]\boldsymbol{C}_s^t\end{aligned} \tag{8}$$

The discretized equations (7) and (8) are established for all the internal nodes. Appropriate boundary conditions are applied at the boundary nodes. The nodal discretized equations of eqn. (7) can be assembled in matrix form as (Guneshwor et al., 2016),

$$[K]_{N\times N}\{h\}_{N\times 1}^{t+\Delta t}=[F]_{N\times N}\{h\}_{N\times 1}^{t}+\{Q\}_{N\times 1} \tag{9}$$

where *N* is the total number of nodes including internal and boundary nodes. $\{h\}^{t+\Delta t}$ is the unknown nodal heads (or concentrations) at current time, $t = t + \Delta t$ while $\{h\}^t$ is its values at the previous time step. $[K]$ is the global coefficient matrix (LHS of eqn. 7) , $[F]$ is the coefficient matrix associated with previous time-step and $\{Q\}$ is the vector representing contributions of the sources or sinks terms. In a similar way, the nodal discretized equation of eqn. (8) can be obtained. Further a similar discretization is performed for unconfined aquifers using eqn (2). Based on the above formulation, a coupled groundwater flow and transport simulation model (CFTM) in 2D using RPCM called meshfree CFTM-RPCM has been developed. The developed model has been verified for its accuracy and effectiveness with respect to available analytical and numerical solutions for various problems.

Particle Swarm Optimization (PSO)

The Particle Swarm Optimization (PSO) is a nature-inspired swarm intelligence algorithm proposed by Kennedy and Eberhart in 1995 (Kennedy and Eberhart, 1995). A swarm is a collection of multiple units known as particles that interact with each other leading to a complex behavior. PSO relies on the

interactions of these particles to find the optimum value of a function. The ability of the PSO algorithm to optimize a given objective function comes from the velocity and position update steps of the algorithm. For each particle in the swarm, the velocity is updated using the following equation (Clerc and Kennedy, 2002):

$$v_i(t+1) = wv_i(t) + c_1 r_1\left[x_b^i(t) - x_i(t)\right] + c_2 r_2\left[x_g(t) - x_i(t)\right] \quad (10)$$

The position is then updated as,

$$x_i(t+1) = x_i(t) + v_i(t+1) \quad (11)$$

Here, i is the index of the particle. Thus, $v_i(t)$ and $x_i(t)$ are the velocity and position respectively of the i^{th}particle at time *t*. The parameters *w*, c_1 and c_2 are coefficients to be-specified by the user and their ranges are: $0 \leq w \leq 1.2$, $0 \leq c_1 \leq 2$ and $0 \leq c_2 \leq 2$. c_1 and c_2 controls the cognitive and social aspects of the particle respectively while *w* controls the inertia of the particle. The values r_1 and $r_2 (0 \leq r_1 \leq 1 \ and \ 0 \leq r_2 \leq 1)$ are random values generated for each velocity update. $x_b^i(t)$ is the individual best candidate solution for the i^{th} particle at time *t*, while $x_g(t)$ refers to the swarm's global best candidate solution at time *t*. Based on the above formulation, a PSO model has been developed and verified for its accuracy and effectiveness.

Simulation-Optimization Model for Source Identification

In Simulation-Optimization (SO) models, the groundwater contaminant source identification problem is formulated as forward-time simulation in conjunction with an optimization model. In this approach, several forward-time simulations of the groundwater solute transport equation are run with different sets or combinations of the potential sources and their strengths. The predicted solute concentrations of these forward runs are compared against the measured spatial and temporal concentration data. Since there are an infinite number of plausible sets of the potential sources, an optimization model is required to find that set of potential sources which lead to minimum difference between the simulated and observed concentrations (the objective function). In this study an SO model (RPCM-PSO-SO model) is being developed using meshfree RPCM as the simulation model and the PSO as the optimizer. Since the forward-time simulation of the groundwater solute transport model needs to be called many times to search for the optimal solution, it may take very large computational time. To overcome this, a concentration response matrix is developed (Gorelick et al., 1983) for evaluation of the concentrations of the contaminant at the observation wells from the forward simulations.

Figure 1 shows the flow chart of the simulation-optimization approach for groundwater contaminant source identification. This approach avoids the mathematical complexities associated with direct inversion of the groundwater flow and solute transport equation.

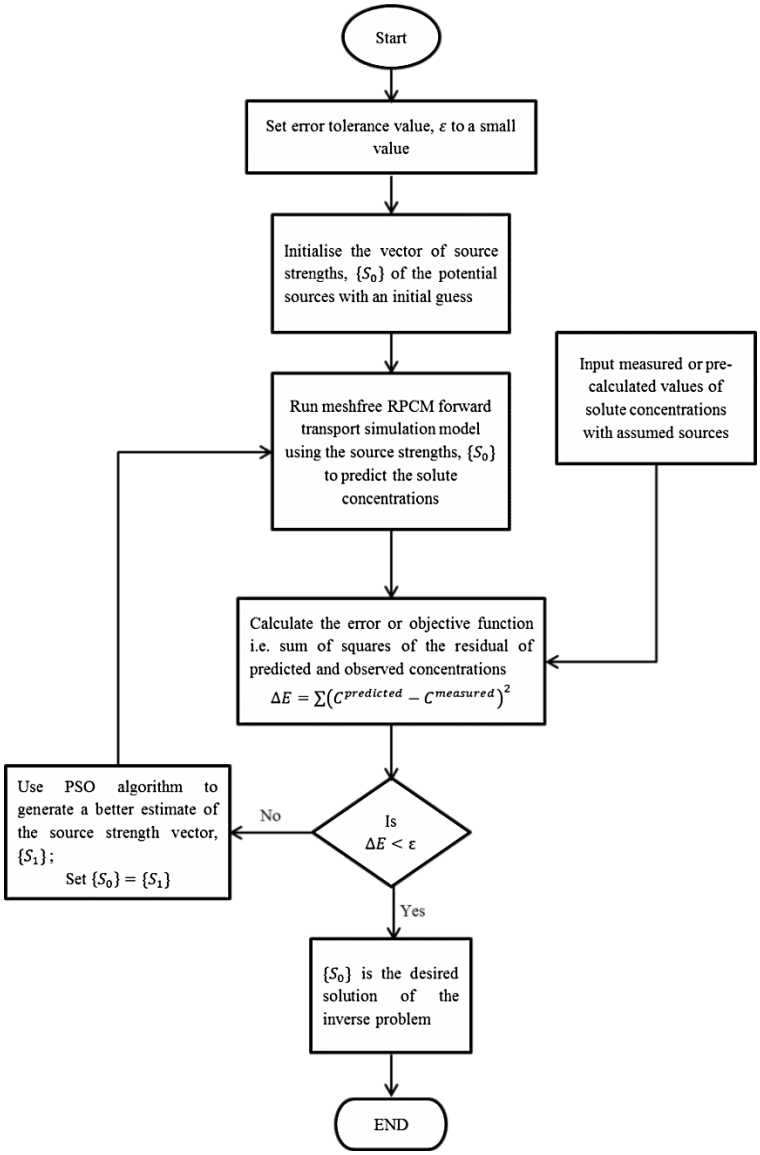

Figure 1: Flow chart of the developed Simulation-Optimization model (RPCM-PSO-SO model)

Objective Function for Optimization

As depicted in the flow chart (Figure1), the simulation-optimization (SO) model seeks to match the concentrations predicted by the model to the measured (observed) concentrations. This matching is done by minimizing the sum of a function of the differences between the simulated and measured concentrations. In this study, the objective function used for minimization is the sum of squared differences between predicted and observed concentrations i.e.

$$S = \sum_{i=1}^{NO}\sum_{j=1}^{NT}\left(C_{i,j}^{Pred} - C_{i,j}^{Obs}\right)^2 \qquad (12)$$

where, NO = no. of observation bore wells, NT = no. of time steps, $C_{i,j}^{Pred}$ =Predicted concentration at i^{th} observation point at the j^{th} time step, $C_{i,j}^{Obs}$ =Observed/measured concentration at i^{th} observation point at j^{th} time step.

Application of the Meshfree RPCM Simulation Model

The meshfree RPCM simulation model is applied to one case study of confined aquifer near Surat, Gujarat (Figure 3). The aquifer is bounded by a lake on the north, north-east, west and south-west boundaries. There are no water bodies on the rest of the boundary. The area to be modeled is approximately 4.5 km^2. A total of 1008 nodes were used corresponding to a separation between the nodes of 49.6 m along *x*-direction (Δx) and 42.8 m along the *y*-direction (Δy). The field measured hydrogeological parameters of the site are obtained from Singh and Sarma (2009). It is observed that the transmissivity of the area varies from a minimum of 30.0 m^2/day to a maximum of 170.0 m^2/day. There is a recharge zone within the model domain which corresponds to a water pond and is known to be leaking water to the aquifer and is observed as a mound in the water table map of the area. The boundaries adjacent to the lake are treated as constant head boundaries while the rest of the boundaries are treated as flux boundaries. The flux boundary values are estimated and adjusted during calibration of the model. The recharge through the pond is estimated from the make-up level of the pond and is adjusted during calibration. Figure 3 shows the head distribution (contours) and velocity vectors from the RPCM flow model. An areal contaminant (assumed to be TDS) source is assumed to be leaking with a concentration of 1000 ppm. The longitudinal dispersivity (α_L) for this problem is 20 m and the transverse dispersivity (α_T) is taken as 10% of the longitudinal dispersivity. The transport model was simulated for a period of 10 year. Meshfree RPCM model was applied to compute the head and concentration distribution in the aquifer. The results were compared to the field measured heads and FEM predicted concentration distributions (Figure 2) and found to be in good agreement (Guneshwor et al. 2016). This validates the applicability of the meshfree CFTM-RPCM model.

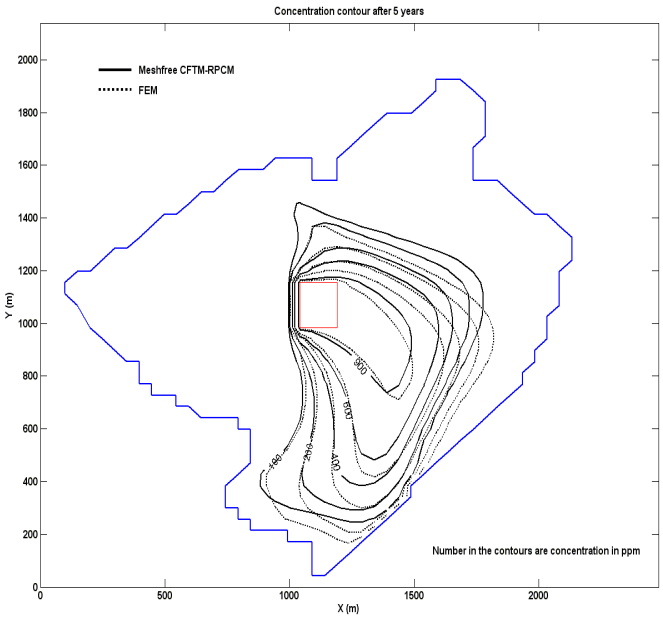

Figure 2: Comparison of concentration predictions of the RPCM model to FEM predictions.

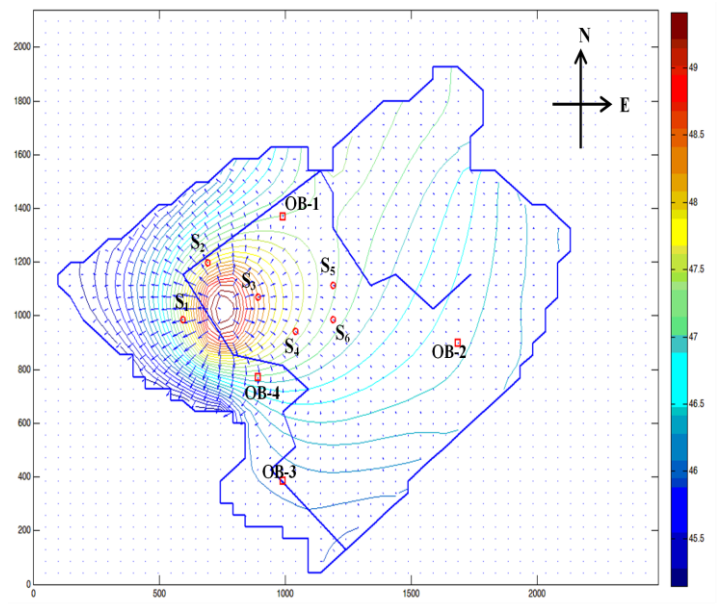

Figure 3: Location of the sources and observation wells for source identification model including contour of groundwater heads (in m) and plot of flow vectors.

Application of the Meshfree RPCM –PSO Simulation-Optimization Model

The developed SO model has been applied to a number of hypothetical and field case problems. Results of two case studies are presented here – the first is a steady state case involving a hypothetical aquifer and the second is a transient field case study.

Case Study 1 (Steady state case): Figure 4 shows the hypothetical aquifer considered for the steady state case. An underground pipe lies in an unsaturated zone above the water table and carries effluent from one end to the other. This problem was studied by Gorelick et al.(1983) and all the parameters are taken from the above work. The aquifer is 10 m thick and is of size 160 m x 240 m with a constant hydraulic conductivity of 0.864 m/day. It is assumed that the effluent (pollutant) has been flowing continuously within the pipe and contains high concentrations of the non-reactive pollutants – chloride and tritium. Several observation borewells are located within the modeling region which is used for detecting and measuring the concentration of the pollutant found in the groundwater. It is assumed that the relatively small volume of effluent that has leaked into the aquifer does not change the original, steady groundwater flow pattern.

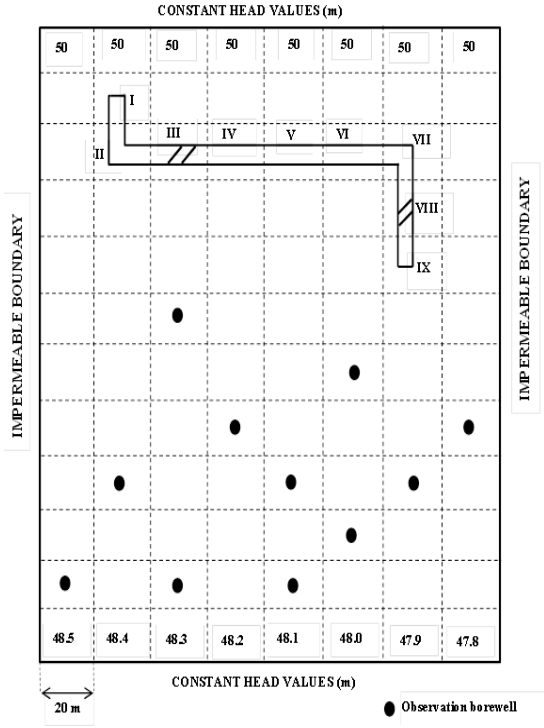

Figure 4: Hypothetical aquifer with an underground pipeline carrying effluent

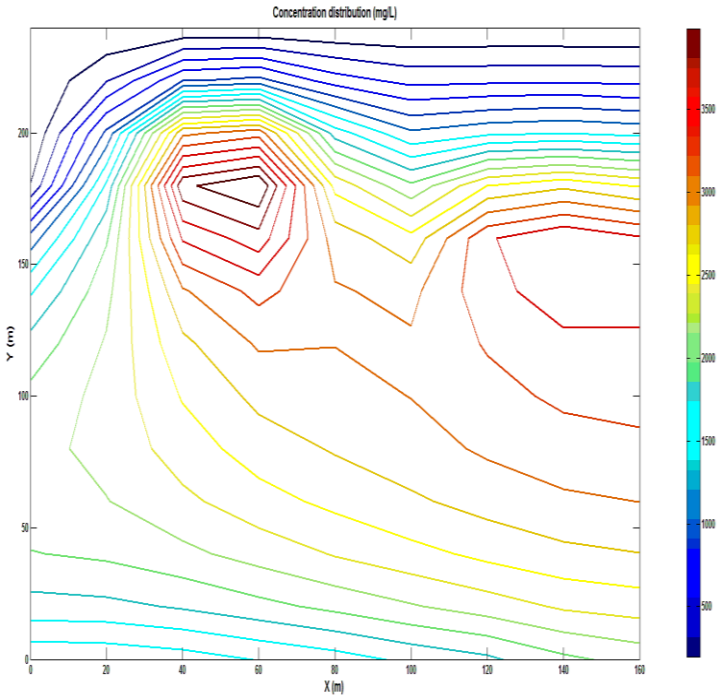

Figure 5: Chloride Concentration distributions (mg/L)

Here the concentration distributions are at steady state. It is required to locate the leak(s) and determine the magnitude of the solute and water flux from each leak from the concentration distributions of the pollutant observed in the water samples of the observation borewells.

Table 1: Source predictions by the meshfree RPCM-PSO-SO model of the present study as compared to other SO models

Potential Source Location	**True Leak Magnitudes(L/d)**	**RPCM-PSO-SO model Predicted Leak Magnitudes (L/d)**	**Leak magnitudes predicted by Gorelick et al. (1983)**	
			Linear Programming(L/d)	**Regression (L/d)**
I	0	0	0.0	-1.0
II	0	0	0.1	-0.6
III	518.4	518.2	518.2	521.1
IV	0	0.2	0	-1.3
V	0	0	0	-1.1
VI	0	0	0.0	-1.5
VII	0	3.2	2.0	-0.4
VIII	259.2	254.8	256.5	259.2
IX	0	2.0	1.0	0.0

The meshfree RPCM groundwater flow and transport simulation was carried out to create the concentration data used in this problem. In the transport model two sources (leaks) were placed at the locations III and VIII. The concentrations of Chloride and Tritium in the effluent are 15,000 mg/L and 15,000 μCi/L respectively. The water flux at first leak (location III) and second leak (location VIII) are respectively 259.2 L/day and 518.4 L/day. Figure 5 shows the chloride concentration distribution from the simulation model. The source predictions by the meshfree RPCM-PSO-SO model of the present study is shown in Table 1 where it has been compared with the SO model used by Gorelick et al. (1983). It is seen that the RPCM-PSO-SO model predictions are comparable to other models.

Case Study 2 (Transient case): The aquifer used for the transient field case study is shown in figure 3. Six hypothetical sources S_1, S_2, S_3, S_4, S_5 and S_6 are assumed to be releasing TDS (Total Dissolved Solids) contaminant through leaching over a period of four years according to the concentration data given in Table 2. It is assumed that after the 4 years of release, the sources stop releasing any contaminants. Four observation wells viz. *OB-1, OB-2, OB-3* and *OB-4* records the contaminant (solute) concentrations due to the releases from the above sources for a simulation period of 10 years.

Table 2**:** Strength of the sources during the leaching period

Release Year	**Source strength (in ppm)**					
	S1	**S2**	**S3**	**S4**	**S5**	**S6**
1st year	1000	1500	890	0	0	500
2nd year	0	1200	1000	0	0	700
3rd year	900	500	0	1000	850	0
4th year	0	0	800	1300	1100	0

The concentration values at the observation bore wells are recorded for every 30 days (monthly) to construct the breakthrough curves at the wells (Figure 6). The breakthrough curves at the four observation bore wells serve as the measured concentration data and are used as the input to the source identification model. The goal of the source identification model is to reconstruct the release history of the sources (Table 2) from this given concentrations data. The result of the source identification model is presented in Table 3.

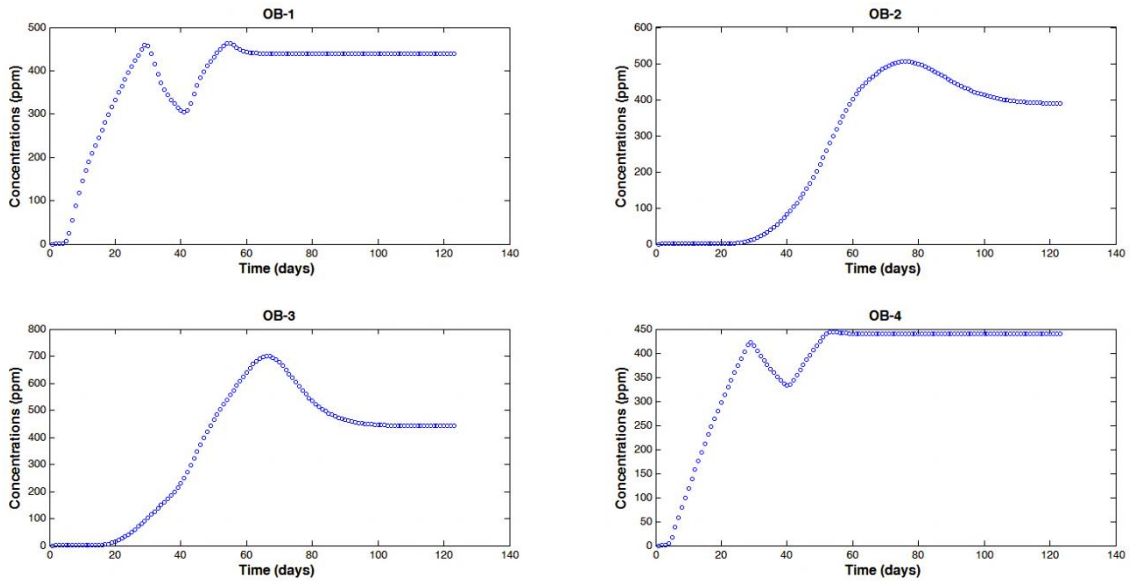

Figure 6: Breakthrough curves at the observation wells

The source strength predictions are shown in brackets (bold) alongside the actual release strengths. 50 x 10^3 iterations of PSO was used to generate this result. It is observed that the source predictions are accurate to within 5% of the true values. It may be observed that a few artificial or spurious sources are also predicted. However their magnitudes are very small and can therefore be safely neglected.

Table 3: Predicted strengths (bolded in bracket) of the sources during the leaching period

Release Year	**Source strength (in ppm)**					
	S1	**S2**	**S3**	**S4**	**S5**	**S6**
1st year	1000 (**1031**)	1500 (**1552**)	890 (**888**)	0 (**0**)	0 (**1**)	500 (**491**)
2nd year	0 (**27**)	1200 (**1257**)	1000 (**999**)	0 (**1**)	0 (**1**)	700 (**691**)
3rd year	900 (**878**)	500 (**462**)	0 (**1**)	1000 (**1000**)	850 (**850**)	0 (**9**)
4th year	0 (**3**)	0 (**6**)	800 (**800**)	1300 (**1300**)	1100 (**1100**)	0 (**4**)

Further, the robustness of the proposed RPCM-PSO-SO model for source identification was examined by considering additional scenarios which simulates cases with limited amount of concentration data, missing or incomplete concentration data, intermittent or irregular data collection etc. Effect of the location of the observation borewells with respect to the sources was also examined by placing the wells randomly and in the contaminant plume path. It was observed that the source identification model was able to reconstruct the release histories satisfactorily in all the above cases. The application of the meshfree RPCM-PSO-SO model was further extended to cases with uncertain

concentration data since errors or uncertainties are inevitable in field measurements. The measurement uncertainties were simulated by perturbing the concentration data with random errors sampled from a normal distribution. Various ways of dealing with erroneous concentration data were examined such as, smoothing of the input data to recover the underlying relationship, imposing global and local constraints on the sources from field information, incorporating field information to rule out spurious predictions, giving weights when such information is conceivable or available etc. The developed source identification model was able to cope with the uncertain input data but the prediction accuracies are reduced with increase in uncertainty. From the above case studies, it can be concluded that the meshfree RPCM-PSO-SO model can be effectively used for groundwater source identification.

Conclusions

Following important conclusions are drawn from the present study:

- A Meshfree RPCM model is developed for groundwater flow and solute transport simulation for both confined and unconfined aquifers. The models are verified with available analytical and numerical solutions using FDM and FEM and found to be in good agreement. The developed model was also applied to a field case study. The results are compared to field measurements and with the results from FEM computation. The results were found to be satisfactory validating the applicability of the RPCM model.
- For the purpose of groundwater source identification, a simulation-optimization (SO) model using meshfree RPCM as the simulator and PSO as the optimizer was developed. The model was verified with other methods available in the literature and found to be effective.
- The source identification model was applied to a field case problem. Robustness of the model was examined by simulating various field scenarios such as limited amount of concentration data, missing concentration data, intermittent or irregular data collection etc. The effects of the location of the observation borewells, with respect to the contaminant plume path, on the model predictions were also examined. The model has been found to be effective for all types of the problems.
- The source identification model was also examined for its capability to handle concentration data with measurement errors. Both moderate and high levels of measurement errors were simulated and it was found that the model could handle the uncertainties involved.
- The RPCM-PSO-SO model developed identified the location and magnitude of the sources to acceptable accuracy and will be a useful tool in remediation of contaminated aquifers.

List of Figures

List of Figures

List of Figures

List of Tables

List of Tables

List of Notations and Abbreviations

Notations

C Concentration (solute)

D_{xx}, D_{yy} Components of dispersion coefficient tensor [L^2T^{-1}]

D^* Effective diffusion coefficient

C_a Sorbed concentration

Cr Courant Number

C_s Shape parameter value

K_d Distribution Coefficient [L^3M^{-1}]

K_{xx} , K_{yy} Hydraulic conductivities [$L\ T^{-1}$]

Pe Peclet Number

Q_w Pumping or extraction rate [L^3T^{-1}]

R_a Retardation Coefficient

T_{xx} , T_{yy} Transmissivities

dc Nodal or grid spacing

n Porosity

Δt Time step size

α_c Multiples of nodal spacing (for shape parameter value calculation)

ρ_b Bulk Density of soil [ML^{-3}]

λ First Order Decay rate constant [T^{-1}]

h Hydraulic head [L]

$h_0(x, y)$ Initial Head distribution in the modeling domain [L]

$h_1(x, y, t)$ Known boundary head [L]

Φ Shape Functions

Ω Modeling domain

$\partial\Omega$ Boundary of the modeling domain

α_L Longitudinal dispersion coefficient

α_T Transverse dispersion coefficient

$\bar{v}$ Seepage velocity

Abbreviations

ADE	Advection Diffusion equation
AI	Artificial Intelligence
ANN	Artificial Neural Networks
ASA	Adaptive Simulated Annealing
BBE	Backward Beam Equation
BEM	Boundary Element method
BNM	Boundary Node Method
BPIM	Boundary Point Interpolation Method
BRPIM	Boundary Radial Point Interpolation Method
CFTM-RPCM	Coupled Flow and Transport Model using Radial Point Collocation Method
CGM	Conjugate Gradient Method
CSRBF	Compactly Supported RBF
DDP	Differential Dynamic Programming
EFG	Element Free Galerkin method
EXP-RBF	Exponential Radial Basis Function
FDM	Finite Difference Method
FEM	Finite Element Method
FIPS	Fully Informed Particle Swarm
GA	Genetic Algorithm
HBRPIM	Hybrid Boundary Radial Point Interpolation Method
LP	Linear Programming
LRPIM	Local Radial Point Interpolation Method
MILP	Mixed Integer Linear Programming
MINLP	Mixed Integer Non Linear Programming
MJBBE	Marching Jury Backward Beam Equation
MLPG	Mess Less Petrov-Galerkin
MLS	Moving Least Squares
MOC	Method of Characteristics
MQ-RBF	Multi-Quadrics Radial Basis Function
MRE	Minimum Relative Entropy
NLP	Non Linear Programming
NLS	Non Linear Least Squares
PAT	Pump and Treat
PDE	Partial Differential Equation
PIM	Point Interpolation Method
PSO	Particle Swarm Optimization
PUFEM	Partition of Unity Finite Element Method

RBF Radial Basis Function

RKPM Reproducing Kernel Particle Method

RMS Root Mean Square

RMSE Root Mean Square Error

RPCM Radial Point Collocation Method

RPCM-GFM Radial Point Collocation Method based Groundwater Flow Model

RPCM-GTM Radial Point Collocation Method based Groundwater Solute Transport Model

RPCM-PSO-SO Radial Point Collocation Method and Particle Swarm Optimization based Simulation-Optimization

RPIM Radial Point Interpolation Method

SO Simulation Optimization

SPH Smoothed Particle Hydrodynamics

SUPG streamline upwind Petrov-Galerkin

TDS Total Dissolved Salts

UST Underground Storage Tank

Chapter 1
Introduction

1.1 General

Groundwater accounts for roughly a third of the source of drinking water for the world's population and is one of the components of the hydrological cycle. In some regions of the world, the share of groundwater as drinking water is as high as 75 percent (Sampat, 2000). Major aquifers are tapped on every continent, and ground- water is the primary source of drinking water for more than 1.5 billion people worldwide. It is predicted that groundwater may become the main source of water in future as many terrestrial sources of fresh water are getting dried up or their water volume is reduced due to global warming and climate changes. In many arid regions, groundwater is the only reliable source of water for drinking and for agricultural activities. As rivers and lakes are stretched to their limits with many of them getting dried up, dams being constructed or polluted, we're growing more and more dependent on groundwater.

Even as our dependence on groundwater increases, the availability of the resource is becoming more limited. Overexploitation of groundwater due to intensive competition among factories, farms, and households, has led to rapid depletion of the water table in many places around the world. On almost every country, many major aquifers are being drained faster than their natural rate of recharge. Groundwater depletion is most severe in many parts of India, China, the United States, North Africa, and the Middle East (Sampat, 2000).

In many coastal areas, salt water intrusion has become a very serious problem as the sea water and groundwater equilibrium is disturbed due to overuse of groundwater. Moreover in many places around the world, groundwater contamination has become a very serious issue due to uncontrolled human and industrial activities. Not only has this rendered the groundwater in many areas unusable, but the soil and groundwater being contaminated by toxic substances pose a threat to human and environmental health as they enters the food chain through absorption by plants. Therefore proper management of this precious source of water on which mankind depends is very important. Remediation and protection of groundwater is very vital to human needs and to maintain nature's ecological balance also. An important aspect in groundwater remediation is to identify the location and estimate the release magnitude of the unknown contaminant sources. The main scope of the present study is groundwater contaminant source identification using a simulation-optimization approach.

1.2 Groundwater pollution problems

Over the past few decades, the groundwater resources of the world have become vulnerable to serious threats of pollution due to rapid industrialization and uncontrolled extraction of groundwater. Areas known to be severely affected are often densely populated areas where groundwater is heavily used and dependent upon as a drinking water source. A wide variety of organic and inorganic chemicals have been identified as potential contaminants in groundwater (Freeze and Cherry, 1979). These include inorganic compounds such as nitrates, brine, and various trace metals; dissolved solids; synthetic organic chemicals such as fuels, chlorinated solvents, and pesticides; radio-active contaminants associated with defense sites; and pathogens.

1.3 Groundwater flow and transport modeling

The growing economic importance of aquifers as a potable water supply and the potential adverse effects that contamination can pose to users of aquifers necessitate the development of improved methods of predicting the transport of contaminants in aquifers both spatially and temporally. The scientific developments in solving partial differential equations numerically, and the technological developments in the computer industry during the past decades, have collectively made it possible to solve complex aquifer flow and aquifer contamination problems in a cost-effective and efficient way. For some aquifer problems, such as wellhead protection and water supply design, groundwater flow modeling is sufficient. However, for a solute transport problem, both groundwater flow and solute transport modeling are required. Groundwater flow and solute transport models are mathematical tools that can range from simple analytical solutions, which can be solved using a calculator, to far more complex numerical models that can only be solved using a digital computer (Bear, 1979). These models can be used to develop optimal groundwater usage and management models, and to develop remedial measures to address the contamination.

Groundwater modeling is one of the main tools used in the hydrogeological sciences for the assessment of the resource potential and prediction of future impact under different circumstances/stresses. Its predictive capacity makes it the most useful tool for planning, design, implementation and management of the groundwater resources.

1.4 Groundwater source identification

While the importance of groundwater as the source of potable water has grown over the years, groundwater pollution has become a serious environmental problem due to rapid industrialization, uncontrolled extraction of groundwater, uncontrolled disposal of industrial and domestic wastes, seepage from urban landfills etc. Once contaminated, it is very expensive to remediate the aquifer. To make the

remediation effective, accurate assessment of the contamination and proper planning is required. Groundwater source identification is vital to the remediation of a contaminated aquifer. Only when the sources are identified, the effective planning for remediation can be taken up. Once identified, the sources can be plugged or prevented from further leakages. Also it will help to fix the responsible facility or unit and take other legal measures (Delleur, 2007).

However, identifying the source of groundwater contamination is not an easy task since the only available information in most of the cases is the contaminant concentration data found from water sampling in an area. Physical approaches such as tracer tests will be difficult to perform in most of the field situations. In this context, the effective method may be to develop computer or numerical models. In the past three decades, several modeling approaches have been proposed for groundwater source identification. Since it is in developmental stages, most of the proposed approaches have serious limitations and limited applicability in field conditions. Among the proposed approaches, the simulation-optimization approach has the potential to handle actual field problems with complex geometries. It couples a groundwater flow and transport model to an optimization model. Since there are many methods to perform the simulation and the optimization, it provides a lot of flexibility in the choice of these models.

1.5 Simulation-Optimization model for source identification

Simulation-optimization models are powerful tools for groundwater source identification with the potential to be widely applicable to a number of field problems. It was the first method proposed for groundwater source identification. A large number of researches towards groundwater source identification have been focused on the SO models due to its flexibility in the choice of simulation and optimization techniques (Gorelick et al., 1983). The basic principle behind SO model is to find the combination of the sources which gives closest match between observed and simulation predicted solute concentrations. This matching is done by defining an objective function. The objective function is usually the sum of squares of the differences between the observed and predicted solute concentrations. Other types of objective functions can also be defined as per the requirements of the problem. A number of conventional (e.g. linear programming, non-linear programming, regression etc.) and heuristic or artificial intelligence based (genetic algorithm, swarm intelligence optimization etc.) optimization techniques may be adopted (Datta et al., 2009). For the simulation model, commonly used methods are the finite-difference and finite element methods. Recently meshfree methods have also been used in simulation of groundwater flow and transport.

1.6 Motivation of the study

Groundwater is a significant source of drinking water for the world's population. In many areas of the world, it is also the main source for irrigation. It is predicted that groundwater may become the main source of water in future as many terrestrial sources of fresh water are getting dried up or their water volume is reduced due to global warming and climate changes. However, groundwater resources of the world are facing serious threats of contamination or are already contaminated due to rapid industrialization, overexploitation or uncontrolled extraction of groundwater, uncontrolled disposal of industrial and domestic wastes, seepage from urban landfills etc. (Freeze and Cherry, 1979). Remediation of contaminated aquifers is very expensive and requires proper planning both to optimize the cost and increase its effectiveness. This calls for accurate tracking and assessment of the groundwater contamination.

A very crucial aspect in the remediation process is to identify the location and release magnitude of the unknown contamination sources. Only then an effective remedial measure can be designed and it will also help to fix the responsibilities. Simulation optimization (SO) models have been found to be very effective for groundwater contamination source identification.

Generally used simulation models are based on Finite Difference Method (FDM) and Finite Element Method (FEM). Compared to these methods, meshfree based methods offer advantageous in that no mesh is required. The construction of mesh is computationally very expensive. Moreover, radial basis functions (RBF) used in meshfree methods such as Radial Point Collocation Method (RPCM) have high interpolation accuracy. High Peclet transport problems are also much easier to deal with meshfree RPCM.

For optimization, compared to generally used traditional methods such as linear programming, non-linear programming etc. have inherent disadvantages. Recently swarm intelligence techniques such as Particle Swarm Optimization (PSO) have been found to be very effective for global optimization. PSO offers easy implementation and also easy integration with simulation model, has fewer parameters to adjust. It can locate the global as well as local optimas unlike conventional gradient based optimizers which can get trapped in local optima.

In this study, the simulation-optimization model has been proposed for groundwater contaminant source identification. Due to the advantages of meshfree method, here the Meshfree Radial Point Collocation Method (RPCM) is proposed as the simulation model. The Particle Swarm Optimization (PSO) is proposed as the optimization model. Both models will be coupled to construct the SO model.

1.7 Objectives of the study

The main aim of this study is to develop methods for locating or tracing the sources of contamination in a given contaminated area. It is assumed that many potential sources of contamination may be present in the area. This is an inverse modeling problem. It is proposed to use a simulation-optimization model in this study to achieve this goal.

The specific objectives of the study are:

- Development of coupled groundwater flow and transport simulation models using meshfree radial point collocation methods (RPCM) for both confined and unconfined aquifer problems.
- Development of optimization model using Particle Swarm Optimization (PSO).
- Coupling of meshfree RPCM simulation model and PSO based optimization model to develop Simulation-Optimization (SO) models for groundwater source identification.
- Validation of the developed models with benchmark problems from published literature.
- Application of the developed SO model to hypothetical and field case studies, and to cases with uncertainty in concentration data.

1.8 Organization of the report

This report is organized in seven chapters including the present one which deals with the general aspects of groundwater and the objectives of the study. **Chapter 2** gives a comprehensive review on the major developments and research works carried out so far in groundwater flow and transport modeling with conventional and with mesh free techniques. It also reviews the developments in contaminant source identification techniques in aquifers and in particular, the use of Simulation-Optimization methods for contaminant sources.

Chapter 3 deals with the fundamental aspects and theoretical developments in groundwater flow and transport modeling and groundwater source identification. **Chapter 4** introduces the mesh free RPCM and elaborates on the numerical formulation of the flow and transport equation with mesh free RPCM methods. It also includes the verification and benchmarking of the formulations developed with several 1D and 2D problems. The developed meshfree RPCM model has also been applied to a field case study. **Chapter 5** deals with the theoretical and numerical aspects of groundwater source identification. A meshfree RPCM and PSO based simulation-optimization model for groundwater source identification has been developed and verified using literature available test problems. **Chapter 6** gives the application of

the developed simulation-optimization model to a wide variety of problems. A field case study is presented with various scenarios that may arise in real field problems of groundwater source identification and to test the robustness of the model. A section on handling uncertain concentration data has been included. **Chapter 7** summarizes the research work carried out in this study, the conclusions drawn from it and the scope for future works.

Chapter 2
Literature review

2.1 Introduction

This chapter discusses the developments and current research directions in groundwater flow and transport modeling, meshfree methods and groundwater contaminant source identification. It also briefly examines the existing methods or techniques in these areas and explores the issues with these methods and their proposed solutions.

2.2 Groundwater flow and transport modeling

Groundwater modeling has, nowadays, become a major part of most projects dealing with groundwater development, protection and remediation. With the improvements in computer hardware and software, the role of groundwater models will continue to increase. Earlier models of groundwater used finite difference method but over the years many new techniques have been applied in groundwater modeling such as finite element method, boundary element method, boundary integral equation method, analytic elements, integrated finite difference, mesh free methods etc. Each of these methods has their own advantages and disadvantages. A brief review of the various groundwater flow and transport modeling techniques and tools are provided herewith.

Pinder (1973) used Galerkin method of approximation to simulate the movement of groundwater contaminants. This paper is among the first application of finite element to groundwater modeling. The main advantages that the author claimed in using finite element in solving the groundwater flow and mass transport equations was that this approach allowed a functional representation of the dispersion tensor, transmissivity tensor, and fluid velocity, as well as an accurate representation of boundaries of irregular geometry. As a field application, he successfully used the method to track chromium contamination on Long Island, New York, and showed that accurate simulations can be obtained by using the Galerkin-finite element approach.

Strack and Haitjema (1981) developed the analytic element method for regional groundwater modeling. This new method avoids the discretization of a groundwater flow domain by grids or element networks. Instead, only the surface water features in the domain are discretized, broken up in sections, and entered into the model as input data. Each of these stream sections or lake sections is represented by closed form analytic solutions: the analytic elements. The comprehensive solution to a complex, regional groundwater flow problem is obtained by superposition of all, a few hundred, analytic elements in the model.

Traditionally, superposition of analytic functions was considered to be limited to homogeneous aquifers of constant transmissivity. However, by formulating the groundwater flow problem in terms of appropriately chosen discharge potentials, rather than piezometric heads, the analytic element method becomes applicable to both confined and unconfined flow conditions, as well as to heterogeneous aquifers. The analytic elements are chosen to best represent certain hydrologic features. For instance, stream sections and lake boundaries are represented by line sinks, small lakes or wetlands may be represented by areal sink distributions. Areal recharge is modeled by areal source distributions (areal sinks with a negative strength). Streams and lakes that are not fully connected to the aquifer are modeled by line sinks or area sinks with a bottom resistance. Discontinuities in aquifer thickness or hydraulic conductivity are modeled by use of line doublets (double layers). Specialized analytic elements may be used for special features, such as drains, cracks, slurry walls, etc.

Ligget (1987) explored the advances of the boundary element method to model groundwater problems. He observed that diffusion and advection-diffusion solutions could be done efficiently including the incorporation of inhomogeneity, anisotropy, and nonlinear diffusion. Some of the problems suggested by the author which are ideally suited for application of the method are the difficult problem of stream-aquifer interaction, flow in fractured media and seawater intrusion forms. These problems are complicated in nature. He suggested that for these and other applications the boundary element method provides an inexpensive technique for calculation where the data preparation and setup time is minimal and programs can be written easily.

Harbaugh and McDonald (1996) developed a finite-difference code for modeling three dimensional groundwater flow. It is one of the most widely used code and also well validated by hydro-geologist around the world. Several commercial codes available today are based on this code. The code has been updated in 1988 and 2000. One of the main feature of this code is its modularity i.e. separate modules can be written and incorporated into the code.

Anderson and Woessner (2002) discussed the various aspects of groundwater flow and transport modeling including calibration and parameter sensitivity. The book deals mainly with the popular methods of finite-difference and finite-element. All the protocols and consideration to be made for a practical groundwater modeling are discussed. Popular codes are reviewed along with the shortcomings.

Zheng and Bennet (2002) discussed all the techniques used for groundwater transport modeling. Theoretical foundations of contaminant transport are elaborately discussed. Several techniques for solving groundwater transport such as finite difference, finite element, method of characteristics (MOC),

modified MOC, hybrid MOC, particle tracking etc. are all discussed. Dedicated chapters are there for handling different solute types, uncertainty and data collection and conceptualization of the model.

Rastogi (2007) discussed latest techniques in numerical modeling of groundwater flow and transport including various applications such as groundwater management, inverse modeling, contaminant migration and remediation.

Desai et al., (2011) illustrated the application of finite element method to groundwater flow and transport simulation. Various aspects of developing FEM models in various areas of scientific and engineering endeavors have been discussed in detail.

2.3 Groundwater modeling with meshfree methods

Meshfree methods offers an alternative approach to the mesh or grid based techniques such as FDM and FEM. Being free from mesh, it gives a number of advantages over mesh based approaches and is increasingly becoming popular. There are various approaches/types of mesh free methods (Liu and Gu, 2005).

Kansa (1990) used a mesh free scheme for solving partial differential equations (PDE) using a globally supported multi-quadrics radial basis functions (MQ-RBF) interpolant. He employed a point collocation discretization of the governing PDEs, known as strong form approach. This globally supported RBF collocation method suffers from ill-conditioning as the number of nodes increases and was also computationally expensive (Gutierrez and Florez, 2008). Many approaches have been proposed to overcome these difficulties. One of the approaches is the use of locally supported RBF interpolant.

To improve the robustness of the Kansa method, Fedoseyev et.al.(2002) proposed an improved Kansa – MQ method by using an additional set of collocations points beyond the boundary and an additional set of collocation equation of the governing equation on these points.

There are many other issues which are yet to be addressed in using the RBF interpolation and collocation approach such as the optimal choice of shape parameter, shape and size of the local support domain etc. A few strategies have been suggested in Kansa and Carlson (1992); Rippa (1999), Schaback and Wendland (2000), Fornberg and Wright (2004) etc. for the optimal choice of the shape parameter. The stability and accuracy of radial basis function interpolations are very sensitive to the value of shape parameter (Driscoll and Fornberg, 2002; Fornberg and Wright, 2004; Larsson and Fornberg, 2005). Another issue with the collocation technique is that of instability at the boundary when it involves singularity or derivative (Neumann) boundary conditions (Zuppa and Cardona, 2003; Bernal et.al.,2009) etc. A discussion of the issues with RBF collocation method can be found in Gutierrez and Florez (2008). The

relative performance of the different variations of the RBF collocation methods has also been discussed in the same paper. The loss of accuracy due to presence of derivative boundary conditions is also well known (Liu and Gu, 2005), though some special treatments are available. Liu and Gu (2005) and Gutierrez and Florez (2008) discussed different strategies of handling the derivative boundary conditions along with the relative performances of each strategy. Chen (2009) has observed that owing to the smoothness and non-locality of radial basis functions, it poses considerable difficulties in solving problem with local features and heterogeneity, and proposed a technique called subdomain strong form collocation to deal with such problems.

In this section, further brief literature review on the application of mesh free methods to groundwater modeling is presented.

Li et al., (2003) developed a mesh less method for modeling groundwater contaminant transport. The algorithm uses collocation method with radial basis functions as the interpolation function. The authors tested and presented numerical results for several cases in two and three dimensions involving pure diffusion, advection and dispersion for continuous source; advection and dispersion for instantaneous source; advection and dispersion for patch-source. For the transient case, they have found that both the Crank-Nicholson and fully implicit time stepping schemes were convergent with similar accuracy. They observed that the method is very simple and accurate.

Chandhini and Sanyasiraju (2007) applied a mesh free method known as radial basis function-finite difference (RBF-FD) for solving steady convection-diffusion equations. This method is a finite-difference type scheme based on radial basis function, first proposed by Wright and Fornberg (2006). The authors have employed multi-quadrics RBF. Convection dominated equations are very challenging as it can lead to oscillations and numerical dispersion. The scheme they have developed was applied to both linear and non-linear problems in one and two dimensions. Several test problems were chosen to check the performance of the mesh free scheme under various conditions such as moderate to high Reynolds number, different types of boundary conditions, regular and irregular grids etc. The authors have reported that the solution obtained with their mesh free scheme was accurate and non-oscillatory.

Kumar and Dodagoudar (2008) applied a mesh free method, the radial point interpolation method (RPIM) with polynomial reproduction, to model the two-dimensional contaminant transport through saturated porous media. In RPIM, the approximate solution is constructed entirely in terms of a set of nodes and no characterization of the interrelationship of the nodes is needed. In their method, the radial basis function is used only for shape function construction which is the only mesh free part, the rest of the method is actually same as FEM. Locally supported domains were used for the shape function creation. An

advection-dispersion equation with sorption was considered to illustrate the applicability of the RPIM. They have implemented Galerkin weak form of the governing equation using two-dimensional mesh free shape functions constructed using thin plate spline radial basis functions. Through three numerical examples, their results are compared with those obtained from the analytical solution and finite element method. Experimental results were also used to validate the approaches. They found that the proposed mesh free method showed no oscillations and also able to tackle to Peclet constraints without modification.

Alhuri et.al., (2011) compared the performance of two types of mesh free collocation method for modeling groundwater contaminant transport. One is based on a globally supported multi-quadric radial basis function (MQ-RBF) for function approximation while the other was based on locally supported compactly supported radial basis functions (CSRBF). Their algorithm uses collocation method with radial basis functions. They have presented numerical results for 1-D, 2-D and 3-D groundwater contaminant transport models and shown that the method was very simple and accurate. The authors observed that CSRBFs with a suitable choice of scaling factor δ performed better than global MQ-RBFs. It was also found that the condition number of MQs scheme increased rapidly with the increase in the number of data points. Using CSRBF technique which enables one to work with sparse banded matrices, the problem of ill-condition was reduced and improved the conditioning of the matrices.

Meenal and Eldho (2011) have applied mesh free point collocation method using Multi-quadrics radial basis function (MQ-RBF) to solve the groundwater flow equation in an unconfined aquifer and applied it to a case study using real field data. This work is the first application of mesh free collocation method to a large scale field study. The authors have employed rectangular local support domain for RBF interpolation and so called dummy nodes are constructed for nodes in the periphery or boundary and for the applications of derivative boundary. The developed method was verified through several one and two dimensional problems. The comparison was done against either analytical solution or FEM or BEM solution, if analytical solution is not available. Sensitivity analysis was performed for time-steps, nodal distance and shape parameter values of the multi-quadric RBF. Calibration was also performed for the field problem. Through their numerical exercises, they have found that the developed mesh free technique was giving very good agreements with field measured data. The authors have highlighted issues such as choosing the optimal value of the shape parameter, which is yet unresolved issue in mesh free method. In this work, an isotropic aquifer was considered but the method developed can be extended to heterogeneous aquifers also.

Meenal and Eldho (2012b) developed a mesh free collocation method to solve a two-dimensional coupled groundwater flow and solute transport problem. This mesh free method was applied to model contaminant transport through groundwater at an industrial complex (refinery) in Gujarat, India. Contaminant transport is a complicated problem as it involves solving both the flow and transport equations and coupling them. The formulation used is similar to what the authors have used in Meenal and Eldho (2011) and is an extension of their earlier work. The verification of the method was carried out by comparing the mesh free solutions with either analytical solutions or FEM solutions, when analytical solutions are not available, for one and two dimensional problems. The mesh free results were found to be in good agreement with standard FEM simulations. However sensitivity analysis reveals that the mesh free model was sensitive to shape parameter value of the MQ-RBF. This is a well-known issue while using RBF function interpolation (Driscoll and Fornberg, 2002). The issue of finding the optimal choice of the shape parameter is not yet addressed so far in mesh free formulations. It is generally found by hit and trial method. This paper demonstrated the applicability of mesh free collocation methods in complex and large scale field problems.

Cifti et al., (2012) applied radial basis function collocation method to investigate the solute transport phenomena under heterogeneous conditions. They studied 1-D and 2-D transport scenarios in which scale-dependent dispersivity fields were taken into consideration and compared it with available analytical solutions. For assessing the sensitivity of their method, different radial basis functions (RBFs) augmented with polynomials of varied orders, were studied. For the designed test cases uniformly distributed interpolation nodes as well as randomly scattered data points were used. The simulation results were compared with the results of MT3DMS (Zheng and Wang, 1998) which is a modular three-dimensional transport model with alternative solution schemes including the method of characteristics, the implicit central finite difference and the third order total variation diminishing finite volume. They reported that the mesh free collocation method predicts the solute concentration behavior in a more accurate manner than MT3DMS. They used the model to simulate a real case of solute transport through a two-layer soil which was set up experimentally. They found that the results were very close to the experimentally measured values and demonstrated the applicability of the mesh free collocation to heterogeneous conditions.

Swathi and Eldho (2013) used Meshless Local Petrov-Galerkin (MLPG) method with strong form of collocation with exponential/Gaussian radial basis function to solve the groundwater flow problem in confined aquifer. MLPG was first proposed in Atluri and Zhu (1998). The developed 1D model was verified with available analytical solution while the 2D model was compared against FEM solutions. Two case studies were taken up –one of them being an aquifer with anisotropy and heterogeneity. The MLPG

results were found to be satisfactory. However it was observed that the accuracy of the MLPG method was affected by various model parameters such as the value of shape parameter of the multi-quadric RBF used, support domain size, nodal distances etc. But these issues are common to most mesh free methods. The authors carried out a sensitivity analysis with regard to the above parameters to study how they affect the accuracy and to determine the optimum values of them. This study demonstrated that the MLPG based Meshless method was very effective in the simulation of groundwater flow problems.

Alice et al., (2014) used reviewed the application of collocation based meshfree method to groundwater flow. A meshFree method based on PCM is discussed and comparison of results obtained with the conventional FEM is presented for groundwater flow problems. They developed PCM- and FEM-based groundwater flow models for confined aquifer in two-dimensional are developed. The PCM model has been applied to hypothetical groundwater flow problems and results are compared with analytical solutions and FEM model results. The meshfree-based PCM model has been found to be more accurate than FEM results when compared with analytical solutions.

2.4 Contaminant Source identification in groundwater

When multiple potential contaminant leakage sources are present, it can be quite a challenge to identify the source of contaminant leakage based on contamination data collected from surveillance bore wells. Detailed information of the potential sources is a pre-requisite to this effort. Most attempts at quantifying contaminant transport have relied on solving some form of a well-known governing equation referred to as advection-dispersion-reaction equation. In identifying the source of pollution we have to solve the governing equations backward in time, a process known as inverse modeling. But modeling contaminant transport using reverse time is an ill-posed problem since the process, being dispersive, is irreversible. Because of this ill-posedness, such problems have discontinuous dependence on data and are very sensitive to the errors in data. Non-uniqueness is another major issue for inverse calculations. In inverse problems, one of the common practices to overcome the stability and non-uniqueness problem is to make assumptions about the nature of the unknown function so that the finite amount of data in observations is sufficient to determine that function. In the case of groundwater pollution source identification, most of the time, additional informations are available such as the location of potential release sites and chemical fingerprints of the plume. Hester and Harrison (2008) discussed the importance of source identification in environmental forensics and the critical role played by it from legal perspectives.

Various methods have been proposed for the identification of contaminant source in groundwater. All the methods attempt to solve the Advection-Dispersion equation (ADE) backward in time in order to identify the pollution sources. These methods may broadly be subdivided into four major groups (Atmadja and

Bagtzoglou, 2001b) namely optimization methods, analytical solution and regression approaches, direct methods, probabilistic and geo-statistical approach. In optimization methods, a forward simulation is run and the solution obtained is checked against the measured/current spatial data observed. Owing to the non-uniqueness of the solution and the infinite number of plausible combinations, an optimization method to obtain the best fitted solution is devised. Direct methods usually reconstruct the plume history. Analytical methods are an inverse method based on analytical solution of the contaminant transport equation and parameter estimation using linear or non-linear regression. Probabilistic and geo-statistical approaches are a group of techniques which attempts to solve the ADE backward in time without relying on optimization approaches. A probabilistic approach involves solving the transport problem with stochastic differential equations backward in time. Each of the methods is subject to significant drawbacks and limitations. A brief review of the various approaches is presented here.

Gorelick et.al.(1983) was among the first who studied the pollution source identification problem using optimization approaches. The groundwater pollution source identification problem was formulated as a forward time simulation with an optimization model. For optimization, they used least squares regression and linear programing for least absolute error estimation combined with groundwater solute transport simulation to identify the locations and magnitudes of aquifer pollutant sources. Pollutant sources were identified by matching simulated and measured non-reacting solute concentration data. They assumed known hydraulic parameters i.e. no uncertainty in the physical parameters of the aquifer but concentration data errors were considered explicitly. The identification models were demonstrated and compared using two hypothetical aquifer systems, one for the steady state case and the other for the transient case. The number of likely leak locations was restricted in the models by employing mixed integer programing and stepwise multiple regressions. By minimizing either least absolute or least squared errors they were successful in identifying pollutant sources. The limitation of the method was the assumption of no uncertainty in aquifer parameter and also the restriction to cases where data are available in the form of breakthrough curves. It also displayed spurious negative values.

Wagner (1992) proposed another optimization method for simultaneous model parameter estimation and source characterization, using inverse modeling that combines groundwater flow and contaminant transport simulation with non-linear maximum likelihood estimation, to determine optimal estimates of the unknown model parameters and source characteristics based on measurements of hydraulic head and contaminant concentration. In this method, a first-order uncertainty analysis provided a means for assessing the reliability of the maximum likelihood estimates and evaluating the accuracy and reliability of the flow and transport model predictions. Hydraulic conductivities, effective porosity, longitudinal and transverse dispersivities, boundary flux, and contaminant flux at the source are estimated for a two-

dimensional groundwater system. Characterization of the history of contaminant disposal or location of the contaminant source was demonstrated through hypothetical examples. One of the limitations of the method is the reduction in accuracy with increasing number of unknown parameters.

Bagtzoglou et.al. (1992) proposed a random walk based backward tracking model. It is the among the first to attempt solving the ADE backward in time without relying on optimization approaches. In their work, they modeled the reversed time transport equation using random walk particle methods, for which the advective part of the transport model is reversed while the dispersive part is left unchanged. They presented a probabilistic framework to identify solute sources in heterogeneous media. Repeated reversed time solute transport simulations with evaluation of the first two moments of the concentration probability density function (pdf) were conducted. Using geo-statistical techniques, they successfully assess the relative importance of each potential source. The proposed scheme provided probabilistic estimates of source locations and spill-time histories. The method assumed the spill incidents to be instantaneous and occurring simultaneously. Also the dispersion part was kept positive.

Wilson and Liu (1994) proposed a probabilistic approach to solve the transport problem with stochastic differential equations backward in time. They kept the dispersion part positive and reversed the advection part. They provided two types of maps, namely, travel time probability and location probability maps. The authors showed that both location and travel time probabilities could be calculated directly, using a backward-in time version of traditional continuum advection-dispersion modeling. The results for travel time probability are in very close agreement with the simulation results from traditional forward-in-time methods.

Snodgrass and Kitanidis (1997) also used a probabilistic approach combining Bayesian theory and geo-statistical techniques. The Bayesian framework is used to derive the best estimate and to quantify the estimation error. In their approach the source function to be estimated is discretized into components that are assigned a known stochastic structure with unknown stochastic parameters. The method incorporates uncertainty in contaminant concentration. The method produces a best estimate of the release history and a confidence interval. Conditional realizations of the release history are generated that can be useful in visualization and risk assessment. This method is an improvement to some other methods in that the solutions are more general and make no blind assumptions about the nature and structure of the unknown source function. This approach was used for cases for which the location of the potential source was known a priori.

Alapati and Kabala (2000) used a non-linear least-squares (NLS) method without regularization to recover the release history of a groundwater contaminant plume from its current measured spatial

distribution. They assumed the flow system to be one-dimensional, with the plume originating from a known single site. The solution was found to be very sensitive to noise and to the extent to which the plume is dissipated. Despite the extreme sensitivity to measurement errors for the gradual release scenario in using the NLS method, it could resolve the release histories for catastrophic release scenarios reasonably well, even in the presence of moderate measurement errors. The authors used a number of synthetic numerical examples for analysis. They suggested that for catastrophic contaminant releases the NLS method may be an alternative to the Tikhonov regularization approach.

Atmadja and Bagtzoglou (2001a) proposed a method called the marching-jury backward beam equation method to solve the ADE equation backwards in time for contaminant source identification. It is an enhancement of the Backward Beam Equation (BBE) method, first developed by (Carasso, 1972), to solve the Advection-Dispersion Equation (ADE) within the context of contaminant source identification. The authors have applied the BBE method for the first time to solve the ADE with heterogeneous parameters. By altering the method, to produce a hybrid between a marching and a jury method called the Marching-Jury Backward Beam Equation (MJBBE), they were able to make the problem practical to solve. Their method was capable of recovering the time history and spatial distribution of a groundwater contaminant plume from measurements of its current position. Using examples involving deterministic heterogeneous dispersion coefficients they showed that the method was robust enough to handle heterogeneous parameters. However the method was sensitive to noise.

Michalak and Kitanidis (2004) extended the geo-statistical approach to inverse modeling to allow for the recovery of the antecedent distribution of a contaminant at a given point back in time, which is critical to the assessment of historical exposure to contamination. These problems are typically strongly underdetermined, with a large number of points at which the distribution is to be estimated. To address this challenge, the authors have applied the adjoint state method to increase the computational efficiency. They have presented the adjoint problem in a format that allows for the reuse of existing groundwater flow and transport codes as modules in the inverse modeling algorithm. Through a few presented applications, they showed that geo-statistical approach combined with the adjoint state method allow for a historical multidimensional contaminant distribution to be recovered even in heterogeneous media, where a numerical solution is required for the forward problem.

Clayton (2005) used a hybrid of global and local search methods to estimate the location of contaminant sources. It is a case of multiple source identification. His method is a linked simulation-optimization technique to solve an inverse problem that uses downstream well data to estimate the source. It is an extension of the method he has developed to estimate the location of a contaminant source in a simplified

two-dimensional setup to the case when there are possibly multiple sources in the same area. In order to handle more than one source, he modified the groundwater transport model, expanded the optimization methods, and created different visualizations of the problem to better understand the solution. The author also compared different optimization methods to find which are best for a multi-source problem, examine the difference between the objective function errors versus the actual solution error, and explore the possibilities of a non-unique solution to the problem.

Milnes and Perrochet (2007) presented a theoretical framework that allows direct identification of a single point-source pollution location and time in heterogeneous multidimensional systems under known flow field conditions. Using the concept of the transfer function theory, they showed that an observed pollution plume contains all the necessary information to predict the concentration at the unknown pollution source when a reversed flow field transport simulation was performed. They obtained the target concentration from a quadratic integral of the observed pollution plume itself. Due to dispersion, backwards simulation of the pollution plume leads to shrinkage of the target concentration contour. In their method, when the target concentration contour reduces to a singular point or becomes a concentration maximum, the position of the pollution source was identified and the backward simulation time indicates the time elapsed since the contaminant release. The theoretical basis of the method was first developed for the ideal case that the pollution plume is entirely known and was illustrated using a synthetic heterogeneous 2D example where all the hydro-dispersive parameters are known. Using the same example, they illustrated the procedure for a more realistic case where only few observation points exist.

Huang et al., (2008) used a conjugate gradient method (CGM), based inverse algorithm determining the unknown space and time-dependent contaminant source for groundwater systems based on the measurements of the concentrations. They assumed that no prior information was available on the functional form of the unknown contaminant release function, classified as the function estimation in the inverse calculations. They examined the accuracy of this inverse mass transfer problem using the simulated exact and inexact concentration measurements in the numerical experiments.

Datta et.al., (2009) developed a method for simultaneous pollution source identification and parameter estimation in groundwater systems based non-linear optimization. The groundwater flow and transport simulator is linked to the nonlinear optimization model as an external module. The simulator defines the flow and transport processes, and serves as a binding equality constraint. The Jacobian matrix which determines the search direction in the nonlinear optimization model links the groundwater flow-transport simulator and the optimization method. Performance of the proposed methodology was evaluated by

solving illustrative problems and they demonstrated the potential applicability of the developed methodology for a fairly large aquifer study area with multiple unknown pollution sources.

Zi and Mao (2011) applied a radial basis collocation method (RBCM) based on the global space-time multi-quadric to solve the inverse problem of groundwater contaminant source identification. Their deterministic method directly induces the problem to a single-step solution of a system of over-determined linear algebraic equations in the entire space-time domain. To overcome the ill-posedness of the linear system, the authors used least-square-based radial basis collocation method. They also performed sensitivity analysis with respect to calculation parameters, observation data and model uncertainty to increase the confidence in the solutions. Through many application examples of contaminant source identification in one- and two-dimensional porous media, they demonstrated that the proposed method poses the mesh free advantage and direct identification of contaminant source with efficiency. The method showed good performance to resist the noisy measurement data and model uncertainty. However estimated release history was found to be very sensitive to the uncertainty of the Darcy velocity. They observed that the errors of the estimated release history were relatively large but the estimated spatial distributions match the true ones very well. They noted that this method provides a robust tool for estimating spatial plume distribution as well as the release history of groundwater contaminant source from concentration measurements.

Jha and Datta (2013) applied an adaptive simulated annealing based method for groundwater contamination source identification in a three-dimensional setting. The inverse problem of source identification problem was solved using a linked simulation-optimization approach. Optimization approaches are used to overcome the non-uniqueness and ill-posedness but such approaches can be computationally intensive and the results obtained tend to be highly susceptible to errors in the measured data and estimated hydrogeological parameters. To address these issues, the authors used an adaptive simulated annealing (ASA) based solution algorithm and found it to be computationally efficient for optimal identification of the source characteristics in terms of execution time and accuracy. The authors noted that the computational efficiency appears to prevail even with moderate levels of errors in estimated parameters and concentration measurement errors. It was also observed that the contaminant concentration monitoring locations are critical in the efficient characterization of the unknown contaminant sources. They presented optimal identification results for different monitoring networks to demonstrate the relevance of a network suitable for efficient source identification.

Gzyla et al., (2014) presents a new multi-step approach aiming at source identification and release history estimation. Their approach consists of three steps: performing integral pumping tests, identifying sources,

and recovering the release history by means of a geostatistical approach. A case study in Poland, situated in the vicinity of a former chemical plant, was studied in which several areal sources were identified. They found that some suspected contamination sources were found to have minor effect on the overall contamination while other suspected sources have been proven to have key significance. They showed the capability of the geostatistical approach to manage a complex real case study.

Zhang et al., (2015) proposed an efficient full Bayesian approach for the optimal design of sampling well location and source parameters identification of groundwater contaminants. The relative entropy is employed, as an information measure, to quantify the information gain from concentration measurements in identifying unknown parameters. The sampling locations that give the maximum expected relative entropy are selected as the optimal design. Then a Bayesian approach based on Markov Chain Monte Carlo (MCMC) is used to estimate unknown parameters. An interpolation method based on the adaptive sparse grid was utilized to reduce the computations by constructing a surrogate for the contaminant transport equation. Through a numerical study, they demonstrated the applicability of their approach.

2.5 Simulation-Optimization models for source identification

Contaminant source identification involves solving the advection-dispersion equation backward in time. One of the approaches to backtrack the pollution source location is to run the forward simulations and check the solutions with the measured spatial data of the contaminant. But owing to the non-uniqueness of the solution and the infinite number of plausible combinations, such a manual search will be almost impossible. Hence one needs to follow an optimization method to obtain the best fitted solution. This combination of simulation and optimization is one of the early source identification techniques. It does not directly solve the advection-dispersion equation backward in time. A brief review of the linked simulation-optimization models for source identification is given below.

Gorelick et al.,(1983) was among the first who studied the pollution source identification problem using optimization approaches. The groundwater pollution source identification problem was formulated as a forward time simulation with an optimization model. For optimization, they used least squares regression and linear programing for least absolute error estimation combined with groundwater solute transport simulation to identify the locations and magnitudes of aquifer pollutant sources. Pollutant sources were identified by matching simulated and measured non-reacting solute concentration data. The limitation of the method was the assumption of no uncertainty in aquifer parameter and also the restriction to cases where data are available in the form of breakthrough curves. It also displayed spurious negative values.

Wagner (1992) proposed another optimization method for simultaneous model parameter estimation and source characterization in which he modeled an inverse model as a non-linear maximum likelihood estimation problem.

Sidauruk et.al. (1998) proposed an inverse procedure based on correlation coefficient optimization to locate groundwater contaminant sources and to identify transport parameters. They used two case scenarios namely, plumes caused by instantaneous and continuous point sources in a two-dimensional uniform groundwater flow field. For these cases the inverse formulas were explicit. They manipulated these expressions to yield linear relations between the logarithm of concentration and certain combination of parameters. By minimizing the correlation coefficient of the linear regression, parameters such as time and space origin of the pollution, groundwater velocity, amount of mass released, dispersion coefficients etc. were determined by explicit formulas similar to linear regression equation. Their procedures allow not only for the delineation of the sampled contaminant plume, but also the tracing and the projection of the plume history. Use of explicit formulas eliminated the need for an initial guess and the subsequent iterations to determine the unknown parameters, avoiding the possibility of divergence or false convergence to local extrema. However the method requires the deployment of wells following a special pattern.

Mahar and Datta (2000) suggested a methodology using a nonlinear optimization model for estimating the unknown magnitude, location and duration of groundwater pollution sources under transient flow and transport conditions. The proposed optimization model incorporates the governing equations of flow and solute transport as binding equality constraints, and simulated the physical processes of transient flow and transient transport in the groundwater systems. Their method identifies unknown sources of pollution by using measured values of pollutant concentration at selected locations. Performance of the proposed model for the identification of unknown groundwater pollution sources was evaluated for an illustrative study area in a hypothetical confined aquifer under different cases of data availability. The effect of observation well location with respect to the pollution source location on identification accuracy was also investigated. Performance of the developed identification model was also evaluated for a condition when concentration measurements were missing during few initial time periods after the pollution sources become active. They also investigated the effect of specified initial guesses of the variable values on the optimal solutions.

Mahar and Datta (2001) proposed another optimization-based methodology for identifying unknown sources of groundwater pollution. This methodology utilizes an optimization model in which the flow and transport equations are embedded as constraints. A nonlinear programming algorithm was used to obtain

as solution the optimal estimates of unknown source characteristics. The input to this model includes measured pollutant concentration at observation sites. The source identification methodology was further extended to the simultaneous estimation of aquifer parameters as well as identification of unknown pollutant sources. Through illustrative examples considering two-dimensional flow and advective-dispersive solute transport, the performance of the developed methodology was evaluated. They examined different cases including variability in data availability, single and multiple potential source locations, and errors in measurement data. They found that the proposed methodology performs satisfactorily in identifying the locations, determining the magnitudes, and specifying duration of the unknown ground-water pollution sources, even when the aquifer parameters were unknown.

Singh and Datta (2004) proposed an artificial neural network (ANN) based method to simultaneously solve the problems of estimating unknown groundwater pollution sources and estimating unknown hydro-geologic parameters (hydraulic conductivity, porosity, and dispersivities). They achieved this by training an ANN to recognize the data patterns. The universal function approximation property of a multilayer, feed-forward ANN was utilized to estimate temporally and spatially varying unknown pollution sources, as well as to provide a reliable estimation of unknown flow and transport parameters. Back-propagation algorithm was used to train the ANN on patterns of simulated data. A set of source fluxes and temporally varying simulated concentration measurements constituted the pattern for training used by the authors. Through an illustrative example, they demonstrated the potential applicability of their method. Performance of the method was evaluated under varying concentration measurement errors. They concluded that the proposed methodology performs reasonably well even with large measurement errors.

Singh and Datta (2006) used a genetic algorithm (GA) based simulation optimization approach for optimal identification of unknown groundwater pollution sources. A flow and transport simulation model was externally linked to the GA-based optimization model to simulate the physical processes involved. In this study, simple as well as complex scenarios of multiple unknown groundwater pollution sources were considered. The simulation model uses potential pollution source characteristics that are evolved by the GA and simulates the resulting concentration measurement values at observation locations. These simulated spatial and temporal pollutant concentration measurement values were used to evaluate the fitness function value of the GA. The external linking of the numerical simulation model with the optimization model makes it feasible to solve the source-identification problems for complex aquifer study areas with multiple unknown pollution sources. Performance was evaluated for combinations of source characteristics (locations, magnitudes, and release periods), data availability conditions, and concentration measurement error levels.

Chadalavada et al., (2012) introduced a feedback-based methodology for identifying the unknown pollution sources in contaminated aquifers. The methodology consists of models within an iterative feedback system, with the capacity of feeding back real-time measurements of pollutant concentrations for the sequential optimal designs and characterization of the contaminated aquifer study area. The resulting linked-simulation optimization model considers the delineation of the contaminant plume, optimally characterizing the site in terms of pollutant sources and the optimal monitoring network leading to the remediation and/or management of the contaminated aquifer. The simulation-optimization code was developed by linking a groundwater flow and transport model with an optimization code for the purpose of identifying the unknown pollution sources. Their method addresses the source identification process with very limited information available regarding the observed contamination data for the identification of unknown pollution sources. They applied it to a chlorinated hydrocarbon contaminated site for the identification of unknown pollution sources. Information regarding the sources such as the magnitude, location and the duration of contamination activity were not known for the study area except the information regarding the likely activities that led to its contamination. Developed methodology was applied to choose the optimal source locations from the identified potential locations. They performed qualitative assessment of the results by utilizing the contamination information obtained during their field investigations.

Srivastavaa and Singh (2014) proposed an ANN based simulation-optimization approach for groundwater source identification by exploiting the capability of universal function approximation by a feed-forward multilayer artificial neural network (ANN) to identify the sources in terms of its location, magnitudes, and duration of activity. Back-propagation algorithm is utilized for training the ANN to identify the source characteristics based on simulated concentration data at specified observation locations in the aquifer. Uniform random generation and the Latin hypercube sampling method of random generation are used to generate temporal varying source fluxes. These source fluxes are used in groundwater flow and the transport simulation model to generate necessary data for the ANN model-building processes. Breakthrough curves obtained for the specified pollution scenario are characterized by different methods. The characterized breakthrough curves parameters serve as inputs to ANN model. Unknown pollution source characteristics are outputs for ANN model. The method was verified using hypothetical examples.

Gurarslan (2015) presented a model for solving problems of groundwater-pollution-source identification using differential evolution algorithm optimization model. The numerical simulations of flow and pollutant transport in groundwater were carried out using MODFLOW and MT3DMS. The performance of the developed model was tested on two hypothetical aquifer models using real and noisy observation

data. Two cases were considered. In one case, the locations of the potential sources are known and second when there is no information on the sources. The results were found be very accurate.

Leichombam and Bhattacharya (2016) proposed a simulation-optimization model where an ANN based surrogate model replaced the complex time-consuming numerical simulation model. They enhanced the model efficiency by developing separate ANN model for each of the observation locations. The number of ANN models is equal to the number of observation wells in the aquifer. A modified formulation was used to find out the optimal numbers of observation wells which will eventually reduce the computational time of the model. The performance of the ANN-based simulation-optimization model was evaluated by identifying the groundwater pollutant sources of a hypothetical study area.

2.6 Critical appraisal of literature review

From the literatures reviewed, it is seen that extensive work has been done towards groundwater flow and transport modeling in the last three decades, various techniques have been suggested and many codes have been written in this regard. Each of the techniques has their own advantages and disadvantages. Out of the available methods, FEM and Mesh free methods are suitable for very complex modeling domain with irregular features. A number of papers have been published and extensive research work was done towards application of mesh free techniques in the last two decades. Though a few issues are yet to be fully addressed, the use of mesh free methods has increased and its successful application in groundwater modeling has been reported along with the advantages it offers.

For invers modeling, there is a substantial increase in the use of optimization based on artificial intelligence based techniques such as ANN, genetic algorithm etc. over the conventional gradient based optimization techniques A number of papers have been published which explores different variations and improvements of these techniques.

A number of techniques or methods have been proposed for the identification of contaminant source in groundwater. At this stage, most of the methods have serious limitations and drawbacks. No general method has been found which can be used in all conditions. All the methods attempt to solve the Advection-Dispersion equation backward in time in order to identify the pollution sources. These methods have been broadly be classified into four major groups namely: optimization methods, analytical solution and regression approaches, direct methods, probabilistic and geo-statistical approach. In optimization methods, a forward simulation is run and the solution obtained is checked against the measured/current spatial data observed. An optimization method is then devised to obtain the best fitted solution to overcome the problem of non-uniqueness of the solution and the infinite number of plausible combinations. From the literature review, it is seen that recent trend towards source identification is the

use of simulation-optimization (SO) methods. In the present study, SO method will be utilized for source identification.

In the last two decades, artificial intelligence or soft computing techniques have increasingly been applied in SO models for source identification. They have also been successfully applied in many scientific and engineering problems which involve optimization. The main advantage of soft computing techniques like GA, PSO etc. is that they can search the global extrema unlike the conventional gradient based methods which can end up finding only the local extrema, depending on the initial guess or start point. A number of papers have been published which utilizes soft computing techniques for contaminant source identification and construction of release history. The present study proposes to employ soft computing techniques for source identification. In particular, particle swarm optimization will be used as it offers additional advantages such as fewer parameters to adjust, simplified structure and implementation.

In the present study, Mesh free method is proposed to be used for coupled flow and transport studies (forward simulation). This mesh free forward simulation model will be linked or coupled with the PSO optimization model. This coupled SO model will be used for the identification of contamination sources by fitting the model predicted concentration to the measured spatial concentration data. The developed model will be tested with hypothetical problems and field case study.

2.7 Closure

Groundwater pollution is a serious problem in many parts of the world. Based on the literature review, it is observed that numerical models are very effective tools for groundwater flow and contaminant transport modeling. Out of the available numerical methods, meshfree methods are found to be efficient to deal with flow and transport problems with complex domain and boundary conditions. A number of research papers dealing with the flow and solute transport model have been published. Meshfree methods are becoming popular in recent days and a lot of research have been conducted to address different issues with these methods and to extend their applications to several areas. For groundwater source identification, a number of different approaches have been proposed and a lot research material has been published in the last three decades. Simulation-optimization approaches have attracted a lot of attention from researchers with various combinations of simulation and optimization models. Artificial intelligence based optimization approaches are gaining popularity as they are global optimizers and less prone to local minima trapping as compared to conventional gradient based approaches.

In the present study, the meshfree RPCM method is proposed as a numerical tool for coupled groundwater flow and transport problems. The meshfree RPCM model based simulation model will be coupled with the PSO optimization model. The coupled SO model is proposed for groundwater source

identification problem. The developed models will be tested initially on hypothetical problems and then it will be applied to field case studies. Robustness of the model will be examined in different field situations.

Chapter 3
Theoretical development - groundwater flow and transport modeling and source identification

3.1 Introduction

Since groundwater moves at a very slow rate in aquifers, groundwater contamination and its source is normally detected much later (Freeze and Cherry, 1979). As a result, before a bore well shows deterioration in its water quality, it is likely that groundwater may have moved several kilometers from the source and a large aquifer area is already contaminated. A large number of surveillance bore wells will be required to properly track the movement of contaminants if the aquifer area involved is very large. It will be prohibitively costly to drill such a large network of bore wells. As is well known, remediation of contaminated groundwater is also a very costly affair. Therefore numerical modeling of groundwater flow and contamination plays a very important in the prediction of the movement of contaminants in an aquifer and also to optimize the remediation efforts.

Significant progress has been there in groundwater flow and contaminant transport modeling over the years. Many techniques have evolved and been applied in groundwater modeling such as finite difference, finite element, particle tracking methods, method of characteristics, modified method of characteristics, random transport models etc. Recently mesh free methods has also been applied to groundwater modeling. This section deals with the theoretical developments and application of mesh free methods to simulate groundwater flow and transport problems.

3.2 Sources of groundwater contamination

Groundwater can become contaminated in many ways. If rain water or surface water comes into contact with contaminated soil while seeping into the ground, it can become polluted and can carry the pollution from the soil to the groundwater. Groundwater can also become contaminated when liquid hazardous substances themselves soak down through the soil or rock into the groundwater. Some liquid hazardous substances do not mix with the groundwater but remain pooled within the soil or bedrock (Bear, 1979). These pooled substances can act as long-term sources of groundwater contamination as the groundwater flows through the soil or rock and comes into contact with them.

Aquifers are normally contaminated by agricultural activities, industrial waste and municipal sewage waste disposal practices. The major sources of groundwater pollution are Underground Storage Tanks (USTs), landfills, septic systems and hazardous waste sites (Freeze and Cherry, 1979). Other sources

include pesticides leaks or spills of industrial chemicals at manufacturing facilities, runoff of salt and other chemicals from roads and highways and fertilizer on agricultural land. Most of water contamination cases generally occur in highly developed areas, agricultural areas, and industrial zones

Groundwater contaminants exist in many forms, and contaminant classification schemes can be based on any of several physicochemical characteristics. For example, contaminants may be classified based on their preference for association with the aqueous phase or with particles (Bear, 1979). Contaminant distinction based on phase preference is important as the phase(s) a contaminant associates with can affect its transport behavior and toxicology. Furthermore, the form taken by a contaminant can also affect the choice of treatment processes that may be implemented to remediate a contaminated area. In general, the physicochemical characteristics of groundwater contaminants and the surrounding aquifer will play critical roles in determining their fate, transport, and effects.

3.3 Mechanisms of Contaminant movement

The principal mechanisms of contaminant transport are advection, diffusion, dispersion, sorption, and decay (Bear, 1979). These processes are briefly discussed in this section in their simplest 1D form. Other processes such as hydrolysis, volatilization, and biotransformation may also play an important role depending on the type and nature of the contaminant and also the soil (Zheng and Bennet, 2002).

3.3.1 Advection

The process by which solutes are transported by the bulk motion of the flowing groundwater is known as advection (Freeze and Cherry, 1979). Owing to advection, non-reactive solutes are carried at an average rate equal to the average linear velocity, $\bar{v}$, of the water. Here

$$\bar{v} = \frac{v}{n} = \frac{1}{n}\left(-K\nabla h\right) \tag{3.1}$$

Here, v is the specific discharge or Darcy flux and n is the porosity. The advection process is also sometimes called convection. An estimation of the flow velocity is needed for an accurate estimation of the advective transport. In sand/gravel aquifers with significant groundwater, the plume movement is dominated by advection. Applying the conservation of mass principle to a control volume, it can be derived that the one dimensional advective transport equation in a homogeneous aquifer (Zheng and Bennet, 2002) as,

$$\frac{\partial C}{\partial t} = -v\frac{\partial C}{\partial x} \tag{3.2}$$

Here C is the concentration of the solute. The main factors that control the advective transport are hydraulic conductivity or transmissivity, effective porosity of the porous material and the hydraulic gradient.

3.3.2 Diffusion

Diffusion is the flux of solute from a zone of higher concentration to one of lower concentration due to the Brownian motion of ionic and molecular species. Under steady-state condition, the diffusion flux F is described by Fick's first law (Bear, 1979),

$$F = -D\vec{\nabla}C \tag{3.3}$$

where D is the diffusion coefficient [L^2 T^{-1}]. For diffusion in porous media, Freeze and Cherry (1979) suggest taking an effective diffusion coefficient, $D^* = \omega D$ to account for the tortuosity of the flow paths with ω ranging from 0.5 to 0.01 for laboratory studies of non-adsorbed ions in porous geological materials. The change of concentration over time inside a control volume subject to diffusion flux is given by Fick's second law,

$$\frac{\partial C}{\partial t} = D^* \frac{\partial^2 C}{\partial x^2} \tag{3.4}$$

The importance of diffusion increases as flow velocities decrease. Thus diffusion may be the governing transport mechanism in unfractured clays with low hydraulic conductivities. Diffusion can generally be neglected in gravel aquifers with high flow velocities. It can also be significant in fractured porous aquifers.

3.3.3 Dispersion

Dispersion is the spreading of the plume that occurs along and across the main flow direction due to aquifer heterogeneities at both the small scale (pore scale) and at the macroscale (regional scale). Dispersion tends to increase the plume uniformity as it travels downstream. Factors that contribute to dispersion include faster flow at the center of the pores than at the edges, some pathways being longer than others, flow velocity larger in smaller pores than in larger ones. This is known as mechanical dispersion. The spreading due to both mechanical dispersion and molecular diffusion is known as hydrodynamic dispersion (Freeze and Cherry, 1979).

Dispersion equation in general is derived using Fick's law, whereas, results from theoretical studies suggest that dispersion is non-Fickian near the source of contaminant and it generally becomes Fickian at larger times or travel distances where a constant dispersivity value is achieved (Anderson, 1984). A

phenomenological coefficient that combines the effects of diffusion and dispersion, known as *dispersion coefficient* is generally defined. As mechanical dispersion is more pronounced in the longitudinal direction than in the transverse direction, a *longitudinal dispersion coefficient* D_L and a *transverse dispersion coefficient* D_T are introduced. These coefficients are defined as,

$$D_L = \alpha_L v + D^* \\ D_T = \alpha_T v + D^* \tag{3.5}$$

where α_L is the longitudinal dispersivity [L], α_T is the transverse dispersivity [L], and v is the pore velocity [LT^{-1}].

3.3.4 Retardation and Reactions

Sorption refers to the exchange of molecules and ions between the solid phase and the liquid phase. It includes adsorption and desorption. Adsorption is the attachment of molecules and ions from the solute to the rock material. Adsorption produces a decrease of the concentration of the solute or, equivalently, causes a *retardation* of the contaminant transport compared with water movement. Desorption is the release of molecules and ions from the solid phase to the solute (Zheng and Bennet, 2002).

The relationship between the solute concentration in the adsorbed phase and in the water phase is called a sorption isotherm. The simplest expression is the linear isotherm, called Henry's equilibrium model,

$$C_a = K_d C \tag{3.6}$$

where C_a is the sorbed concentration as mass of contaminant per mass of dry rock matrix dimensionless, C is the dissolved concentration in mass of contaminant per volume of water [ML^{-3}], and K_d is the distribution coefficient [$L^3\ M^{-1}$]. This expression implies that there is equilibrium between the adsorbed concentration and the dissolved concentration. This can be assumed when the adsorption process is fast compared with advection of contaminant. Apart from the Henry's model, many adsorption models are also used (Rastogi, 2007).

The adsorption causes retardation in the migration of contaminants compared with advection. The contaminant transport gets more retarded as the fraction adsorbed increases. This effect can be described by a retardation factor R_a , which for a linear isotherm, is

$$R_a = 1 + \frac{(1-n)\rho_s}{n} K_d \tag{3.7}$$

where n is the porosity and ρ_s is the density of the solids. The retardation coefficient may take values from 1 to 10,000. The velocity of the solute front v_c (where the concentration is half that of the original concentration) is given by

$$v_c = \frac{v}{R_a} \tag{3.8}$$

If sorption is taken into account, the 1D advection–dispersion equation then becomes,

$$\frac{\partial C}{\partial t} = -\frac{v}{R_a}\frac{\partial C}{\partial x} + \frac{D_L}{R_a}\frac{\partial^2 C}{\partial x^2} \tag{3.9}$$

where the term on the left side represents the time rate of change in storage of contaminant in the control volume, the first term on the right-hand side represents the retarded advective inflow–outflow, and the last term represents the retarded diffusion and dispersion.

When there is chemical reaction (degradation) whereby the solute changes its form or if the solute undergoes radioactive decay, it decreases the concentration of the solute. The simplest model for decay of contaminants without transport is first order model,

$$\frac{\partial C}{\partial t} = -\lambda C \tag{3.10}$$

where λ is the first order decay rate constant [T^{-1}]. This relation also applies to radioactive decay and degradation processes. Integration of equation (3.10) gives $C = C_0 e^{-\lambda t}$ where C_0 is the concentration at time $t = 0$ and

$$\lambda = \frac{\ln 2}{T_{1/2}} \tag{3.11}$$

$T_{1/2}$ is the half-life of the radioactive isotope or of the degraded contaminant. The degradation causes a mass λC to disappear per unit volume per unit of time. The transport equation including decay is then obtained by simply appending the quantity $-\lambda C$ to the right-hand side of equation (3.9).

3.4 Governing equations and Boundary conditions

3.4.1 Groundwater Flow

The governing equation describing the groundwater flow in a two dimensional inhomogeneous confined aquifer is given as (Bear, 1979)

$$\frac{\partial}{\partial x}\left[T_x \frac{\partial h}{\partial x}\right] + \frac{\partial}{\partial y}\left[T_y \frac{\partial h}{\partial y}\right] = S\frac{\partial h}{\partial t} + Q_w \delta(x - x_i)(y - y_i) - q \tag{3.12}$$

Following initial conditions are used for transient analysis,

$$h(x, y, 0) = h_0(x, y) \qquad x, y \in \Omega \tag{3.13}$$

Generally, the boundary conditions can be of two types, the prescribed head or flux. It can be written as:

$$h(x, y, t) = h_1(x, y, t) \qquad x, y \in \partial\Omega_1 \tag{3.14}$$

$$T\frac{\partial h}{\partial n} = q_1(x, y, t) \qquad x, y \in \partial\Omega_2 \tag{3.15}$$

For an unconfined aquifer, the governing equation is given as (Bear, 1979) ,

$$\frac{\partial}{\partial x}\left[K_x h \frac{\partial h}{\partial x}\right] + \frac{\partial}{\partial y}\left[K_y h \frac{\partial h}{\partial y}\right] = S_y\frac{\partial h}{\partial t} + Q_w \delta(x - x_i)(y - y_i) - q \tag{3.16}$$

For unconfined aquifer problems, the boundary conditions are:

$$h(x, y, t) = h_1(x, y, t) \qquad x, y \in \partial\Omega_1 \tag{3.17}$$

$$Kh\frac{\partial h}{\partial n} = q_2(x, y, t) \qquad x, y \in \partial\Omega_2 \tag{3.18}$$

where , $h(x, y, t)$ is the Piezometric head (m) which is the state variable, K_x, K_y are the hydraulic conductivities in *x* and *y* directions, T_x, T_y are the transimissivities (m^2/d) in *x* and *y* directions, S is the storage coefficient, Sy is the specific yield, Q_w is the source or sink term (m^3/d/m2). The flow region is represented by Ω while the boundary is denoted by ∂Ω. $\frac{\partial}{\partial n}$ denotes the normal derivative to the boundary. $h_0(x, y)$ is the initial head in the flow domain (m), $h_1(x, y, t)$ is the known head value of the boundary head (m) and $q(x, y, t)$ is the known inflow rate (m^3/d/m).

3.4.2 Groundwater Solute Transport

The governing equation for contaminant transport of a single chemical constituent in groundwater is given by (Freeze and Cherry, 1979; Wang and Anderson, 1982; Desai et al., 2011 etc.)

$$R\frac{\partial C}{\partial t} = \frac{\partial}{\partial x}\left(D_{xx}\frac{\partial C}{\partial x}\right) + \frac{\partial}{\partial y}\left(D_{yy}\frac{\partial C}{\partial y}\right) - \frac{\partial}{\partial x}(V_x C) - \frac{\partial}{\partial y}(V_y C) - \frac{c'w}{nb} - R\lambda C + \frac{q_w C}{n} \tag{3.19}$$

where,

V_x , V_y ≡ Seepage velocity in x and y direction [LT^{-1}]

D_{xx} , D_{yy} ≡ components of dispersion coefficient tensor in x and y direction [L^2T]

C is the concentration of the dissolved species [ML^{-3}]; λ is the reaction rate constant [T^{-1}];
w =elemental recharge rate with solute concentration c'; n = porosity; b = aquifer thickness;
R = Retardation factor = $1 + \rho_b K_d/n$, in which ρ_b is the media bulk density, K_d is the sorption coefficient and q_w = volumetric pumping rate from a source.

The initial condition is,

$$C(x, y, 0) = f(x, y, 0) \qquad (x, y) \equiv \Omega \tag{3.20}$$

And the boundary conditions are of the form,

Dirichlet boundary condition: $$C(x, y, t) = g_1(x, y, t) \quad (x, y) \equiv \partial\Omega_1; \tag{3.21}$$

Neumann boundary condition: $$\left(D_{xx}\frac{\partial C}{\partial x}\right)n_x + \left(D_{yy}\frac{\partial C}{\partial y}\right)n_y = g_2(x, y, t) \in \partial\Omega_2 \tag{3.22}$$

Where Ω is the flow domain, Ω = boundary region ($\partial\Omega_1 \cup \partial\Omega_2 = \partial\Omega$; f is a given function in Ω; g_1, g_2 are functions along boundaries; and n_x, n_y are the components of the unit outer normal vector to the given boundary.

The seepage velocities V_x, V_y are evaluated from the flow equations by the following relations,

$$V_x = -\frac{K_x}{n}\frac{\partial h}{\partial x} \; ; \; V_y = -\frac{K_y}{n}\frac{\partial h}{\partial y} \tag{3.23}$$

where n is the porosity of the medium. The elements of the dispersion coefficient tensor are evaluated from the longitudinal dispersivity (α_L) and transverse dispersivity (α_T) from the relations (Bear, 1979):

$$D_{xx} = \frac{\alpha_L V_x^2 + \alpha_T V_y^2}{V^2} \; ; D_{yy} = \frac{\alpha_L V_y^2 + \alpha_T V_x^2}{V^2} \; ; D_{xy} = D_{yx} = \frac{(\alpha_L - \alpha_T)V_x V_y}{V^2} \tag{3.24}$$

where, $V^2 = V_x^2 + V_y^2$. Equations (3.23) and (3.24) together provide the linkage or coupling between the groundwater flow and transport equations. The velocities computed from the flow equation are used as input to the transport equation.

3.5 Groundwater flow and transport modeling - numerical methods

Every groundwater model design consists of the following steps (Anderson and Woessner, 2002):

1. Establish the purpose of the model. It will determine the governing equations and code to be selected
2. Develop a conceptual model of the system

3. Select the mathematical model (governing equation and computer code)
4. Model design
5. Calibration
6. Calibration sensitivity analysis
7. Model verification
8. Prediction
9. Presentation of results
10. Post audit

Figure 3.1 shows a flow chart of the groundwater modeling process (Anderson and Woessner, 2002).

The laws which govern the groundwater flow and solute transport are usually expressed in terms of partial differential equations (PDEs). For the vast majority of geometries and problems, these PDEs cannot be solved with analytical methods. Instead, an approximation of the equations can be constructed, based upon different types of discretization. These discretization methods approximate the governing PDEs with numerical model equations, which can be solved using numerical methods. The solution to the numerical model equations are, in turn, an approximation of the real solution to the PDEs. There are various discretization schemes for solving PDEs. The most widely used methods are the finite difference method (FDM) and finite element method (FEM). Both methods require the construction of a grid or mesh of the solution domain which can be computationally very costly. Meshfree method which does not require the construction of a mesh is gaining popularity in recent days. Brief descriptions of these methods are provided in this section.

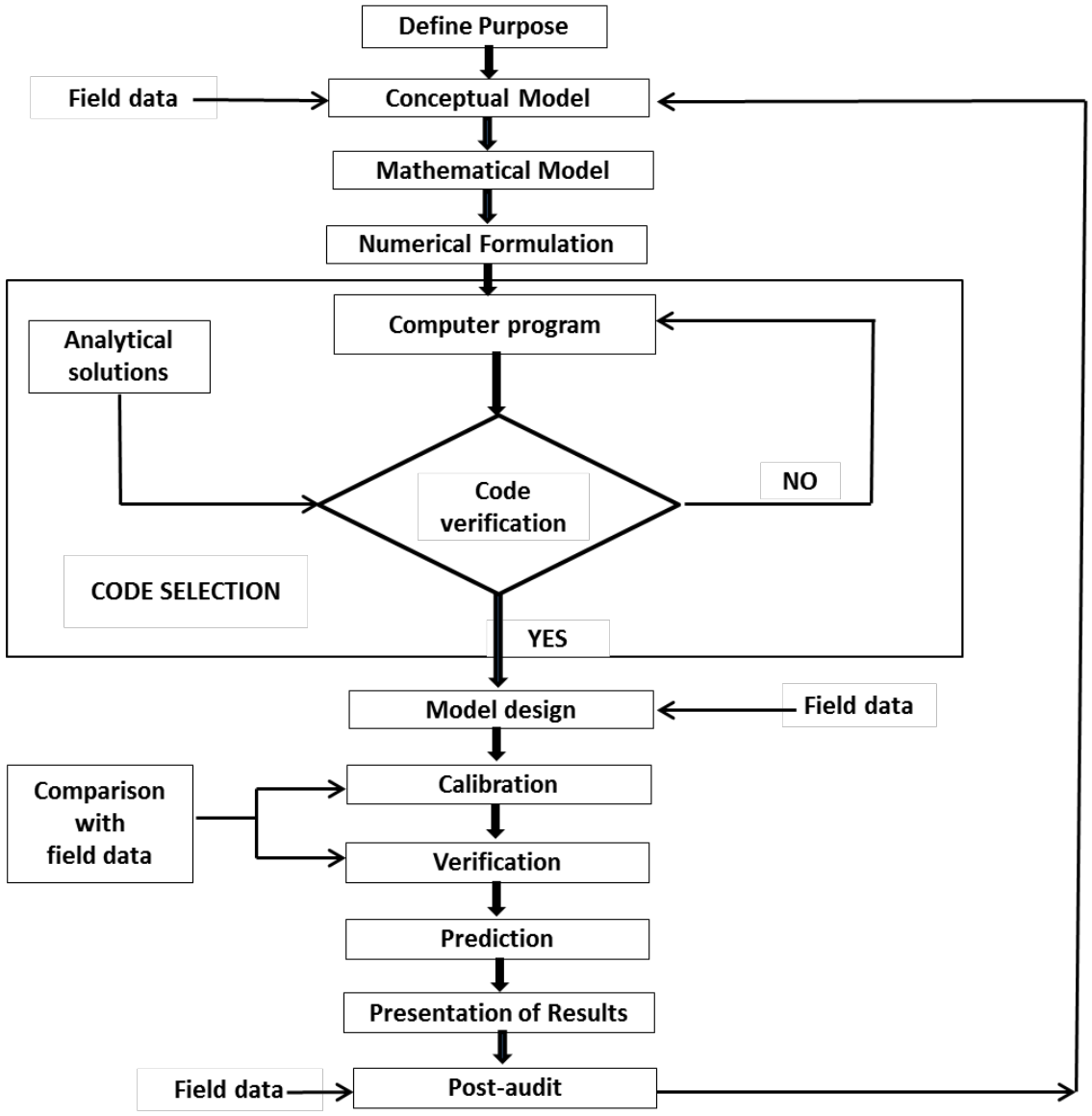

Figure 3.1: Steps in Groundwater modeling

3.5.1 Finite Difference Method

Finite difference methods (FDM) are numerical methods for solving differential equations by approximating them with difference equations, in which the derivatives are approximated by finite differences. The difference approximations of the derivatives of a function $f(x)$ can be obtained from a Taylor series expansion (Wang and Anderson, 1982):

$$f(x_0 + \Delta x) = f(x_0) + \frac{f'(x_0)}{1!}\Delta x + \frac{f''(x_0)}{2!}\Delta x^2 + \cdots + \frac{f^n(x_0)}{n!}\Delta x^n + R_n(x) \qquad (3.25)$$

The first derivative of the function can be obtained by truncating the series as,

$$f(x_0 + \Delta x) = f(x_0) + f'(x_0)\Delta x + O(\Delta x^2)$$

$$or, \qquad f'(x_0) = \frac{f(x_0 + \Delta x) - f(x_0)}{\Delta x} + O(\Delta x) \tag{3.26}$$

This is known as the forward difference approximation of the first derivative. The backward difference approximation can be obtained by using Taylor series expansion for $f(x_0 - \Delta x)$. Centered difference approximations can be obtained by combining the Taylor series expansions of $f(x_0 + \Delta x)$ and $f(x_0 - \Delta x)$. The centered difference approximation for the second derivative is obtained as (Wang and Anderson, 1982),

$$f''(x_0) = \frac{f(x_0 + \Delta x) - 2f(x_0) + f(x_0 - \Delta x)}{\Delta x^2} + O(\Delta x^2) \tag{3.27}$$

To use finite difference method, the domain over which the differential equation is to be solved for is divided into a grid of discrete points (nodes). The differential equation is then written (discretized) on each node using the finite difference approximations of the derivatives i.e. FDM is a point wise approximation of the differential equation on each node. Appropriate boundary conditions are applied at the domain boundaries. The resulting system of equations is then solved using a numerical technique such as Gauss elimination or iterative method to get the nodal solutions.

Finite difference methods are one of the most popular methods for solving partial differential equations due to its simplicity. The MODFLOW codes (Harbaugh and McDonald, 1996) used for groundwater flow modeling and MT3DMS (Zheng and Wang, 1998) for solute transport modeling are both FDM codes. However, FDM has its own limitations. Its main drawback is that it cannot properly represent complex domains accurately and efficiently. It also has difficulty in implementing dissimilar or variable material properties.

3.5.2 Finite Element method

In contrast to the FDM, the finite element method (FEM) divides the solution domain into simply shaped regions or elements (Desai et al., 2011). An approximate solution is then developed for each of these elements. The total solution is then generated by coupling together (assembling) the individual solutions over each element taking care to ensure continuity at the inter-element boundaries. FEM thus uses continuous, piecewise smooth functions to approximate the unknown quantity. FEM is characterized by the following three basic features (Desai et al., 2011),

1. The domain of the problem is represented by a collection of simple sub-domains, called finite elements. The collection of finite elements is called the finite element mesh
2. Over each finite element, the physical process is approximated by functions of desired type (polynomials or otherwise), and algebraic equations relating physical quantities at selective points, called nodes, of the elements are developed
3. The element equations are assembled using continuity and /or "balance" of physical quantities

The use of elements, rather than a rectangular grid, allows a much accurate representation of complex and irregularly shaped domains. Further, the values of the unknown variable can be generated continuously across the entire domain rather than at isolated grid points.

The main steps involved in a FEM solution of a PDE are (Desai et al., 2011; Segerlind, 1984):

1. Discretization of the domain into finite elements
2. Development of element equations: develop element equations to approximate the solution for each element. This consists of two steps:
   (i) Choose an appropriate function (called trial function) to approximate the solution. The trial function has parameters which have to be determined so that it satisfies the differential eqn. as closely as possible. Usually the approximation function is a linear combination of basis functions:

$$u(\boldsymbol{x}) = \sum_{i=0}^{n} \phi_i(\boldsymbol{x}) u_i \tag{3.28}$$

   where $\phi_i(\boldsymbol{x})$'s are known as basis functions or shape functions and u_i are the nodal values of the unknown function $u(\boldsymbol{x})$

   (ii) Since it is not an exact solution, substitution of the trial function into the differential equation will produce an error (called residual), $R(\boldsymbol{x})$. The coefficients of the trial functions are evaluated such that it approximates the solution in an optimal way i.e. the residual (or error) is made as small as possible (minimized) or forced to be zero. The residual is usually multiplied with a weight function, $w_i(\boldsymbol{x})$ before minimization i.e.

$$min \int_{\Omega} w_i(x) R(x) dx \tag{3.29}$$

3. Assembly of element equations taking care of continuity and/or balance of physical quantities

4. Application of boundary conditions
5. Solving the system of equations
6. Post-processing of the solution

It may be noted that finite element method approximates a solution by minimizing the associated error function (residual). The minimizing process automatically finds the linear combination of basis functions which is closest to the solution (Zienkiewicz and Taylor, 2000).

In FDM the differential operators are approximated from Taylor's series expansions while in FEM the unknown variable itself is approximated with a shape function of one's choice. This provides enormous flexibility with FEM in approximating the unknown function. The shape of the elements can also be chosen by the modeler according to the requirements of the problem domain. These flexibilities, together with the ability to represent any complex geometry makes FEM one of the most widely used approach for solving PDEs. Several commercial softwares based on FEM are available for performing simulations in various areas of engineering and scientific endeavors (Pepper and Heinrich, 1992).

However, creating a grid or mesh for FEM can be computationally very costly. Consequently FEM is not suitable for those applications which require frequent meshing such as adaptive analysis, simulation of large deformation, crack propagation, breakage of materials etc.

3.5.3 Meshfree Methods

Meshfree methods provide an alternative to the mesh based methods and seeks to address the inherent shortcomings of numerical methods that rely on meshes. A truly meshfree method requires only a set of scattered nodes within and on the boundary to represent the modeling domain and no information is required on the connectivity of the nodes throughout the process of solving the problem (Liu and Gu, 2005). However, for most of the methods classified as meshfree methods, the connectivity of the nodes is determined at the run time. In conventional numerical methods (FDM, FEM etc.), the definition of the connectivity of the nodes needs to be determined *a priori.*

The minimum requirement for a meshless method is that a predefined mesh is not necessary at least in field variable interpolation. Unlike FEM where shape functions are determined for each element, meshless methods compute the shape functions using a support domain. A support domain of a point is a collection of nodes used to approximate the function value at that point (Liu and Gu, 2005). The equations of a mesh free method can be formulated using the shape functions and a strong or weak form system equation. The procedures of forming system equations are slightly different for different meshfree methods. Several variants of meshfree methods have been proposed in the last three decades. These methods have been discussed in Liu and Gu (2005), Nguyen et al. (2008), Belytschko et al.(1996) etc.

3.5.4 Comparison of FEM and Meshfree model

The solution procedures of FEM and meshfree methods are as shown in the Figure 3.2 (Liu and Gu, 2005). Both the methods follow similar procedures. The differences are at the 2nd and 3rd stages viz., mesh generation and shape function construction. FEM requires a mesh but meshfree methods require only the nodal coordinates.

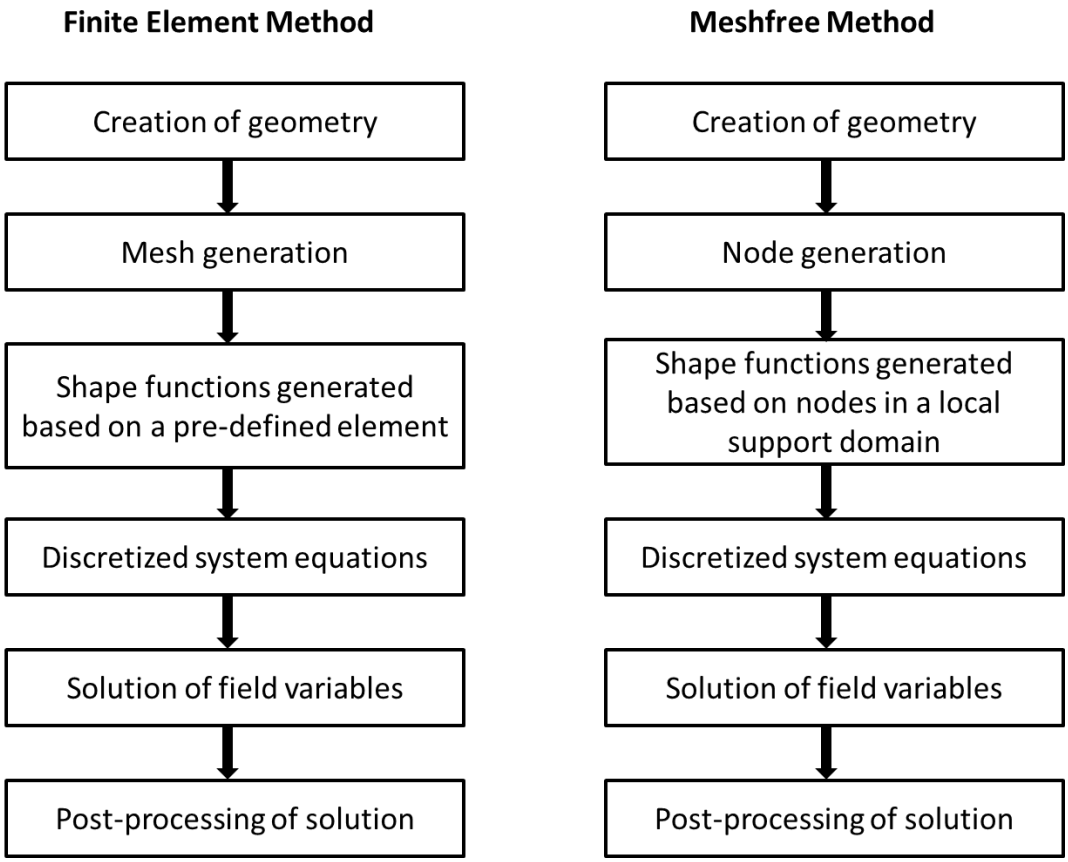

Figure 3.2: Comparision of solution procedures of FEM and Meshfree methods

The construction of the shape functions in these two methods is also quite different. In the finite element method, the shape functions are constructed using predefined elements, and the shape functions are the same for the entire element. But in MFree methods, the shape functions constructed are usually only for a particular point of interest based on selected local nodes located within a small region called the support domain of the point of interest (Liu and Gu, 2005). As such the shape functions can change when the point of interest changes. Once the global discretized system equation is established, the two methods follow the same procedure. The main differences between FEM and meshfree methods are listed below (Liu and Gu, 2005):

1. FEM requires the creation of a mesh while meshfree methods requires only the generation of nodes.
2. Shape function creation in FEM is based on pre-defined elements while in meshfree methods it is based on a local support domain
3. Imposition of essential boundary condition is easy in FEM but the same will require special treatments in meshfree methods
4. Computational speeds are in general slower in meshfree methods as compared to FEM
5. Meshfree methods, in general, yields more accurate solutions as compared to FEM
6. Due to the requirement of a mesh, carrying out adaptive analysis with FEM is difficult especially in 3D. The same can be done much easier in meshfree methods
7. It may be mentioned that FEM is a well-developed method whereas meshfree methods are in developmental stages with many issues yet to be addressed. Consequently while there are several commercial software packages for FEM, only a few codes are available for meshfree methods.

Since the solution procedure is the same for FEM and meshfree methods after the global discretized system is obtained, many of the techniques developed for FEM can be applied to meshfree methods also.

3.6 Groundwater source identification

Contaminant transport in groundwater is governed by advection-dispersion equation (ADE). Contaminant source identification involves solving the advection-dispersion equation backward in time .The problem of contaminant source identification is illustrated with a one dimensional case here. For a non-reactive contaminant, the one-dimensional (1-D) heterogeneous transport in a semi-infinite domain, described by the ADE is (Atmadja and Bagtzoglou, 2001b):

$$\frac{\partial C}{\partial t} = \frac{\partial}{\partial x}\left[D(x)\frac{\partial C}{\partial x}\right] - \frac{\partial}{\partial x}\left[u(x)C\right] \tag{3.30}$$

with initial and boundary conditions :

$$C(x_1, t) = C_{in}(t) \qquad 0 \le t \le T_{obs} \tag{3.31}$$

$$C(\infty, t) = 0 \qquad 0 \le t \le T_{obs} \tag{3.32}$$

$$C(x, T_{obs}) = C_T(x) \qquad 0 \le x \le \infty \tag{3.33}$$

where *u(x)* is the transport velocity in the x-direction and x is distance. In the pollution source location identification, the source (x_1) information is not known, but measurements of the spatial distribution of the plume are given at time, T_{obs}. For the release history reconstruction, usually the source location is assumed to be known, but the contaminant source function,$C_{in}(t)$ is unknown. Finding the source

location and the time history of the solute in groundwater can be categorized as a problem of time inversion. This means solving the governing equations backward in time. Modeling contaminant transport using reverse time is an ill-posed problem since the process, being dispersive is irreversible. Because of this, the solutions have discontinuous dependence on data and are sensitive to errors in the data.

A problem is categorized as a well-posed problem if (1) the solution exists; (2) the solution is unique; and (3) the solution is stable (Ortega and Rheinboldt, 1970). Problems that do not satisfy these criteria are called ill- posed. For the groundwater contamination problem, the plume has to have originated from someplace, therefore, physically, the plume exists. However, in rigorous mathematical terms, the fact that there exists a present day plume concentration does not necessarily mean that we satisfy the existence criterion. The solution exists only when we have perfect and consistent model and data that satisfy extremely restrictive conditions. Satisfying the stability criterion is a difficult task to accomplish since numerical schemes, which are usually implemented as a marching procedure are unstable for negative time steps, and make it impossible to solve contaminant transport problems backward in time.

Regarding the non-uniqueness of the solution, there is no method that can bypass this inherent problem. In inverse problems, one of the common practices to overcome the stability and non-uniqueness criteria is to make assumptions about the nature of the unknown function so that the finite amount of data in observations is sufficient to determine that function (Ala and Domenico, 1992). This can be achieved by converting the ill-posed problem to a properly posed one by stabilization or regularization methods. In the case of groundwater pollution source identification, additional information such as potential release sites and chemical fingerprints of the plume are usually available to make this possible.

3.6.1 Source identification Methods

A number of source identification techniques have been proposed. An overview of the developed methodologies can be found in Atmadja and Bagtzoglou (2001b), Michalak and Kitanidis (2004) and Sun et al. (2006). These methods may broadly be subdivided into four major groups (Atmadja and Bagtzoglou, 2001b) namely: optimization methods, analytical solution and regression approaches, direct methods, probabilistic and geo-statistical approach. Each of the methods is subject to significant drawbacks and limitations. A broad classification of the proposed methods is discussed below.

3.6.1.1 Direct inversion of advection-diffusion equation

This class of approaches uses deterministic direct methods to solve the governing equations backward in time to reconstruct the release history of the contaminant plumes. The inversion is achieved by using appropriate integral equations or other transformations to represent the contaminant transport. Methods falling into this class of approaches are the Tikhonov regularization approach (Skaggs and Kabala, 1994),

method of quasi-reversibility (Skaggs and Kabala, 1995), the minimum relative entropy (MRE) inversion method (Woodbury et al.,1998), Fourier series based inversion technique (Birchwood, 1999), the marching-jury backward beam equation (MJBBE) method (Atmadja and Bagtzoglou, 2001a) etc. These methods have been applied to reconstruct the spatial and temporal plume release history in homogeneous and heterogeneous media. However, such methods are very sensitive to noise or errors in the concentration data and in some cases can only recover the plume history partially.

3.6.1.2 Analytical solution and regression

Analytical methods are an inverse method based on analytical solution of the contaminant transport problems and parameter estimation using linear or non-linear regression. Sidauruk et al., (1998) presented an inverse method based on the analytical solution that provides a complete estimate of the dispersion coefficients, flow velocity, amount of pollutant, its initial location and time of origin. Ala and Domenico (1992) developed an inverse analytical technique that can determine the source strength, the advective position of the contaminant front for the instantaneous contaminant plumes at air force base. Other analytical solutions methods were proposed by Butcher and Gauthier (1994), Alapati and Kabala (2000) etc. The analytical solution and regression techniques have been applied only to very simple geometries and flow conditions. They are also very sensitive to noise in the input data. Consequently their utility is very limited.

3.6.1.3 Probabilistic and geo-statistical method

Probabilistic and geo-statistical approaches employ probabilistic techniques such as geo-statistics to deduce the probability of the location of the sources. These techniques are among the first which attempts to solve the ADE backward in time without relying on optimization approaches. Methods belonging to this class are the random walk particle method (Bagtzoglou et al., 1992), backward in time solution of stochastic differential equations (Wilson and Liu, 1994), adjoint method (Neupauer and Wilson, 1999), probabilistic approach combining Bayesian theory and geo-statistical techniques (Snodgrass and Kitanidis, 1997) etc. The probabilistic and geo-statistical techniques have been used to assess the relative importance of each potential source and produce the maps of time and location probability. These techniques have limitations in application to complex geometries. Some of the methods require that potential sources be known a priori and that the release incidents are assumed to be instantaneous and occurring simultaneously.

3.6.1.4 Simulation-Optimization (SO) approach

These approaches were among the first to be proposed for groundwater source identification. In these methods, a forward simulation is run with different possible sets of sources and the predicted solution is

compared to the measured spatial and temporal concentration data. Since an infinite number of plausible combinations of sources are there, an optimization model is required. The optimization model searches for the particular combination of sources which leads to minimum differences with the observed data. Simulation-optimization approaches were first proposed by Gorelick et al., 1983) using linear programming and regression as the optimizer. Since then several such approaches have been proposed using various optimization methods, some of which also includes simultaneous parameter estimation. Wagner, (1992) used non-linear maximum likelihood for simultaneous source identification and parameter estimation. Other optimization technique proposed include non-linear optimization model (Mahar and Datta, 2000), artificial neural network (ANN) (Singh and Datta, 2004), genetic algorithm (GA) (Singh and Datta, 2006) etc. SO approaches have been applied to both steady state and transient source identification problems, hydro-geologic and source parameters identification and groundwater quality monitoring. It has the potential to be applicable in field scale problems with complex geometries. However, non-uniqueness of groundwater source identification and sensitivity to noise in input data pose a challenge for these methods.

3.7 Stability criterion

There are certain stability issues associated with the numerical modeling of groundwater flow and solute transport. These issues arise from the approximations used in spatial and temporal discretization. In this section, some of the issues which can drastically affect the outcome of the numerical model of the groundwater flow and solute transport are discussed (Bear, 1979; Zheng and Bennet, 2002).

Stability in time integration: Of the different time-stepping techniques, the explicit method is the most simple. However it is only conditionally stable. When the size of the time step, Δt exceeds a certain limit, the numerical errors incurred by the solution will be amplified as the time marches forward leading to a situation where the solution is dominated by the errors and becomes an invalid or unstable solution. Consider the one-dimensional groundwater flow in a confined equation,

$$T\frac{\partial^2 h}{\partial x^2} = S\frac{\partial h}{\partial t} \tag{3.34}$$

The explicit method is stable only when the following relation holds between the spatial grid size (Δx) and the time step size (Δt) (Wang and Anderson, 1982):

$$\frac{T\Delta t}{S(\Delta x)^2} \leq \frac{1}{2} \tag{3.35}$$

Thus the nodal spacing and time step size cannot be independently chosen when using the explicit method. For the two dimensional problem, the stability condition is,

$$\frac{T\Delta t}{S(\Delta x^2 + \Delta y^2)} \leq \frac{1}{4} \tag{3.36}$$

Similarly, for the one-dimensional advection-dispersion equation (Zheng and Bennet, 2002),

$$\frac{\partial C}{\partial t} = D\frac{\partial^2 C}{\partial t^2} - v\frac{\partial C}{\partial x} \tag{3.37}$$

the explicit method is stable only when,

$$\frac{D\Delta t}{(\Delta x)^2} \leq \frac{1}{2} \quad \Rightarrow t \leq \frac{(\Delta x)^2}{2D} \tag{3.38}$$

The explicit method is a special case of the general θ- method of time integration (Richtmyer and Morton, 1967). In this technique, the time derivative is replaced by a simple forward difference while the solution is replaced by a weighted value of the previous time-step solution and current solution e.g. for the groundwater flow problem, $h = \theta h^{t+\Delta t} + (1-\theta)h^{t}$, $\theta \in [0,1]$. When $= 0$, it reduces to the explicit method. The θ-method is unconditionally stable only when $\theta \geq 1/2$, otherwise it is only conditionally stable.

Artificial oscillation and Numerical dispersion: Artificial oscillation and numerical dispersion are two issues encountered in numerical modeling of advectively dominated transport problems**.** The root cause of these instabilities is the truncation error incurred by the derivative terms. To illustrate the idea, let us consider the one dimensional transport problem (eqn. 3.37). From Taylor series expansion (Zheng and Bennet, 2002),

$$C(x+\Delta x) = C(x) + \Delta x \cdot \frac{\partial C}{\partial x} + \frac{(\Delta x)^2}{2} \cdot \frac{\partial^2 C}{\partial x^2} + O(\Delta x^3)$$

$$\Rightarrow \frac{\partial C}{\partial x} = \frac{C(x+\Delta x) - C(x)}{\Delta x} - \frac{\Delta x}{2} \cdot \frac{\partial^2 C}{\partial x^2} - O(\Delta x^2) \tag{3.39}$$

Substituting this expression, eqn. (3.39) into the RHS of eqn. (3.37) and neglecting terms with $O(\Delta x^2)$, we get,

$$\frac{\partial C}{\partial t} \approx D\frac{\partial^2 C}{\partial t^2} - v\left(\frac{C(x+\Delta x) - C(x)}{\Delta x} - \frac{\Delta x}{2} \cdot \frac{\partial^2 C}{\partial x^2}\right) \tag{3.40}$$

Re-arranging the terms,

$$\frac{\partial C}{\partial t} = \left(D + v\frac{\Delta x}{2}\right)\frac{\partial^2 C}{\partial x^2} - v\left(\frac{C(x+\Delta x) - C(x)}{\Delta x}\right) \tag{3.41}$$

It may be observed that an artificial dispersion term has been added with dispersion coefficient, $v\,\Delta x/2$ as a truncation error. If $D \leq v\,\Delta x/2$, then the artificial dispersion term starts dominating over the actual dispersion and the solution will be invalid.

Artificial oscillation: Oscillations are the overshoot or undershoot in the numerical solution. It arises when a sharp concentration front is present i.e. when the problem is advection-dominated. The degree to which the transport problem is dominated by advection is measured by a quantity called Peclet number (Pe) (Zheng and Bennet, 2002). For a one-dimensional uniform flow field, it is given by:

$$Pe = v\frac{\Delta x}{D} \tag{3.42}$$

A smaller value of Peclet number is desirable to for an oscillation free numerical solution. It has been shown that when $Pe \leq 2$, numerical oscillations are removed (Huyakorn and Pinder, 1983). Larger the physical dispersion (D), smaller the Peclet number. The Peclet number is also dependent on the grid spacing used. Smaller grid spacing leads to smaller *Pe*. However to keep the Peclet number within a small value, the grid spacing Δx may have to be so small as to be impractical. There are several ways to deal with high Peclet number flow problems such as upstream weighting, streamline upwind Petrov-Galerkin (SUPG) etc. (Onate, 1998)

Courant number: Another source of numerical dispersion lies in the approximation of the time derivative. A quantity used to estimate numerical dispersion while solving the advection-dispersion (AD) equation is the Courant number (Zheng and Bennet, 2002). The Courant number (Cr) reflects the number of cells (or the fraction of a cell) that a solute particle will traverse by advection in one time step. It is defined as,

$$Cr = \frac{v\Delta t}{\Delta x} \tag{3.43}$$

The numerical dispersion is dependent on the Courant number and is used as the accuracy requirement for the solution of AD equation (Zheng and Bennet, 2002). When advection dominates dispersion, designing a model with a small (<1) Courant number will decrease oscillations, improve accuracy and decrease numerical dispersion. To obtain sufficiently accurate solutions, it is generally required that Cr be less than or equal to one. The Courant number requirement nevertheless put a limit on the time-step size to be used in implicit or Cranck-Nicholson schemes, even though these schemes are unconditionally stable.

3.8 Closure

This chapter has discussed the various physical processes which are associated with groundwater flow and solute transport. The partial differential equations (PDE) that governs these processes have been

elaborated along with the available numerical methods for solving them such as FDM, FEM and the meshfree methods. Each of these methods has its own strengths and weaknesses. Over and above these, various numerical stability issues also arises during groundwater flow and solute transport modeling and they have been briefly discussed. The primary root cause of these stability problems is the truncation or approximation errors that are implicit in the numerical methods. This chapter also discussed the broad classifications of the methods used for groundwater source identification and the limitations of each of them. The next chapter proposes a meshfree method for modeling groundwater flow and solute transport. Meshfree methods can overcome some of the difficulties associated with mesh based approaches.

Chapter 4

Groundwater flow and transport modeling using meshfree method

4.1 Introduction

Commonly used methods for solving groundwater flow and transport equations such as FDM, FEM, and BEM are grid based methods requiring the construction of a mesh. This necessitates a lot of pre-processing and also leads to difficulties in adaptive analysis. Mesh Free methods, on the other hand, use a set of nodes scattered within the problem domain as well as sets of nodes scattered on the boundaries of the domain to represent (not discretize) the problem domain and its boundaries. These sets of scattered nodes are called field nodes, and they do not form a mesh, meaning it does not require any a priori information on the relationship between the nodes for the interpolation or approximation of the unknown functions of field variables (Liu and Gu, 2005). The solution procedure for Meshfree methods is shown in the Figure 4.1 where it has been compared to FEM.

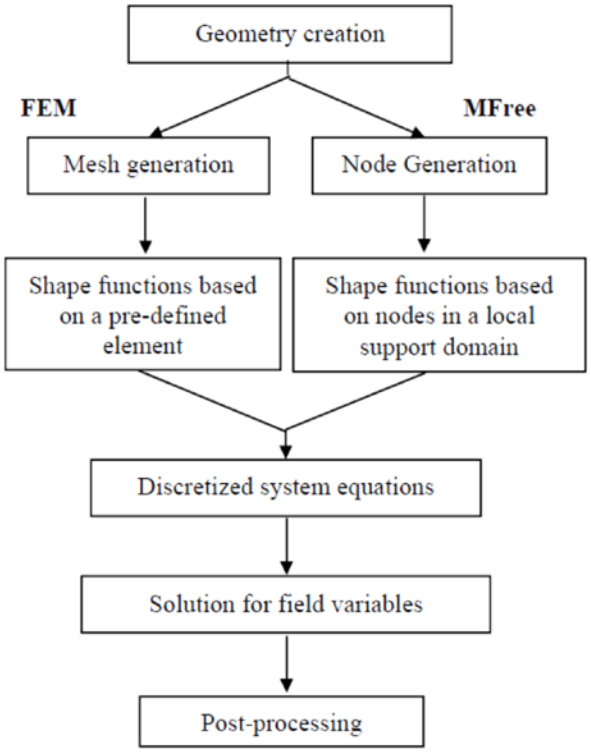

Figure 4.1: Comparison of steps in Mesh Free and FEM

4.2 Meshfree method - theoretical background

Mesh free methods use a set of *nodes* scattered within the problem domain as well as sets of nodes scattered on the boundaries of the domain to *represent* (not discretize) the problem domain and its boundaries (Liu and Gu, 2005). The set of scattered nodes are called *field nodes.* Mesh free method does not require any *a priori* information on the relationship between the nodes for the *interpolation* or *approximation* of the unknown functions of field variables i.e. a mesh is not required.

The *ideal* requirement for an MFree method will be that no mesh is required throughout the process of formulating and solving the problem, of a given arbitrary geometry, governed by a partial differential system equations subject to given boundary conditions. However, many of the methods classified as meshfree methods do not fulfill the ideal requirement as stated above. For many of these methods the connectivity of the nodes is determined at the run time. The *minimum* requirement for a method to be called mesh free method is that a predefined mesh is not required in the field variable interpolation or approximation.

Over the last three decades, several types of mesh free methods have been developed and it continues to attract the attention of researchers around the world till today. Many mesh free methods have found good applications in several areas of scientific and engineering endeavors and have shown to be a very good potential to become a powerful numerical tools. However, these methods are still in their developmental stage, and there are technical issues that need to be resolved before the methods can become efficient tools for complex engineering problems.

4.2.1 Developments in meshfree methods

The first of the meshfree methods developed was the smooth particle hydrodynamics (SPH) method by Lucy, (1977) and Gingold and Monaghan, (1977). It was developed to solve problems in astrophysics such as modeling exploding stars and dust clouds that had no boundaries. Its application was later extended to fluid dynamics (Bonet and Kulasegaram, 2000, Monaghan, 1982, Monaghan, 1988). Libersky et al., (1993) were the first to use SPH in solid mechanics. SPH is based on a strong form. Meshfree methods based on weak form were developed in the 1990s such as the element-free Galerkin (EFG) method developed in 1994 by Belytschko et al., (1994). EFG was one of the first meshfree methods based on a global weak form. Since then several other weak-form meshfree methods such as reproducing kernel particle method (RKPM) (Liu et al.,1995), the meshless local Petrov-Galerkin method (MLPG) (Atluri and Zhu, 1998), the point interpolation method (Liu and Gu, 1999), *hp*-cloud method (Armando and Oden, 1995), the partition of unity finite element method (PUFEM) (Melensk and Babuska, 1996) etc.

were developed. Kansa (1990) first applied collocation based meshfree method to solve partial differential equations using a globally supported support domain.

4.2.2 Different types of meshfree method

Meshfree methods can be classified based on the formulation procedure, according to the function approximation schemes and the domain representation. There are three main ways of formulating mesh free methods namely, weak-form formulation, strong-form formulation (collocation) and combination of weak-form and strong-form. Mesh free methods also differs from each other in the schemes with which the function approximations are performed. The main function approximation techniques are the moving least squares approximation (MLS), integral representation method of function approximation, point interpolation method (PIM), *hp*-cloud method and the partition of unity method. When it comes to domain representation, meshfree methods falls into two categories namely domain-type and boundary-type meshfree methods. The boundary-type is an extension of the boundary integral equation. Table 4.1 below list the various meshfree methods classified according to the criterion mentioned above (Liu and Gu, 2005).

Table 4.1: Classification of meshfree methods (Liu and Gu, 2005)

Feature or basis for classification	**Categories**	**Examples of the meshfree methods falling in a category**
Interpolation or approximation method	Meshfree methods using MLS	EFG, MLPG etc.
	Meshfree methods using integral representation method for function approximation	SPH
	Meshfree method using PIM	RPIM, LRPIM etc.
	Meshfree method using other interpolation schemes	PUFEM (partition of unity) *hp*-cloud

Formulation procedure of the governing equation	Meshfree methods formulated based on strong-form	Meshfree collocation methods, FPM etc.
	Meshfree methods formulated based on weak-form	EFG, RPIM, MLPG, LRPIM etc.
	Meshfree methods formulated based on combination of weak-form and strong-form	MWS
Domain representation	Domain-type meshfree methods	SPH, EFG, RPIM, MLPG, LRPIM etc.
	Boundary-type meshfree methods	BNM, BPIM, BRPIM, HBRPIM etc.

4.2.3 Radial point collocation method

Radial point collocation is a strong-form meshfree method wherein the governing equations are formulated using point collocation method and the function approximation (interpolation) is achieved by using a class of functions known as the radial basis functions (RBF) (Liu and Gu, 2005). The function interpolation is performed by using nodes within a small region around the point of interest. This region in the neighborhood of the point of interest is known as the local support domain of the point and is different for each point. The chosen approximation function passes through all the points within the support domain. This type of interpolation is known as the point interpolation method (PIM). In other function approximation such as the moving least squares approximation, the function need not pass through the individual points.

4.3 Meshfree method- modeling procedure

The process of solution of a given PDE by mesh free methods proceeds as in FEM but with differences in the way the domain representation and shape function creation are handled (Figure 4.1). These can be seen from the steps listed below (Liu and Gu, 2005).

4.3.1 Domain representation

In the Mesh free method, the problem domain and its boundary are first modeled and represented by using sets of nodes scattered in the problem domain and on its boundary. Since these nodes carry the values of

the field variables in a meshfree formulation, they are often called field nodes. The density of the nodes depends on the accuracy required and resources available.

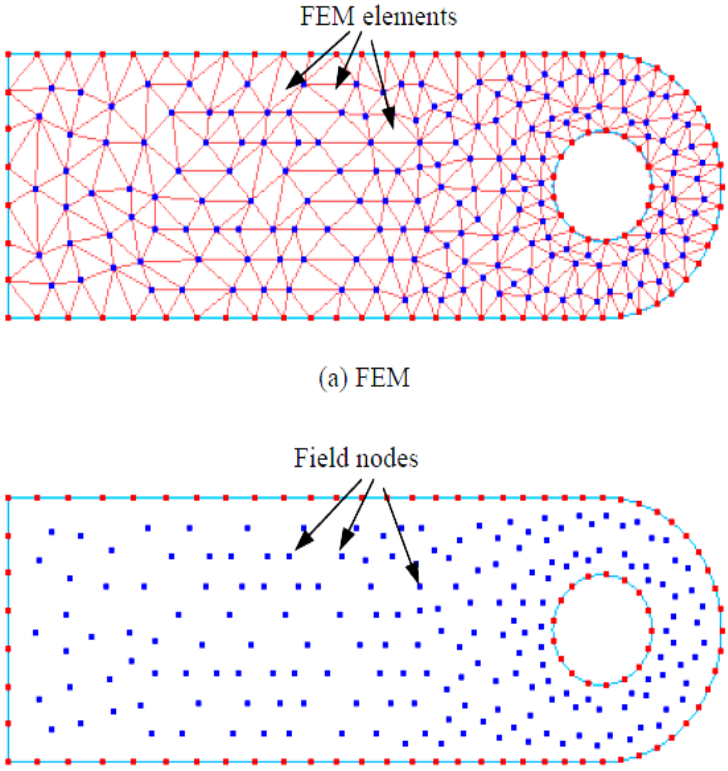

Figure 4.2: Domain representation in (a) FEM and (b) Mesh free methods

Unlike in FEM, no connectivity data among the nodes is required i.e. no mesh is required, only the coordinates of the nodes is required. This difference in the domain representation is illustrated in Figure 4.2 (Liu and Gu, 2005).

4.3.2 Function interpolation or approximation

To solve any PDE, first the unknown field variable is approximated using trial or shape functions. A local support domain of a point *x* determines the number of nodes to be used to approximate the function value at *x*. It is a set of nodes in the neighborhood of the point. The constructed shape function will not be used or is regarded as zero outside this local support domain; hence it is called locally supported. The support domain can have different shapes and also its dimension and shape can be different for different points of interest *x*, as shown in Figure 4.3 (Liu and Gu, 2005). Circular or rectangular support domains are the most commonly used shapes.

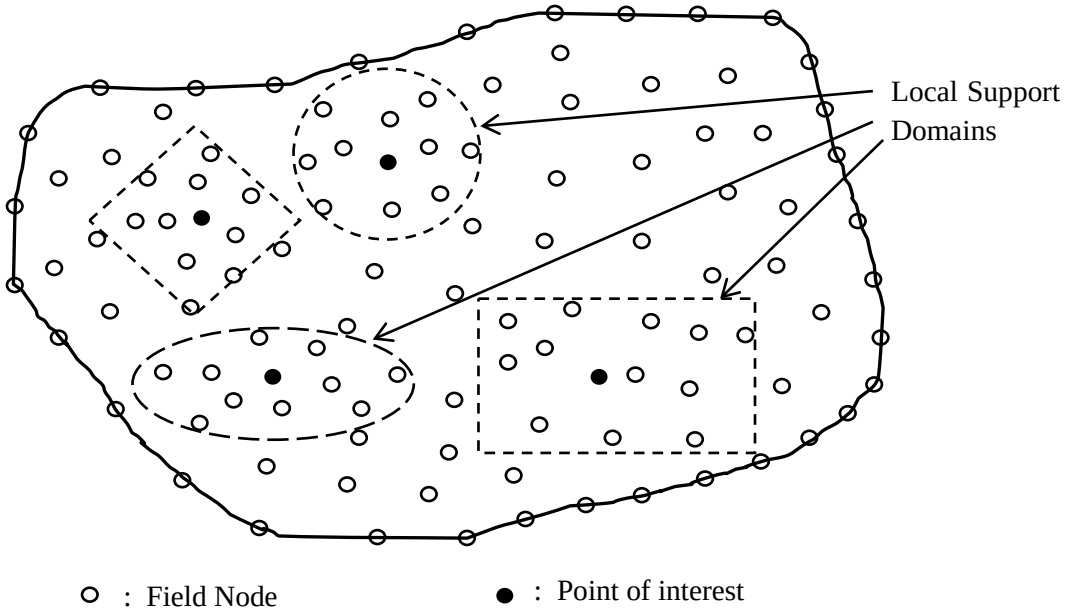

Figure 4.3 : Local support domains

4.3.3 Formation of system equations

The discrete equations of a meshfree method can be formulated using the shape functions and strong or weak form system equation. These equations are often written in nodal matrix form and are assembled into the global system matrices for the entire problem domain. The discretized system equations of meshfree methods are similar to those of FEM in terms of bandedness and sparseness, but they can be asymmetric depending on the method used.

4.3.4 Solve the global Mesh free equations

The resulting system of equations is solved to get the desired solution, as in FEM, except that solvers for asymmetric matrix systems may be needed, if locally supported domain is used in the function approximation. When the function interpolation is based on globally supported domain i.e. all the nodes are used in the function approximation, the system matrix can be conditionally unstable and is also unbanded.

4.4 Radial point interpolation and shape function evaluation

The approximation of a function $u(\mathbf{x})$ within a local support domain can be constructed as a linear combination of n radial basis functions and m polynomial basis functions as below (Liu and Gu, 2005):

$$u(\boldsymbol{x}) = \sum_{i=1}^{n} a_i R_i(\boldsymbol{x}) + \sum_{j=1}^{m} P_j(\boldsymbol{x}) b_j = \boldsymbol{R}^T(\boldsymbol{x})\boldsymbol{a} + \boldsymbol{P}^T(\boldsymbol{x})\boldsymbol{b} \tag{4.1}$$

where $R_i(\boldsymbol{x})$ is a radial basis function (RBF) such as a Multi-Quadrics or Gaussian, *n* is the number of points in the support domain, a_i and b_j are unknown coefficients to be determined. $P_j(x)$ are polynomial basis functions. *m* is the number of polynomial basis functions. When *m* = 0, pure RBFs are used. Otherwise, the RBF is augmented with *m* polynomial basis functions.

The above interpolation could have been accomplished using polynomials. But the major drawback of using polynomial for point interpolation method (PIM) is that it may yield a moment matrix that is badly conditioned or even singular depending on the locations of the nodes in the support domain and the terms of the monomials used in the basis. This may render the moment matrix non-invertible. To create a nonsingular moment matrix, radial basis functions (RBF) are used for constructing shape functions. PIM using radial basis function is termed radial PIM (RPIM).

In the RBF, $R_i(\boldsymbol{x})$, the only variable is the distance between the point of interest $\boldsymbol{x}$, called the data site and a node at $\boldsymbol{x}_i$, known as the center point,

$$r_i = \sqrt{(x - x_i)^2 + (y - y_i)^2} \quad \text{(in case of 2D problems)} \tag{4.2}$$

There are several types of radial basis functions. Kansa (1990), Franke and Schaback (1997), Sharan et al.(1997) etc. have extensively investigated the characteristics of RBFs. Table 4.2 lists some of the widely used RBF functions and their definitions. In this work, two of the most widely used RBF functions viz., the multi-quadrics RBF (MQ-RBF) and the Exponential or Gaussian RBF (EXP-RBF) have been used for function interpolation.

Table 4.2 : Typical radial basis functions with dimensionless shape parameters

	Name	Expression	Shape Parameters
1	Multi-quadrics(MQ)	$R_i(x,y) = \left(r_i^2 + C_s^2\right)^q = [(x - x_i)^2 + (y - y_i)^2 + C_s^2]^q$	C_s, q
2	Gaussian (EXP)	$R_i(x,y) = \exp\left(-cr_i^2\right) = \exp\{-c[(x - x_i)^2 + (y - y_i)^2]\}$	c
3	Thin plate spline (TPS)	$R_i(x,y) = r_i^\eta = [(x - x_i)^2 + (y - y_i)^2]^\eta$	η
	Logarithmic RBF	$R_i(r_i) = r_i^\eta \log r_i$	η

where q, C_s, c, η are known as the shape parameters of the RBF and. The standard MQ-RBF has $q = \pm 0.5$, but this parameter can also be left as an additional open parameter (Wang and Liu, 2002a). In this study, the parameter q has been kept at 0.98 as in Liu and Gu (2005). It was observed that changing this parameter to the standard value of 0.5 did not produce any significant effect on the accuracy and stability of the solutions in this study. The shape parameter of the MQ-RBF, C_s is usually defined in terms of a characteristic length (d_c) i.e. $C_s = \alpha_c d_c$. This characteristic length (d_c) is related to the nodal spacing in the local support domain. The value of the shape parameter of the RBFs has a very profound impact on the quality of the interpolation within a support domain and hence on the overall solution accuracy. Choosing the optimum value of this parameter is very crucial. Currently there is no unique criterion or established method for finding the optimum value of this parameter and is generally found by sensitivity or parametric studies. Some strategies of choosing the shape parameter can be found in Schaback and Wendland (2000), Rippa (1999) and Wright (2003).

The unknown coefficients a_i and b_j in equation (4.1) can be determined by enforcing the interpolation function to pass through all *n* nodes within the support domain (Liu and Gu, 2005). The interpolation of the function at the k^{th} point has the following form:

$$u(x_k, y_k) = h_k = \sum_{i=1}^{n} a_i R_i(x_k, y_k) + \sum_{j=1}^{m} b_j P_j(x_k, y_k) \quad , k = 1, \quad \dots \ , n \tag{4.3}$$

which yields *n* simultaneous linear algebraic equations with $n + m$ unknowns. The additional *m* equations can be obtained from the following *m* constraint equations imposed on the polynomial term to guarantee unique approximation (Goldberg et al., 1999) :

$$\sum_{i=1}^{n} P_j(x_i, y_i) a_i = \boldsymbol{P}_m^T \boldsymbol{a} = 0 \ , \quad j = 1,2, \dots \dots m \tag{4.4}$$

Equation (4.3) can be written in matrix form as:

$$U_s = R_0 \boldsymbol{a} + P_m \boldsymbol{b} \tag{4.5}$$

where,

$$U_s = \{u_1 \ u_2 \ \cdots \ u_n\}^T \tag{4.6}$$

$$R_0 = \begin{bmatrix} R_1(r_1) & R_2(r_1) & \cdots & R_n(r_1) \\ R_1(r_2) & R_2(r_2) & \cdots & R_n(r_2) \\ \vdots & \vdots & & \vdots \\ R_1(r_n) & R_2(r_n) & \cdots & R_n(r_n) \end{bmatrix}_{(nxn)} \tag{4.7}$$

$$P_m{}^T = \begin{bmatrix} 1 & 1 & \cdots & 1 \\ x_1 & x_2 & \cdots & x_n \\ y_1 & y_2 & \cdots & y_n \\ \vdots & \vdots & \ddots & \vdots \\ p_{m(\boldsymbol{x_1})} & p_{m(\boldsymbol{x_2})} & \cdots & p_{m(\boldsymbol{x_n})} \end{bmatrix}_{(mxn)} \tag{4.8}$$

$$a^T = \{a_1 \quad a_2 \quad \cdots \quad a_n\};\ b^T = \{b_1 \quad b_2 \quad \cdots \quad b_m\} \tag{4.9}$$

R_0 is the moment matrix of RBFs while P_m^T is the moment matrix of polynomials. In the above, $r_k\ in\ R_i(r_k)$ is defined as:

$$r_k = \sqrt{(x_k - x_i)^2 + (y_k - y_i)^2} \tag{4.10}$$

Combining equations (4.4) and (4.5), the following set of equations is obtained,

$$\widetilde{\boldsymbol{U}}_s = \begin{bmatrix} \boldsymbol{U}_s \\ \boldsymbol{0} \end{bmatrix} = \begin{bmatrix} R_0 & P_m \\ P_m{}^T & 0 \end{bmatrix} \begin{Bmatrix} \boldsymbol{a} \\ \boldsymbol{b} \end{Bmatrix} = G\boldsymbol{a}_0 \tag{4.11}$$

Solving this set of equations,

$$\boldsymbol{a}_0 = \begin{Bmatrix} \boldsymbol{a} \\ \boldsymbol{b} \end{Bmatrix} = G^{-1}\widetilde{\boldsymbol{U}}_s \tag{4.12}$$

Equation (4.1) can be written as,

$$u(\boldsymbol{x}) = R^T(\boldsymbol{x})\boldsymbol{a} + p^T(\boldsymbol{x})\boldsymbol{b} = \{R^T(\boldsymbol{x}) \quad p^T(\boldsymbol{x})\} \begin{Bmatrix} \boldsymbol{a} \\ \boldsymbol{b} \end{Bmatrix} \tag{4.13}$$

Substituting the coefficients from equation (4.12) back into equation (4.13), the interpolation can be expressed as,

$$u(\boldsymbol{x}) = \boldsymbol{\Phi^T}(\boldsymbol{x})\boldsymbol{u_s} \tag{4.14}$$

where $\boldsymbol{\phi}(\mathbf{x})$, is known as the shape functions and expressed as:

$$\boldsymbol{\Phi^T}(\boldsymbol{x}) = \{\phi_1(x,y) \quad \phi_2(x,y) \quad \ldots \quad \phi_n(x,y)\} \tag{4.15}$$

and, $\boldsymbol{u}_s = \{u_1\ u_2\ \cdots u_n\}^T$ is the vector of nodal values of the function at the support domain nodes.

The shape functions depend only upon the position of the nodal points. The derivatives of $u(x,y)$ at any point $\boldsymbol{x}_I(x_I, y_I)$ can be easily determined as below:

$$u(\boldsymbol{x}_I) = \boldsymbol{\Phi}^T\boldsymbol{u}_s = \sum_{i=1}^{n} \phi_i u_i \tag{4.16}$$

$$\frac{\partial \boldsymbol{u}_I}{\partial x} = \frac{\partial \boldsymbol{\Phi}^T}{\partial x}\boldsymbol{u}_s = \sum_{i=1}^{n} \frac{\partial \phi_i}{\partial x} u_i \quad ; \quad \frac{\partial^2 \boldsymbol{u}_I}{\partial \boldsymbol{x}^2} = \frac{\partial^2 \boldsymbol{\Phi}^T}{\partial x^2}\boldsymbol{u}_s = \sum_{i=1}^{n} \frac{\partial^2 \phi_i}{\partial x^2} u_i \tag{4.17}$$

$$\frac{\partial \boldsymbol{u}_I}{\partial y} = \frac{\partial \boldsymbol{\Phi}^T}{\partial y}\boldsymbol{u}_s = \sum_{i=1}^{n} \frac{\partial \phi_i}{\partial y} u_i \quad ; \quad \frac{\partial^2 \boldsymbol{u}_I}{\partial \boldsymbol{y}^2} = \frac{\partial^2 \boldsymbol{\Phi}^T}{\partial y^2}\boldsymbol{u}_s = \sum_{i=1}^{n} \frac{\partial^2 \phi_i}{\partial y^2} u_i \tag{4.18}$$

4.4.1 Approximation using radial point collocation method (RPCM)

In this section, the approximation or discretization of differential equations using point collocation method is demonstrated (Liu and Gu, 2005). The discretization techniques developed here are applied to the governing equations of groundwater flow and transport in the next section.

Let us consider the following second-order one-dimensional differential equation:

$$A_2(x)\frac{d^2u}{dx^2} + A_1(x)\frac{du}{dx} + A_0(x)u + q_a(x) = 0 \tag{4.19}$$

where u is the unknown scalar field variable, the coefficients A_0, A_1 and $A_2$are given functions of the independent variable x, q_a is the source or sink term which may also be a function of *x*. Let the boundary conditions be:

$$B_1(x)\frac{du(x)}{dx} + B_0(x)u(x) + q_b = 0 \quad (Neumann\ or\ derivative\ BC) \tag{4.20}$$

$$u(x) - \bar{u} = 0 \quad (Dirichlet\ BC) \tag{4.21}$$

where B_0 and B_1 are given functions of *x*, q_b is a source term on the flux boundary and $\bar{u}$ is the specified value of the field variable on the Dirichlet boundary points. Let us assume that the above equation is valid over the domain shown in Figure 4.4 where the nodal distributions are also shown. The domain ranges from $x = x_1$to $x = x_L$ and it has been sub-divided into *N* discrete points, not necessarily spaced equally. The Dirichlet boundary is at $x = x_1$while the Neumann or derivative boundary is at $x = x_L$. The collocation points to be used for the discretization of eqn.(4.19) can be different from the grid or field nodes used to sub-divide the domain.

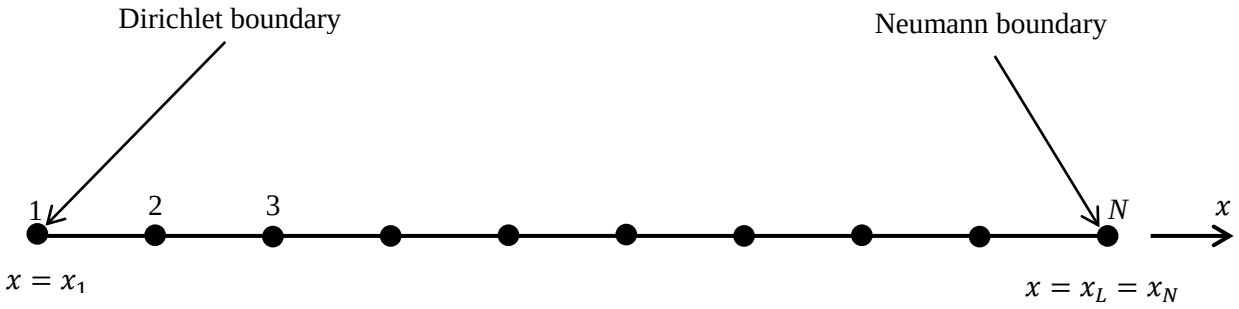

Figure 4.4: Nodal distribution of the problem domain

Using the meshfree shape function derived in the preceding section (given in eqns. 4.16 through 4.18), the approximation (u^h) of the unknown function (u) and its derivatives at the collocation point at $x = x_I$ are :

$$u_I^h = u^h(x_I) = \boldsymbol{\Phi}^T \boldsymbol{u}_s \tag{4.22}$$

$$\frac{\partial u_I^h}{\partial x} = \frac{\partial \boldsymbol{\Phi}^T}{\partial x} \boldsymbol{u}_s \tag{4.23}$$

$$\frac{\partial^2 u_I^h}{\partial x^2} = \frac{\partial^2 \boldsymbol{\Phi}^T}{\partial x^2} \boldsymbol{u}_s \tag{4.24}$$

For all the internal points (all points except the end points where BC are applied) of the domain, the discretization of the equation (4.19) is obtained by simple collocation at each of the points and using the approximation in eqn. (4.22). For the node at $= x_I$, the resulting equation is:

$$\left(A_2(x_I) \frac{d^2 \boldsymbol{\Phi}^T}{dx^2} + A_1(x_I) \frac{d\boldsymbol{\Phi}^T}{dx} + A_0(x_I) \right) \boldsymbol{u}_s = -q_a(x_I) \; ; \;\; for\ all\ I = 2, 3, \ldots, N-1 \tag{4.25}$$

Or in matrix form,

$$\boldsymbol{K}_I \boldsymbol{u}_s = f_I \; ; \quad for\ all\ I = 2,3, \ldots, N-1 \tag{4.26}$$

Where $\boldsymbol{K}_I$ is the nodal matrix for the collocation at x_I. Expanding the expression,

$$\begin{aligned} \boldsymbol{K}_I &= A_2(x_I) \frac{d^2 \boldsymbol{\Phi}^T}{dx^2} + A_1(x_I) \frac{d\boldsymbol{\Phi}^T}{dx} + A_0(x_I) \\ &= \left\{ A_2(x_I) \frac{d^2 \phi_1}{dx^2} + A_1(x_I) \frac{d\phi_1}{dx} + A_0(x_I) \ldots . A_2(x_I) \frac{d^2 \phi_n}{dx^2} + A_1(x_I) \frac{d\phi_n}{dx} + A_0(x_I) \right\} \end{aligned} \tag{4.27}$$

Here, $f_I = -q_a(x_I)$. The Dirichlet boundary condition (eqn.4.21) can be implemented as,

$$\boldsymbol{\Phi}^T \boldsymbol{u}_s = \bar{u} \Rightarrow \boldsymbol{K}_1 \boldsymbol{u}_s = f_1 \tag{4.28}$$

where $\boldsymbol{K}_1 = \boldsymbol{\Phi}^T = \{\phi_1\ \phi_2\ \ldots \phi_n\}$ is the nodal matrix for the collocation node at x_1 ; the ϕ_i's are created by using the *n* nodes in the support domain of node 1 and $f_1 = \bar{u}$. The Neumann boundary condition at the other end of the domain i.e. $x = x_N$ requires special treatment as derivative boundary conditions are known to cause instability and poor accuracy, specially with irregular grids, in collocation methods (Liu and Gu, 2005). A number of strategies have been proposed in Liu and Gu (2005) to deal with derivative boundary conditions such as direct collocation, method of fictitious points, Hermite-type collocation, method of regular grids, dense nodes method and weak-strong form method. In this study, the direct collocation approach has been implemented. In the direct collocation method for derivative boundary, a discretization scheme, similar to that for the internal nodes, is constructed at the derivative boundary nodes. Substituting the function approximation in eqn. (4.20) into the Neumann boundary (eqn. 4.22), we obtain,

$$\left(B_1(x_N)\frac{d\boldsymbol{\Phi}^T}{dx} + B_0(x_N)\boldsymbol{\Phi}^T\right)u_s = -q_b(x_N) \tag{4.29}$$

Or, in matrix form,

$$\boldsymbol{K}_N\boldsymbol{u}_s = f_N \tag{4.30}$$

where $\boldsymbol{K}_N$ is the nodal matrix for the collocation node at x_N and $f_N = -q_b(x_N)$. $\boldsymbol{K}_N$ can be expanded as,

$$K_N = B_1(x_N)\frac{d\boldsymbol{\Phi}^T}{dx} + B_0(x_N)\boldsymbol{\Phi}^T = \left\{B_1(x_N)\frac{d\phi_1}{dx} + B_0(x_N)\phi_1 \ldots\ B_1(x_N)\frac{d\phi_n}{dx} + B_0(x_N)\phi_n\right\} \tag{4.31}$$

Now assembling the eqns. (4.25), (4.28) and (4.29), the discretized system equation is obtained as,

$$\boldsymbol{K}_{NxN}\boldsymbol{U}_{Nx1} = \boldsymbol{F}_{Nx1} \tag{4.32}$$

where the global system matrix , $\boldsymbol{K}$ has the form,

$$\boldsymbol{K} = \begin{bmatrix} K_{11} & K_{12} & \cdots & K_{1(N-1)} & K_{1N} \\ K_{21} & K_{22} & \cdots & K_{2(N-1)} & K_{2N} \\ \cdots & \cdots & \ddots & \cdots & \cdots \\ K_{(N-1)1} & K_{(N-1)2} & \cdots & K_{(N-1)(N-1)} & K_{(N-1)N} \\ K_{N1} & K_{N2} & \cdots & K_{N(N-1)} & K_{NN} \end{bmatrix} \tag{4.33}$$

and the global source or load vector $\boldsymbol{F}$ is of the form,

$$\boldsymbol{F} = \begin{Bmatrix} \bar{u} \\ -q_a(x_2) \\ \vdots \\ -q_a(x_{N-1}) \\ -q_b(x_N) \end{Bmatrix} \tag{4.34}$$

The vector $\boldsymbol{U}$ collects all the nodal values of the unknown function u and is of the form,

$$\boldsymbol{U} = \begin{Bmatrix} u_1 \\ u_2 \\ \vdots \\ u_{N-1} \\ u_N \end{Bmatrix} \tag{4.35}$$

Solving eqn. (4.32) will give the nodal values of the unknown field variable u at all the nodes. It may be observed that the assembling of the global system matrix has been done by stacking together row-by-row for each of the nodes, quite different from the assembling procedure of FEM.

Two dimensional equation: The general form of the second-order PDE defined in a domain Ω is given by,

$$A_{11}(\boldsymbol{x})\frac{\partial^2 u}{\partial x^2} + 2A_{12}(\boldsymbol{x})\frac{\partial^2 u}{\partial x \partial y} + A_{22}(\boldsymbol{x})\frac{\partial^2 u}{\partial y^2} + A_{10}(\boldsymbol{x})\frac{\partial u}{\partial x} + A_{20}(\boldsymbol{x})\frac{\partial u}{\partial y} + A_{00}(\boldsymbol{x})u + q_a(x) = 0 \tag{4.36}$$

where u is the unknown field function, q_a is the source term and A_{11} through A_{00} are coefficients which can be a function of the spatial coordinates, $\boldsymbol{x} = (x, y)$. The boundary conditions can be of Dirichlet or Neumann type.

- Dirichlet boundary condition:

$$u = \bar{u} \;\; on \;\; \partial\Omega_{\mathrm{u}}$$

- Neumann (derivative) boundary condition:

$$\boldsymbol{n}^T \cdot \nabla u + q_b = 0 \quad on \;\; \partial\Omega_{DB}$$

where q_b is a specified source term on the Neumann boundary, $\partial\Omega_{DB}$; $\boldsymbol{n}$ is the vector of the unit outward normal and the gradient operator ∇ is defined as,

$$\nabla u = \begin{Bmatrix} \dfrac{\partial}{\partial x} \\ \dfrac{\partial}{\partial y} \end{Bmatrix} u = \begin{Bmatrix} \dfrac{\partial u}{\partial x} \\ \dfrac{\partial u}{\partial y} \end{Bmatrix}$$

The point collocation discretization derived above can be easily extended to this general second-order PDE. The meshfree function approximations derived in eqns. (4.16), (4.17) and (4.18) can be employed to obtain the discretization of the given equation.

4.5 RPCM formulation for groundwater flow problem

In the present work, the meshfree RPCM or strong form formulation as proposed in Liu and Gu (2005) is used for discretizing the groundwater flow and transport equations. The governing equation is discretized using point collocation method with the state variable, i.e. hydraulic head or solute concentration approximated by using point interpolation method (PIM) as described in the previous section 4.4. The radial basis functions used in this study are the Multi-quadrics (MQ) and the Gaussian or Exponential (EXP) RBFs. In this section, this discretization process is demonstrated for both the confined and unconfined aquifers. Steady state and time-dependent cases of both the aquifers have been also considered.

4.5.1 2D confined flow problem

The equation which governs the two-dimensional groundwater flow in a confined aquifer is given by eqn.(3.12). In steady-state case the governing equation is given by,

$$\frac{\partial}{\partial x}\left[T_x \frac{\partial h}{\partial x}\right] + \frac{\partial}{\partial y}\left[T_y \frac{\partial h}{\partial y}\right] = Q_w \delta(x - x_i)(y - y_i) - q \tag{4.37}$$

Using the meshfree shape functions derived in eqn. (4.16), the groundwater head can be approximated as,

$$h(x, y) = \sum_{i=1}^{n} \phi_i(x, y) h_i = \boldsymbol{\Phi}^T(x, y) \boldsymbol{h}_s \tag{4.38}$$

where $\boldsymbol{h}_s = \{h_1\ h_2 \ldots h_n\}$ is the nodal heads for the nodes in the support domain of the point of interest (x, y), n is the number of nodes in its support domain. Collocation of the governing eqn. (4.37) at the point $\boldsymbol{x}_r = (x_r, y_r)$ using the approximation in eqn. (4.37) yields,

$$T_x(\boldsymbol{x}_r) \frac{\partial^2 \boldsymbol{\Phi}^T}{\partial x^2} \boldsymbol{h}_s + T_y(\boldsymbol{x}_r) \frac{\partial^2 \boldsymbol{\Phi}^T}{\partial y^2} \boldsymbol{h}_s = Q_w \delta(\boldsymbol{x} - \boldsymbol{x}_r) - q(\boldsymbol{x}_r)$$

Or,

$$\left[T_x(\boldsymbol{x}_r) \frac{\partial^2 \boldsymbol{\Phi}^T}{\partial x^2} + T_y(\boldsymbol{x}_r) \frac{\partial^2 \boldsymbol{\Phi}^T}{\partial y^2}\right] \boldsymbol{h}_s = Q_w \delta(\boldsymbol{x} - \boldsymbol{x}_r) - q(\boldsymbol{x}_r) \tag{4.39}$$

The above discretized equation is established for all the internal nodes, $\boldsymbol{x}_r$'s. The Dirichlet boundary condition in eqn. (3.14) can be easily discretized, using the function approximation (eqn.4.38), as below:

$$\boldsymbol{\Phi}^T \boldsymbol{h}_s = h_1 \tag{4.40}$$

The Neumann boundary condition in eqn. (3.15) is discretized by using the direct collocation technique as described in the preceding sections to yield,

$$T(\boldsymbol{x})\frac{\partial \Phi^T}{\partial n} = q_1(\boldsymbol{x}) \tag{4.41}$$

Now, assembling the discretized eqns. (4.39), (4.40) and (4.41), the global system of equations can be obtained and it will have a similar form as in eqn. (4.32).

4.5.1.1 Time-dependent confined flow problem

For time-dependent case, the nodal groundwater head approximation using the meshfree RPIM shape functions can be written as,

$$h(\boldsymbol{x},t) = \sum_{i=1}^{n} \phi_i(\boldsymbol{x}) h_i(t) = \boldsymbol{\Phi}^T(\boldsymbol{x})\boldsymbol{h}_s(t) \tag{4.42}$$

in which *n* is the number of nodes used in the local support domain. The time-dependence appears only in the nodal head values whereas the shape functions are only a function of the nodal coordinates.

The discretization of the governing equation (3.12) is achieved by simple collocation at all the internal nodes and using the above approximation for the groundwater head. Thus by collocation at the point $\boldsymbol{x}_r(x_r, y_r)$, the governing equation (3.12), for a homogeneous and isotropic aquifer, is discretized as:

$$T(\boldsymbol{x}_r)\left[\frac{\partial^2 \boldsymbol{\Phi}^T}{\partial x^2} + \frac{\partial^2 \boldsymbol{\Phi}^T}{\partial y^2}\right]\boldsymbol{h}_s(t) = S(\boldsymbol{x}_r)\left(\frac{\partial h}{\partial t}\right)_{\boldsymbol{x}_r} + Q_w\delta(\boldsymbol{x}_r - \boldsymbol{x}_i) - q(\boldsymbol{x}_r) \tag{4.43}$$

Using nodal indices, the above equation can be re-written as,

$$T_r\left[\frac{\partial^2 \boldsymbol{\Phi}^T}{\partial x^2} + \frac{\partial^2 \boldsymbol{\Phi}^T}{\partial y^2}\right]\boldsymbol{h}_s(t) = S_r\left(\frac{\partial h}{\partial t}\right)_r + Q_w\delta(\boldsymbol{x}_r - \boldsymbol{x}_i) - q_r \tag{4.44}$$

The time discretization can be done by using the θ- method which is the most commonly used algorithm for time discretization. In this method, the time derivative is replaced by a simple forward difference while the solution is replaced by a weighted value of the previous time-step solution and current solution as below (Richtmyer and Morton, 1967):

$$\frac{\partial h}{\partial t} = \frac{h^{t+\Delta t} - h^t}{\Delta t} \tag{4.45}$$

and

$$h = \theta h^{t+\Delta t} + (1-\theta)h^t \tag{4.46}$$

Here, θ is a relaxation parameter which lies in the interval [0, 1] and is used to control the accuracy and stability of the algorithm. This method is unconditionally stable for all $\theta \geq 1/2$ (Richtmyer and Morton, 1967). Commonly used values of θ are 0, ½, 2/3 and 1. When θ < 1/2, the algorithm is only conditionally stable. When $= {}^{1}/_{2}$, it is known as the Cranck-Nicholson time stepping method and the same is used in this study. Substituting equations (4.45 and 4.46), the discretized equation (4.44) can be written as,

$$S_r \frac{\boldsymbol{\phi^T h_s}^{t+\Delta t} - h_r^t}{\Delta t} + Q_w \delta(\boldsymbol{x}_r - \boldsymbol{x}_i) - q_r = \theta T_r \left[\frac{\partial^2 \boldsymbol{\phi^T}}{\partial x^2} + \frac{\partial^2 \boldsymbol{\phi^T}}{\partial y^2}\right] \boldsymbol{h}_s^{t+\Delta t} + (1-\theta) T_r \left[\frac{\partial^2 \boldsymbol{\phi^T}}{\partial x^2} + \frac{\partial^2 \boldsymbol{\phi^T}}{\partial y^2}\right] \boldsymbol{h}_s^t \tag{4.47}$$

It is assumed that the nodal heads, h_r^t at time t are known and is used as the initial condition to advance the solution to the next time level, $t = t + \Delta t$. Re-arranging the terms,

$$\left[S_r \boldsymbol{\phi^T} - \theta \Delta t T_r \left(\frac{\partial^2 \boldsymbol{\phi^T}}{\partial x^2} + \frac{\partial^2 \boldsymbol{\phi^T}}{\partial y^2}\right)\right] \boldsymbol{h}_s^{t+\Delta t} = S_r h_r^t + \Delta t(1-\theta) \left[\frac{\partial^2 \boldsymbol{\phi^T}}{\partial x^2} + \frac{\partial^2 \boldsymbol{\phi^T}}{\partial y^2}\right] \boldsymbol{h}_s^t - Q_w \delta(\boldsymbol{x}_r - \boldsymbol{x}_i) + q_r \tag{4.48}$$

The above equation is established for all the internal nodes. Appropriate boundary and initial conditions are applied. An assembling of the discretized nodal equations, as discussed in the preceding section 4.4.1, is performed and the resulting global equation is solved.

4.5.2 2D unconfined flow problem

The governing equation for an unconfined aquifer in two dimensions is non-linear (eqn. 3.16). Hence a linearization technique needs to be applied to apply the mesh free formulation. In this work Newton-Raphson iteration (Ortega and Rheinboldt, 1970 ; Onate, 1998) is applied.

Given a system of equations, $\boldsymbol{K}(\boldsymbol{h}) = 0$ Newton-Raphson method use successive approximations /iterations to find the solution to the equation, $\boldsymbol{h}_{n+1} = \boldsymbol{h}_n - \Delta \boldsymbol{h}$ where $\mathbf{\Delta h} = \boldsymbol{J}^{-1}.\boldsymbol{K}(\boldsymbol{h}_n)$ is the successive corrections or refinements to the solution. $\boldsymbol{J}$ is the Jacobian matrix, also called gradient matrix. The procedure for creating the system matrix (**K**) and the Jacobian(**J**) for implementing Newton-Raphson iteration method is illustrated here. The hydraulic conductivities terms have been neglected for the sake of simplicity since they appear as constants factors.

The non-linear terms in the equation of the unconfined aquifer are discretized as below:

$$\frac{\partial}{\partial x}\left(h\frac{\partial h}{\partial x}\right)=\left(\frac{\partial h}{\partial x}\right)^2+h\frac{\partial^2 h}{\partial x^2}=\left(\sum_{i=1}^{n}\frac{\partial \varphi_i}{\partial x}h_i\right)^2+\left(\sum_{i=1}^{n}\varphi_i h_i\right)\left(\sum_{i=1}^{n}\frac{\partial^2 \varphi_i}{\partial x^2}h_i\right) \tag{4.49}$$

Similarly,

$$\frac{\partial}{\partial y}\left(h\frac{\partial h}{\partial y}\right)=\left(\frac{\partial h}{\partial y}\right)^2+h\frac{\partial^2 h}{\partial y^2}=\left(\sum_{i=1}^{n}\frac{\partial \varphi_i}{\partial y}h_i\right)^2+\left(\sum_{i=1}^{n}h_i\right)\left(\sum_{i=1}^{n}\frac{\partial^2 \varphi_i}{\partial y^2}h_i\right) \tag{4.50}$$

The (j,r)th element of the Jacobian matrix element is then given by:

$$\begin{aligned}[J]_{jr}=\frac{\partial K_j}{\partial h_r}&=2\frac{\partial \phi_r}{\partial x}\left(\sum_{i=1}^{n}\frac{\partial \phi_i}{\partial x}h_i\right)+\frac{\partial^2 \phi_r}{\partial x^2}\left(\sum_{i=1}^{n}\phi_i h_i\right)+\phi_r\left(\sum_{i=1}^{n}\frac{\partial^2 \phi_i}{\partial x^2}h_i\right)\\&+2\frac{\partial \phi_r}{\partial y}\left(\sum_{i=1}^{n}\frac{\partial \phi_i}{\partial y}h_i\right)+\frac{\partial^2 \phi_r}{\partial y^2}\left(\sum_{i=1}^{n}\phi_i h_i\right)+\phi_r\left(\sum_{i=1}^{n}\frac{\partial^2 \phi_i}{\partial y^2}h_i\right)\end{aligned} \tag{4.51}$$

The discretization of the Dirichlet boundary condition is done in a similar way as in eqn. (4.40). However, the Neumann or derivative boundary condition is also non-linear for an unconfined aquifer. As noted earlier, the presence of derivative boundary condition, also called Neumann type BC, drastically deteriorates the accuracy of the solution and the solution can also be unstable (Liu and Gu, 2005). A number of strategies to handle derivative boundary conditions have been mentioned in Liu and Gu (2005). In the present study, the direct collocation method has been used which is a simple way to treat derivative boundary conditions (BC) with satisfactory accuracy.

The generalized expression for derivative or Neumann type boundary conditions is (Liu and Gu, 2005)

$$\frac{\partial h(\boldsymbol{x_i})}{\partial \boldsymbol{n}}=l_{xi}\frac{\partial h(\boldsymbol{x_i})}{\partial x}+l_{yi}\frac{\partial h(\boldsymbol{x_i})}{\partial y} \tag{4.52}$$

Where $\boldsymbol{n}$ is the vector of unit outwards normal; l_{xi} and l_{yi} are the direction cosines for the outward normal at the Neumann node $\boldsymbol{x_i}\equiv(x_i,y_i)$ defined by,

$$\begin{cases}l_{xi}=\cos(\boldsymbol{n},x_i)\\l_{yi}=\cos(\boldsymbol{n},y_i)\end{cases}$$

For an unconfined aquifer, the boundary condition is also non-linear .The discretization of derivative BC can be done as below:

$$c_1\left(h\frac{\partial h}{\partial \boldsymbol{n}}\right)+c_0=g(x)\ \text{ or, }\ c_1\left[l_{xi}\left(h\frac{\partial h}{\partial x}\right)+l_{yi}\left(h\frac{\partial h}{\partial y}\right)\right]+c_0=g(x)$$

$$\text{or,}\qquad c_1\left[l_{xi}\left\{\left(\sum_{i=1}^{n}\phi_i h_i\right)\left(\sum_{i=1}^{n}\frac{\partial \phi_i}{\partial x}h_i\right)\right\}+l_{yi}\left\{\left(\sum_{i=1}^{n}\phi_i h_i\right)\left(\sum_{i=1}^{n}\frac{\partial \phi_i}{\partial y}h_i\right)\right\}\right]+c_0=g(x)$$

The (j,r)[th] element of the Jacobian or gradient matrix corresponding to the Neumann boundary nodes will be given by,

$$[J]_{jr}=\frac{\partial K_j}{\partial h_r}=c_1[l_{xi}\left\{\phi_r\left(\sum_{i=1}^{n}\frac{\partial \phi_i}{\partial x}h_i\right)+\frac{\partial \phi_r}{\partial x}\left(\sum_{i=1}^{n}\phi_i h_i\right)\right\}+\ l_{yi}\left\{\phi_r\left(\sum_{i=1}^{n}\frac{\partial \phi_i}{\partial y}h_i\right)+\frac{\partial \phi_r}{\partial y}\left(\sum_{i=1}^{n}\phi_i h_i\right)\right\}] \tag{4.53}$$

The eqns. (4.49), (4.50), (4.51) and (4.53) can be established for all the nodes in the domain to form the system matrix (**K**) and the Jacobian (**J**). The steps for implementing Newton-Raphson iterations is:

1. Start with an initial guess solution
2. Compute the corrections to the previous guess using $\mathbf{\Delta h}=\boldsymbol{J^{-1}}.\boldsymbol{K}(\boldsymbol{h}_n)$
3. Compute the improved solution: $\boldsymbol{h}_{n+1}=\boldsymbol{h}_n-\Delta\boldsymbol{h}$
4. Repeat steps 2 and 3 until the preset convergence criteria is satisfied

4.5.3 Modeling sources and sinks

The presence of singular sources or sinks such as pumps leads to instability of the solution and loss of accuracy in the whole domain, known as pollution effect. This has been studied by Tornberg and Engquist (2004), Ashyraliyev et.al., (2007), Rude et al., (2003) and Jung (2009). Many techniques have been proposed to overcome this problem. In this study, the Gaussian function regularization as suggested in Jung (2009) has been implemented which is a very simple yet very effective method.

In this approach, the singular δ-function i.e. the source or sink term is regularized as

$$\delta_N^{\epsilon}(x)=\frac{1}{\epsilon\sqrt{2\pi}}e^{-\frac{x^2}{2\epsilon^2}}$$

where the constant ϵ is given by, $\epsilon=2/N$ and

$$\lim_{N\to\infty}\int_{1}^{+1}\delta_N^{\epsilon}(x)dx=1$$

As observed in Jung (2009), this approach yields more regularized δ-function approximation on the collocation points. For the choice of parameter ϵ, Jung (2009) suggested that the parameter ϵ should be chosen properly so that $\delta_N^{\epsilon}(x)$ can be smoothly defined on the collocation points to guarantee the regularity within the approximation with given *N*. It was shown by the author that this approach yields only a first order convergence near the jump discontinuity. In this study, we have observed that this first order convergence is sufficient for regularizing the singularities i.e. sources or sinks in groundwater modeling.

4.5.4 Velocity computation

Velocity computations are performed by applying equation (3.23) which is Darcy's law (Bear, 1979),

$$V_x = -\frac{K_x}{n}\frac{\partial h}{\partial x} \; ; \; V_y = -\frac{K_y}{n}\frac{\partial h}{\partial y}$$

Applying the meshfree approximation, $h(\boldsymbol{x_I}, t) = \boldsymbol{\Phi}^T \boldsymbol{h}_s(\boldsymbol{t}) = \sum_{\boldsymbol{i=1}}^{\boldsymbol{n}} \phi_i h_i(t)$**,** the nodal velocities at the node *i* can be computed as,

$$V_{x_i} = -\frac{K_{x_i}}{n}\frac{\partial \boldsymbol{\phi}^T}{\partial x}\boldsymbol{h}_s(\mathrm{t}); \quad V_{y_i} = -\frac{K_{y_i}}{n}\frac{\partial \boldsymbol{\phi}^T}{\partial y}\boldsymbol{h}_s(t) \tag{4.54}$$

4.5.5 Dealing with anisotropy and heterogeneity

The groundwater flow and transport equations are given for confined and unconfined aquifers in eqns. (3.12), (3.16) and (3.19). For heterogeneous and anisotropic cases, the RPCM formulations are same as for in preceding sections for homogeneous cases except that the domain is divided into zones. The transmissivity of a zone is considered for all the nodes lying in that particular zone. The detail formulations and changes to be considered are discussed in section 4.9.

4.6 RPCM formulation for contaminant transport problem

The meshfree RPCM formulation of the groundwater solute transport equation can be done in a similar way to the formulation for groundwater flow equations. However, the transport equation requires seepage velocities in *x* and *y* directions to be calculated from the flow model. These velocities are also required for the computation of dispersion coefficients (eqn. 3.24). In this section, the RPCM formulation of the groundwater solute transport problem is demonstrated for both one and two dimensional cases. For the sake of simplicity not all processes / terms has been taken into account e.g. sources or sinks, reaction terms etc. have been neglected. Discretizing such terms does not pose any challenge to the RPCM formulation. Unlike groundwater flow equations, numerical modeling of solute transport suffers from instability when the advection term dominates over the dispersion term. A quantity called the Peclet

number is defined to measure the degree to which the transport problem is dominated by advection. Section 3.5 briefly discussed the instability caused by advection dominated flow. Liu and Gu (2005) discussed several ways in which this instability can be overcome while using meshfree RPCM formulation.

4.6.1 1D transport problem

Consider the one dimensional advection-diffusion equation

$$\frac{\partial C}{\partial t} = -v\frac{\partial C}{\partial x} + D_L\frac{\partial^2 C}{\partial x^2} \tag{4.55}$$

The meshfree RPIM approximation for the concentration function may be written as,

$$C(x,t) = \sum_{i=1}^{n} \phi_i(x) C_i(t) = \boldsymbol{\Phi}^T \boldsymbol{C}_s \tag{4.56}$$

where ϕ_i's are the shape functions as derived in eqn.(4.16) and $\boldsymbol{C}_s = \{C_1\ C_2 \dots C_n\}$ is a vector of concentrations at the nodes in the local support domain of the point, *x*. The seepage or linear velocity, *v* may be obtained from the flow model by using the computations as in eqn. (4.54). This computed seepage velocity may be used in eqn. (3.24) to compute the dispersion coefficient.

Now collocating at an internal (not on the boundary) node $x = x_r$ and substituting the function approximation in eqn. (4.56) to the one dimensional transport eqn. (4.55), the discretized equation is obtained as,

$$\left(\frac{\partial C}{\partial t}\right)_{x_r} = -v(x_r)\frac{\partial \boldsymbol{\Phi}^T}{\partial t}\boldsymbol{C}_s + D_L(x_r)\frac{\partial^2 \boldsymbol{\Phi}^T}{\partial t^2}\boldsymbol{C}_s \tag{4.57}$$

For time discretization, the θ-method, as discussed in the preceding sections, is applied. Eqn. (4.57) is then transformed as,

$$\frac{C_r^{t+\Delta t} - C_r^t}{\Delta t} = \theta\left\{-v_r\frac{\partial \boldsymbol{\Phi}^T}{\partial t} + D_{L_r}\frac{\partial^2 \boldsymbol{\Phi}^T}{\partial t^2}\right\}\boldsymbol{C}_s^{t+\Delta t} + (1-\theta)\left\{-v_r\frac{\partial \boldsymbol{\Phi}^T}{\partial t} + D_{L_r}\frac{\partial^2 \boldsymbol{\Phi}^T}{\partial t^2}\right\}\boldsymbol{C}_s^t \tag{4.58}$$

where the nodal index has been used to represent the collocation node e.g. v_r denotes $v(x_r)$. $\boldsymbol{C}_r^{t+\Delta t}$ is the nodal concentration at the current time t=$t + \Delta t$ while $\boldsymbol{C}_s^t$ is the concentration in the previous time step $t = t$. It is required that the nodal values of the concentration are known at the pervious time step to advance to the next time step.

Eqn. (4.64) is established for all the internal nodes. The implementation of the Dirichlet and Neumann boundary conditions can be performed in a similar way as demonstrated in the preceding sections for the flow equation. The terms of eqn. (4.64) can be re-arranged as,

$$\left[1+\theta\cdot\Delta t\left\{v_r\frac{\partial\boldsymbol{\Phi}^T}{\partial t}-D_{L_r}\frac{\partial^2\boldsymbol{\Phi}^T}{\partial t^2}\right\}\right]C_s^{t+\Delta t}=C_r^t+\Delta t(1-\theta)\left\{-v_r\frac{\partial\boldsymbol{\Phi}^T}{\partial t}+D_{L_r}\frac{\partial^2\boldsymbol{\Phi}^T}{\partial t^2}\right\}\boldsymbol{C}_s^t \tag{4.59}$$

Assembling the discretized equations for all the nodes (including the boundary conditions) will yield a matrix equation of the form,

$$[K]_{N\times N}\{C\}_{N\times 1}^{t+\Delta t}=[F]_{N\times N}\{C\}_{N\times 1}^{t} \tag{4.60}$$

Here $\boldsymbol{K}$ is the global system matrix arising out of the LHS of eqn. (4.65) while $\boldsymbol{F}$ is a coefficient matrix arising from the RHS of the same equation. $C^{t+\Delta t}$ is the vector of the nodal concentration values at the time $t=t+\Delta t$ and is the unknown in the above equation. With the initial condition is as the starting concentration values, eqn. (4.65) is used to evaluate the concentrations at the successive time steps.

4.6.2 2D transport problem

The discretization of the two dimensional transport equation (3.19) can be done in a similar manner as for the one dimensional case. The RBF point interpolation approximation of the concentration, $C(\boldsymbol{x},t)$ in this case is:

$$C(\boldsymbol{x},t)=\sum_{i=1}^{n}\phi_i(\boldsymbol{x})C_i(t)=\boldsymbol{\Phi}^T\boldsymbol{C}_s \tag{4.61}$$

The point collocation discretization using the function approximation in eqn. (4.67) yields the following equation at the node *r*, neglecting the source and reaction terms:

$$\begin{aligned}\left[R\boldsymbol{\Phi}^T-\theta\Delta t\left(D_{xx_r}\frac{\partial^2\boldsymbol{\Phi}^T}{\partial x^2}+D_{yy_r}\frac{\partial^2\boldsymbol{\Phi}^T}{\partial y^2}-V_{x_r}\frac{\partial\boldsymbol{\Phi}^T}{\partial x}-V_{y_r}\frac{\partial\boldsymbol{\Phi}^T}{\partial y}\right)\right]\boldsymbol{C}_s^{t+\Delta t}\\ =RC_r^t+(1-\theta)\Delta t\left[D_{xx_r}\frac{\partial^2\boldsymbol{\Phi}^T}{\partial x^2}+D_{yy_r}\frac{\partial^2\boldsymbol{\Phi}^T}{\partial y^2}-V_{x_r}\frac{\partial\boldsymbol{\Phi}^T}{\partial x}-V_{y_r}\frac{\partial\boldsymbol{\Phi}^T}{\partial y}\right]\boldsymbol{C}_s^t\end{aligned} \tag{4.62}$$

The seepage velocities V_x , $V_y$can be evaluated from the groundwater flow equation solutions using equation (4.54) as,

$$V_{x_r}=-\frac{K_r}{\theta}\frac{\partial\boldsymbol{\Phi}^T}{\partial x}\boldsymbol{h}_s\;;\;\;V_{y_r}=-\frac{K_r}{\theta}\frac{\partial\boldsymbol{\Phi}^T}{\partial y}\boldsymbol{h}_s \tag{4.63}$$

With the seepage velocities evaluated, the dispersion coefficients are computed using equation (3.29). Equation (4.62) are formed for all the internal nodes. For the boundary nodes, the proper boundary conditions have to be imposed as illustrated in previous sections. Let N be the total number of nodes including internal and boundary nodes. Then nodal discretized equations derived above for the groundwater flow equation can be assembled in matrix form as,

$$[K]_{N\times N}\{C\}_{N\times 1}^{t+\Delta t} = [F]_{N\times N}\{C\}_{N\times 1}^{t} \tag{4.64}$$

This equation can be solved, using any of the matrix inversion methods or by using iterative methods, for the concentrations at the current time $\{C\}^{t+\Delta t}$ given the concentrations at the previous time $\{C\}^{t}$.

4.7 RPCM model development

Based on the RPCM formulations presented in the previous sections, groundwater flow models (RPCM-GFM) for confined and unconfined aquifers, groundwater solute transport models (RPCM-GTM) and coupled groundwater flow and transport models (CFTM-RPCM) are developed. In this section, the stepwise model development process is being described.

4.7.1 Confined aquifer

The model development for confined aquifers is shown in the flow chart in Figure 4.5. Here the hydro-geological parameters to be collected (step1) are transmissivities, storativity, porosity, recharges and sources or sinks within the model domain. The transmissivity and storativity values are determined in the field using pumping tests and are normally a spatially variable quantity. The model is able to take into account varying zones for the hydro-geological parameters. These quantities are adjusted during the calibration of the model. The boundary conditions are also determined from the field data. Specified heads are obtained from river stages or water levels (connected to mean sea level) of the adjoining water bodies. The flux boundary conditions, being difficult to be determined by field experiments, are however determined and adjusted usually during the calibration process.

Following are the important steps in the groundwater flow model development:

Step 1: Model development starts with delineation of the model domain and collection of field measured hydro-geological data such as transmissivity, hydraulic conductivity, porosity, recharges, sources or sinks etc. The total simulation time and time-step size may also be decided at this stage

Step 2: Nodes are generated within the model domain and on its boundaries to represent the

domain in the numerical model.

Step 3: From the nodes generated, the RPIM shape functions are computed for each of the nodes by determining its local support domain.

Step 4: The groundwater heads are initialized to begin the simulation.

Step 5: The governing equations are discretized at each node by using the RPCM formulations derived in section 4.5 and by incorporating the field measured hydro-geological parameters and by applying the appropriate boundary conditions. These discretized nodal equations are then assembled to form the global system of equations.

Step 6: The global system equation is then solved using any of the numerical solvers such as Gauss-elimination, LU decomposition or iterative solvers.

Step 7: At this stage, calibration of the model parameters may be performed.

Step 8: Once the solution is obtained, the groundwater heads are re-initialized with the new solutions to proceed to the next time step. The solution process is repeated for all the time steps till the total simulation period is reached.

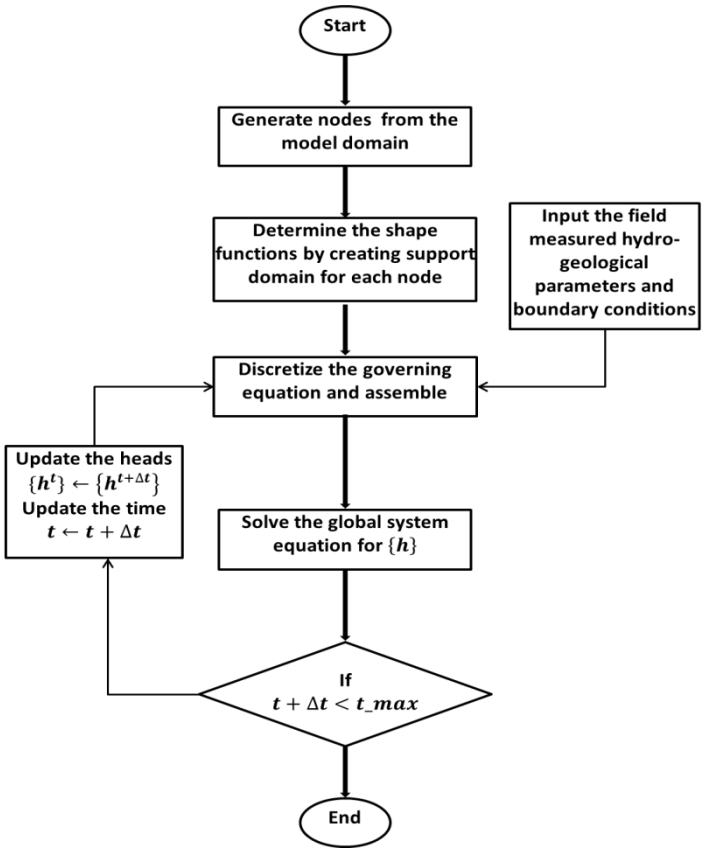

Figure 4.5 : Groundwater flow model development

4.7.2 Unconfined aquifer

For unconfined aquifers, the groundwater flow model development proceeds in the same manner as for the confined aquifer except that, being non-linear equation, the global system equation must be solved iteratively e.g. with the Newton-Raphson iterative method. Some the hydro-geological parameters are also different from the unconfined aquifer e.g. transmissivity and storativity are replaced by hydraulic conductivity and specific yield respectively.

Using Newton-Raphson iteration method for solving the global system matrix requires additional computations for evaluating the Jacobian and system matrix at every iteration step. The main steps of implementing Newton-Raphson iteration are:

Step 1: Set the convergence criteria

Step 2: Start with an initial guess for the hydraulic heads, $\{h^0\}$

Step 3: Compute the Jacobian matrix, J and the global system matrix, $K(h)$ using the guess solution

Step 4: Compute the corrections to the initial guess heads using the following formula:

$\{\Delta h\} = J^{-1}K(h_n)$ where h_n is the vector of guess solutions at n^{th} iteration

Step 5: Update the guess solution with the improved solution as,

$$\{h_n\} = \{h_n\} - \{\Delta h\}$$

Step 6: Repeat steps 3 to 5 until the convergence criteria is satisfied

4.7.3 RPCM transport model

The flow chart for developing RPCM groundwater solute transport model is shown in the Figure 4.6 and is based on the numerical formulations described is section 4.6. Following are the important steps in the groundwater solute transport model development:

Step 1: Model development starts with delineation of the model domain and collection of field measured data such as longitudinal and horizontal dispersivities, K_d values, bulk density of the soil, porosity, solute sources or sinks, reaction mechanisms of the solutes etc. The total simulation time and time-step size may also be decided at this stage

Step 2: Nodes are generated within the model domain and on its boundaries to represent the domain in the numerical model.

Step 3: From the nodes generated, the RPIM shape functions are computed for each of the nodes by determining its local support domain.

Step 4: The solute concentrations in the model domain are initialized to begin the simulation.

Step 5: The governing equations are discretized at each node by using the RPCM formulations

derived in section 4.6. At this stage the field measured hydro-geological parameters are incorporated and appropriate boundary conditions are then applied. The seepage velocities used in discretizing the transport equation are obtained from the flow model and using these velocities the dispersion coefficients are computed.

Step 6: These discretized nodal equations are then assembled to form the global system equation.

Step 7: The global system equation is then solved using any of the numerical solvers such as Gauss-elimination, LU decomposition or iterative solvers.

Step 8: At this stage, calibration of the model parameters may be performed.

Step 9: Once the solution is obtained, the initial solute concentrations are updated with the new solutions to proceed to the next time step. The solution process is repeated for all the time steps till the total simulation period is reached.

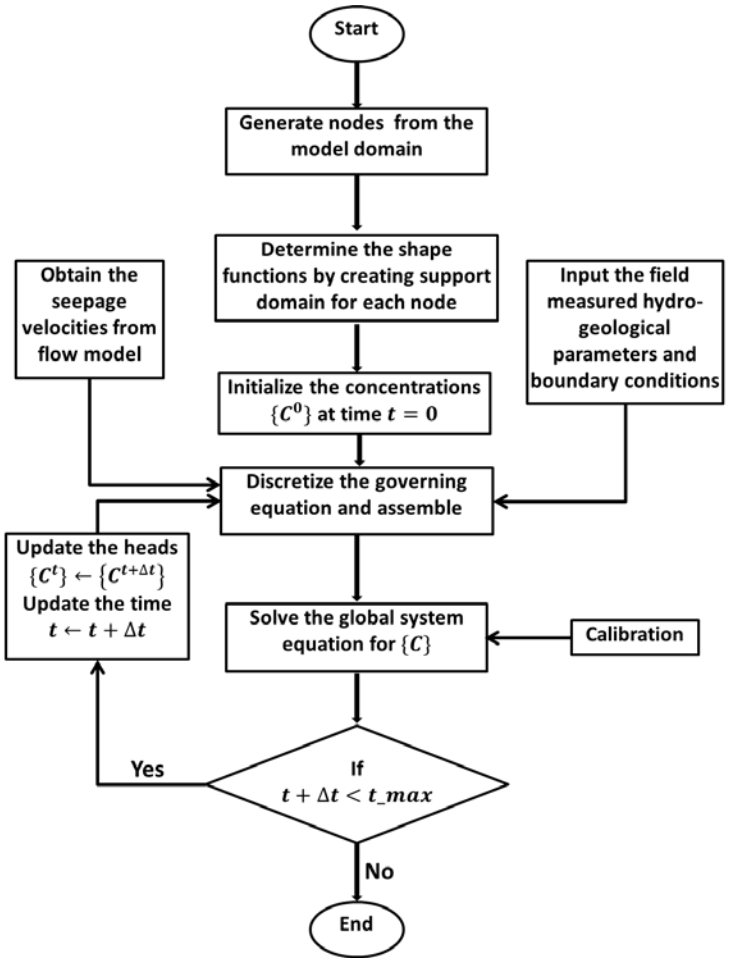

Figure 4.6: Flow chart for RPCM transport model

4.7.4 Coupled flow and transport model

The coupled flow and transport model is a coupling of the flow and transport models. Both the models are run at every time step. The flow chart for the coupled flow and transport model is shown in Figure 4.7. The coupling is provided through the transfer of the seepage velocity computations from the flow model to the transport model. As such at every time step, the flow model is solved first so that the seepage velocities can be computed using eqn. (4.54) and then the dispersion coefficients using eqn. (3.24). These computed values are used as inputs to the solute transport model.

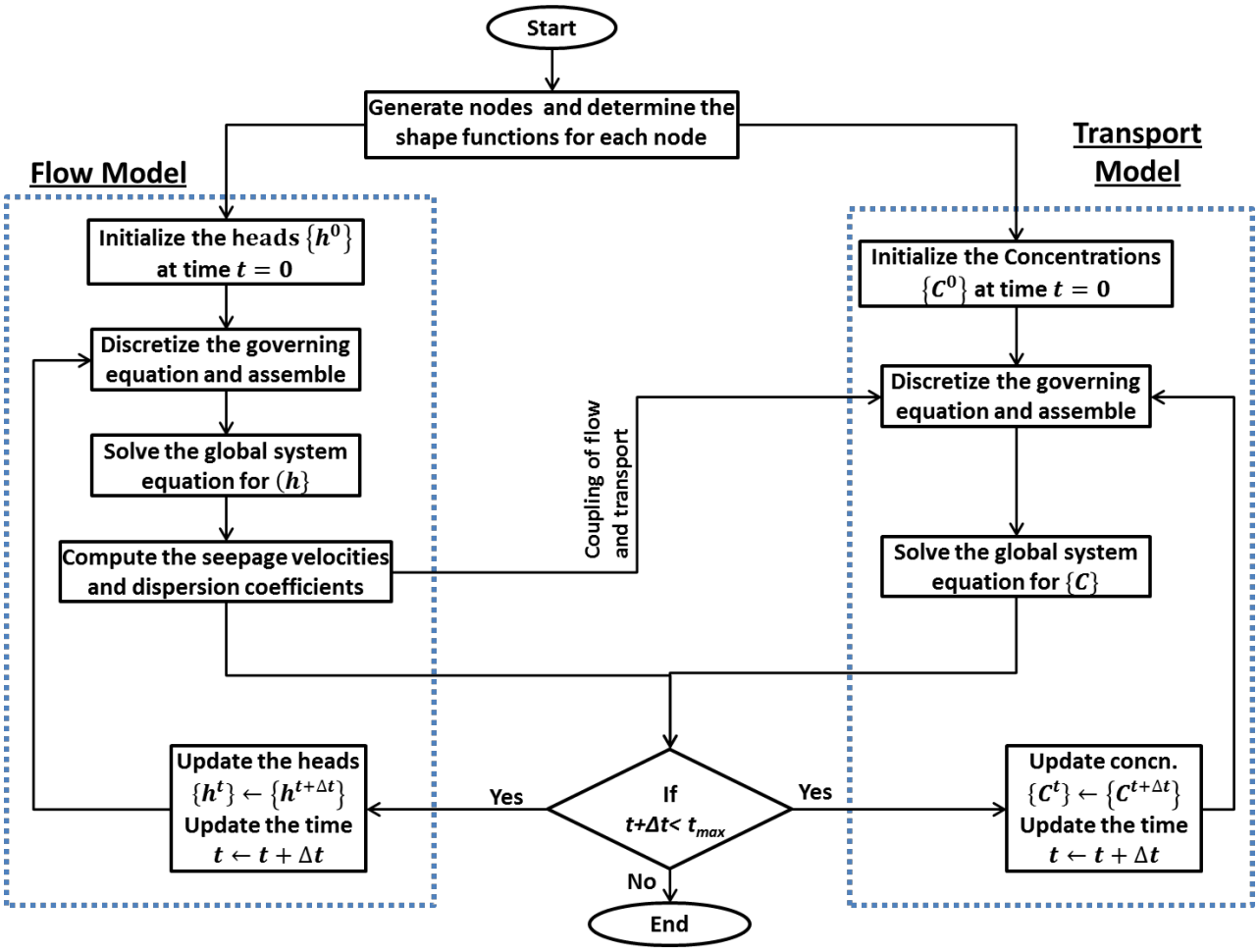

Figure 4.7: Flow chart of coupled groundwater flow and transport model

4.7.5 Model performance evaluation

The performance of the meshfree RPCM model can be measured using various metrics or error indicators, depending on the aspects to be examined. For the cases where the exact analytical solution is known, the

following error metrics or norms are defined for measuring the performance of the RPCM method (Liu and Gu, 2005):

Normalized RMS error of the solution, *u*:

$$e_0 = \left(\frac{\sum_{i=1}^{N} \left(u_i^{exact} - u_i^{num} \right)^2}{\sum_{i=1}^{N} \left(u_i^{exact} \right)^2} \right)^{1/2} \tag{4.65}$$

Errors in the first *x*-derivative of the function, *u*:

$$e_x = \left(\frac{\sum_{i=1}^{N} \left(u_{i,x}^{exact} - u_{i,x}^{num} \right)^2}{\sum_{i=1}^{N} \left(u_{i,x}^{exact} \right)^2} \right)^{1/2} \tag{4.66}$$

Errors in the first *y*-derivative of the function, *u*:

$$e_y = \left(\frac{\sum_{i=1}^{N} \left(u_{i,y}^{exact} - u_{i,y}^{num} \right)^2}{\sum_{i=1}^{N} \left(u_{i,y}^{exact} \right)^2} \right)^{1/2} \tag{4.67}$$

e_0 is a normalized root mean square error of the solution while the other two error metrics are for the derivatives of the solution or the dependent variable, *u*. Here u_i^{exact} are the exact values of the function, and u_i^{num} are the numerical values of the function obtained using the numerical method (meshfree RPCM). $u_{i,x}^{exact}$ is the exact values of the first *x*-derivative, and $u_{i,x}^{num}$ is the numerical value of the first *x*-derivative obtained using RPCM method while $u_{i,y}^{exact}$ is the exact values of the first *y*-derivative, and $u_{i,y}^{num}$ is the numerical value of the first *y*-derivative.

Apart from the above measures of error, the absolute Root Mean Square (RMS) error and maximum error (percentage) are also used to measure the performance of the RPCM solution.

4.8 Model verifications

The models developed in the preceding section 4.7, using the RPCM formulations of section 4.5 and 4.6 , are verified using analytical and numerically available solutions.

4.8.1 Model verification for two dimensional mesh free RPCM flow equation

The RPCM groundwater flow model (RPCM-GFM) developed is verified for both the confined and unconfined aquifers in this section. An additional general PDE is being solved using the meshfree RPCM formulation to demonstrate its general applicability.

4.8.1.1 General 2D-PDE equations with RPCM formulation

The RPCM formulation for a general 2D problem is verified with the following problem given in Xin (2006) and also in Liu and Gu (2005):

$$\nabla^2 u + u = (2 + 3x)e^{x-y} \quad , \quad (x, y) \in [0,1] \times [0,1] \tag{4.68}$$

with the boundary conditions

- Dirichlet BC:

$$u(x,y)|_{x=0} = 0 \;\; ; \;\; u(x,y)|_{y=0} = xe^{x} \tag{4.69}$$

- Neumann(Derivative) BC:

$$\left.\frac{\partial u}{\partial x}\right|_{x=1} = 2e^{1-y} \;\; ; \;\; \left.\frac{\partial u}{\partial y}\right|_{y=1} = -xe^{x-1} \tag{4.70}$$

The exact analytical solution to the above PDE is:

$$u^{exact}(x,y) = xe^{x-y} \tag{4.71}$$

The problem domain and the boundary conditions for this problem are shown in Figure 4.8. Dirichlet boundary conditions are imposed on the left and bottom boundaries are while Neumann boundary conditions are applied to the right and top boundaries. However, both the Neumann and Dirichlet boundary values vary as a function of the spatial coordinates. Also shown in the figure is the nodal distribution for a grid size of 11x11 nodes. A uniform grid size has been used along both the *x* and *y* directions in this case for simplicity. However, the node distribution need not be regular.

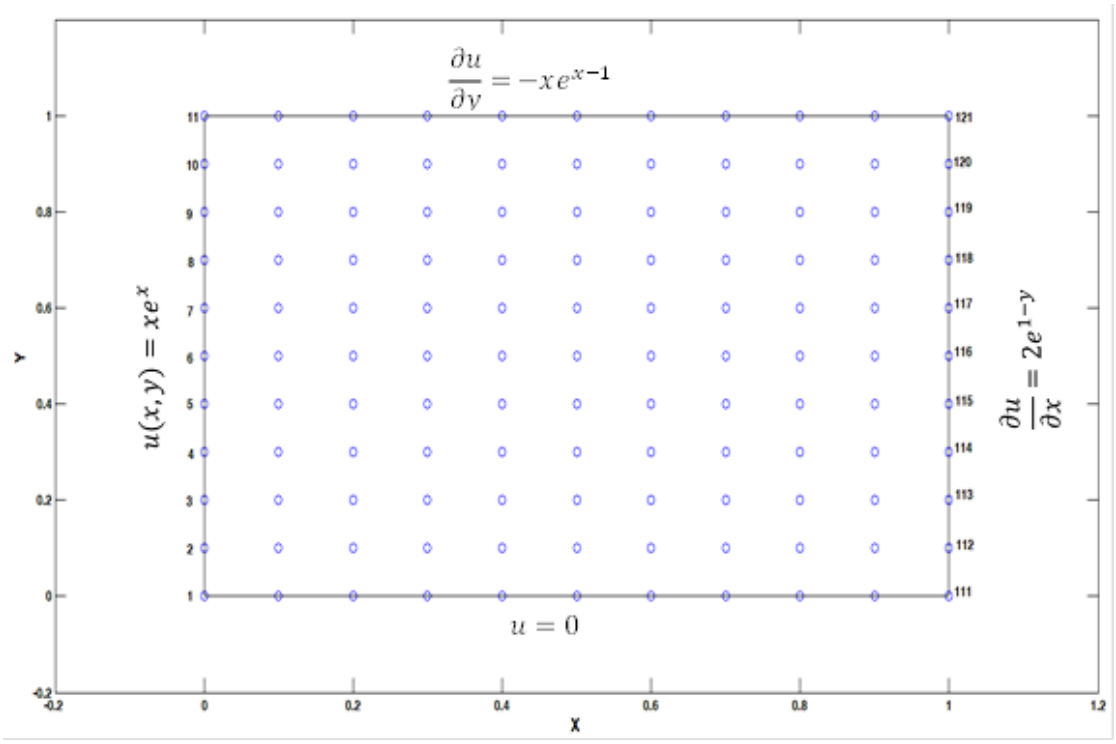

Figure 4.8: Problem domain, boundary conditions and nodal distribution (for 11x11 grid)

Eqn. (4.74) is solved by the RPCM flow model with the nodal distribution as shown in the Figure 4.8. The shape parameter (C_s) has been set to 3 times the nodal spacing and the radius (size) of the circular

support domain has also been set at 3 times the nodal spacing. These values have been set arbitrarily. The optimal values must been found by a sensitivity study. Figure 4.9 shows a comparison of the contour plots of the output from the meshfree RPCM model to the analytical solution. It is observed that the RPCM solution is indistinguishable from the analytical solution in this plot as the differences are in second or third decimal points. However an analysis of the error (percentage) shows that the maximum error is around 12% and that most of the errors are less than 5% of the true values. This may be observed from Figure 4.10 where the node wise comparison of the RPCM and analytical solutions is shown along with the node wise error (percent) of the RPCM solution.

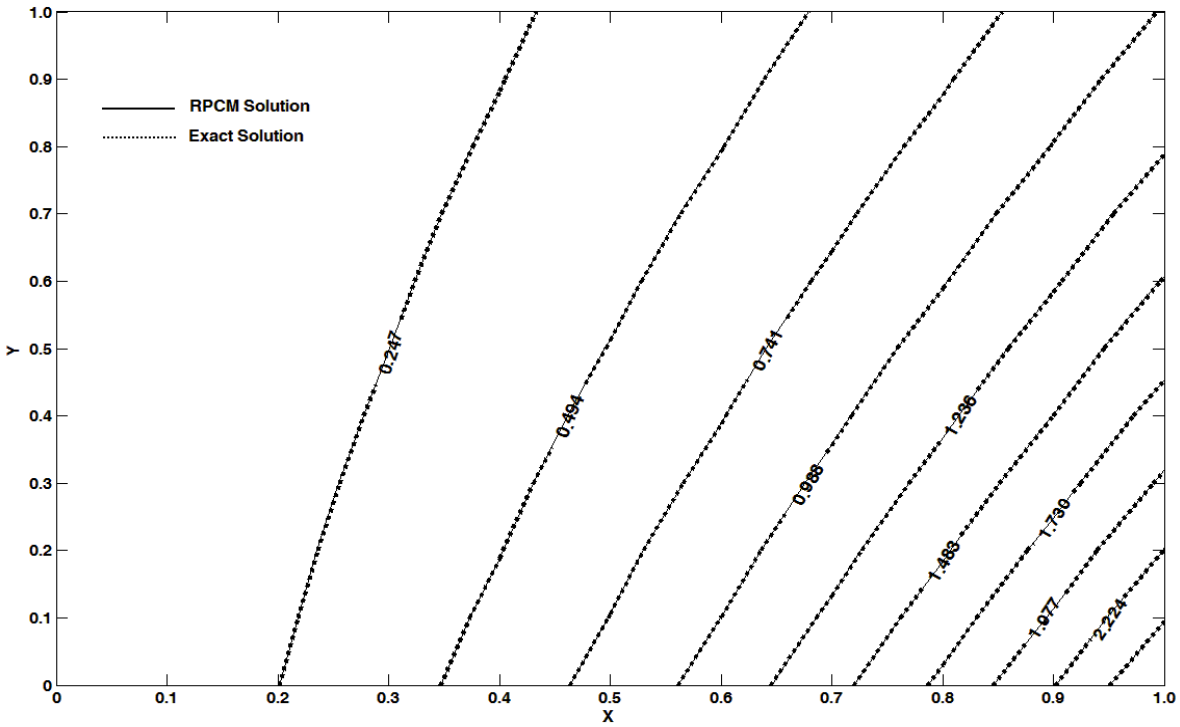

Figure 4.9: Comparison of meshfree RPCM solution with the analytical solution

It may be noted however that the parameters of the RPCM such as shape parameter and size of support domain used to obtain the above solutions have not been optimized. Also the grid spacing can also be reduced to obtain very accurate solutions. The effect of grid size, size of the support domain and value of shape parameter (α_c) on the accuracy of the RPCM solution are shown in Table 4.3 and Table 4.4. It has been found that the shape parameter C_s has the greatest impact on the accuracy and stability of the solution. Its' optimal value is range bound. A small value leads to poor accuracy. The solution accuracy improves as C_s becomes larger till an upper limit beyond which the solution becomes unstable and the method breaks down. As mentioned earlier, this upper limit has to be determined by numerical experimentation.

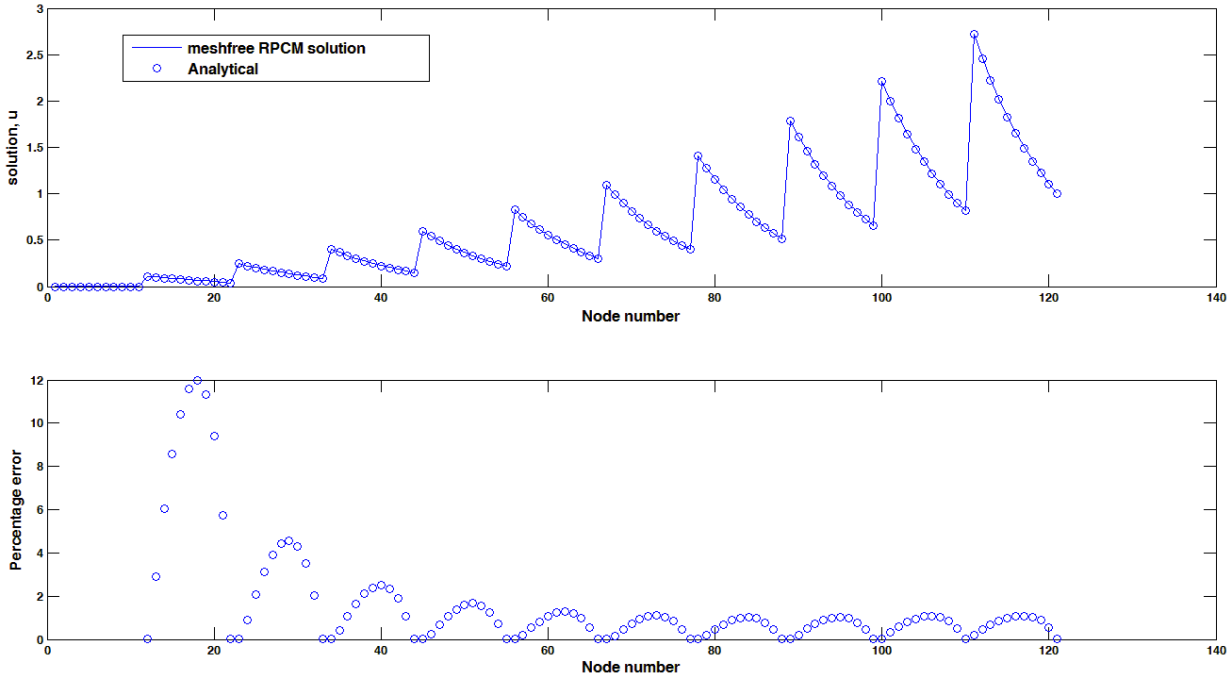

Figure 4.10: Node wise comparison of the RPCM and analytical solution and error

The local support domain size also influences the accuracy and the computational time. It was found that a local support domain size of 3 or 4 times the nodal distance leads to very good accuracy. Larger support domain sizes leads to much higher computational times without commensurate improvement in the accuracy of the solution. The number of grid points plays a role similar to finite difference and finite element methods. A very dense grid points can lead to a huge increase in the computational time.

Table 4.3 : Error measurements of the RPCM solution (radius of support domain=3 x nodal distance (dc)

	$\alpha_c = 3$			$\alpha_c = 5$		
Grid	20 x 20	30 x 30	40 x 40	20 x 20	30 x 30	40 x 40
Maximum error (%)	0.0059	0.0024	0.0087	0.0037	0.0018	6.192e-4
RMS Error	1.002e-4	3.82e-5	9.88e-5	6.58e-5	2.138e-5	4.85e-6
e_0	0.0024	0.0014	0.0048	0.0016	7.77e-4	2.347e-4
e_x	0.0031	0.0016	0.0026	0.0015	8.68e-4	4.53e-4
e_y	0.0091	0.0086	0.0182	0.0051	0.0027	0.0017

Table 4.4 : Effect of size of support domain (expressed as multiples of nodal distance, dc) on the solution (grid size: 30 x 30)

	$\alpha_c = 3$			$\alpha_c = 5$		
Size of support domain	2*dc	3*dc	4*dc	2*dc	3*dc	4*dc
Maximum error (%)	0.0244	0.0024	0.0063	0.0048	0.0018	0.0016
RMS Error	3.64e-4	3.82e-5	8.11e-5	5.86e-5	2.14e-5	1.90e-5
e_0	0.0132	0.0014	0.0029	0.0021	7.77e-4	6.91e-4
e_x	0.0059	0.0016	0.0022	0.0016	8.68e-4	6.75e-4
e_y	0.044	0.0086	0.0098	0.0072	0.0027	0.0024

4.8.1.2 Confined aquifer

For the verification of the mesh free RPCM formulation to two-dimensional groundwater flow problem, a hypothetical confined aquifer as shown in the Figure 4.11 is considered. This problem is found in Segerlind (1984). The aquifer is of dimension 5 km by 3 km and is bounded by impermeable layers on the northern and southern sides while on the eastern and western boundaries the piezometric head is maintained at 100m. The hydraulic transmissivities are $T_x = 30\, m/day$ and $T_y = 30\, m/day$ i.e the aquifer is isotropic. Two pumps are operating within the confined aquifer with pumping rates 400 m^3 /day (P2) and 600 m^3 /day (P1) as shown in the figure. As the presence of singular sources can lead to numerical instability of the solution (as discussed in section 4.5.3) if special treatments are not implemented, this problem will also demonstrate the effectiveness of the mesh free RPCM method to handle singular sources and sinks. The governing equation (steady state) for the confined aquifer with pumping is (see Eqn. 3.12)

$$T_x \frac{\partial^2 h}{\partial x^2} + T_y \frac{\partial^2 h}{\partial y^2} = Q\delta(x - x_p)(y - y_p) \tag{4.72}$$

As there is no analytical solution available for this problem, the mesh free RPCM solution is compared to the solution from FEM (COMSOL® Multiphysics). To examine the effect of the pumps, two cases are studied – one with only one pump (P1) operating and the other when both the pumps P1 and P2 are operating. The grid used for the mesh free solution is 51 x 31 i.e. 50 equal divisions along *x*-direction and 30 equal divisions along *y*-direction, corresponding to a regular grid with equal *x*- and *y*- sub-division size of 100 m, for a total of 1581 nodes. The nodal distribution is shown in Figure 4.12. In comparison, the FEM mesh used consists of 584 triangular elements and a total of 1231 nodes. The FEM mesh was generated by Delaunay triangulation. The size or radius of the local support domain is 4 times the nodal distance i.e. 200 m and the shape parameter is 3 times the nodal distance 150 m.

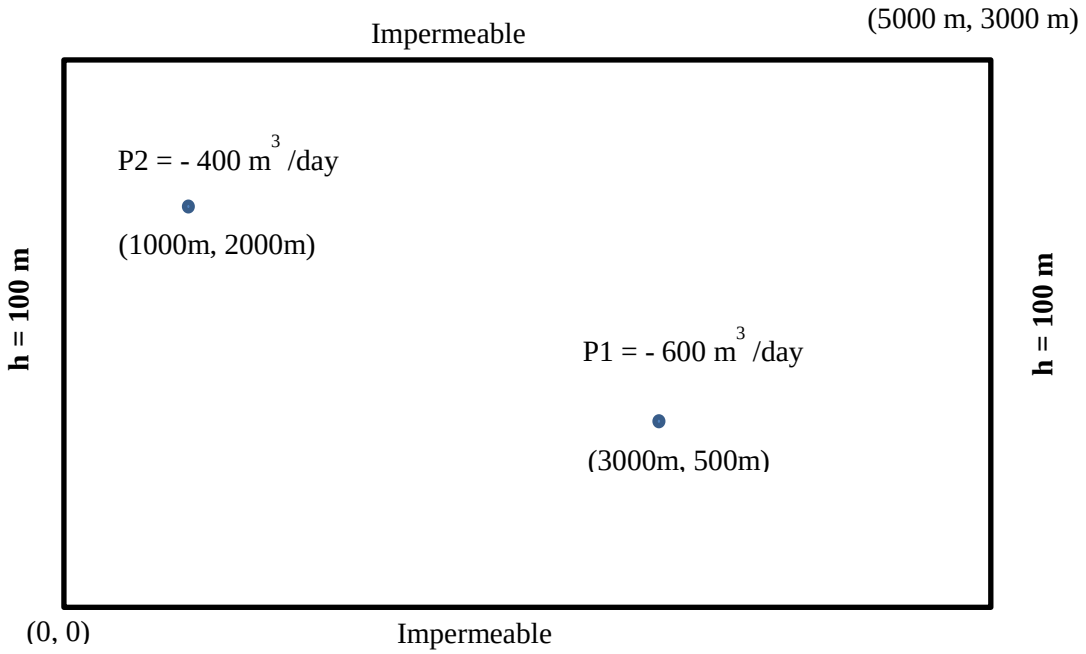

Figure 4.11 : Confined aquifer problem domain with two pumping wells

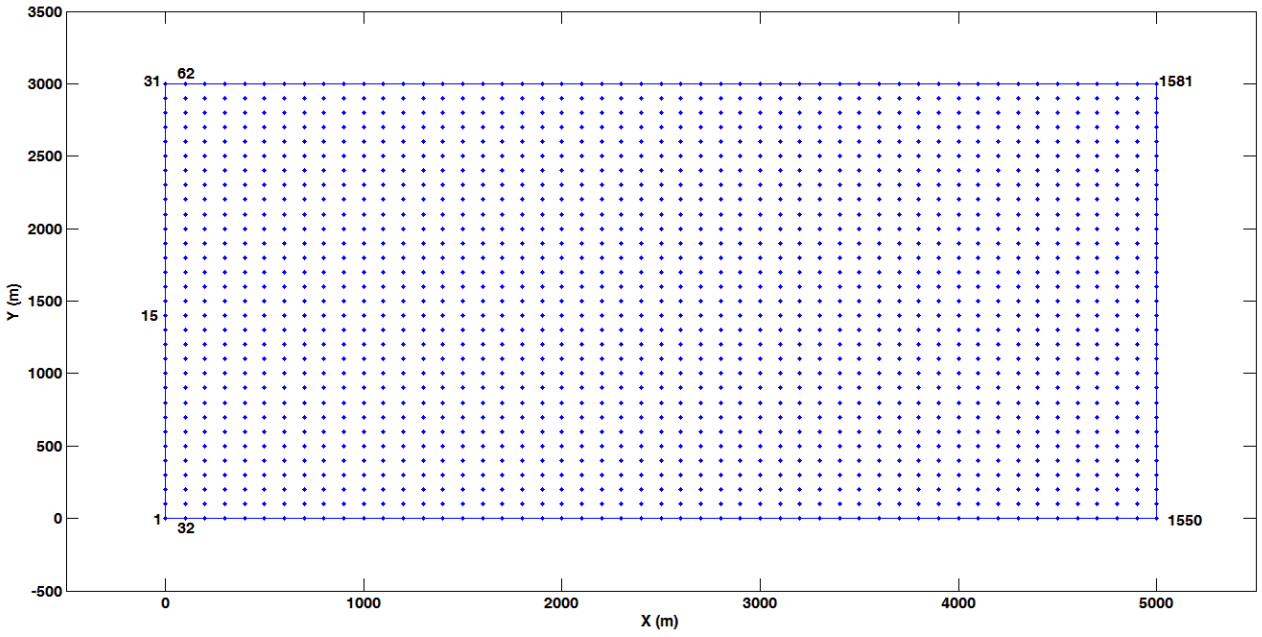

Figure 4.12: Nodal distribution used in the meshfree RPCM solution

Case 1: A single pump, P1 is assumed to be operating. A contour plot of the output from mesh free RPCM solution is shown in Figure 4.13. The solution obtained by FEM (COMSOL) is also shown alongside for comparison. It is seen that the mesh free and FEM solution agrees very well.

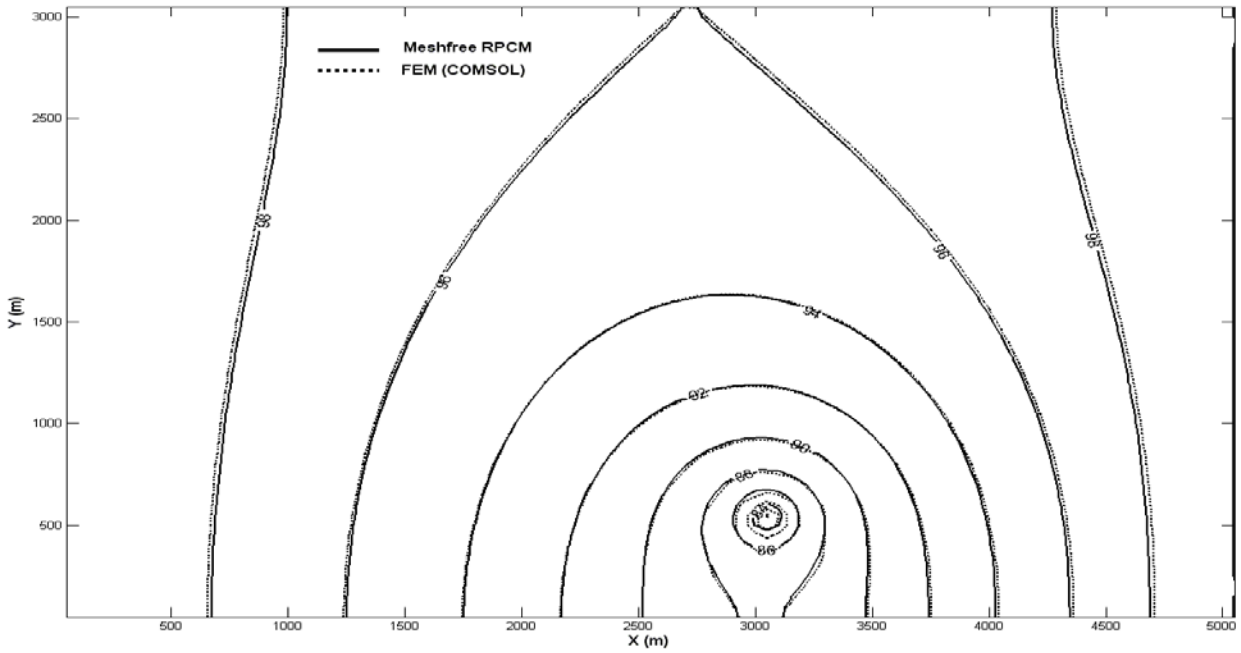

Figure 4.13: Comparison of Mesh free RPCM and FEM solution for the single pump case

Case 2: Here it is assumed that both the pumps P1 and P2 are operating. This case highlight the effect of one pump over another. Figure 4.14 shows a contour plot of the output from mesh free RPCM formulation. The effect of the simultaneous operation of the two pumps on the head distribution is clearly seen. Figure 4.15 shows a contour plot comparison of the solution from mesh free RPCM and FEM for this case. It is seen that the mesh free RPCM results agrees very well with the FEM results.

From the above comparative studies, it is observed that the RPCM solutions agree very well with FEM solutions. As the results show, with a simple Gaussian function representation of the pumping wells (singular sources) as described in section 4.5.3, the meshfree RPCM method is able to overcome the numerical instability very well and also gives very smooth contours near the wells. The RPCM solution may be made more efficient by employing lesser number of nodes. This can be done by employing an irregular node distribution where there are denser nodes in regions near the pumping wells and coarse nodes elsewhere. The FEM mesh uses this type of node distribution. However, in this demonstration example, for the sake of simplicity regular node distribution has been used regardless of the presence of the pumping wells. This case study demonstrates that the RPCM method can be effectively used for solving confined aquifer flow problems with pumping wells.

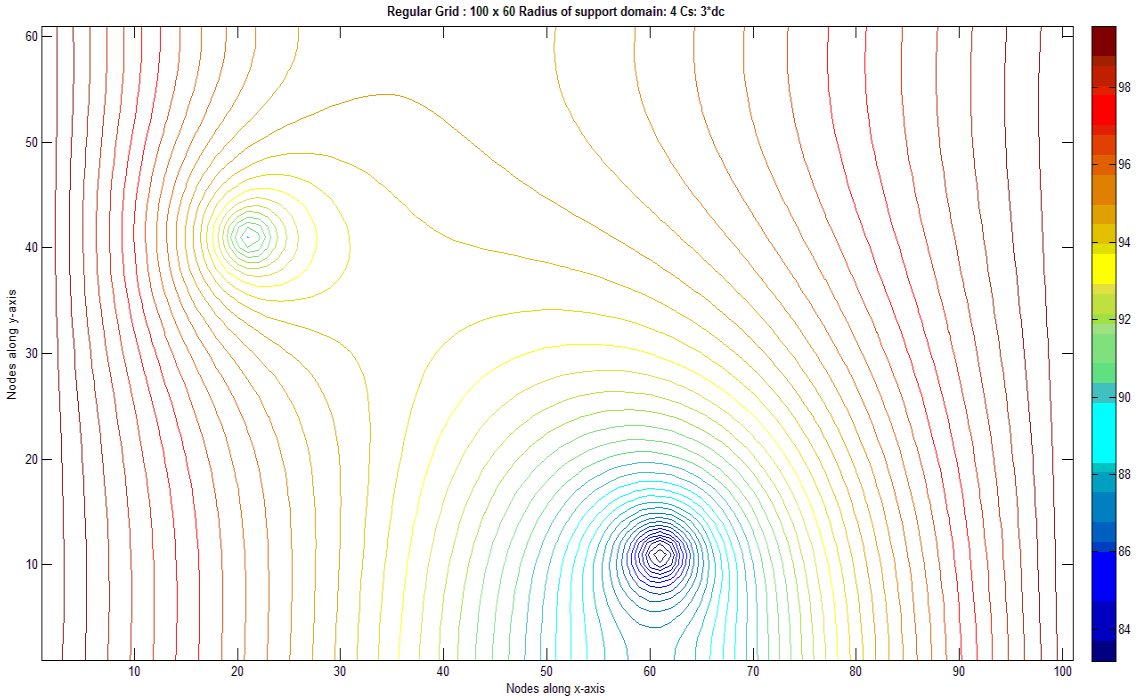

Figure 4.14: Mesh free RPCM solution of the confined aquifer problem with two pumps operating

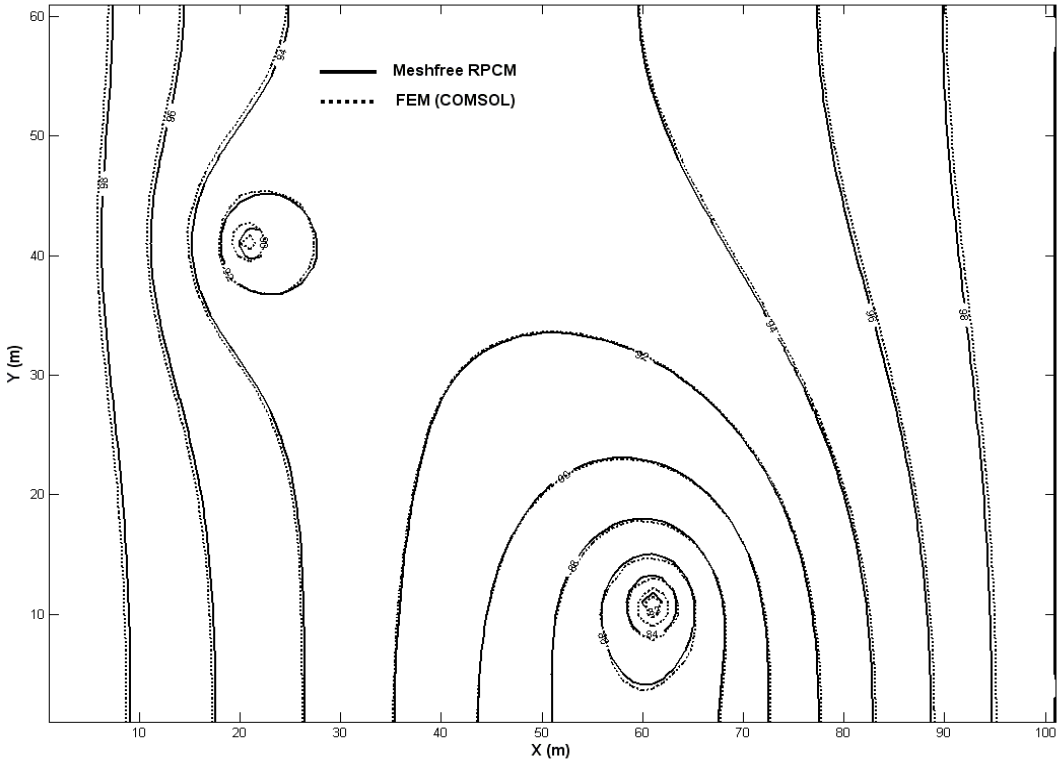

Figure 4.15: Comparision of mesh free RPCM and FEM solution for the confined aquifer problem with two pumps operating

4.8.1.3 Unconfined aquifer

As observed in section 4.5.2, the governing equation for two dimensional groundwater flow in an unconfined aquifer is non-linear and hence must be linearized first with a technique such as Newton-Raphson iteration method. To verify the applicability of the mesh free RPCM solution for this non-linear equation, a hypothetical aquifer as shown in Figure 4.16 below is considered. The boundary conditions are arbitrarily prescribed as in the figure to check the ability of the mesh free RPCM to handle all kinds of boundary conditions. It is also assumed that there are no sources or sinks or recharge taking place.

The governing equation for this unconfined aquifer is:

$$\frac{\partial}{\partial x}\left(\frac{\partial h}{\partial x}\right)+\frac{\partial}{\partial y}\left(\frac{\partial h}{\partial y}\right)=0 \tag{4.73}$$

The aquifer is assumed to be of dimension 100 m by 100 m. On the west and southern boundary, the head is prescribed (Dirichlet boundary condition). On the northern boundary, no flow boundary condition is imposed while on the eastern side, the flux is specified.

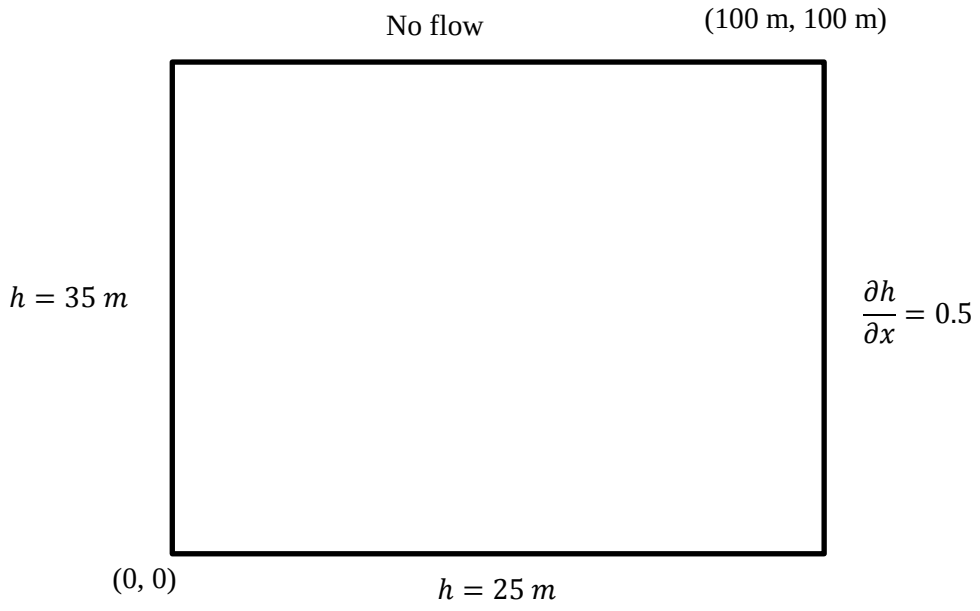

Figure 4.16 : An unconfined Aquifer

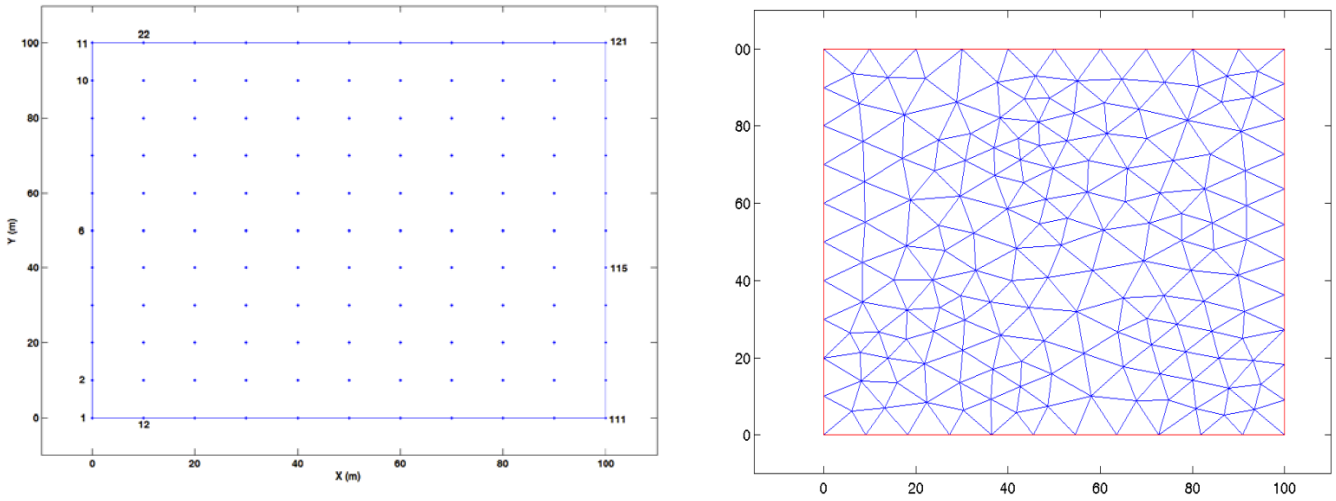

Figure 4.17: Node distribution used in RPCM solution (left) and mesh used in FEM solution (right)

The domain is subdivided into a 10 x 10 grid so that $\Delta x = \Delta y = 10\ m$ for a total of 121 nodes. The size (radius) of the support domain used was 4 times the nodal distance. The governing non-linear equation is solved by mesh free RPCM by using Newton-Raphson iteration method as formulated in section 4.5.2. The convergence criterion used for this problem is:

$$\frac{h^{j+1} - h^{j}}{h^{j}} \leq 0.1\% \tag{4.74}$$

where j is the iteration number. It was observed that convergence was achieved after 6 iterations. The same problem is solved by finite element method (FEM) using the PDETOOL toolbox of MATLAB for checking the performance of the mesh free RPCM method. The mesh used for the FEM solution consists of 318 triangular elements with 181 nodes. Figure 4.17 shows the node distribution used in the RPCM solution and the mesh employed in the FEM solution.

Figure 4.18 shows the comparison of the contour plot of the solution by FEM and Mesh free RPCM while Figure 4.19 shows the comparison of the mesh free and FEM solutions on node to node basis. The two figures show that both FEM and RPCM results agree very well.

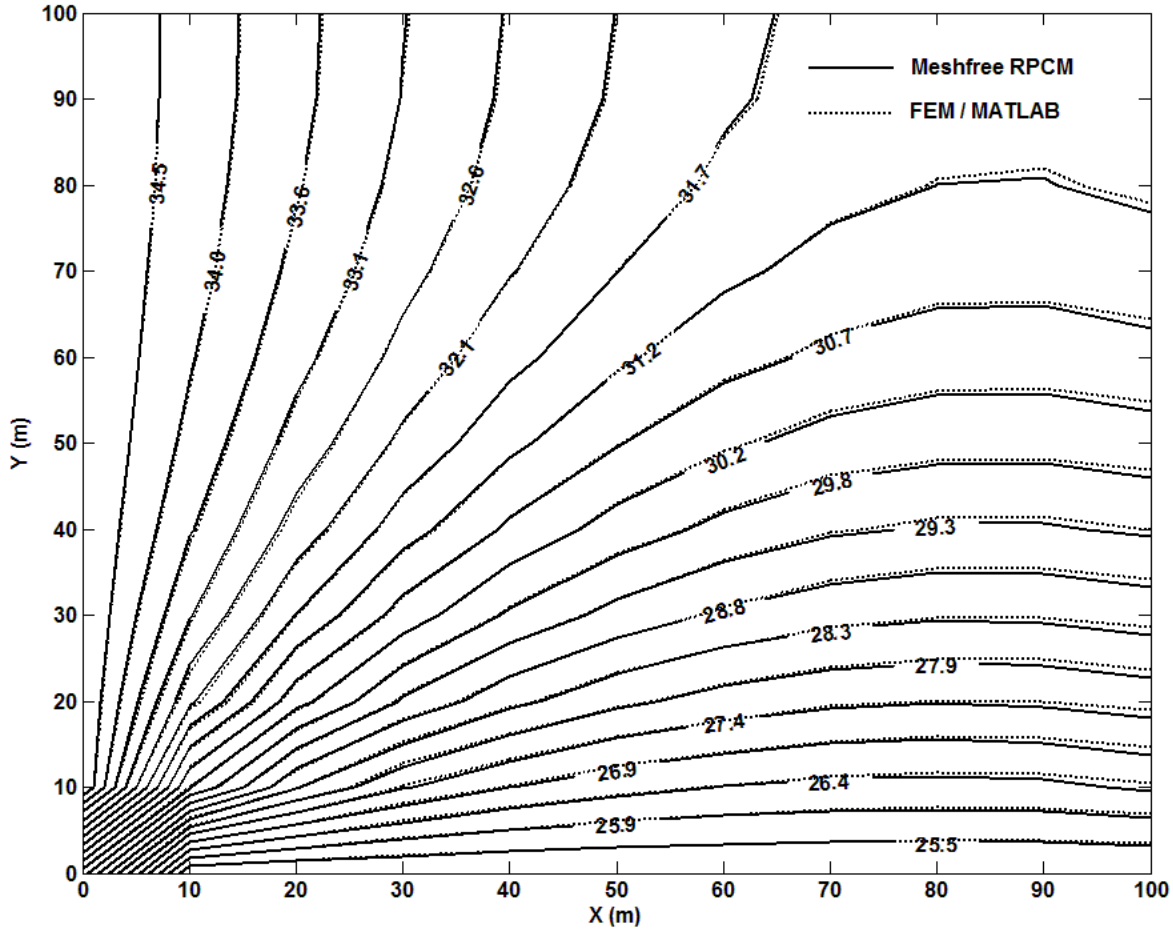

Figure 4.18 : Contour plot comparison of Mesh free RPCM and FEM (PDETOOL of MATLAB) solutions

To measure the agreement between the two results, the following metric called the root mean square error or difference is defined

$$RMSE = \sum_{i=1}^{N} \frac{(h^{RPCM} - h^{FEM})^2}{N} \quad , \text{ where } N \text{ is the number of nodes/points in the domain} \qquad (4.75)$$

The RMSE value for the present case is found to be 0.0028 which indicates the two results agree with each other up to the second decimal point. This confirms the very good agreement between meshfree RPCM and FEM (MATLAB PDETOOL). This problem demonstrates that the mesh free RPCM method can effectively be used for non-linear equations also.

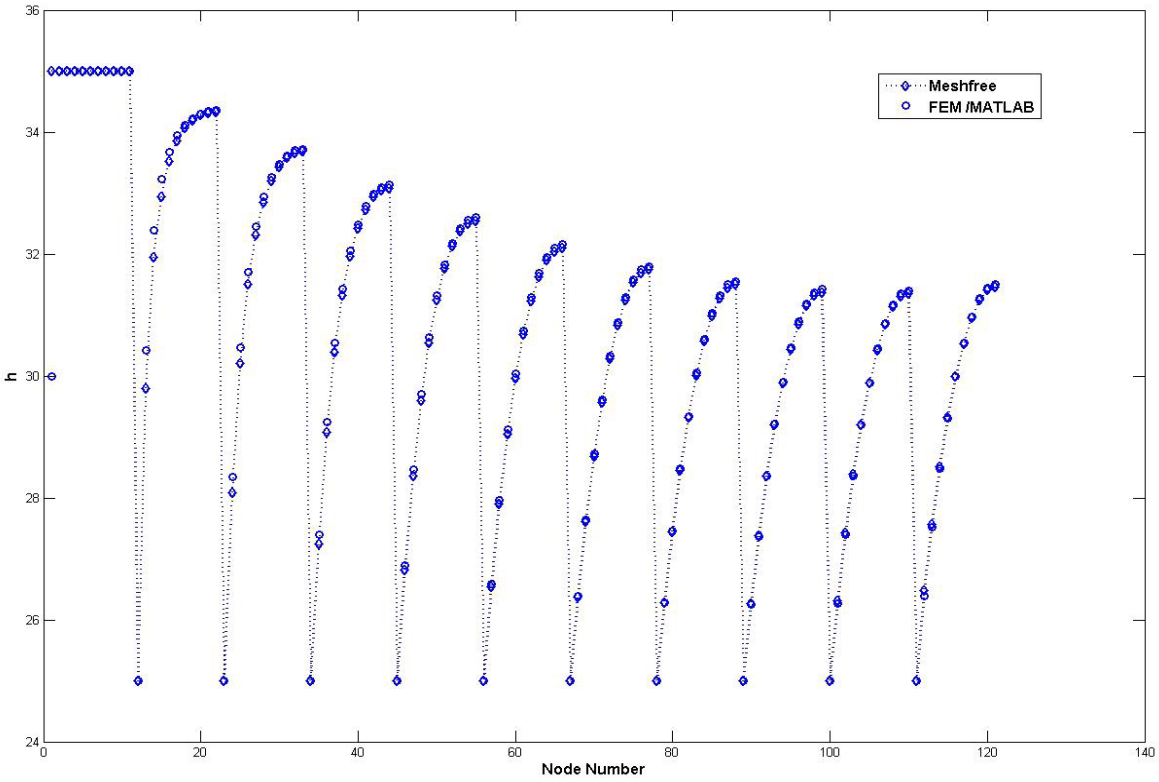

Figure 4.19 : Nodal plot of solution (in m) to the unconfined aquifer

4.8.2 One dimensional transport problem

For verification of one dimensional RPCM transport model, the following combined advection-dispersion equation is considered,

$$\frac{\partial C}{\partial t} = -v\frac{\partial C}{\partial x} + D_L\frac{\partial^2 C}{\partial x^2} \tag{4.76}$$

The boundary and initial conditions for the problem considered are:

Initial Condition: $C(x,0) = 0 \;\; , \; x \geq 0$;

Boundary conditions: $C(0,t) = C_0 \;\; , \;\; t \geq 0$ and $C(\infty,t) = 0 \; , \;\; t \geq 0$

The analytical solution to this problem has been given by Ogata and Banks (1961) as,

$$C(x,t) = \frac{C_0}{2}\left[erfc\left(\frac{x-vt}{2\sqrt{D_L t}}\right) + \exp\left(\frac{vx}{D_L}\right) erfc\left(\frac{x+vt}{2\sqrt{D_L t}}\right)\right] \tag{4.77}$$

where is x the distance from the injection point. To verify the RPCM method for this 1D transport problem, a one dimensional domain as depicted in Figure 4.20a is considered. Solute (contaminant) of concentration $C_0 = 500\, mg/L$ is injected at $x = 0$ and it is required to find the concentration at different a downstream distances ($x > 0$) after 2 years. The parameters used for this problem are (Delleur, 2007):

pore flow velocity (v) = 0.0259 m/day and longitudinal dispersion coefficient (D_L) = 0.0360 m^2 /day. The modeling domain is considered to be 1000 m in length, sufficient enough for the boundary condition $C(\infty, t) = 0$, $t \geq 0$ to be satisfied i.e. far away from the points where concentration is required. Considering the very small pore flow velocity of 0.0259 m/day, the above assumption regarding zero concentration boundary condition is justified since the simulation time considered is only 2 years. Figure 4.20b illustrates the construction of local support domain for a support domain size equal to twice the nodal separation (d_c).

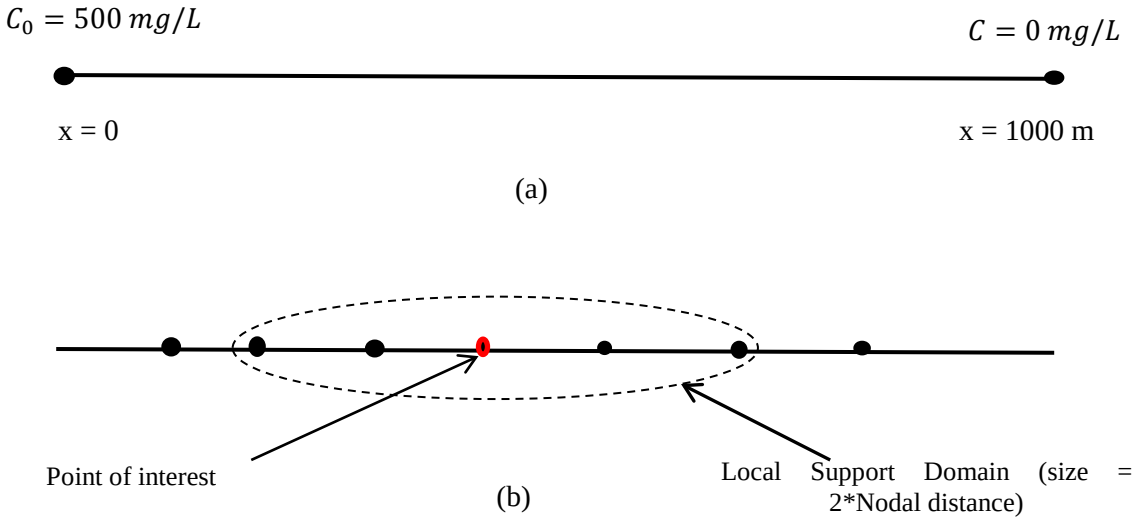

Figure 4.20 : One Dimensional Transport Problem

For finding the optimum value of the shape parameters for the RBF function used in the interpolation, a sensitivity analysis is performed. The RBF functions used in this study are the Multi-Quadrics and Exponential or Gaussian RBF. Figure 4.21 and Figure 4.22 shows respectively the results of the sensitivity analysis for each of the RBFs. It is found that for the MQ-RBF, the values of the shape parameter ($C_s = \alpha_c d_c$) in the range of 3 to 7 times the nodal separation gave very good accuracy whereas for the exponential RBF very good accuracy was observed when the shape parameter (α_c) was in the range from 0.1 to 0.08. It was observed that the exponential RBF was more sensitive to changes in the shape parameter values as compared to MQ-RBF. The values of the shape parameter can further be refined using some of the recent approaches suggested in Schaback and Wendland (2000), Rippa (1999), Wright (2003) etc. to obtain the optimum value.

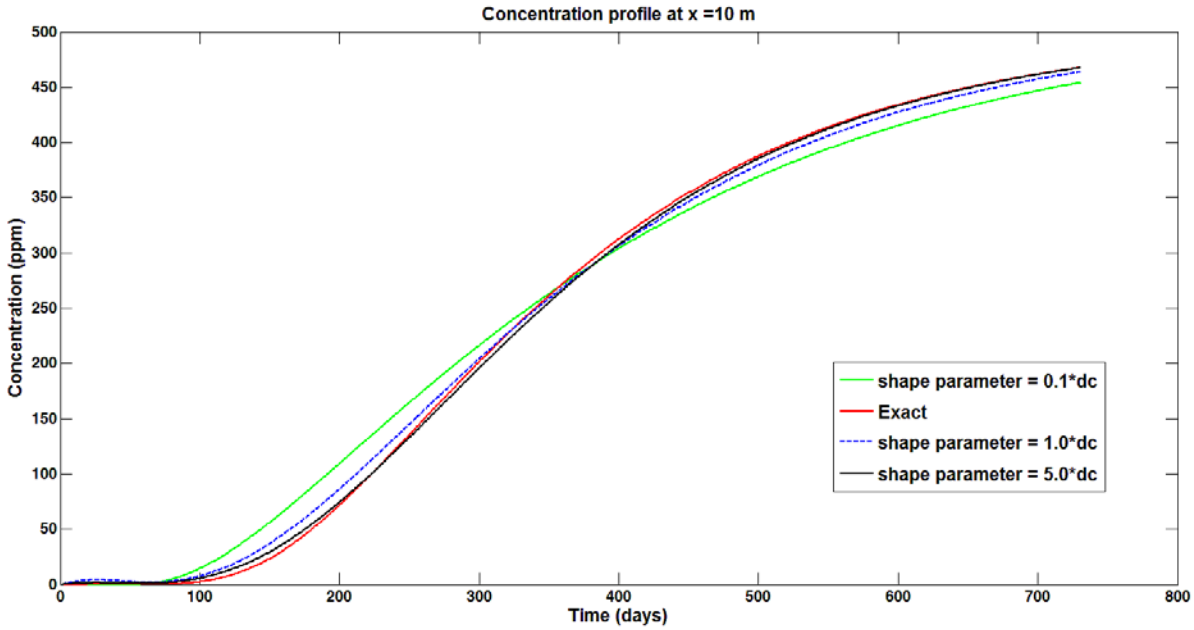

Figure 4.21 : Meshfree Concentration profile at 10m downstream as compared to the analytical result for various values of the shape parameter of the MQ-RBF (number of nodes : 301, size of support domain : 4 *dc)

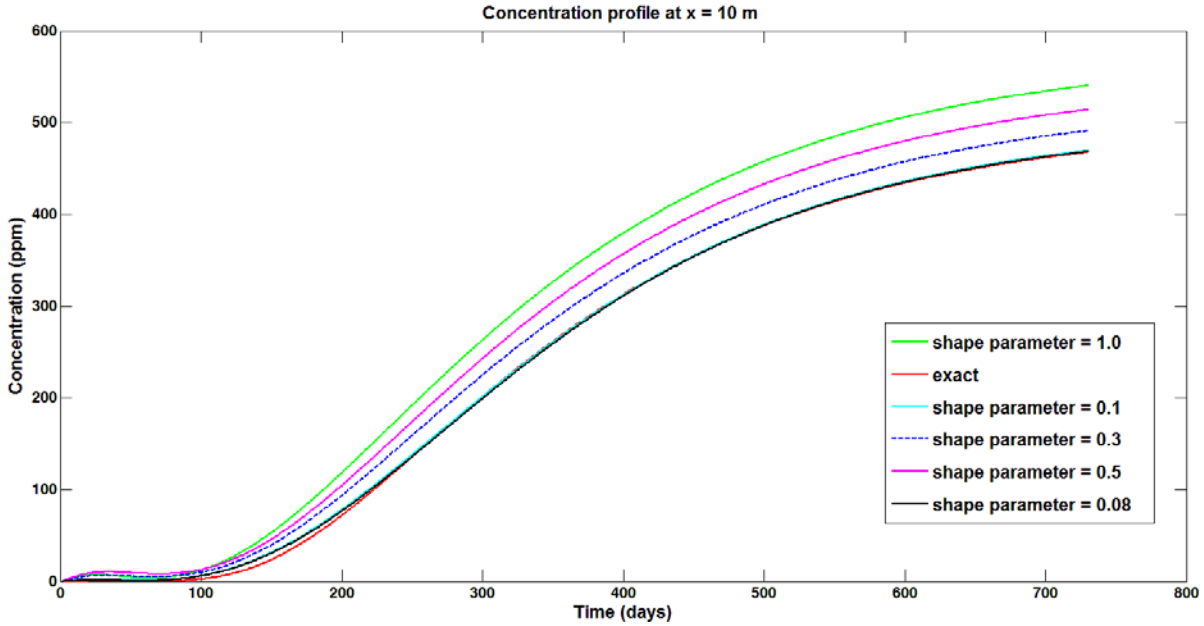

Figure 4.22 : Meshfree Concentration profile at 10 m downstream as compared to the analytical result for various values of the shape parameter of the EXP-RBF (number of nodes:301; size of support domain: 4*dc)

With the shape parameters determined, the 1D transport equation is solved and Figure 4.23 shows the concentration profiles at two downstream distances as compared to the exact solution of Ogata and Bank (1961). Results of using MQ-RBF and EXP-RBF as interpolation functions are also shown for comparison.

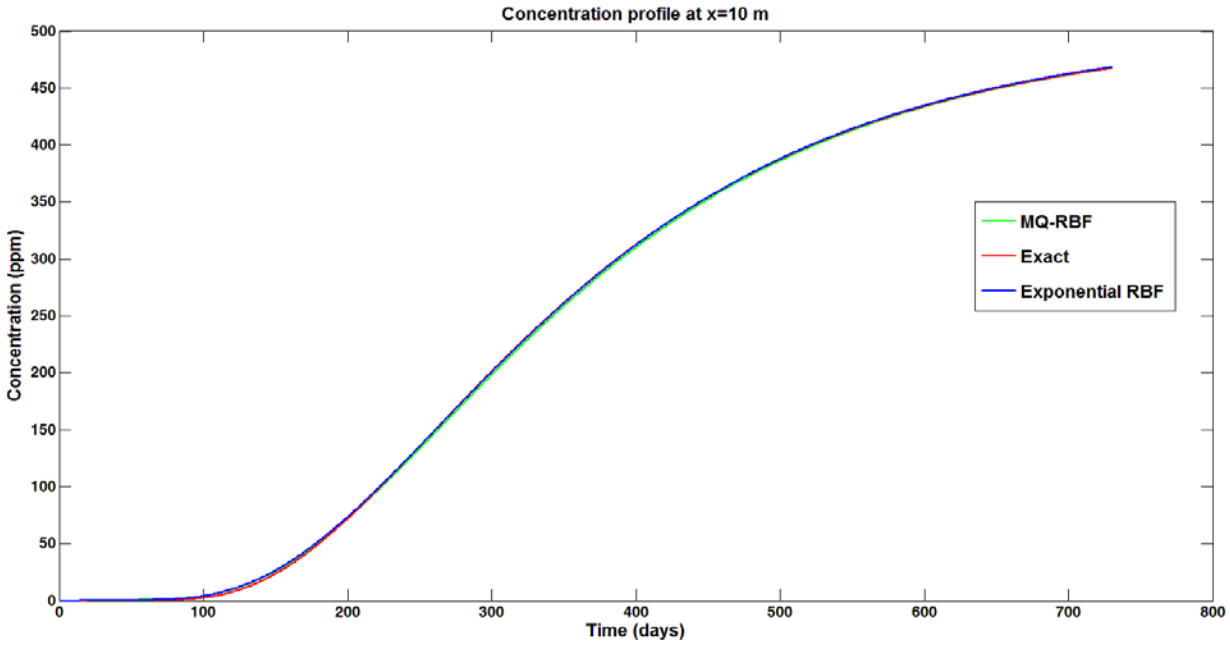

(a) Concentration profile at *x = 10 m*

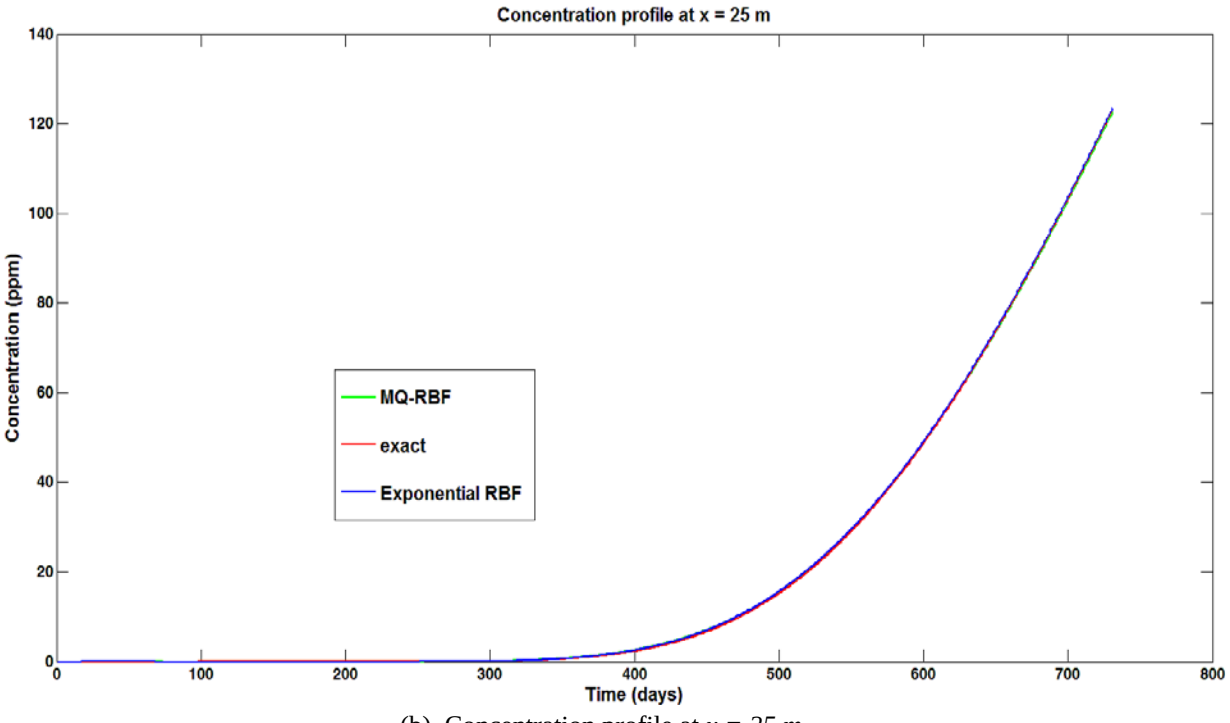

(b) Concentration profile at *x = 25 m*

Figure 4.23 : Concentration profile at downstream distance (a) x = 10 m and (b) x = 25m

In the above figures, number of nodes used for the simulation is 401 and the size of the support domain is 4 times the nodal separation (d_c). Since the analytical solution is known, the root mean square error (RMSE) as defined below is used as the measure of error:

$$RMSE = \sum_{i=1}^{N} \sqrt{\frac{\left(C_i^{num} - C_i^{exact}\right)^2}{N}} \tag{4.78}$$

Table 4.5 below shows the RMS error measures of the above plots:

Table 4.5: Error measures of the concentration profile plots of Fig. 4

RBF	***x = 10m***	***x = 25 m***
	RMSE	RMSE
Multi-quadrics	1.4	0.4
Exponential	1.6	0.6

From Figure 4.23a and b and Table 4.5, it can be seen that there is very good agreement between the mesh free calculated concentration values and the analytical results. It is also seen that both the MQ-RBF and EXP-RBF gave almost equally good results.

4.8.3 Two dimensional coupled flow and transport problem

For verification of the coupled groundwater flow and solute transport model, a two-dimensional transport of solute injected continuously from a point source in a steady-state uniform flow field is considered (Zheng and Wang, 1998). In this problem, it is assumed that a contaminant enters at a point, such as an injection well or toxic spill, and spreads through the aquifer with time.

The study area is shown in Figure 4.24. The flow model is surrounded by constant-head boundaries on the east and west borders and no-flow boundaries on the north and south borders. The head values at the

constant-head boundaries are arbitrarily chosen to establish the required hydraulic gradient so as to give a uniform flow field with groundwater seepage velocity (v) = 1/3 m/day. The simulation period is chosen so that the plume developed from the point source does not reach the boundaries. The model parameters used in the simulation are listed below (Zheng and Wang, 1998):

Cell width along rows (Δx) = 10 m, Cell width along columns (Δy) = 10 m, Layer thickness (Δz) = 10 m, Porosity (θ) = 0.3, Longitudinal dispersivity = 10 m, Ratio of transverse to longitudinal dispersivity = 0.3, Volumetric injection rate = 1 m^3 /day, Concentration of the injected water = 1000 ppm, Simulation time (t) = 365 days

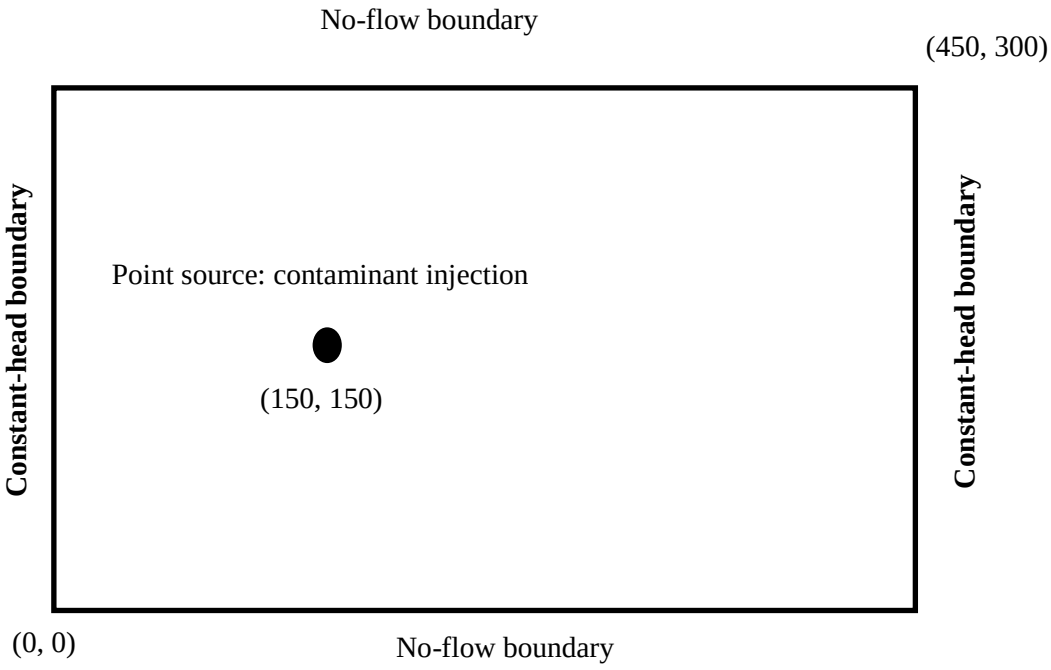

Figure 4.24 : Confined aquifer considered as benchmark for coupled flow and transport simulation

The study area has been divided into a 46 x 31 uniformly spaced nodes, along the x and y axes respectively and meshfree RPCM formulation as formulated in section 4.4.1 was applied. Figure 4.25 shows the nodal distribution used in the RPCM model .The node numbering scheme is also shown in the figure. The Crank-Nicholson scheme was implemented for time discretization with a time step of 5 days.

The same problem was solved with FEM using 1092 triangular elements and 585 nodes in COMSOL Multiphysics (www.comsol.com) for the purpose of comparison.

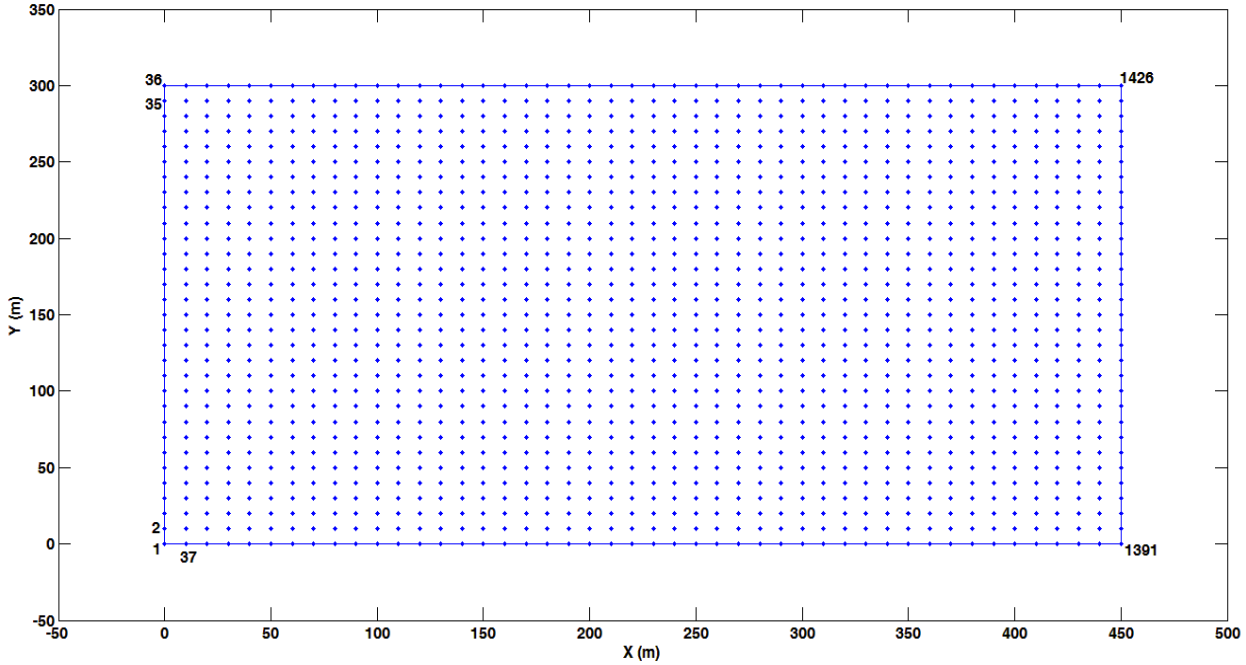

Figure 4.25: Node distribution for 2D transport problem

As in the 1D case, a numerical sensitivity analysis with respect to the size of support domain and the shape parameter value was conducted to arrive at an optimum value of these parameters taking into account the balance between accuracy, stability and computational time. While the support domain size mostly affects the computational time, the shape parameter has a profound impact on the accuracy and stability of the method. A support domain size (radius) of 3 to 4 times the nodal separation yielded sufficient accuracy within acceptable computational time.

For finding the optimum value of the shape parameter, a sensitivity analysis is performed for both the RBF functions viz. MQ-RBF and EXP-RBF. It is found that for the MQ-RBF, the values of the shape parameter ($C_s = \alpha_c d_c$) in the range of 3 to 7 times the nodal separation gave very good accuracy whereas for the EXP-RBF the optimum values of the shape parameter (α_c) was in the range from 0.1 to 0.08. It can be noted that the ranges of the shape parameters are same as for the 1D transport case.

Figure 4.26 shows the contour plot of the contaminant distribution at the end of the simulation time i.e. 365 days obtained by meshfree RPCM method using both the MQ-RBF and EXP-RBF as interpolation functions. It is observed that both MQ-RBF and EXP-RBF produces almost identical results and there is no way to conclude which RBF function is superior to the other. This means that we can freely choose either of the RBF functions provided the proper shape parameter values are used. The result from the FEM (COMSOL) simulation is also shown alongside for comparison. From the figure, it can be seen that there is good agreement between the meshfree RPCM and FEM results.

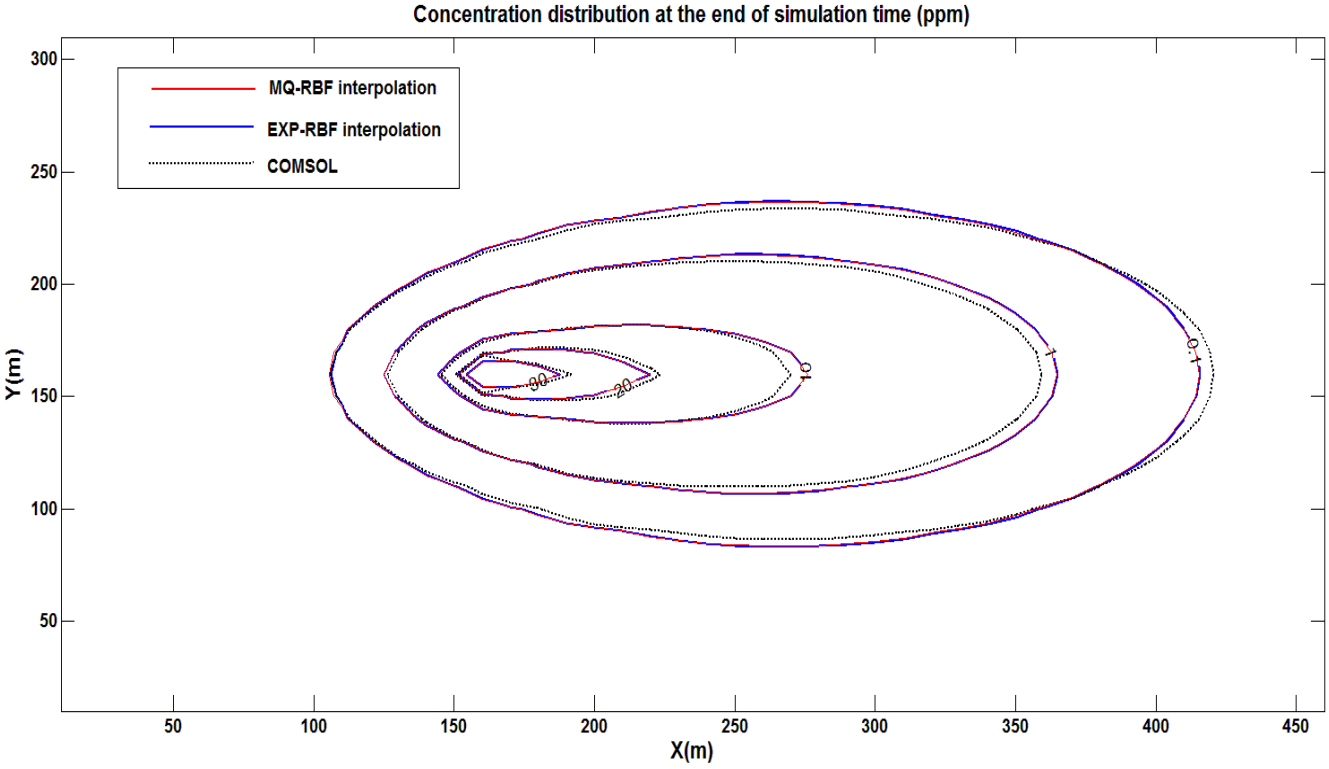

Figure 4.26 : Comparison of the meshfree RPCM and FEM solutions for two-dimensional transport from a continuous point source in a confined aquifer

4.9 Heterogeneous and anisotropic problem

Though the RPCM method offers implementation simplicity and exponential convergence in solving partial differential equations, the smoothness and non-locality of radial basis functions poses considerable difficulties in solving problems with local features and heterogeneity, specially when there is abrupt changes in the material properties (Chen, 2009). Presently, there is also a dearth of literature in addressing

the solvability of problems with heterogeneity and material interfaces using this class of methods. In groundwater modeling, there can be several zones of transmissivity or conductivity in a given modeling domain. The possibility of sudden change in conductivity from one zone to the other must be considered in developing meshfree methods.

For such problems with heterogeneity and material interfaces, application of the RPCM presents two major difficulties. One is due to the non-locality of the RBF, where the local characters cannot be precisely represented by the nonlocal approximation. The other is the difficulty of approximating derivative discontinuity across the material interface by the smooth RBF.

Chen (2009) has proposed the sub-domain radial basis collocation method to deal with such problems. In this approach, the whole domain is partitioned into different subdomains according to the heterogeneity of the problem. The solution of each subdomain is approximated only by the RBFs with source points located in the particular subdomain and on the boundaries of the subdomain. The strong form (collocation) of the original problem is first imposed at the collocation points in each subdomain using the RBFs in the same subdomain in such a way that they are treated as separate subdomain problems. The solution of the total domain is then obtained by gluing or joining the solution along the interfaces of the subdomains by imposing interface conditions with direct collocation. These interface conditions and the direct collocation of strong form and the associated boundary conditions are then solved simultaneously to obtain the overall solution of the original problem. The critical consideration in this approach is the type of interface conditions to be imposed.

4.9.1 Formulation of sub-domain collocation

We first consider the original heterogeneous problem of the following form:

$$L^{\tau}u^{\tau} = f^{\tau} \quad in \quad \Omega \tag{4.79}$$

$$B^{\tau}u^{\tau} = q^{\tau} \quad in \quad \partial\Omega \tag{4.80}$$

where Ω is the open domain, $\partial\Omega$ is the boundary of Ω; L^{τ} is the differential operator in Ω, B^{τ} is the boundary operator defined on $\partial\Omega$ which contains both the Dirichlet and Neumann boundary operators, f^{τ} is the source term, q^{τ} is a source term associated with boundary conditions. The superscript τ denotes the heterogeneity of the problem.

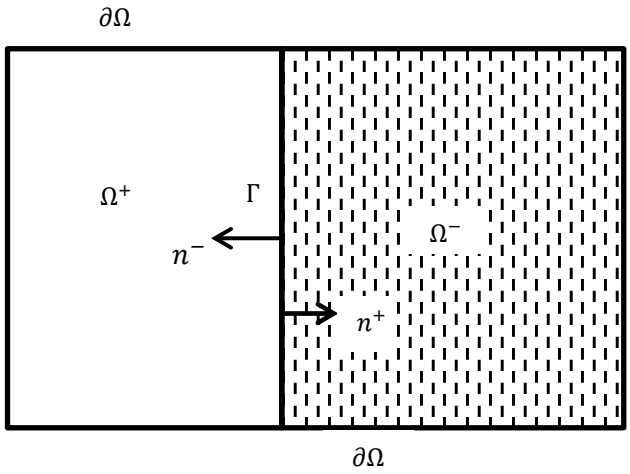

Figure 4.27 : Sub-Domains of a problem with material heterogeneity

For easy illustration we consider a domain composed of two materials, each occupies Ω^+ and Ω^- as shown in Figure 4.27. We denote by $\partial\Omega^+$ and $\partial\Omega^-$ the boundaries of Ω^+ and Ω^-, respectively; and closed domains $\bar{\Omega} = \Omega \cup \partial\Omega$, $\bar{\Omega}^+ = \Omega^+ \cup \partial\Omega$, $\bar{\Omega}^- = \Omega^- \cup \partial\Omega^-$, and we have $\bar{\Omega} = \bar{\Omega}^+ \cup \bar{\Omega}^-$, $\Omega^+ \cap \Omega^- = \emptyset$ and $\Gamma = \partial\Omega^+ \cap \partial\Omega^-$ is the interface. In each subdomain, the material is homogeneous. We consider the transformation of the original problem to the following subdomain problem:

$$\begin{aligned} L^+u^+ &= f^+ \quad in \quad \Omega^+ \\ B^+u^+ &= q^+ \quad on \quad \partial\Omega^+ \cap \partial\Omega \end{aligned} \tag{4.81}$$

$$\begin{aligned} L^-u^- &= f^- \quad in \quad \Omega^- \\ B^-u^- &= q^- \quad on \quad \partial\Omega^- \cap \partial\Omega \end{aligned} \tag{4.82}$$

$$I(u^+, u^-) = 0 \quad on \quad \Gamma \tag{4.83}$$

Where *I* is the operator representing interface conditions on Γ , which plays a crucial role on the accuracy and convergence of the proposed method. The solution of the originally heterogeneous problem in equations (4.79) & (4.80) is now solved in each subdomain i.e. equations (4.81) and (4.82), separately, with additional interface condition in equation (4.83) to 'glue' the two subdomain solutions together. Appropriate construction of the interface condition operator is important. In case of groundwater modeling, both the Dirichlet and Neumann boundary conditions are implemented as the interface conditions. The Dirichlet boundary condition ensures the continuity of the head across the interface while Neumann boundary condition ensures the continuity of Darcy flux across the interface. The solution in each subdomain is approximated by separate set of basis functions

$$u^h(x) = \begin{cases} u^{h+}(x) = g_1^+(x)a_1^+ + \cdots + g_{N_s^+}^+(x)a_{N_s^+}^+, & \boldsymbol{x} \in \bar{\Omega}^+ \\ u^{h-}(x) = g_1^-(x)a_1^- + \cdots + g_{N_s^-}^-(x)a_{N_s^-}^-, & \boldsymbol{x} \in \bar{\Omega}^- \end{cases} \tag{4.84}$$

Where N_s^+ and N_s^- are the number of source points in the two subdomains, and $\{g_I^+\}_{I=1}^{N_s^+}$ and $\{g_I^-\}_{I=1}^{N_s^-}$ are two sets of RBFs with their corresponding source points $\{x_I^+\}_{I=1}^{N_s^+}$ and $\{x_I^-\}_{I=1}^{N_s^-}$ located in $\overline{\Omega}^+$ and $\overline{\Omega}^-$ respectively. The coefficients $\{a_I^+\}_{I=1}^{N_s^+}$ and $\{a_I^-\}_{I=1}^{N_s^-}$ are obtained by solving strong form collocation and interface conditions of equations (4.82) - (4.84) simultaneously.

4.9.2 Numerical example

To illustrate the sub-domain collocation approach, let us consider the confined aquifer as shown in Figure 4.28. This problem is adapted from Zheng and Wang (1998). The hydraulic conductivity of the aquifer is 1.474 x 10^{-4} m/s except for a zone of low conductivity (shaded in the figure) where the conductivity is 1.474 x 10^{-7} m/s i.e. the conductivity is 1000 times lesser than other areas of the aquifer. This means there is a very sharp transition of conductivity values from this zone to the rest of the domain. The boundary conditions are as shown in the figure. The top and bottom boundaries are constant head boundaries (with specified head values as in Figure 4.28) while the left and right boundaries are impermeable boundaries.

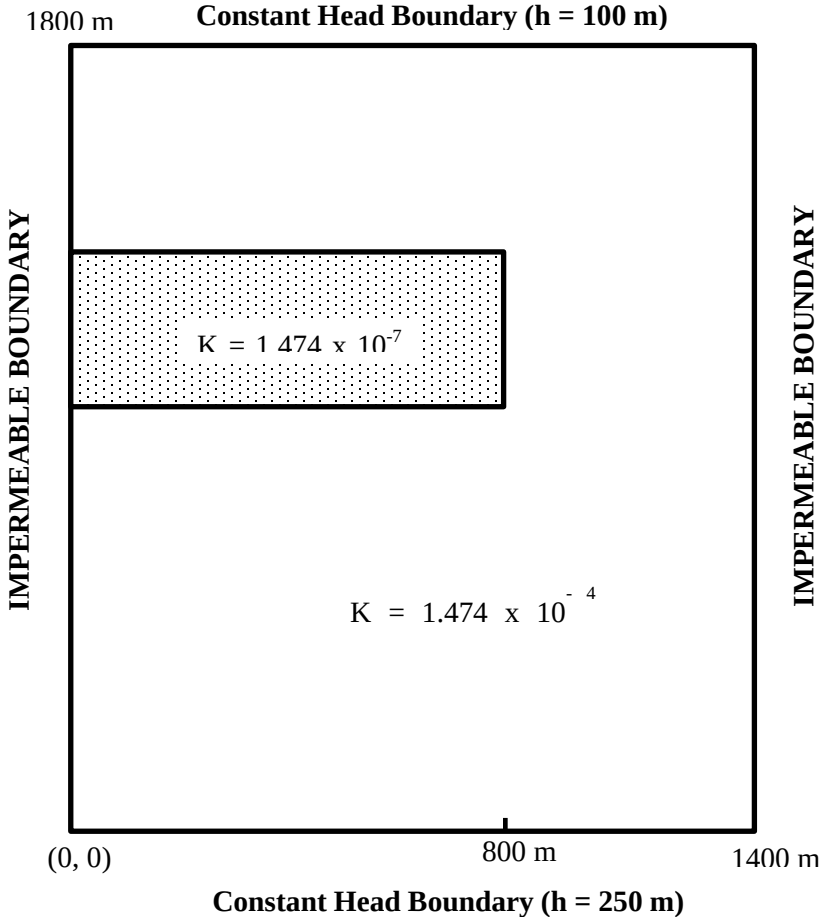

Figure 4.28 : An aquifer with a zone of very small conductivity

This problem is solved first by using RPCM without implementing sub-domain collocation. The domain was divided into uniform grids of size 100m x 100m. Figure 4.29 shows the contour plot of the groundwater heads as calculated by the RPCM method. It is very clear from this figure that RPCM method is unable to capture the heterogeneity of the problem. Reducing the grid size to 25 m x 25 m (a relatively fine grid) produced the same output. This failure to capture the heterogeneity is due to the smooth nature of the RBF functions used in the interpolation.

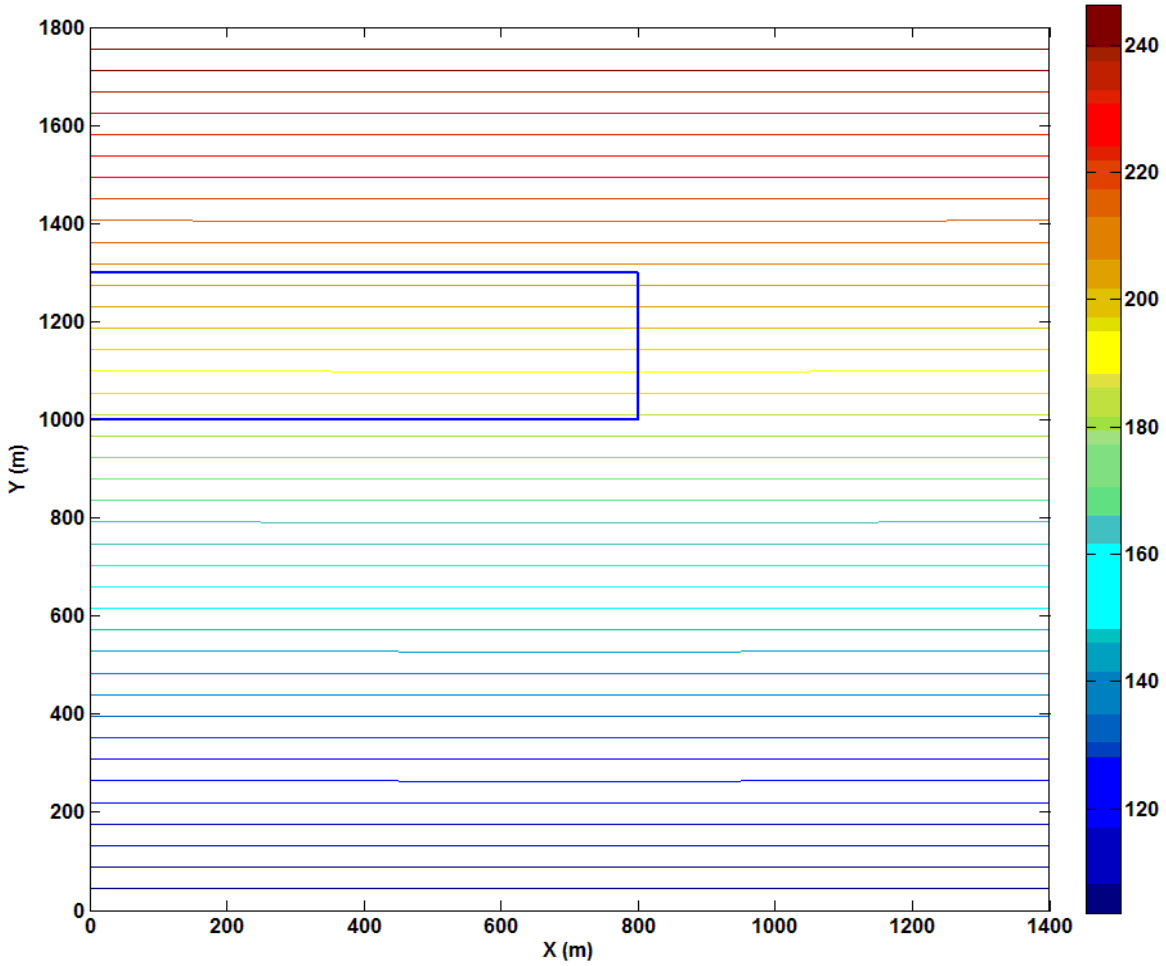

Figure 4.29: Contour of groundwater heads (m) calculated by RPCM method without implementing sub-domain collocation

The same problem is solved using the sub-domain collocation approach (Chen, 2009). The interface conditions used are- Dirichlet and flux continuity. The Dirichlet condition ensures the continuity of the piezometric head across the interface while the flux continuity conserves the Darcy flow flux across the interface. The output from the program is shown below in Figure 4.30. Also shown is the FEM (COMSOL) solution of the same problem for comparison purpose (Figure 4.31). The FEM mesh had

1884 triangular elements with 971 nodal points. The RMSE error (as defined in 4.78) calculated for this case study is 0.152 which confirms the very good agreement between FEM and the meshfree RPCM results. Table 4.6 shows the numerical comparision between the heads (in m) as predicted RPCM and FEM (COMSOL) for certain selected points as shown in Figure 4.32. It is clear that by implementing sub-domain collocation approach, RPCM method is able to capture the heterogeneity of the problem.

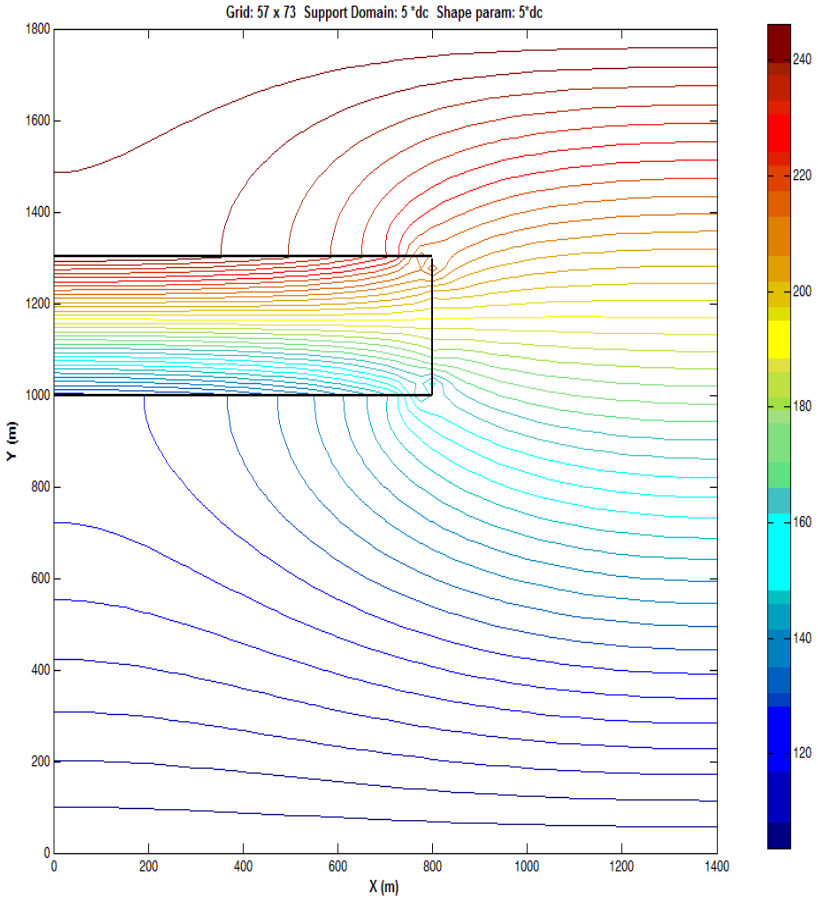

Figure 4.30: Meshfree RPCM Output

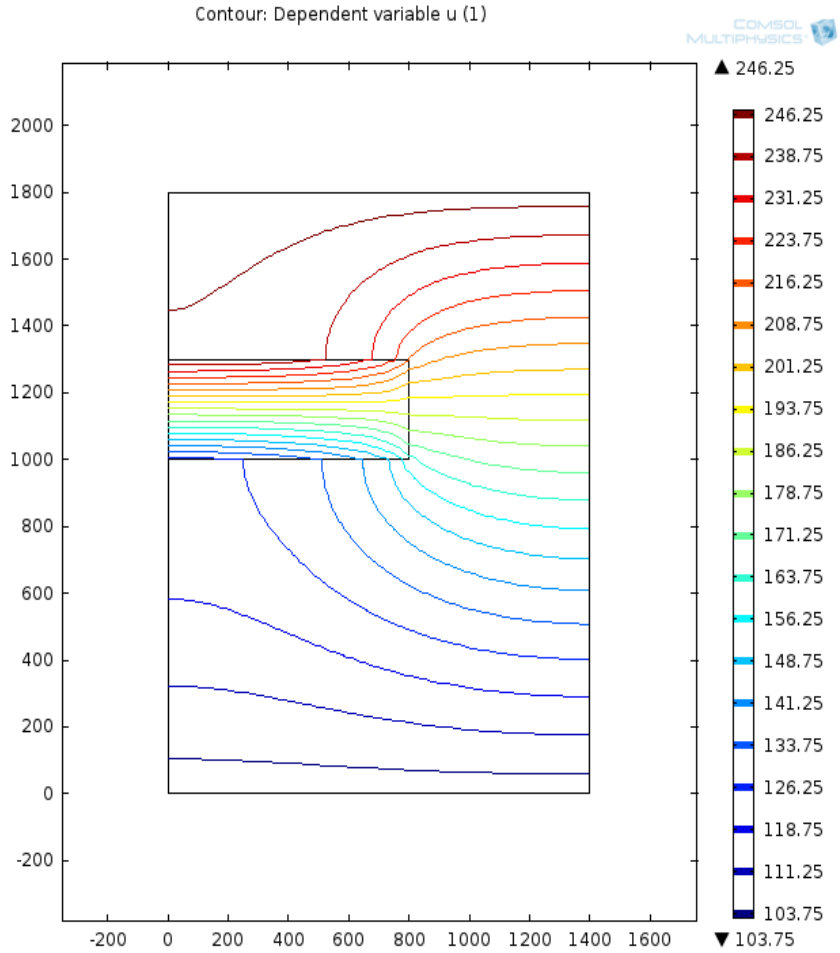

Figure 4.31: COMSOL output

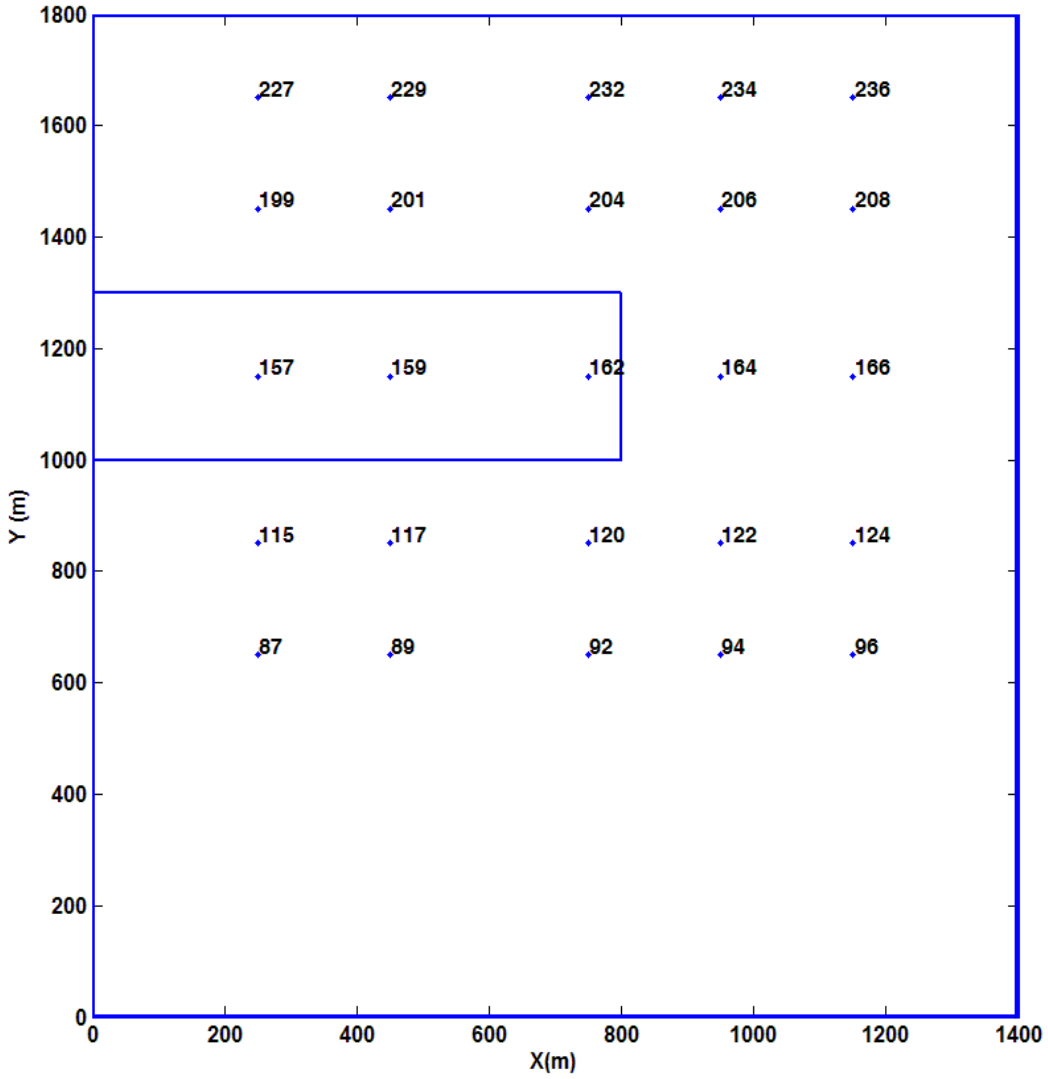

Figure 4.32: Nodal points selected for comparison

Table 4.6: Comparison of COMSOL and RPCM results

Node No.	COMSOL	RPCM	% difference
87	121.7668	118.42	2.7478
89	125.2258	121.64	2.8625
92	133.6622	130.16	2.6218
94	139.32	136.67	1.901
96	142.9443	140.92	1.4181
115	125.3457	121.20	3.3038
117	130.0705	125.31	3.6568
120	144.4531	138.45	4.159
122	154.7504	151.98	1.7911
124	159.4981	157.55	1.2187
157	185.4667	183.73	0.9366
159	186.2374	184.57	0.8952
162	188.1826	186.89	0.6852
164	188.8459	187.67	0.6245
166	189.2544	187.98	0.6712
199	245.1029	245.98	0.3567
201	242.0313	243.62	0.6563
204	231.1199	234.17	1.3215
206	222.9303	223.14	0.0957
208	219.5765	219.06	0.2342
227	247.5379	247.95	0.1653
229	246.0823	246.77	0.2788
232	241.9401	242.77	0.3423
234	239.0541	239.33	0.1146
236	237.4028	237.27	0.057

4.10 Solution of highly advective transport problem

Since in case of transport problems, higher Peclet numbers ($Pe = \frac{v}{D_L} * \Delta x$) causes numerical instability, it is important to analyze the capability of the meshfree RPCM method to handle such instability issues. Two simple approaches to handle the numerical instability are considered in this study (Liu and Gu, 2005). One obvious way is to reduce the nodal separation (Δx), thereby reducing *Pe* itself. The other is to increase the size of the local support domain so as to capture the upstream information which is the source of the numerical instability. This later approach is not easy to implement in FDM or FEM where the mesh is predefined but in meshfree RPCM it can be easily implemented.

The one-dimensional transport problem (Ogata and Banks, 1961) from section 4.8.2 is analyzed here to examine the capability of the meshfree RPCM method to handle high Peclet transport simulation. For the purpose of analysis here, the pore flow velocity is increased by 10 times to 0.259 m/day resulting in a Peclet number value of 72, for a nodal separation of 10 m (corresponding to 100 equal subdivision of the domain). In addition to the RMSE defined in equation (4.78), an additional measure of error (Liu and Gu, 2005) as defined below is also used for the analysis viz.,

$$e_0 = \sqrt{\frac{\sum_{i=1}^{N}\left(C_i^{num} - C_i^{exact}\right)^2}{\sum_{i=1}^{N}(C_{i=1}^{exact})^2}} \tag{4.85}$$

Table 4.7 below shows the results of the two approaches of handling numerical instability where the meshfree RPCM results are compared to the exact solution. Figure 4.33 and Figure 4.34 shows the stabilization of the numerical instability by using a combination of enlargement of local support domain and using denser node distribution. MQ-RBF interpolation has been used in this analysis. But the results will apply to EXP-RBF interpolation also.

Table 4.7 : Effect of different nodal separations and sizes of the local support domain on the RMS error of meshfree RPCM method (concentrations taken at the end of simulation time)

Size of local support domain (multiples of nodal separation)	**Number of Nodes** (N = 101) *Pe* = 72		**Number of Nodes** (N = 201); *Pe* = 36		**Number of Nodes** (N = 401) ; *Pe* = 18	
	RMSE	e_0 **(%)**	**RMSE**	e_0**(%)**	**RMSE**	e_0 **(%)**
2	12.54	5.8	3.3	1.5	1.2	0.5
3	7.7	3.5	1.2	0.5	0.5	0.2
4	5.7	2.6	1.1	0.5	0.2	0.09
5	5.2	2.4	1.0	0.46	0.2	0.1

It can be seen that the combination of enlargement of the local support domain and reducing the nodal separation is very effective in handling numerical instability present in high Peclet number problems. The advantage of using meshfree RPCM method is that this approach can be implemented very easily. Other approaches for stabilization can be found in Liu and Gu (2005).

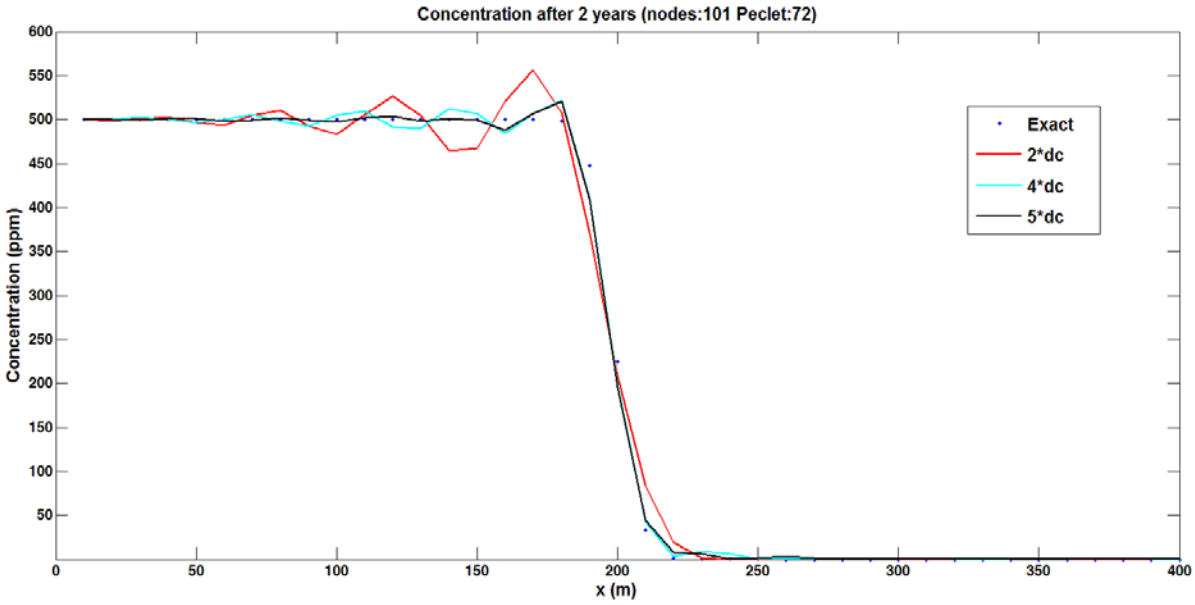

Figure 4.33: Stabilizing effect of enlargement of local support domain for high Peclet transport problem (number of nodes: 101 ; concentrations obtained after simulation of 2 years)

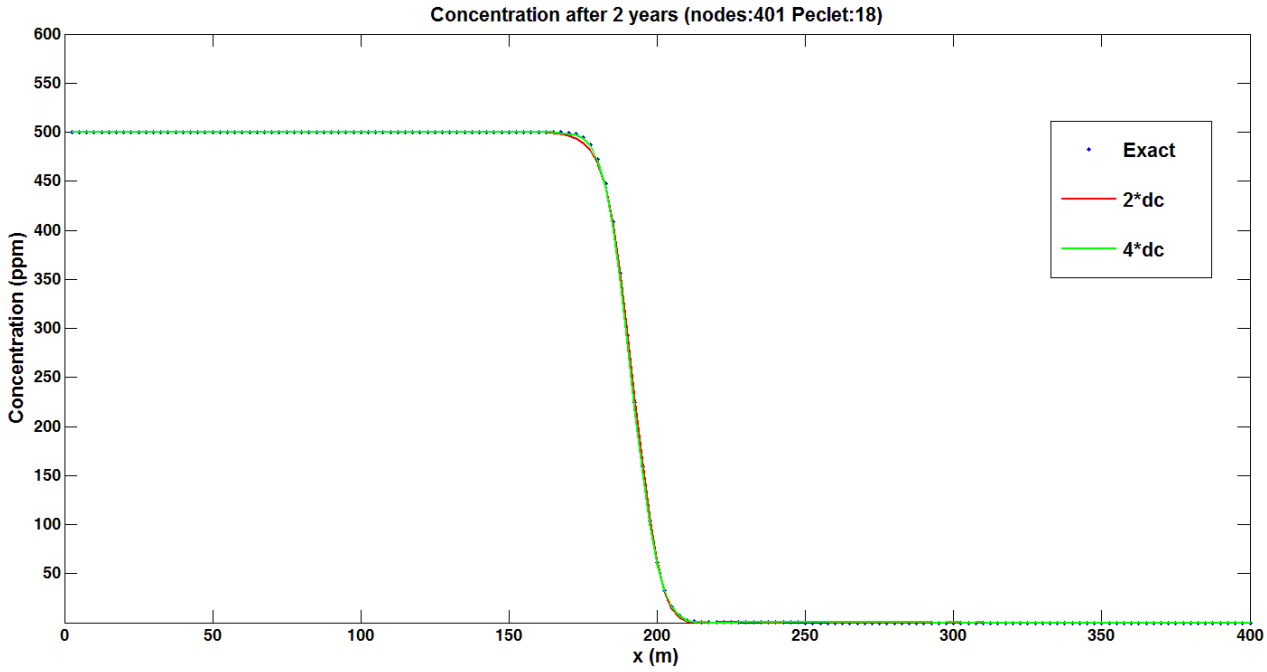

Figure 4.34: A combination of enlargement of local support domain and increasing the nodal density has nearly removed the numerical instability observed in the previous figure (number of nodes: 401; concentrations obtained after simulation of 2 years)

4.11 Sensitivity study of meshfree RPCM model parameters

A parameter sensitivity study is generally required in order to determine the optimal values of the parameters used in the meshfree RPCM method namely, the value of the shape parameter and the size of the support domain. The choice of these parameters is subjective, no definite criteria for choosing these parameters has been found so far. The test example problem discussed in section 4.8.1.1 is taken up for studying the sensitivity analysis. The same metrics defined in that section for measuring the performance of the meshfree RPCM methods is being used here.

Sensitivity to support domain size: A sensitivity study with respect to support domain size is conducted. The grid size is fixed at 5 x 5 nodal points and the value of shape parameter has been kept at twice the nodal or grid spacing (dc). The results of this sensitivity study are shown in Table 4.8 and also in Figure 4.35. It may be observed that the accuracy of the meshfree RPCM results improve with increase in the size (radius) of the support up to 4 times the grid spacing (dc) but beyond this value there is no improvement. This can also be clearly seen in the Figure 4.35 which shows the percentage normalized RMS error of the meshfree RPCM output as compared to the exact results. Hence a support domain radius of 3 to 4 times the grid spacing is optimal for this problem.

Table 4.8: Sensitivity of support domain size

Grid size: 5 x5 , shape parameter: 3*dc			
Support domain size (*dc)	e_0 (%)	e_x(%)	e_y(%)
1	67.28	69.7	376.62
2	1.18	1.46	6.5
3	1.4	1.17	4.25
4	0.69	0.91	3.84
5	0.78	1.02	4.21
6	0.79	1.04	4.13
7	0.79	1.04	4.03

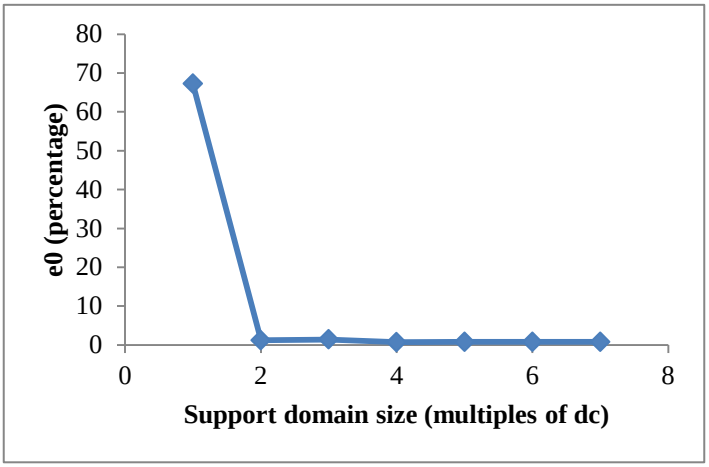

Figure 4.35: Sensitivity w.r.t. support domain size

Sensitivity to shape parameter value **(C_s)**: A sensitivity study with respect to value of the shape parameter used in the calculations is conducted. The grid size is fixed at 5 x 5 nodal points and the radius of the support domain has been fixed at twice the grid spacing. The results of this sensitivity study are shown in Table 4.9 and also in Figure 4.36. It may be observed that the accuracy of the meshfree RPCM results continues to improve with increase in the value of the shape parameter. However, the improvements are insignificant or marginal beyond $C_s = 5 * dc$. This trend is clearly visible from Figure 4.36. Hence the optimal value of the shape parameter (C_s) ranges from 4 to 5 times the grid spacing (dc).

Table 4.9: Sensitivity w.r.t. shape parameter value

Grid size: 5 x5 Size of support domain: 2*dc			
Shape parameter (*dc)	e_0 (%)	e_x (%)	e_y (%)
1	4.□1	4.37	18.24
2	1.89	2.32	9.4
3	1.18	1.46	6.5
4	0.89	1.06	5.16
5	0.74	0.84	4.42
6	0.66	0.72	3.98
7	0.□2	0.65	3.69
8	0.59	0.6	3.5
9	0.57	0.57	3.36

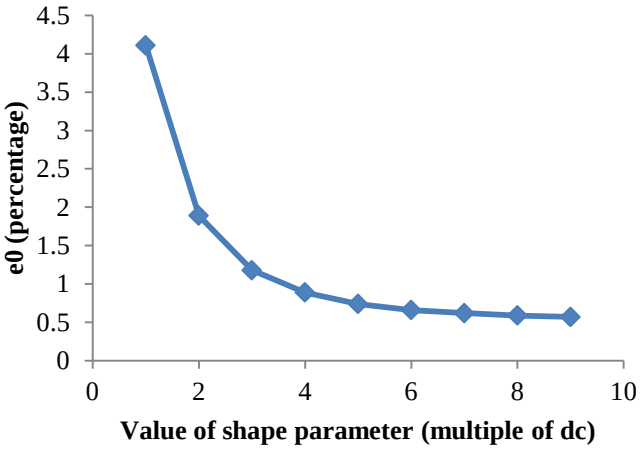

Figure 4.36: Error, e_0 (percent) variation with the value of shape parameter

4.12 Case study - groundwater flow and transport modeling

This section is deals with the application of the RPCM model developed to solve the problems faced in field situations. To test the effectiveness of the developed model for a field problem, a case study of a confined regional aquifer is considered for coupled flow and contaminant transport modeling (Guneshwor et al., 2016). For this case study, the MQ-RBF has been used as the interpolation function. This choice is arbitrary since as demonstrated in previous examples, both the MQ-RBF and EXP-RBF produces nearly the same results. Figure 4.37 shows the location map of the study area. The site is a power plant complex near Vyara, Surat (Gujarat), India. The field measured hydrogeological parameters of the site are obtained from Singh and Sarma (2009). It is bounded by a lake on the north, north-east, west and south-west boundaries. There are no water bodies on the rest of the boundary. The area to be modeled is approximately 4.5 km^2. The aim of the study is to track the movement of any contaminant released inadvertently by the plant so that the groundwater used by the population around the site is safe and any remedial action can be planned based on the contaminant movement.

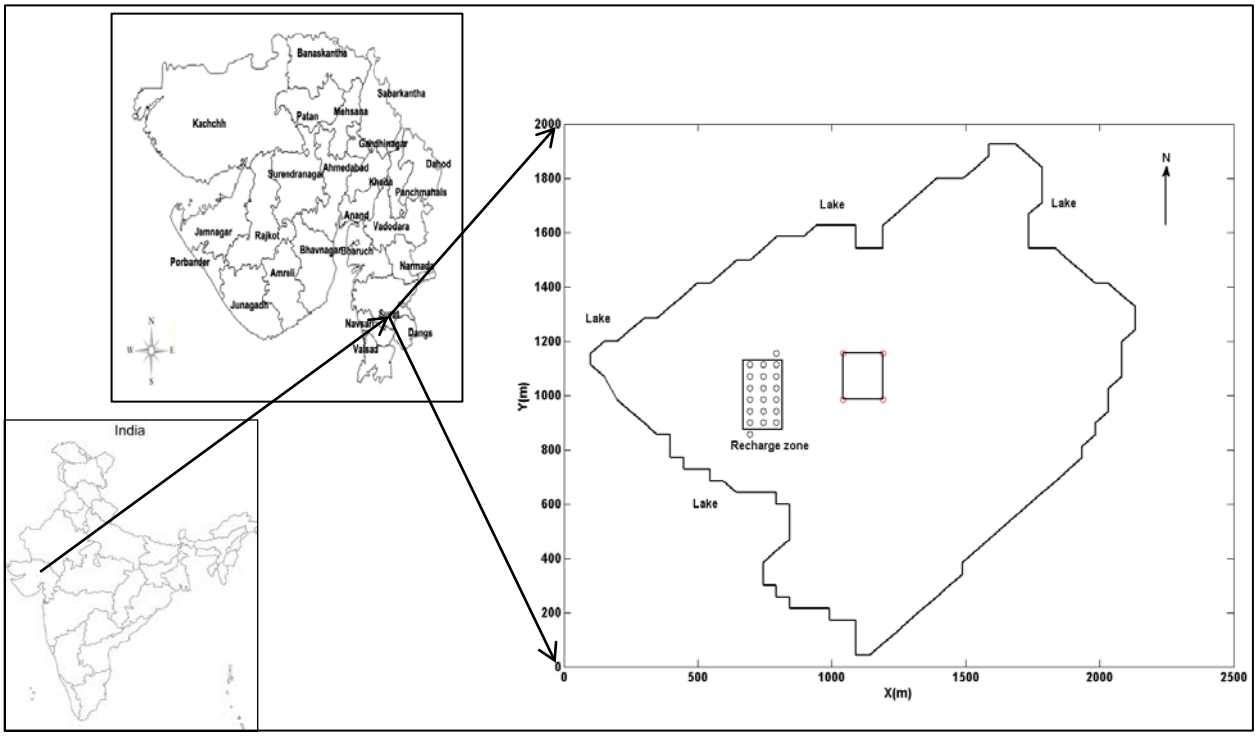

Figure 4.37 : Location map of the study area

Figure 4.38 shows the case study site and the nodal distribution used for discretization of the governing equations. A total of 1008 nodes were used corresponding to a separation between the nodes of 49.6 m along x-direction (Δx) and 42.8 m along the y-direction (Δy). As shown in the figure, there is a recharge zone within the model domain which corresponds to a water pond and is known to be leaking water to the aquifer. The presence of this recharge zone to the aquifer is observed as a mound in the water table map of the area (Singh and Sarma, 2009). Also shown is an area within the complex with underground containers which is assumed to be the contaminant source location.

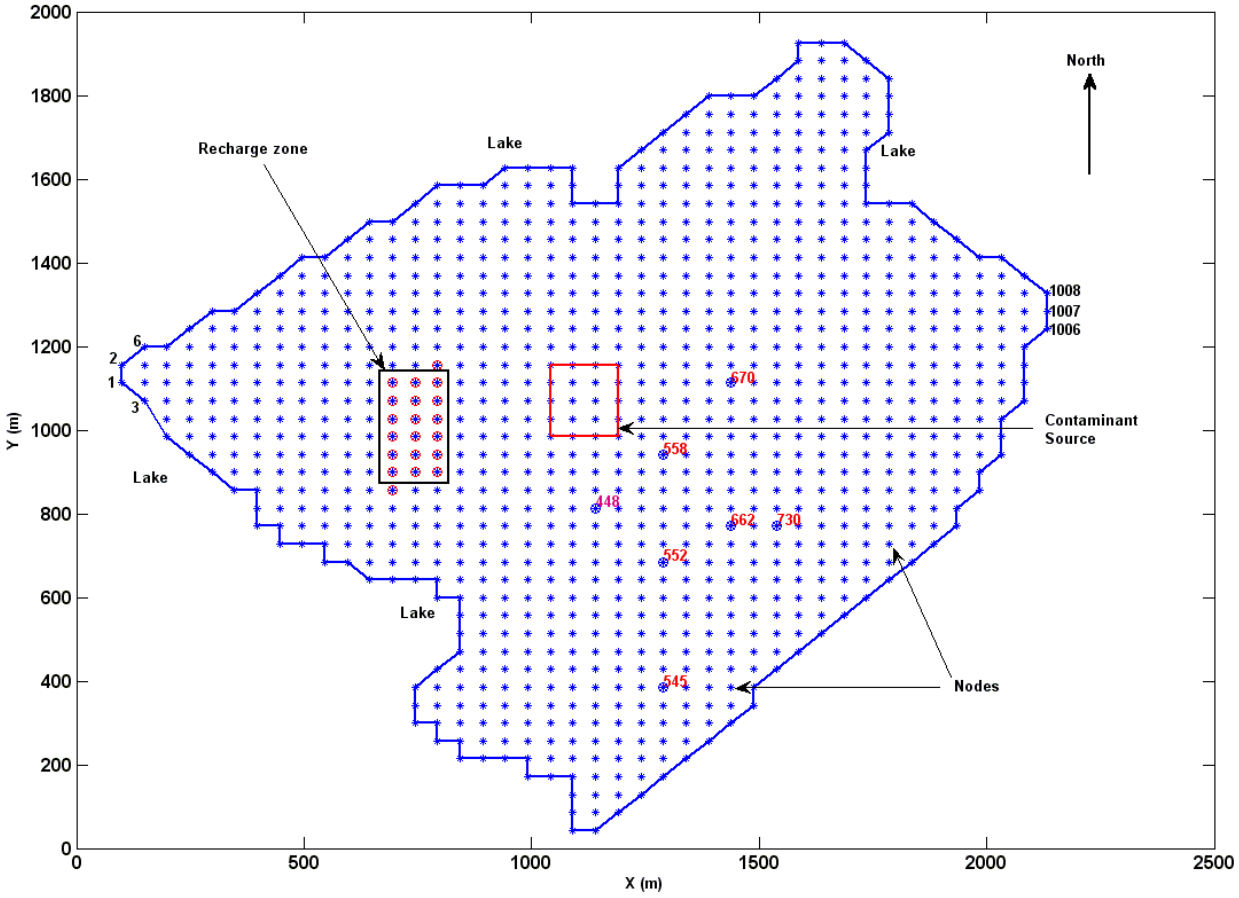

Figure 4.38 : Nodal distribution map and boundaries of the field case study (numbers in the model area

The boundaries adjacent to the lake are treated as constant head boundaries while the rest of the boundary is treated as flux boundaries. The level of water in the lake is maintained by the irrigation department of the local government. This water level, adjusted to mean sea level, is used as the constant head value at the boundaries bounded by the lake. The flux boundary value is estimated and adjusted during calibration of the model. The best estimated value of this flux obtained from model calibration is 6.1x 10^{-5} m^2/d. The distribution of transmissivity is obtained from pumping tests carried out at five different sites within the modeling zone (Singh and Sarma, 2009). Figure 4.39 shows the different transmissivity zones inferred from the field experiments. It is observed that transmissivity of the area varies from a minimum of 30.0 m^2/day to a maximum of 170.0 m^2/day. Other required aquifer parameters are also obtained from the same reference. The recharge through the pond is

estimated from the make up level of the pond and is adjusted during calibration. The final recharge value used was 0.045 m/day. During calibration of the model, the hydrogeologic parameters are adjusted within a range of 20% from their field estimated values.

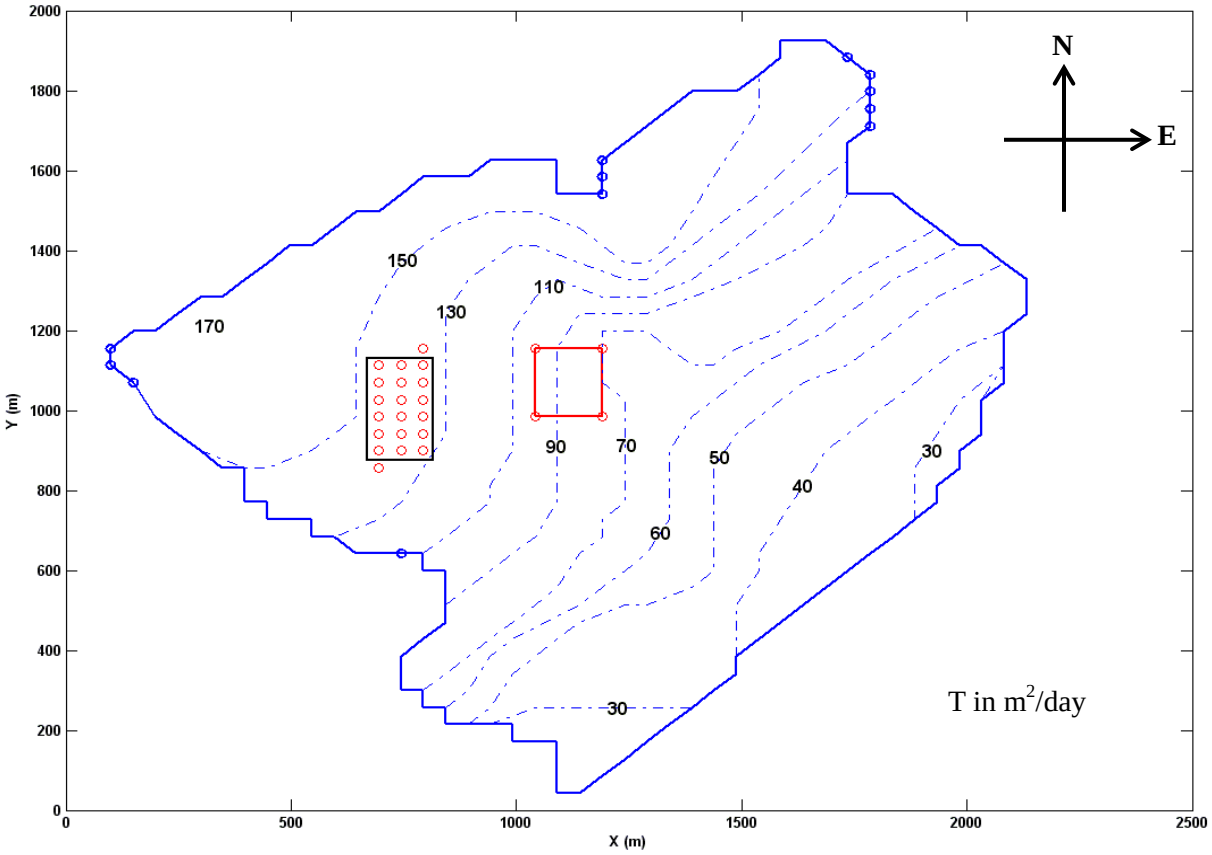

Figure 4.39 : Transmissivity distribution map of the study area

A mesh free RPCM groundwater flow model of the site is constructed using the hydrogeological parameters described above (Singh and Sarma, 2009) and the node distribution as in Figure 4.38. The governing groundwater flow equation (eqn. 3.12) is solved in steady state for obtaining hydraulic heads at the nodes. The level of water in the lake is maintained as also the water level of the recharging pond. Being a confined aquifer, rainfall recharge is negligible. Therefore the groundwater flow is basically steady state. Calibration of the RPCM model was done against the field measured heads. Table 4.10 shows the comparision of actual field measured heads in selected monitoring borewells at the site to the meshfree RPCM model predicted heads, after calibration of the model. For

comparision, using the same calibrated values of the hydro-geological parameters, an FEM model was constructed in COMSOL Multiphysics using 1812 triangular elements with 2165 nodes. The heads predicted by this FEM model is also shown in the same table.

Table 4.10 : Comparision of field measured heads at selected monitoring borewells to FEM and Meshfree RPCM models

Borewell no.(*)	**Field measured head (m)**	**FEM model prediction (m)**	**Meshfree RPCM Model prediction (m)**
1	47.995	48.0	48.3
2	48.383	48.0	48.4
3	48.147	47.8	48.4
4	48.112	47.2	47. 4
5	46.004	46.7	46.7
6	45.799	46.7	46.8
7	45.129	46.9	46.9
8	46.194	47.0	47.1
9	45.82	46.7	46.8
10	45.719	46.6	46.6
11	45.704	46.6	46.6
14	45.619	46.6	46.7
15	45.469	46.6	46.6
16	45.439	46.5	46.6
17	45.387	46.6	46.6
18	45.699	46.0	45.9
19	45.319	46.0	46.0
20	45.139	46.1	46.1
21	44.934	46.0	46.0

* Ref. (Singh & Sarma, 2009)

Figure 4.40 compares the contour map of the hydraulic heads as predicted by mesh free CFTM-RPCM and FEM (COMSOL) models. It can be seen that both the models predicts more or less the

same hydraulic head distribution in the modeling domain. This confirms the good agreement between RPCM model and FEM models.

Table 4.11 : Comparision of head output of Meshfree RPCM and FEM models

Nodes	Head from Mesh free RPCM model (m)	Head from FEM model (m)	Percentage difference
448	46.9	46.8	0.21
558	46.9	46.8	0.21
662	46.6	46.5	0.22
552	46.6	46.5	0.22
670	46.9	46.8	0.21
730	46.5	46.5	0
545	46.1	46.1	0

Table 4.11 above shows the comparison of meshfree RPCM flow model results and those from FEM at 7 selected nodes (shown in Figure 4.37) viz., nodes 448, 545, 552, 558 ,662, 670 and 730 of the nodal distribution. These nodes are also used for validating the transport model. It is seen that there is good agreement between the heads predicted by the meshfree RPCM and FEM models. Figure 4.41 shows the distribution and directions of the flow velocity vectors in the aquifer.

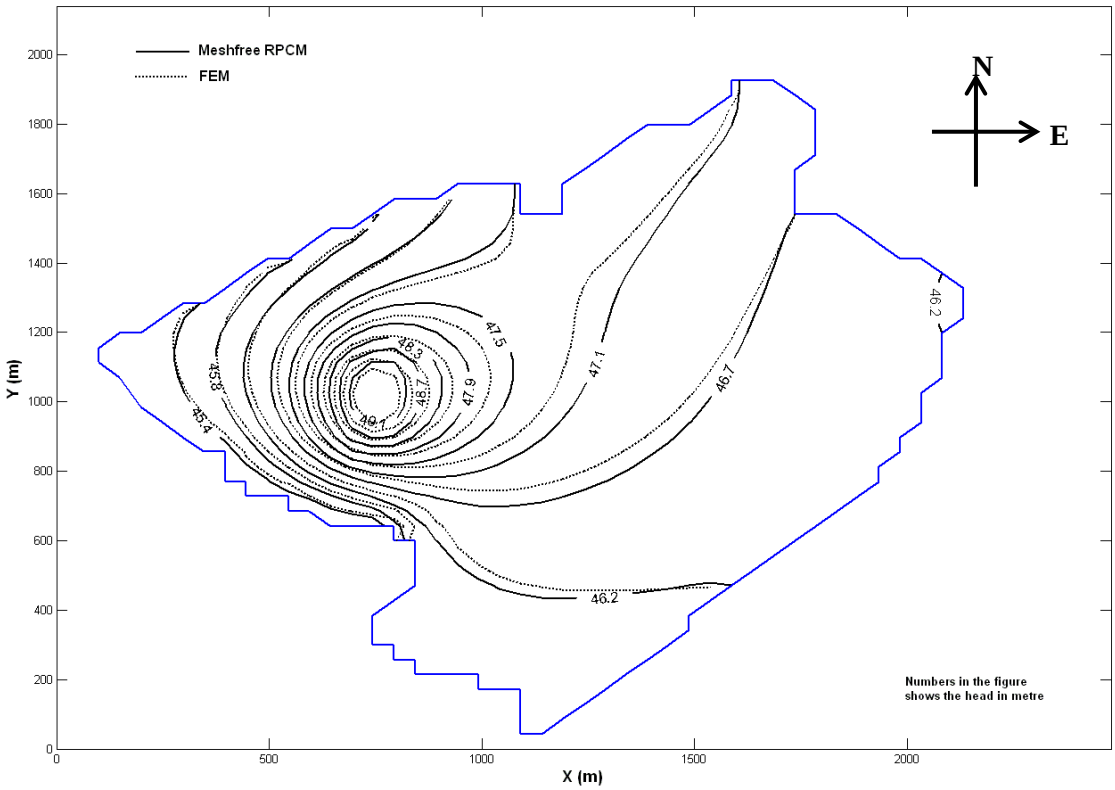

Figure 4.40 : Comparison of head contour predicted by Mesh free RPCM and FEM

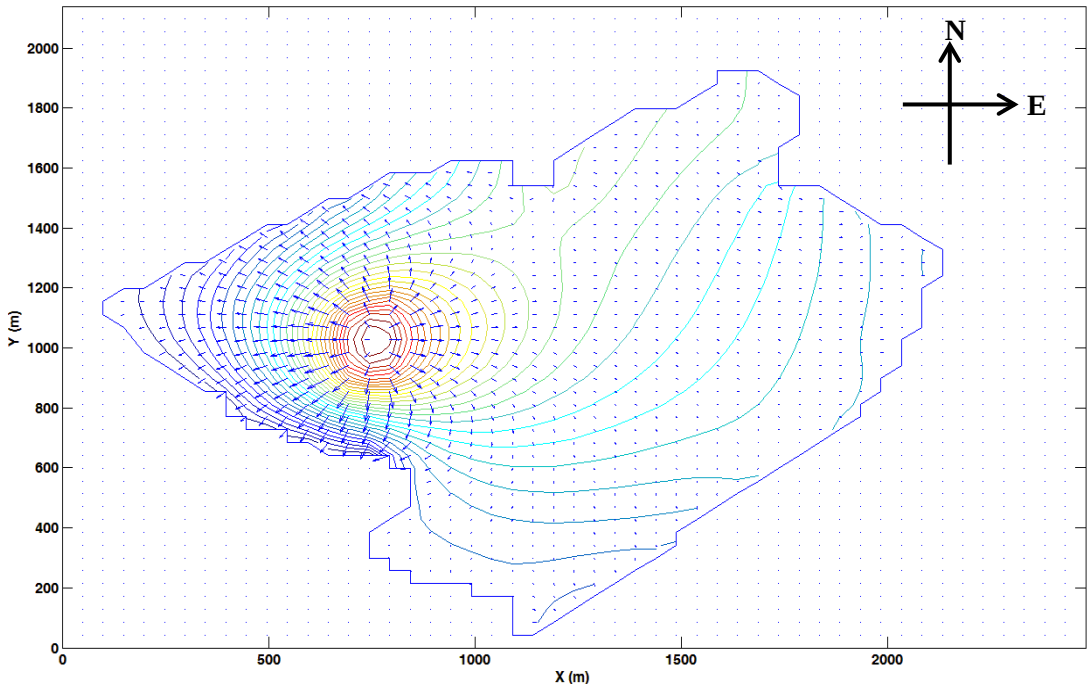

Figure 4.41: Flow velocity distribution

Groundwater flow and transport modeling using meshfree method

With the flow model validated, a non-reactive contaminant transport model is constructed and coupled to the flow model. Steady state head values from the flow model are considered as the initial head distribution. The source of contaminant is an areal source as shown in the Figure 4.38 and corresponds to a particular area in the domain with underground containers which may act as potential sources of contaminants. This model aims to track the spreading of the contaminants in a postulated structural failure scenario where the containers are leaking the contaminants to the groundwater continuously for the period of simulation.

The contaminant transport is governed by equation (3.19). The longitudinal dispersivity (α_L) for this problem is 20 m and the transverse dispersivity (α_T) is taken as 10% of the longitudinal dispersivity. The areal contaminant source is assumed to be leaking contaminant of concentration 1000 ppm. The boundaries of the model are set to a concentration value of zero i.e. Dirichlet boundary condition. The same nodes (Figure 4.38) used for the flow model are also used for the transport model. The time step size used is $\Delta t = 5$ days and it is assumed that the whole area was pristine when simulation starts i.e. have zero concentration as the initial condition. For time-stepping, the Crank-Nicholson method ($\theta = 1/2$) was implemented. The total simulation time was 10 years corresponding to 730 time steps. The size of the local support domain was 3 times the average of the nodal distances along *x* and *y*-directions while the shape parameter of the multi-quadrics RBF was kept at 5 times the average nodal distance. These parameters were determined also in the verification problems discussed in the previous sections.

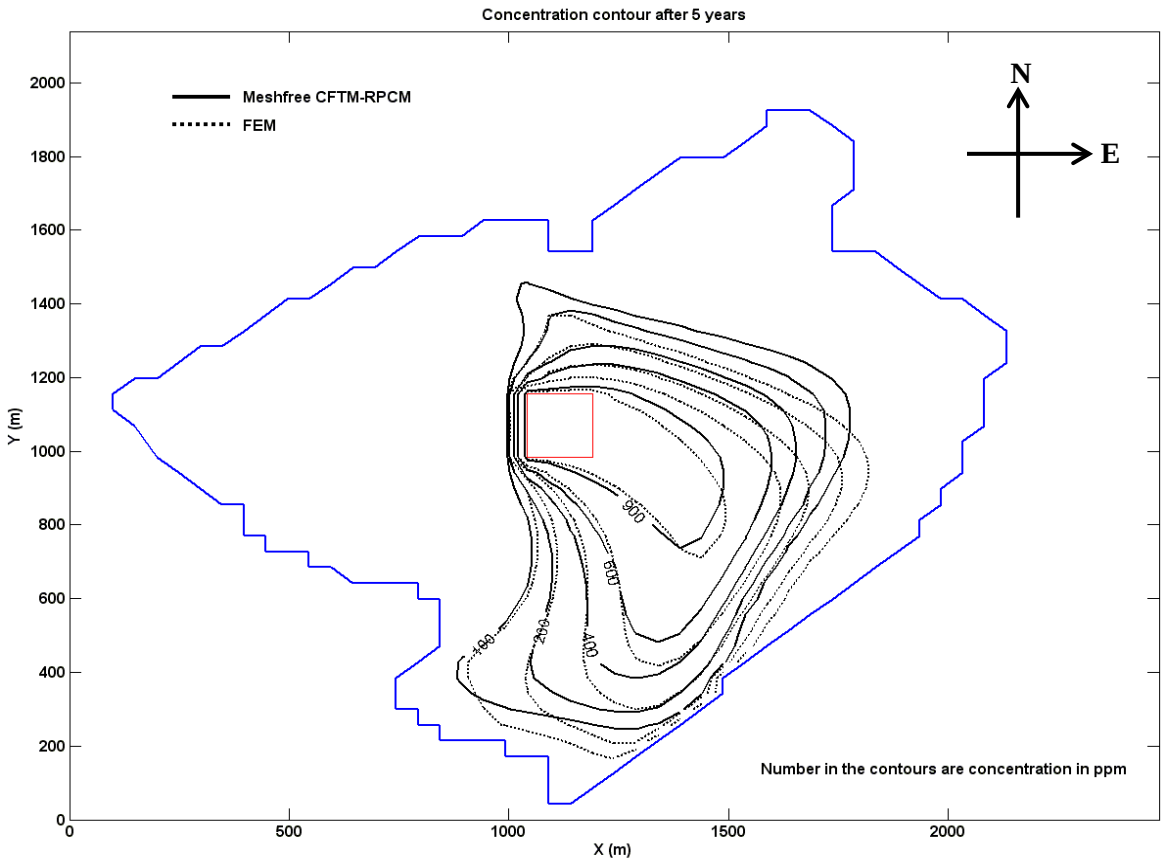

Figure 4.42 : Comparision of concentration plume predicted by meshfree CFTM-RPCM and FEM after 5 years of simulation

Figure 4.42 shows the contaminant plume after 5 years of continuous discharge. The output from FEM is also shown alongside for comparison. The path of the contaminant plume is in the south-eastern direction. Table 4.12 below shows a comparison of the concentrations predicted by meshfree CFTM-RPCM and FEM models at the 7 selected nodes viz. nodes 448, 545, 552,558, 662, 670 and 730 in the direction of the contaminant plume. The locations of these nodes have been shown in Figure 4.38. From Table 4.12 and Figure 4.42, it can be seen that the meshfree CFTM-RPCM results agrees very well with the FEM prediction.

Figure 4.43 shows the concentration profiles for the above selected nodes. It is seen that the nodes 558,662 and 730 receives the highest concentrations being directly along the centerline of the plume while node 448 receives the lowest concentration value being in the flank.

Table 4.12 : Comparison of concentration predicted by CFTM-RPCM and FEM models

Node	Concentration (ppm) after 5 years			Concentration(ppm) after 10 years		
	RPCM	FEM	Percentage difference	RPCM	FEM	Percentage difference
448	442	451	2.0	442	451	2.0
558	985	976	1.0	986	975	1.1
662	905	927	2.4	959	944	1.6
552	732	720	1.6	733	722	1.5
670	781	757	3.1	792	767	3.2
730	785	804	2.4	964	930	3.5
545	502	538	7.2	618	662	7.1

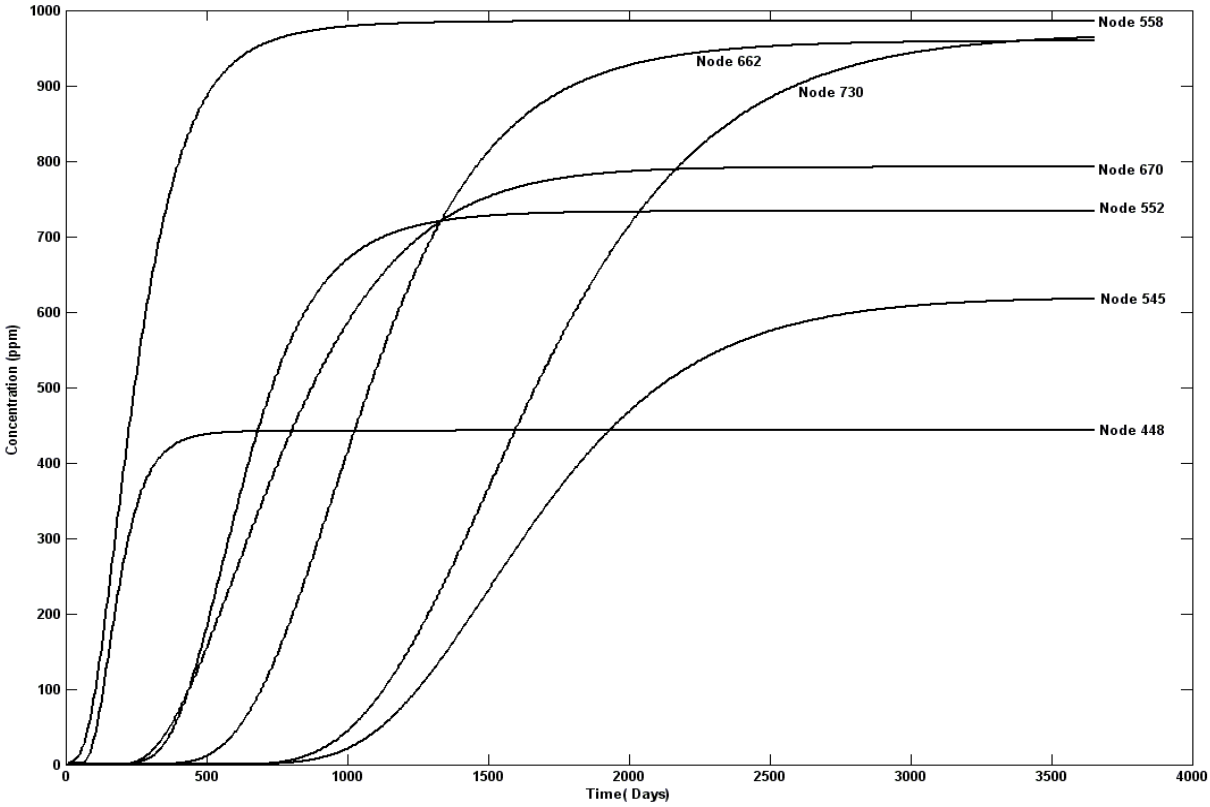

Figure 4.43 : Concentration profile at selected nodes along the path of the contaminant plume

Figure 4.44 shows the snapshot of the contaminant plume at the end of 1, 3, 5 and 10 years of simulation showing the propagation of the contaminant. The movement of the contaminant plume is towards the south-eastern boundary of the model domain.

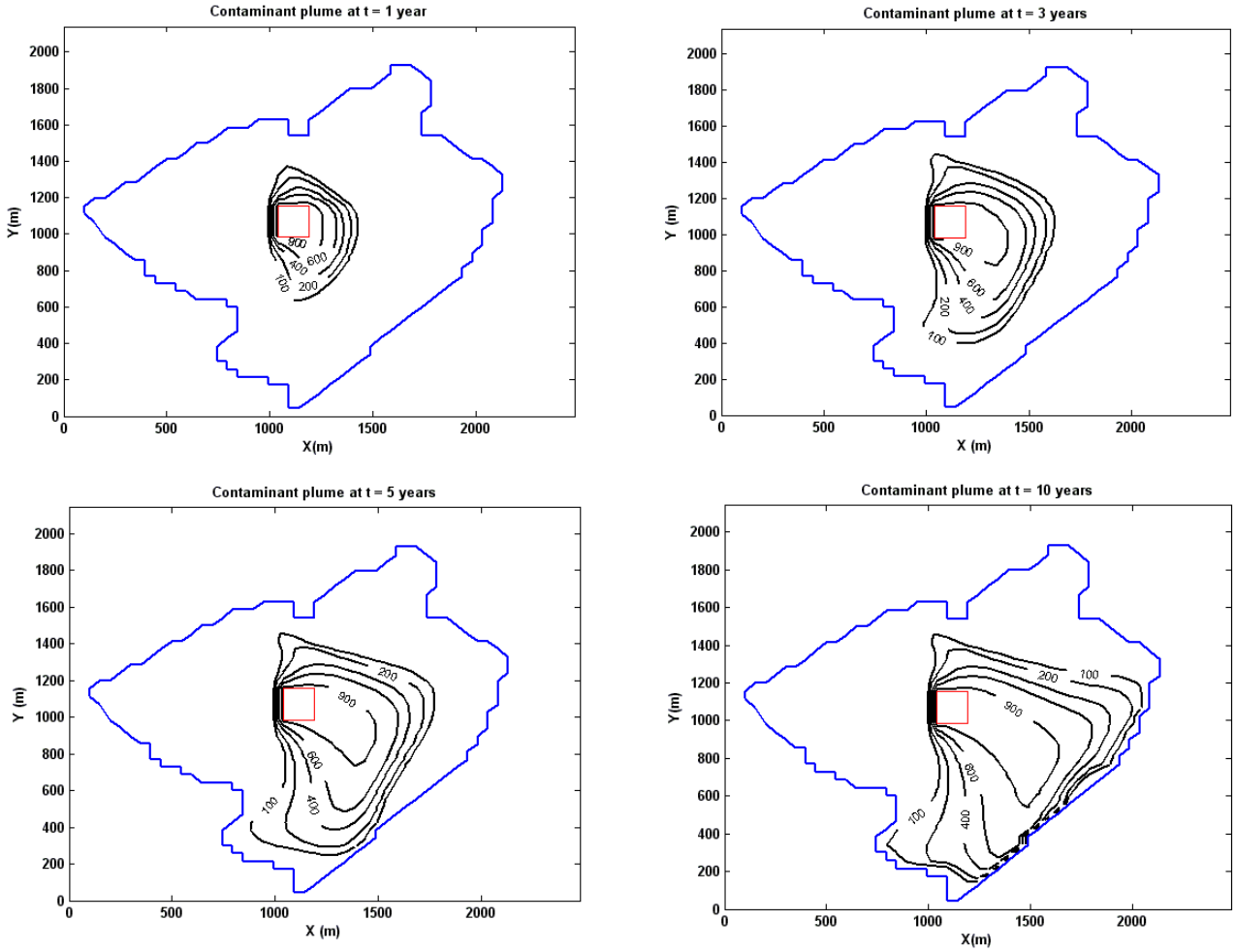

Figure 4.44 : Propagation of the contaminant plume in the aquifer (number in the figure shows concentration in ppm)

This study has demonstrated that meshfree CFTM-RPCM model can be effectively used to model coupled groundwater flow and transport simulations as an alternative to the grid based methods such as FDM or FEM. This method requires only a set of scattered nodes, instead of a mesh with all the nodal interconnection information. The implementation of the model is very simple regardless of the dimension of the problem and complexity of the model geometry. Boundary conditions are also easily

incorporated. A few issues in the application of the meshfree RPCM method though are yet to be addressed such as choosing the optimal value of shape parameters, size and shape of the local support domain etc. In particular, the value of shape parameter has a profound impact on the accuracy. But it was found that these issues do not pose any significant hurdle in application of the method. With a simple numerical sensitivity or parametric analysis, these parameters can be determined.

4.13 Closure

Grid based methods such as FDM, FEM etc. are widely used for numerical solution of partial differential equations. However the requirement for grid in these methods leads to several computational and practical problems. Meshfree methods do away with the requirement to create a mesh. In this chapter a meshfree methods called the RPCM method has been developed to solve the governing equations for groundwater flow and solute transport. The developed method has been verified using analytical and other numerical techniques such as FEM. Various issues that arises while applying the meshfree RPCM method has been examined and ways to overcome or address them have been discussed. The developed method has been applied to a real field problem and the results were found to be good in comparison to field measurements and the output from FEM solutions. This validates the applicability of the meshfree RPCM method to practical problems. The meshfree RPCM method is proposed to be used as the groundwater flow and transport simulator in the simulation-optimization method developed in the next chapter for groundwater source identification.

Chapter 5

Simulation-Optimization models for source identification

5.1 Introduction

Once a system is mathematically modeled, computer-based simulations provide the information about its behavior. Parametric simulation methods can be used to improve the performance of a system. In this method, the input of each variable is varied with other parameters remaining constant and the effect on the design objective is observed. This is a time-consuming method and improves the performance partially. To obtain the optimal solution with minimum computation and time, the problem is solved iteratively where in each iteration the solution moves closer to the optimum solution by integrating with an optimization technique. Such methods are known as 'numerical optimization' or simulation- optimization model.

In this chapter, the simulation-optimization model as applied to groundwater source identification is discussed.

5.2 Simulation-Optimization model in groundwater

Simulation-based optimization integrates optimization techniques into simulation analysis. In simulation experiment, the goal is to evaluate the effect of different values of input variables on a system, which is called running simulation experiments. However the interest is sometimes in finding the optimal value for input variables in terms of the system outcomes. One way could be running simulation experiments for all possible input variables. However this approach is not always practical due to several possible situations and it just makes it intractable to run experiment for each scenario. For example, there might be so many possible values for input variables, or simulation model might be so complicated and expensive to run for suboptimal input variable values. In these cases, the goal is to find optimal values for input variables rather than trying all possible values. This process is called simulation-optimization (SO) model. SO models have been widely used in groundwater management, calibration of groundwater flow and transport models, groundwater remediation etc. (Meenal and Eldho, 2012a).

Two sets of variables are associated with SO models: *decision variables* and *state variables*. The variables that can be used to define and differentiate alternative decisions are known as decision variables (Zheng and Bennet, 2002). Decision variables can be specified or managed in the calculation process to identify their best combination also referred to as the optimal management policy or strategy. For example, in a groundwater pumping management problem, the decision

variables are the pumping or injection rate of wells, location of the wells etc. The variables that describe the flow and transport conditions are known as state variables. Examples of state variables are hydraulic heads, concentration etc. In an SO model, the simulation model updates the state variables while the optimization model determines the optimal values of all decision variables.

The basic goal of an optimization based model for groundwater source identification or characterization is to identify source characteristics (location, disposal duration, and solute mass flux or volume disposal rates). The objective is to search for a feasible set of source characteristics which minimize some function of the deviations between the observed and the simulated values of concentrations. This can be achieved by minimizing the weighted sum of the squared deviations (or absolute deviations) between observed values of spatially and temporally varying concentrations, and the corresponding simulated values of concentrations. Given the initial and boundary conditions, withdrawal from and recharge into the aquifer, an optimization model for identification of pollution sources can be formulated. The groundwater source identification model can be formulated as (Datta et al., 2009):

$$Min\left(\sum_{i,k\in Z_h}\langle W_i^k\rangle_c\left[\langle c_i^k\rangle_{obs}-c_i^k\right]^2\right) \tag{5.1}$$

subject to the constraints,

$$\boldsymbol{c}=\boldsymbol{f}(\boldsymbol{p_m},\boldsymbol{q}) \tag{5.2}$$

$$\boldsymbol{c}^L\le\boldsymbol{c}\le\boldsymbol{c}^U \tag{5.3}$$

$$\boldsymbol{q}^L\le\boldsymbol{q}\le\boldsymbol{q}^U \tag{5.4}$$

where c is the solute concentration, q is the set or vector of sources, f is the transport model, p_m are the parameters of these transport model, W_i are the weights associated with the i^{th} data (concentration)

The constraints in equations (5.2) represent the groundwater flow and solute transport simulation model. They are non-linear constraints. The source of nonlinearity in the decision model is different from the nonlinearity inherent in the numerical simulation model. The source identification model is a decision model where nonlinearity is introduced due to the combination of decision variables, i.e., as a product of variables. Treating the parameters as decision variables, along with the source fluxes, increases the nonlinearity of the decision problem many fold. Therefore, the source identification seems a more challenging problem computationally. In the combined optimization–simulation approach, where the simulation model is linked as a separate module to the optimization model, it is

necessary to iterate between the optimization model and the groundwater flow and transport simulator.

The constraint sets in equations (5.3) and (5.4) essentially reduce the feasible search space. From practical considerations, these two sets of constraints ensure that once a set of sources q (q is the decision variable in the optimization formulation) are assumed, the resulting hydraulic heads and concentrations are evaluated at different observation well locations at various times. Only those set of q are considered acceptable, which result in simulated concentrations within some predefined lower and upper bounds on the actually observed measurement data. The actual values of these bounds may be calculated by subtracting and adding, respectively, some tolerances to the observed concentration values. The lower and upper bounds on the sources in equations (5.4) ensure that practically acceptable ranges of values are considered.

The simulation has been performed using meshfree RPCM method formulated and developed in chapter 4. The optimization model is a particle swarm optimization (PSO) model and has been described in subsequent sections of this chapter. A pre-requisite for the application of the SO model is the existence of a calibrated flow and transport simulation model. It may be noted that the uncertainties inherent in simulation models will obviously affect the identification of optimal solutions.

5.2.1 Simulation models

Simulation models for groundwater use numerical methods such as finite-difference, finite-element, boundary element methods, meshfree methods etc. to analyze the groundwater flow and transport processes. These models gives predictions of hydraulic heads for groundwater flow and solute concentration values for contaminant transport problems.

Similarly, one of the approaches to backtrack the pollution source location is to run forward simulations of the transport model and check the solutions with the field measured data. The procedure is to link the simulation model with an optimization model so as to minimize the difference between predicted and measured values. Owing to the non-uniqueness of the solution and the infinite number of plausible combinations, one needs to follow an optimization method to obtain the best fitted solution. Such a model where forward simulation is linked to an optimization model is generally known as simulation-optimization (SO) model.

5.2.2 Optimization models

An optimization model is defined in terms of an objective function and a set of constraints. The objective function represents the management policy or strategy. Depending on the problem

requirement the objective function is either minimized or maximized. For example, for a contamination remediation design problem, the objective function may be to maximize the contaminant mass removal. The exact form of the objective function is determined by the nature of the individual problem. Because of the complexity of the simulation, the objective function may become difficult and expensive to evaluate in some cases. In some problem, multiples objective functions may need to be achieved. Such problems are known as multi-objective problems.

In all the cases, the management objectives must be achieved within a set of constraints, which can be derived from technical, legal or political conditions associated with the project. These constraints may apply to both decision variables and state variables and mathematically, may take the form of equalities or inequalities. There are several optimization techniques available. Conventional techniques include linear programming (LP), non-linear programming (NLP), mixed-integer linear programming (MILP), mixed-integer non-linear programming (MINLP), differential dynamic programming (DDP) etc. NLP and DDP are gradient based methods and have much wider applicability. However such methods may not be able to find the global optimal solution as they may get trapped in local optima. Several modern artificial intelligence (AI) based optimization methods have become popular in recent days. Some of the important AI based optimization techniques include Genetic algorithm (GA), particle swarm optimization (PSO) and simulated annealing etc. These techniques can avoid local optima trapping and find the global optimum and are also gradient-free methods. However, these techniques generally require intensive computational efforts.

In the present study PSO is being proposed as the optimizer for the SO model for groundwater source identification. Unlike other techniques, PSO has a very simple structure and its implementation is also easy. It can be very easily integrated with simulation models. In the subsequent sections, the different theoretical and practical aspects of PSO have been discussed in detail.

5.3 Particle Swarm Optimization

A Particle Swarm Optimizer (PSO) is a nature-inspired swarm intelligence algorithm (Kennedy and Eberhart, 1995). Swarm intelligence is a problem-solving technique that relies on interactions of simple processing units (also known in artificial intelligence as agents). The notion of a swarm implies multiple units that are capable of interacting with each other resulting in a complex behavior. The notion of intelligence suggests that this approach is successful. PSO was developed by Kennedy and Eberhart in 1995 (Kennedy and Eberhart, 1995) inspired by the flocking and schooling patterns of birds, fish and swarms of insects.

The initial ideas of Kennedy and Eberhart (1995) were to combine cognitive abilities with social interaction. These ideas were developed into the Particle Swarm Optimizer. Since then many different applications and variants have been developed. Every PSO uses a population of particles. The number of particle in a swarm is typically far less than the number of individuals in an evolutionary algorithm. A particle in this population is interconnected to other particles. This interconnection is called the neighborhood topology. Neighborhood refers to a communication structure rather than a geographical neighborhood. To use these particles to explore the search space a so-called change rule is needed. This rule moves the particles through the search space at a given moment t in time depending on its position at moment $t-1$ as well as the position of its previous best location. This is the cognitive aspect of the PSO. The social aspect is introduced by an interaction rule. A particles position is not only dependent on its own best position in history, but also on the best position in history of its neighbors.

5.3.1 Standard or Canonical PSO Algorithm

In PSO a number of entities called particles, which represent a candidate solution, are placed in the search space of some problem or function, and each evaluates the objective function at its current location. Each particle then determines its movement through the search space by combining some aspect of the history of its own current and best (best-fitness) locations with those of one or more members of the swarm, with some random perturbations. The next iteration takes place after all particles have been moved. Eventually the swarm as a whole, like a flock of birds collectively foraging for food, is likely to move close to an optimum of the fitness function.

Each particle maintains its position, composed of the candidate solution and its evaluated fitness, and its velocity. Additionally, it remembers the best fitness value it has achieved thus far during the operation of the algorithm, referred to as the *individual best fitness*, and the candidate solution that achieved this fitness, referred to as the *individual best position or individual best candidate solution*. Finally, the PSO algorithm maintains the best fitness value achieved among all particles in the swarm, called the *global best fitness*, and the candidate solution that achieved this fitness, called the *global best position or global best candidate solution*. In essence, the algorithm consists of the following three main steps which are repeated until the stopping criterion is met:

1. Evaluate the fitness of each particle
2. Update individual and global best fitnesses and positions
3. Update velocity and position of each particle

Fitness evaluation is conducted by supplying the candidate solution to the objective function. Individual and global best fitnesses and positions are updated by comparing the newly evaluated

fitnesses against the previous individual and global best fitnesses, and replacing the best fitnesses and positions as necessary.

The velocity and position update step is responsible for the optimization ability of the PSO algorithm. The velocity of each particle in the swarm is updated using the following equation (Clerc and Kennedy, 2002):

$$v_i(t+1) = wv_i(t) + c_1 r_1[\hat{x}_i(t) - x_i(t)] + c_2 r_2[g(t) - x_i(t)] \quad (5.5)$$

The index of the particle is represented by *i*. Thus, $v_i(t)$ is the velocity of particle *i* at time *t* and $x_i(t)$ is the position of particle *i* at time *t*. The parameters *w*, c_1 and c_2 ($0 \leq w \leq 1.2$, $0 \leq c_1 \leq 2$ and $0 \leq c_2 \leq 2$) are user-supplied coefficients. The values r_1 and r_2 ($0 \leq r_1 \leq 1$ and $0 \leq r_2 \leq 1$) are random values regenerated for each velocity update. The value $\hat{x}_i(t)$ is the individual best candidate solution for particle *i* at time *t*, and *g(t)* is the swarm's global best candidate solution at time *t*.

Each of the three terms of the velocity update equation have different roles in the PSO algorithm. The first term $wv_i(t)$ is the *inertia component*, responsible for keeping the particle moving in the same direction it was originally heading. The value of the inertial coefficient *w* is typically between 0.8 and 1.2, which can either dampen the particle's inertia or accelerate the particle in its original direction (Shi and Eberhart, 1998). Generally, lower values of the inertial coefficient speed up the convergence of the swarm to optima, and higher values of the inertial coefficient encourage exploration of the entire search space.

The second term $c_1 r_1[\hat{x}_i(t) - x_i(t)]$, called the cognitive component, acts as the particle's memory, causing it to tend to return to the regions of the search space in which it has experienced high individual fitness. The cognitive coefficient c_1 is usually close to 2, and affects the size of the step the particle takes toward its individual best candidate solution, $\hat{x}_i$.

The third term $c_2 r_2[g(t) - x_i(t)]$ called the social component causes the particle to move to the best region the swarm has found so far. The social coefficient c_2 is typically close to 2, and represents the size of the step the particle takes toward the global best candidate solution *g(x)* the swarm has found up until that point.

The random values r_1 in the cognitive component and r_2 in the social component cause these components to have a stochastic influence on the velocity update. This stochastic nature causes each

particle to move in a semi-random manner heavily influenced in the directions of the individual best solution of the particle and global best solution of the swarm.

Once the velocity for each particle is calculated, each particle's position is updated by applying the new velocity to the particle's previous position:

$$x_i(t + 1) = x_i(t) + v_i(t + 1) \tag{5.6}$$

Figure 5.1 illustrates the position update of a particle in PSO where the influence of the various aspects pf the PSO namely, inertia, cognitive component (memory) and social component (cooperation) has been depicted clearly.

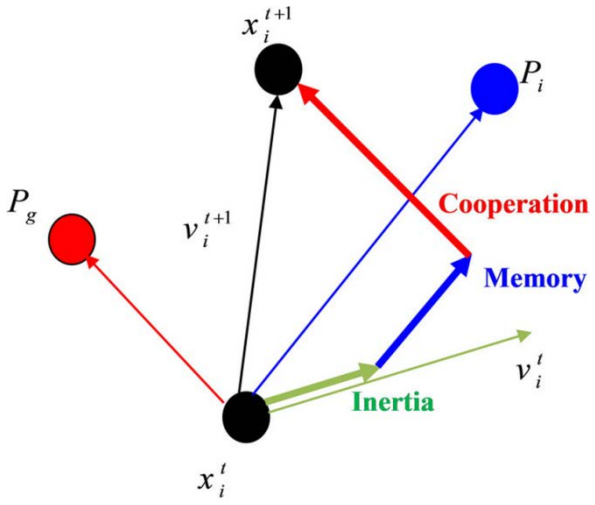

Figure 5.1: Schematic diagram of position update of a particle in PSO

This process is repeated until some stopping condition is met. Some common stopping conditions include: a preset number of iterations of the PSO algorithm, a number of iterations since the last update of the global best candidate solution, or a predefined target fitness value.

The two parameters, c_1 and c_2, are responsible for the optimizing behavior of the swarm. These parameters are often called acceleration coefficients, because they control the magnitude of the adjustments towards the particles personal best and its global best. c_1 controls the cognitive aspect (adjustment towards the personal best), while c_2 controls the social aspect (adjustment towards the global best).

5.3.2 Fully Informed Particle swarm

In the standard version of PSO, the effective sources of influence are in fact only two: self and best neighbor. Information from the remaining neighbors is unused. Kennedy and Mendes have revised

the way particles interact with their neighbors (Kennedy and Mendes, 2002). Whereas in the traditional algorithm each particle is affected by its own previous performance and the single best success found in its neighborhood, in the fully informed particle swarm (FIPS), the particle is affected by all its neighbors, sometimes with no influence from its own previous success. In this manner, information of the total neighborhood is used as opposed to information from the best particle alone. The remaining part of the algorithm is the same as the algorithm for the canonical PSO.

The FIPS algorithm does not perform very well while using the global best topology, or, in general, with any neighborhood topology with a high degree of interconnections (a particle is interconnected to many other particles in the swarm). FIPS performs better at topologies with a lower degree such as the local best (ring lattice) topology or topologies where particles have very few (approximately three) neighbors. Intuitively, it seems obvious that information from many neighbors can result in conflicting situations, since these neighbors may have found their successes in different regions of the search space. Therefore, this averaged information is less likely to be helpful as opposed to the canonical PSO where more neighbors will tend to yield better information, as it is more likely to have a particle with a high solution quality in the neighborhood.

With good parameters, FIPS appears to find better solutions in less iteration than the canonical algorithm, but it is much more dependent on the population topology (Kennedy and Mendes, 2002).

5.3.3 PSO algorithm

Each individual in the particle swarm is composed of three *D*-dimensional vectors, where *D* is the dimensionality of the search space. These are the current position,$\overrightarrow{x_i}$, the previous best position $\overrightarrow{p_i}$ and the velocity $\overrightarrow{v_i}$. The current position $\overrightarrow{x_i}$ can be considered as a set of coordinates describing a point in space. On each iteration of the algorithm, the current position is evaluated as a problem solution. If that position is better than any that has been found so far, then the coordinates are stored in the second vector, $\overrightarrow{p_i}$. The value of the best function result so far is stored in a variable that can be called $pbest_i$ (for "previous best"), for comparison on later iterations. The objective, of course, is to keep finding better positions and updating $\overrightarrow{p_i}$ and $pbest_i$. New points are chosen by adding $\overrightarrow{v_i}$ coordinates to $\overrightarrow{x_i}$, and the algorithm operates by adjusting $\overrightarrow{v_i}$, which can effectively be seen as a step size.

The algorithm for the canonical PSO can thus be written as (Kennedy and Eberhart, 1995):

1. Initialize a population array of particles with random positions and velocities on *D* dimensions in the search space.

2. loop
    i. For each particle, evaluate the desired optimization fitness function in *D* variables.
    ii. Compare particle's fitness evaluation with its $pbest_i$. If current value is better than $pbest_i$ then set $pbest_i$ equal to the current value, and $\overrightarrow{p_i}$ equal to the current location $\overrightarrow{x_i}$, in *D*-dimensional space.
    iii. Identify the particle in the neighborhood with the best success so far, and assign its index to the variable g.
    iv. Change the velocity and position of the particle according to the following equation

$$\overrightarrow{v_i} \leftarrow \overrightarrow{v_i} + \vec{U}(0, \phi_1) \otimes (\overrightarrow{p_i} - \overrightarrow{x_i}) + \vec{U}(0, \phi_2) \otimes (\overrightarrow{p_g} - \overrightarrow{x_i}) \quad (5.7)$$

$$\overrightarrow{x_i} \leftarrow \overrightarrow{x_i} + \overrightarrow{v_i} \quad (5.8)$$

    v. If a criterion is met (usually a sufficiently good fitness or a maximum number of iterations), exit loop.
3. end loop

here,

$\vec{U}(0, \phi_i)$: represents a vector of random numbers uniformly distributed in [0,ϕ_i] which is randomly generated at each iteration and for each particle

$\otimes$: is component-wise multiplication

5.3.4 Velocity clamping

In order to keep the particles from moving too far beyond the search space, we use a technique called velocity clamping to limit the maximum velocity of each particle. For a search space bounded by the range $[-x_{max}, x_{max})]$, velocity clamping limits the velocity to the range $[-v_{max}, v_{max})]$, where $v_{max} = k \times x_{max}$. The value k represents a user-supplied velocity clamping factor and usually, $0.1 < k < 1.0$. The choice of the value of the clamping factor is subjective and may be problem specific. In many optimization tasks, such as the ones discussed in the paper, the search space is not centered around 0 and thus the range $[-x_{max}, x_{max})]$ is not an adequate definition of the search space. In such a case where the search space is bounded by $[x_{min}, x_{max})]$, we define $v_{max} = k \times (x_{max} - x_{min})/2$.

5.3.5 Confinement

In PSO, the particles sometimes tend to leave the search space. Confinement prevents the particles from leaving the feasible search space. A simple confinement can be implemented by the following pseudo code:

$$if\ x(t+1) > x_{max}\ \ then\ x(t+1) \leftarrow x_{max}\ ;\ v(t+1) \leftarrow 0$$
$$if\ x(t+1) < x_{min}\ \ then\ x(t+1) \leftarrow x_{min}\ ;\ v(t+1) \leftarrow 0 \quad (5.9)$$

Several methods are used to prevent particle from leaving the search space, but they all induce some bias, most of the time in favour of the centre of the search space and also often in favour of the boundaries. However not all methods give the same biases and therefore it is possible to combine two of them in order to obtained a less biased way. Several confinement methods, including hybrid or combination of confinement methods methods, have been proposed by Clerc (http:// clerc.maurice.free.fr/pso/ Confinements_and_bias.pdf). In the present work, the simple confinement presented above has been implemented.

5.3.6 Regrouping – dealing with stagnation

Particle swarm optimization (PSO) is known to suffer from stagnation when particles prematurely converged to any particular region of the search space. Once the particle swarm gets attracted to a suboptimal (local optimum) solutions, they continue the search process within a minuscule region of the solution space, and does not escape from this local optimum. Clerc (2006) studied the stagnation behavior of particle swarms. To overcome the stagnation problem with PSO, several modifications to the standard PSO have been suggested by Evers and Ghalia (2009), Worasucheep (2008), Napoles et al., (2012) etc. In this study, the regrouping PSO suggested by Evers and Ghalia (2009) have been adopted. In this technique, stagnation of the swarm is avoided by triggering a swarm regrouping when premature convergence is detected thereby liberating the particles from the stagnation zone (suboptimal solution) and enabling further search towards the true global optimum. Along each dimension, the particles are regrouped within a range proportional to the degree of uncertainty implied by the maximum deviation of any particle from the globally best position.

5.3.7 Neighborhood topology

Another factor with a major influence on the behavior of a PSO is its neighborhood topology (Figure 5.2). A particle in the population is interconnected to other particles. This interconnection is called the neighborhood topology. This neighborhood is not defined in the Euclidian search space. Instead it is preset connectivity relation between the particles (Clerc and Kennedy, 2002). Two topologies are commonly used from the development of PSOs called: global best and local best. Where the global best topology is a fully interconnected population in which every particle can be influenced by every other particle in the swarm. The local best topology is a ring lattice. Every particle is connected to two immediate neighboring particles in the swarm. The advantage of this structure is that parts of the

population can converge at different optima. Thus, while it is mostly slower to converge, is less likely to converge at local sub-optima.

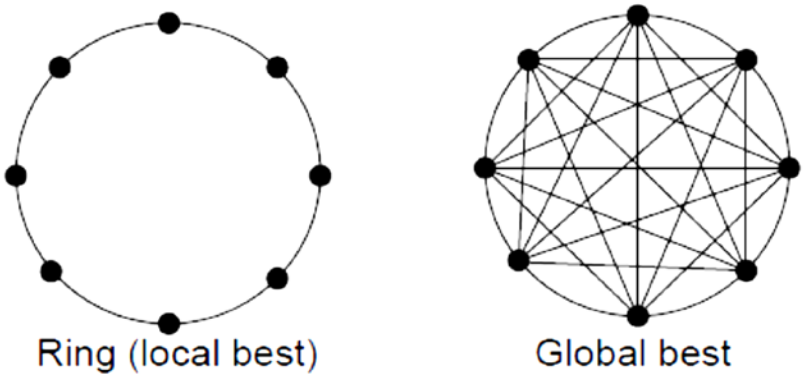

Figure 5.2 : Neighborhoods Topology

5.3.8 PSO model development

The flow chart which describes the PSO model development is shown in Figure 5.3. The main steps in the PSO model development is depicted in the pseudo code below (Kennedy and Eberhart, 1995):

```
For each particle
    Initialize particle
END
Do
    For each particle
        Calculate fitness value
        If the fitness value is better than the best fitness value (pBest) in history
            Set current value as the new pBest
    End
    Choose the particle with the best fitness value of all the particles as the gBest
    For each particle
        Calculate particle velocity according equation (a)
        Update particle position according equation (b)
    End
While maximum iterations or minimum error criteria is not attained
```

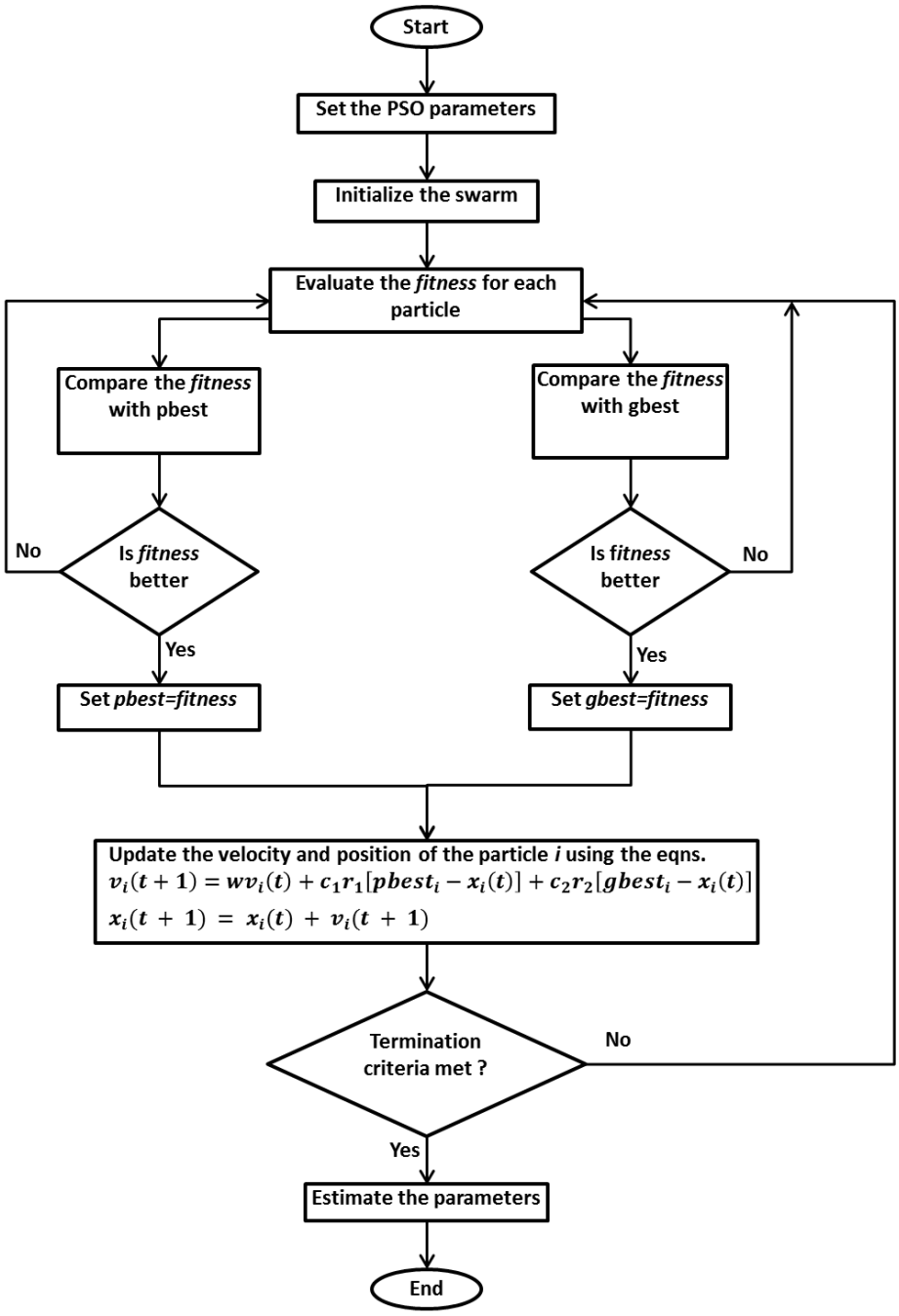

Figure 5.3: Flow chart of PSO model development

5.3.9 PSO model verification

The PSO program is verified through the following benchmark functions.

1. **Rastrigin function function**

The Rastrigin function is a non-convex function used as a performance test problem for optimization algorithms. It is a typical example of non-linear multimodal function. Finding the minimum of this

function is a fairly difficult problem due to its large search space and its large number of local minima. The two-dimensional Rastrigin function is defined by,

$$f(x,y) = 10^2 + x^2 + y^2 - 10\cos(2\pi x) - 10\cos(2\pi y) \;\; \forall\, (x,y) \in [-5.12 \;\; 5.12]$$

It has a global minimum at $(x,y) = (0,0)$ with $f(0,0) = 0$. The result of running the PSO program with 5000 iterations for this function is:

$$f_{min} = 1.199 \times 10^{-7}\,; \;\; (x_{min}\,, y_{min}) = (0.1935 \times 10^{-4}, -0.1517 \times 10^{-4})$$

The location of the minima is accurate to 4 decimal points while the minimum value is accurate to 6 decimal places

2. Six-Hump Camel back function

The six –Hump Camel back function is defined by,

$$f(x,y) = \left(4 - 2.1x^2 + \frac{x^4}{3}\right)x^2 + xy + (-4 + 4y^2)y^2 \;\; \forall \;\; x \in [-1.9 \;\; 1.9], y \in [-1.1 \;\; 1.1]$$

It has six local minima, two of which are global. The global minimum is $f_{min} = -1.0316$ and located at $(x_{min}\,, y_{min}) = (0.0898, -0.7126) \;\; and \;\; (-0.0898, 0.7126)$

The results of finding the minima of this function with the 5000 iterations of the PSO program:

$$f_{min} = 1.0316\,; \;\; (x_{min}\,, y_{min}) = (-0.898\,, 0.7127)$$

It may be seen that the minimum value is correctly found and one of the locations of the minima has also been accurately identified. For finding multiple minima, the PSO has to be modified.

3. Peaks function

The peaks function (MATLAB) is a complex function with multiple maxima and minima and is defined as,

$$f(x,y) = 3(1-x)^2 e^{-x^2-(y+1)^2} - 10\left(\frac{x}{5} - x^3 - y^5\right)e^{-x^2-y^2} - \frac{1}{3}e^{-(x+1)^2-y^2}$$

Defined in the interval $\in [-5.0 \; 5.0], y \in [-5.0 \; 5.0]$.

The results of finding the minima of this function with the 5000 iterations of the PSO program:

	Actual value	PSO predicted value
f_{min}	0.2	0.2267
x_{min}	-1.6	-1.6236
y_{min}	-6.531	-6.551

5.4 Source identification using Simulation-Optimization (SO) models

In simulation-optimization models, the groundwater pollutant source identification problem is formulated as an optimization model. The optimization model incorporates a simulation (response) model of groundwater solute transport as a series of constraints. The objective of the optimization model is to select that set of simulated potential sources which results in simulated concentrations representing the closest match with local groundwater solute concentration data.

A concentration response matrix $[R]$ was developed to describe the simulated concentrations that would result at the measurement sites as a function of the combined effects of effluent leaks along the pipe (Gorelick et al., 1983). With this information the optimization model seeks to locate those pollutant sources (leaks) and their corresponding leak magnitudes which bring the simulated concentrations and measured concentrations into agreement. The constructions of the concentration response matrix are different for the steady state and transient cases.

Steady state concentration response matrix

The construction of the concentration response matrix is in the following manner (Gorelick et al., 1983). Each of the potential source locations was considered separately. For each source, unit leaks were simulated. The concentrations ,resulting at the measurement sites, from each simulation show the response if a leak were to have occurred at only one location. The concentration at any location is a linear function of the unit leaks. Each row of the concentration response matrix is composed of concentration corresponding to a particular measurement site and which result from a unit leak at each location i.e.

$$R_{m\times n} = \begin{bmatrix} C_{11} & C_{12} & \cdots & C_{1n} \\ C_{21} & C_{22} & \cdots & C_{2n} \\ \vdots & \vdots & \ddots & \vdots \\ C_{m1} & C_{m2} & \cdots & C_{mn} \end{bmatrix} \tag{5.10}$$

Where,

$R = [C_{ij}] = concentration\ at\ j^{th}\ measurement\ point\ due\ to\ unit\ leak\ at\ i^{th}\ source$

$m = number\ of\ observation\ borewells\ or\ measurement\ points$

$$n = number\ of\ potential\ sources\ of\ effluents\ or\ contaminants$$

The concentrations at the measurement points due to sources of given strength (source flux magnitudes), $q_1, q_2, \ldots\ldots, q_n$ from the potential sources located at points/cells *1, 2, . . ., n* is then given by,

$$\begin{bmatrix} C_1 \\ C_2 \\ \vdots \\ C_m \end{bmatrix} = [R][q] = \begin{bmatrix} C_{11} & C_{12} & \cdots & C_{1n} \\ C_{21} & C_{22} & \cdots & C_{2n} \\ \vdots & \vdots & \ddots & \vdots \\ C_{m1} & C_{m2} & \cdots & C_{mn} \end{bmatrix} \begin{bmatrix} q_1 \\ q_2 \\ \vdots \\ q_n \end{bmatrix} = \begin{bmatrix} q_1 C_{11} + q_2 C_{12} + \ldots + q_n C_{1n} \\ q_1 C_{21} + q_2 C_{22} + \ldots + q_n C_{1n} \\ \vdots \\ q_1 C_{m1} + q_2 C_{m2} + \ldots + q_n C_{mn} \end{bmatrix} \quad (5.11)$$

Transient case concentration response matrix

To construct the concentration response matrix, each of the potential source locations are considered in isolation with unit leaks (i.e. source strengths). The concentrations resulting at the observation points (wells) from each simulation are the concentrations (response) in the aquifer if a leak were to have occurred at only at that location. The concentration at any location when there are simultaneous multiple leaks (sources) is a linear function of these unit leaks (Gorelick et al., 1983).

For the case studies considered in this study, each column of this matrix stores the breakthrough curves at the observation bore wells resulting from unit release from each of the sources in a particular release year. For example, the first column stores the concentrations at every recorded time steps for the observation bore wells due to a unit release from the first source in the first year. The second column corresponds to the unit release from the 2nd source in the first year of release; the third column corresponds to unit release from the 3rd source and so on. When the columns (block) for all the sources in the first year of release are completed, the columns (block) for the second of year of release are populated. This is followed by the blocks for the remaining years of the releases.

Using concentration response matrix offers a big saving on computational time when using optimization programs like PSO. In PSO, the objective function is evaluated for each particle in every iteration and the number of iterations tends to be several thousands. Without using the concentration response matrix, the groundwater transport program needs to be called each time the objective function is evaluated which can be several thousand evaluations. Consequently the computational time will be very large, in some cases even unacceptable depending on the convergence rate of the optimization algorithm. By using the concentration response matrix, the simulations of unit leak from each source can be run only once and is saved in a matrix.

5.4.1 RPCM Simulation model

The formulation of the meshfree RPCM flow and transport simulation model has been described in chapter 4. This simulation model is used to generate the concentration distributions in the aquifer which is then used as the observed concentration data in the SO model. It is also used to construct the concentration response matrix as described in the previous section. Without using the concentration response matrix, this simulation model will be called in every iteration of the optimization model to compute the fitness or objective function. This can lead to huge computational time if the simulation period is large and time step size is small. It may be mentioned that calibrated hydro-geological parameters must be used in the simulation model.

5.4.2 PSO optimization model

The model for standard PSO has been used in the present study. The parameters of the PSO such as swarm size, acceleration coefficients; topology has been decided through sensitivity analysis. These parameters have a profound impact on the performance of the PSO. The trade-off between exploration and exploitation is controlled by the acceleration coefficients and also by the neighborhood topology (section 5.3.7). The ring topology facilitates more extrapolation since it interacts with fewer particles while the star (global best) topology encourages exploitation since it interacts with every particle in the swarm. The stopping or convergence criteria are decided by using both the maximum number of iterations and a preset value of the fitness function. Whichever criterion is achieved first will decide the stoppage of the iteration.

5.4.3 RPCM-PSO SO model development

The developed SO model uses meshfree RPCM simulation model for generating the solute concentrations while PSO is used as the optimizer to search for the sources (location and magnitude) which leads to the best match between predicted and observed solute concentrations. The PSO iterations calls the simulation model to compute the objective function whenever it generates a new set of the plausible sources. This happens in every iteration of the PSO. This provides the coupling between the optimization and the simulation models. As mentioned earlier, the simulation model is not directly used in these iterations, rather the use of concentration response matrix allows the model to avoid repeated call of the simulation model and make the evaluation of concentration predictions efficient computationally. Figure 5.4 shows the flow chart of the developed RPCM-PSO-SO model.

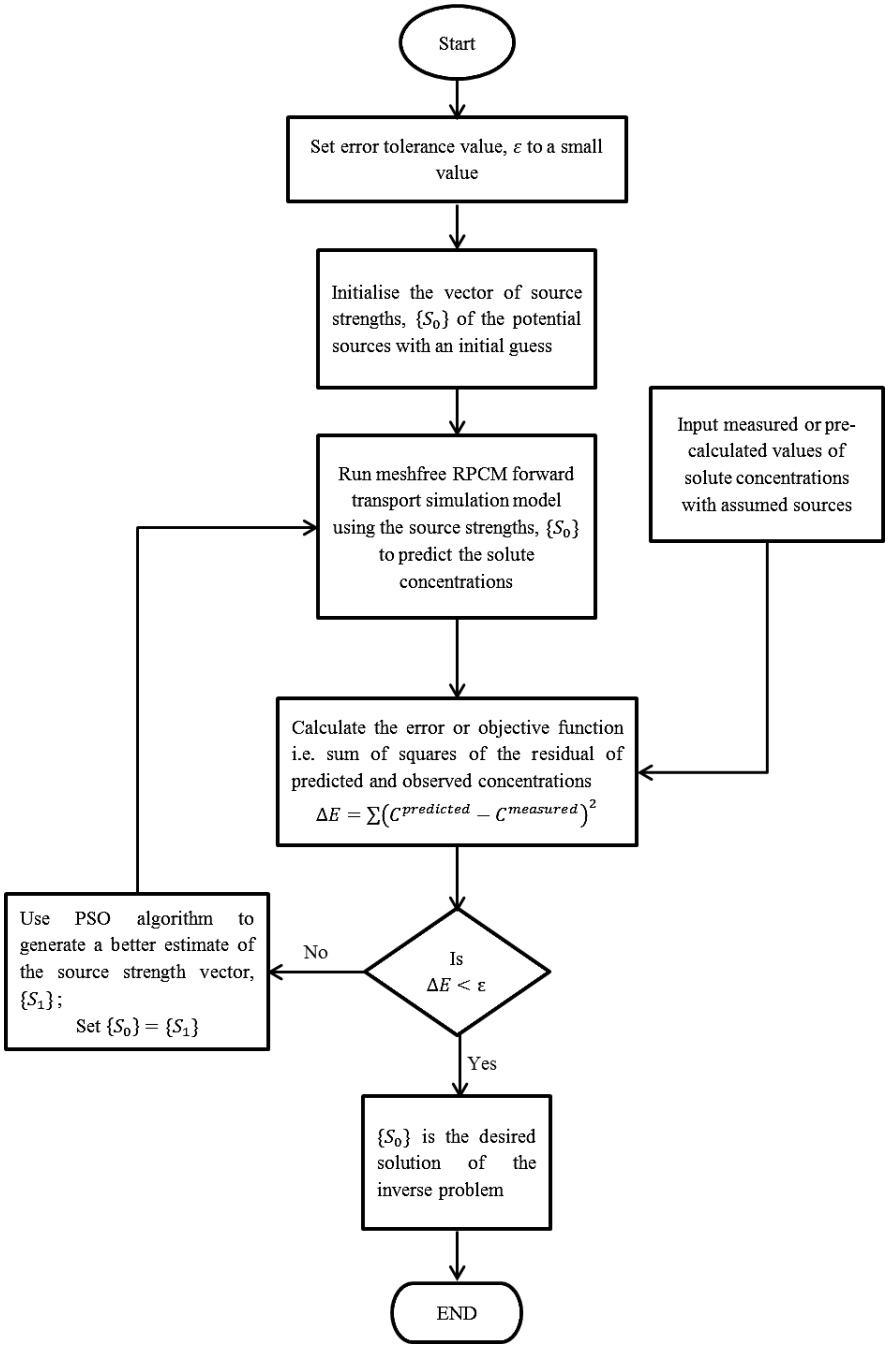

Figure 5.4: Flow chart of the Simulation -Optimization model

5.5 Verification of SO models for source identification

The developed RPCM-PSO-SO model is verified with problems solved by other source identification models. This allows the direct comparison of the performance of the proposed method with other existing models.

5.5.1 Problems considered

In this section, the RPCM-PSO-SO model for contaminant source identification is demonstrated through contamination problems in hypothetical aquifers. This hypothetical problem was studied by Gorelick et al., (1983) and has been chosen so that the performance of the PSO based model can be compared to the techniques proposed by the authors. The use of optimization based source identification model was first proposed by the above mentioned authors with two scenarios of contaminant release. The first case, which is a steady state case, involves simulating continuous release of contaminants from an underground pipe running through the hypothetical aquifer. The second case study involves periodic releases from some randomly distributed disposal sites and represents the transient case study. The optimization methods used in the above mentioned work is least squares regression and linear programming. After this comparative study with the techniques proposed by Gorelick et al. (1983), a parameter sensitivity study is conducted with regard to the PSO parameters namely, swarm population size, acceleration coefficient and the constriction coefficient.

5.5.2 Steady state source identification –effluent flow through an underground pipe

For demonstrating source identification with simulation-optimization model, here we consider the hypothetical aquifer system as shown in Figure 5.5 in which groundwater pollutant sources are to be identified. It is assumed that an underground pipe lies in an unsaturated zone above the water table and carries effluent from one end to the other. The groundwater head boundaries at the top and bottom are also shown in the figure. This problem was studied by Gorelick et al.(1983) and all the parameters are taken from the above work. It is assumed that the effluent (pollutant) has been flowing continuously within the pipe and contains high concentrations of the non-reactive pollutants – chloride and tritium. Several observation or measurement borewells are located within the modeling region which is used for detecting and measuring the concentration of the pollutant found in the groundwater. The detection of the pollutant in the water samples collected from the observation borewells indicates that a small leak or series of leak in the pipe has taken place resulting in the pollution of the groundwater. It is assumed that the relatively small volume of effluent that has leaked into the aquifer has left the original, steady groundwater flow pattern unchanged. Flow from the leak(s) through the unsaturated zone is assumed to be vertical to the water table.

Here the concentration distributions are at steady state. It is required to locate the leak(s) and determine the magnitude of the solute and water flux from each leak from the concentration distributions of the pollutant observed in the water samples of the observation borewells.

A preliminary groundwater flow and transport simulation was carried out to create the concentration data used in this problem. First a steady state groundwater flow model was constructed with the boundary conditions as described in the Figure 5.5. It also shows the grid used by Gorelick et al. (1983). The same nodal distribution has been used in this study. A constant hydraulic conductivity (Gorelick et.al. 1983) of 0.864 m/day was used. The aquifer is 10 m thick and is of size 160 m x 240.m. After the flow model is created, a steady state solute transport model constructed and coupled to the flow model. In the transport model two sources (leaks) were placed at the locations III and VIII, as in Figure 5.5.

Following parameters (Gorelick et.al., 1983) are used in the transport model:

Chloride concentration in the pipe water: 15,000 mg/L

Tritium concentration in the pipe water: 15,000 µCi/L

Solute flux in the first leak (at location III): 90.0 mg/sec chloride and 90.0 µCi/sec Tritium

Solute flux in the second leak (at location VIII): 45.0 mg/sec chloride and 45.0 µCi/sec Tritium

From the above solute concentrations in the pipe and the solute fluxes at the leaks, the water flux from the pipe may be calculated as follows:

Water flux at first leak (at location III) = (45.0 mg/sec) / (15,000 mg/L Chloride) * (86,400 sec/day)
= 259.2 L/day

Water flux at first leak (at location III) = (90.0 mg/sec) / (15,000 mg/L Chloride) * (86,400 sec/day)
= 518.4 L/day

Other transport parameters are:

Longitudinal dispersivity = 40 m

Transverse dispersivity = 20 m

Porosity = 0.3

Figure 5.6 shows the steady state head distribution and flow vectors of the aquifer system subject to the boundary conditions as specified above. The Chloride concentration distribution at steady state is shown in the Figure 5.7. Tritium concentration follows a similar distribution. A total of 11 random measurement points or surveillance borewells are chosen for monitoring the chloride and tritium concentrations. The locations of these borewells are as shown in the Figure 5.5. All the borewells are placed in the downstream direction (refer to Figure 5.6). The concentrations of chloride and tritium in these borewells forms the baseline data i.e. observed concentration data for the source identification model.

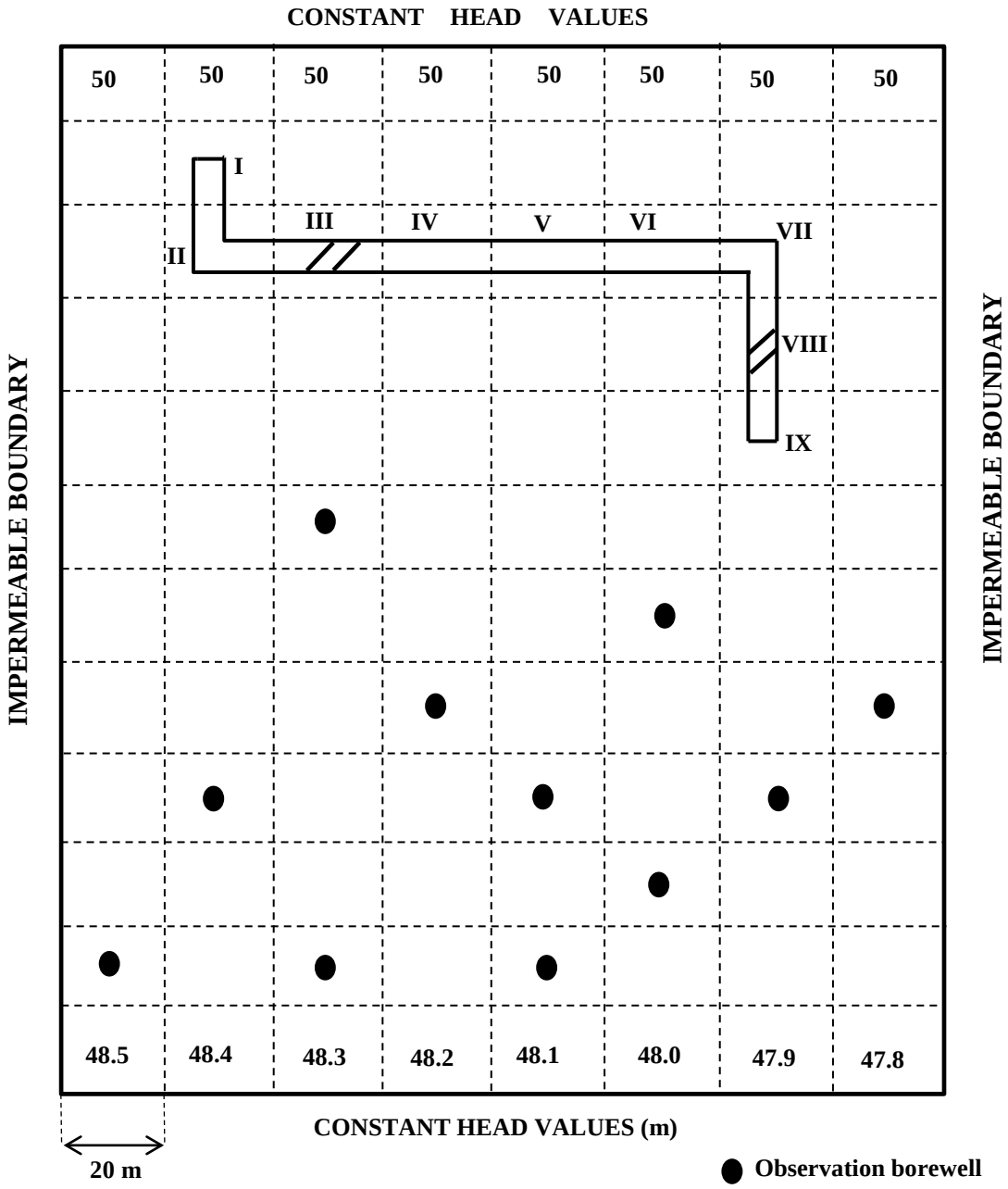

Figure 5.5: Hypothetical Aquifer system for steady state pollutant source identification. Potential leak locations are marked by I through IX

Given this concentration data and the location of all the potential sources, the optimization model seeks to find a set of simulated sources (or source strength vector) which yields closest match to the

concentration data. The error metric which is used to measure this matching can be the least squares residual defined as follows:

$$R = \sum_{i=1}^{N} \left(C_i^{predicted} - C_i^{observed}\right)^2 \qquad N = number\ of\ observation\ points \tag{5.12}$$

But as pointed out by Gorelick et.al.(1983), the use of this ordinary residual introduces a bias in favour of pairs with higher numerical values. Hence a normalized residual as defined below is employed:

$$R = \sum_{i=1}^{N} \left(\frac{C_i^{predicted} - C_i^{observed}}{C^*}\right)^2 \quad \text{where } C^* = C^{observed} \text{ or some smoothed value of } C^{observed} \tag{5.13}$$

The optimization model seeks to minimize the value of *R* with respect to various sets of the source strength vector in order to determine the pipe leak locations and leak magnitudes. Since PSO is being used for optimization in this work, the sets of source strength vectors acts as the particle of the swarm. Several particles are generated randomly to start the search process. Each particle moves around (i.e. is perturbed) in the search space trying to find the lowest value of the objective function (referred to as fitness function in this context) till all the particles converge to the global minima. Additional constraints are applied to stop the particles from crossing the search boundary. In the present case, the constraint on the source strength is that it cannot be negative but the upper limit is unbounded. The displacement (or perturbation) of the particle is also restricted in order to allow exhaustive search of the space.

The results of the source identification using PSO optimization is shown in Table 5.1. It tabulates the source fluxes from the 9 potential sources as predicted by the simulation-optimization model. This table shows the results for 20 independent runs of the SO model and the final result is found by taking average from these runs. As can be seen from the table, the sources at locations III and VIII are identified with acceptable accuracy. However the model has also predicted spurious minor sources at locations VII and VIII. The model has also predicted non-zero source fluxes from locations I, II, and IV. However these fluxes are very small and can be safely neglected. For locations V and VI, the model has correctly identified them as not leaking. Further a sensitivity study of the PSO parameters has been done in section 5.6. As shown in that section, this sensitivity study will allow the determination of the optimal values of the PSO parameters and improve the accuracy of the model predictions significantly. The spurious sources or noises will also be reduced.

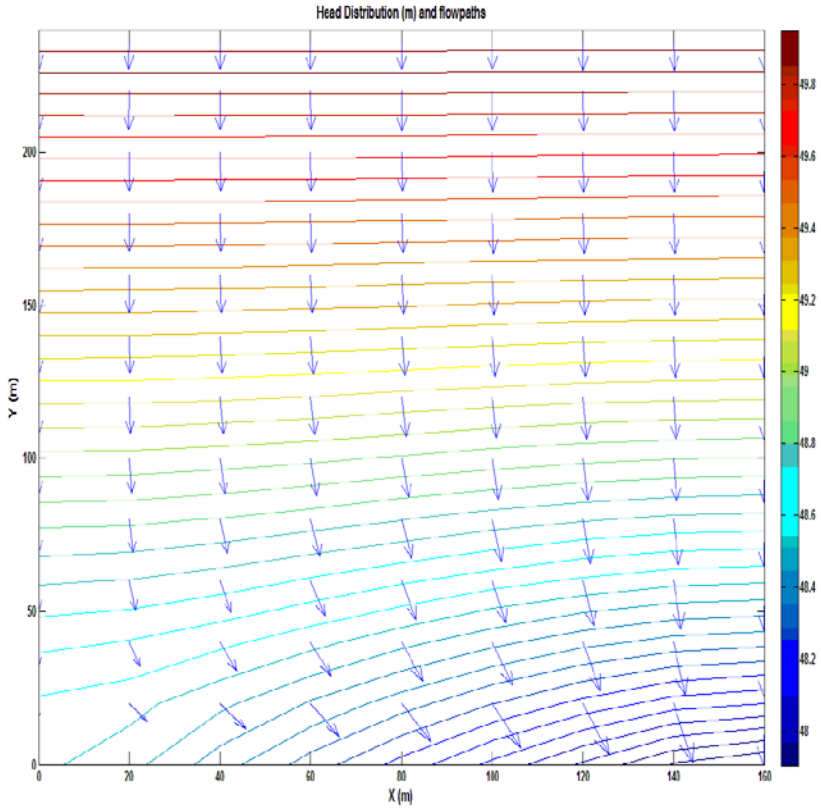

Figure 5.6: Head distribution (in m) and flow vectors of the aquifer system

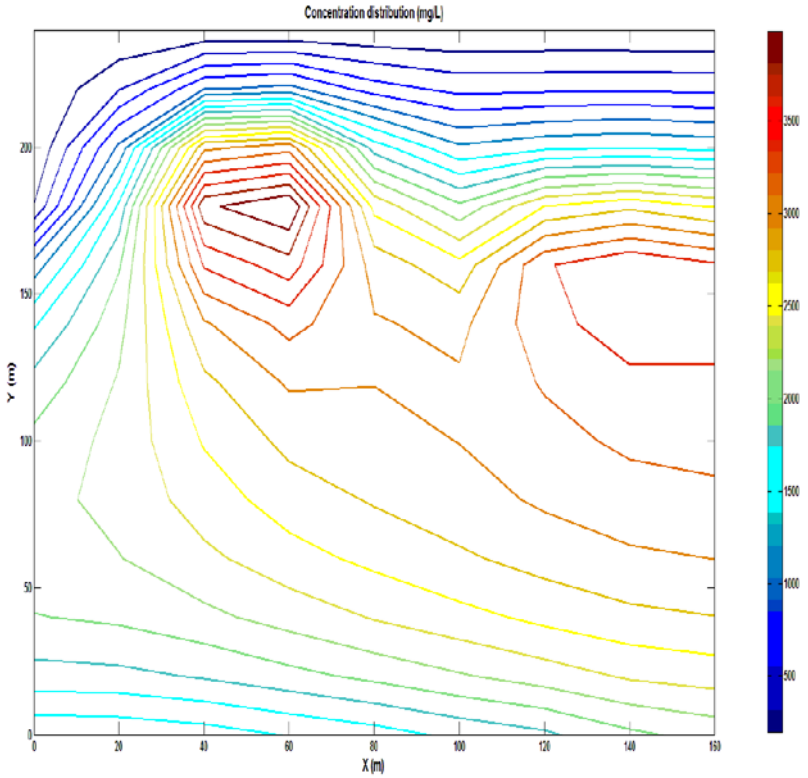

Figure 5.7: Steady state Chloride concentrations in the aquifer system

Table 5.1 : Results of source identification by using Particle Swarm Optimization

Serial	Iterations	Residual	Source location points								
			I	**II**	**III**	**IV**	**V**	**VI**	**VII**	**VIII**	**IX**
1	900000	0.0061	0	0	518.2757	0.1391	0	0	4.8818	252.6626	2.3862
2	900000	0.0073	0	0	518.2645	0.1513	0	0	5.3556	252.0304	2.616
3	900000	0.0136	0	0	518.2139	0.2077	0	0	7.3066	249.4182	3.5691
4	900000	0.0193	0	0	518.1808	0.2452	0	0	8.7208	247.5249	4.2603
5	900000	0.0188	0	0	518.1824	0.2437	0	0	8.6011	247.681	4.2051
6	900000	0.0341	0	0	518.1034	0.3312	0	0	11.5767	243.6995	5.6565
7	900000	0.0364	0	0	518.0962	0.3393	0	0	11.963	243.1851	5.8431
8	900000	0.0106	0	0	518.2335	0.186	0	0	6.4576	250.5504	3.158
9	900000	5.13E-04	0	0	518.3641	0.0401	0	0	1.42	257.2991	0.6935
10	900000	0.0123	0	0	518.2262	0.1946	0	0	6.9454	249.9006	3.394
11	900000	0.0419	0	0	518.0781	0.3605	0	0	12.8401	242.006	6.2763
12	900000	0.0218	0	0	518.1656	0.2617	0	0	9.2627	246.7997	4.5247
13	900000	0.0069	0	0	518.2676	0.1482	0	0	5.1901	252.2485	2.5379
14	900000	0.0136	0	0	518.2141	0.2077	0	0	7.3081	249.416	3.5701
15	900000	4.59E-04	0	0	518.3659	0.0381	0	0	1.344	257.4006	0.6567
16	900000	0.0076	0	0	518.2604	0.1558	0	0	5.4663	251.8815	2.6705
17	900000	0.0038	0	0	518.3015	0.1102	0	0	3.8717	254.0136	1.8939
18	900000	0.0302	0	0	518.1264	0.3059	0	0	10.8996	244.6081	5.3247
19	900000	1.18E-05	0.0004	0.0002	518.3939	0.0052	0	0	0	259.1993	0
20	900000	0.0274	0	0	518.141	0.2899	0	0	10.3879	245.2947	5.0735
Average or Leak magnitudes predicted by SO model (L/day)			**0.0**	**0.0**	**518.2**	**0.2**	**0**	**0**	**6.9**	**249.8**	**3.4**
True values of source flux (L/day)			**0**	**0**	**518.4**	**0**	**0**	**0**	**0**	**259.2**	**0**

Table 5.2 below compares the source strengths predictions of the PSO based source identification model to that of the least squares and linear programming model of Gorelick et al.,(1983).

Table 5.2 : Comparision of leak magnitude predictions

Potential Source Location	True Leak Magnitudes (l/d)	PSO Predicted Leak Magnitudes (l/d)	Leak magnitudes predicted by Gorelick (1983) et.al.	
			Linear Programming	Regression
I	0	0	0.0	-1.0
II	0	0	0.1	-0.6
III	518.4	518.2	518.2	521.1
IV	0	0.2	0	-1.3
V	0	0	0	-1.1
VI	0	0	0.0	-1.5
VII	0	6.9	2.0	-0.4
VIII	259.2	249.8	256.5	259.2
IX	0	3.4	1.0	0.0

It can be seen that the PSO based source identification model gives about the same accuracy as that of the linear programming and regression based models of Gorelick et al.,(1983). It may be observed that the linear programming model give slightly better predictions than PSO model. However, it may be noted that the PSO parameters used in the above calculations have not been optimized. As discussed in section 5.6, with optimized parameters the predictions of the model can be significantly improved and be better than the traditional optimization methods. Further it may be noted that the traditional optimization techniques is prone to getting trapped in local optima instead of finding the global optima. The main advantage of artificial intelligence based optimization techniques is that they do not suffer from this issue and has a better chance of finding the global optima.

5.5.3 Transient source identification –waste release from disposal sites

Consider the hypothetical aquifer as shown in Figure 5.8 with five sources of contamination i.e. disposal sites. This problem was studied by Gorelick et al.(1983) and is being adapted in this study to compare the performance of the PSO based SO source identification model to the optimization methods proposed by Gorelick et al.(1983). The five disposal sites S_1, S_2, S_3, S_4 and S_5 are shown in the Figure 5.8. Three observation wells W_1, W_2 and W_3 shown in the figure records the contaminant concentrations over a 15

year period. The thickness of the aquifer is 30.5 m while the hydraulic conductivity is 0.01 cm/s and is considered to be isotropic. Effective porosity is taken to be 0.3. Longitudinal and transverse dispersivities are 7.6 and 2.3 m respectively. The recharge rate of the pond has been taken as 0.0067 m/day and contributes roughly around 21% of the total flow through the system. The waste disposal rate has been kept at a low value of 1 L/s so that it does not significantly affect the groundwater hydraulic head distribution. The disposal flux, which is the product of the liquid volume disposal rate and the solute concentration of the waste, from the disposal sites has been kept at same values as in Gorelick et. al (1983) to have a comparative study. Table 5.3 shows the schedule of the contaminant disposals from the sites and the magnitude (disposal fluxes) of these disposals. The disposals are assumed to happen during a four year period and stopped thereafter.

Table 5.3: Contamination release schedule from the sources

Year of release	**Disposal fluxes from the disposal sites (in gm/s)**				
	Site 1	Site 2	Site 3	Site 4	Site 5
1st	51	15	47	27	0
2nd	0	9	44	35	0
3rd	0	11	8	0	12
4th	24	0	0	0	16

A groundwater flow and transport model using meshfree RPCM was constructed to generate the breakthrough curves at the observation wells. The nodal grid used in the meshfree RPCM flow and transport simulation is shown in Figure 5.9. A total of 177 nodal points are used in the simulation. The nodal spacing is 91.4 m in both the *x*- and *y*- directions. A circular support domain (Guneshwor et al., 2016) was employed with a radius equal to three times the nodal separation. The simulation was carried out for 15 years period with a time step size of 40 days. Additionally the time steps included all the multiples of 365 days i.e. the end of each year of the 15 years period. The breakthrough curves at the three designated observation borewells obtained from the simulation are shown in Figure 5.10. These breakthrough curve data are be treated as the observed concentration data for the source identification model.

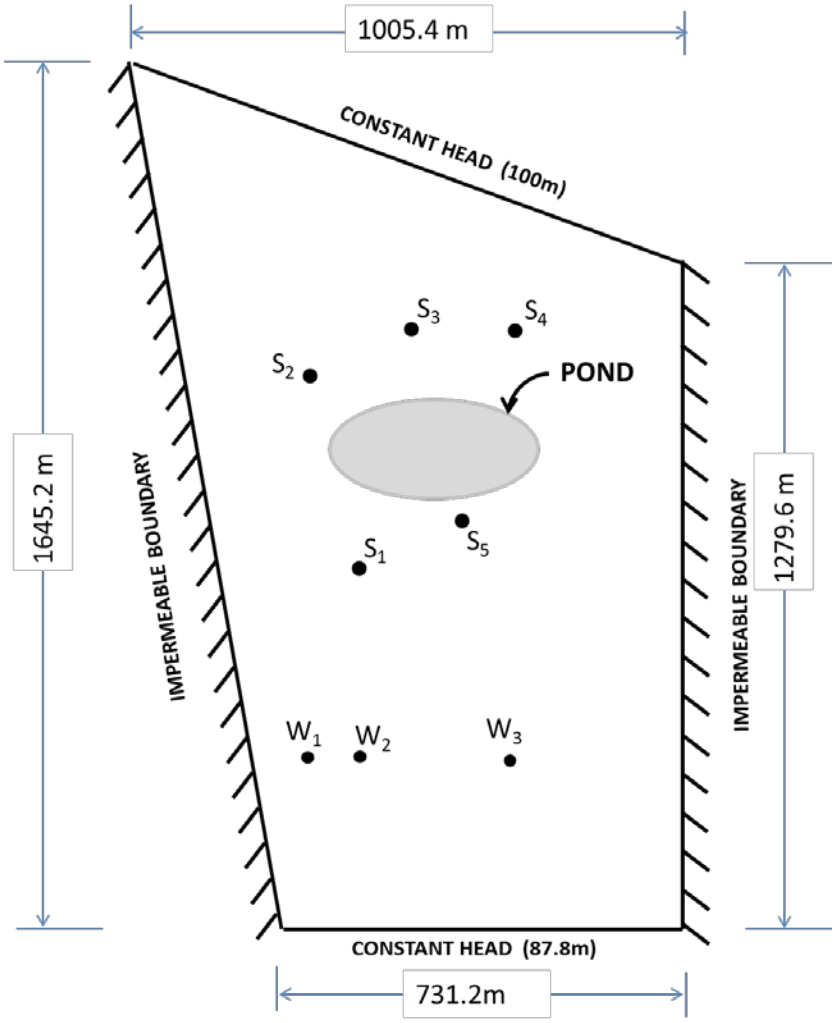

Figure 5.8: Hypothetical aquifer with 5 contaminant disposal sites

To construct the concentration response matrix, the simulation model was run to generate the breakthrough curves corresponding to unit releases from each of the five disposal sites for each year of release. There are a total of twenty 1-year disposal events in this case study (Table 5.3) and the simulation model was run for each of these disposal events. The breakthrough curves from these simulations are then used to construct the concentration response matrix. Each column of this matrix stores the breakthrough curves at the observation wells resulting from simulation of the unit release disposal events.

The observed concentration data and the concentration response matrix are then fed to the PSO based source identification model for prediction of the disposal fluxes from the sources or sites. The PSO optimizer tries to find that set of disposal fluxes that minimize the objective function (defined in equation 5.14) which is the sum of squared differences between predicted and observed concentrations i.e.

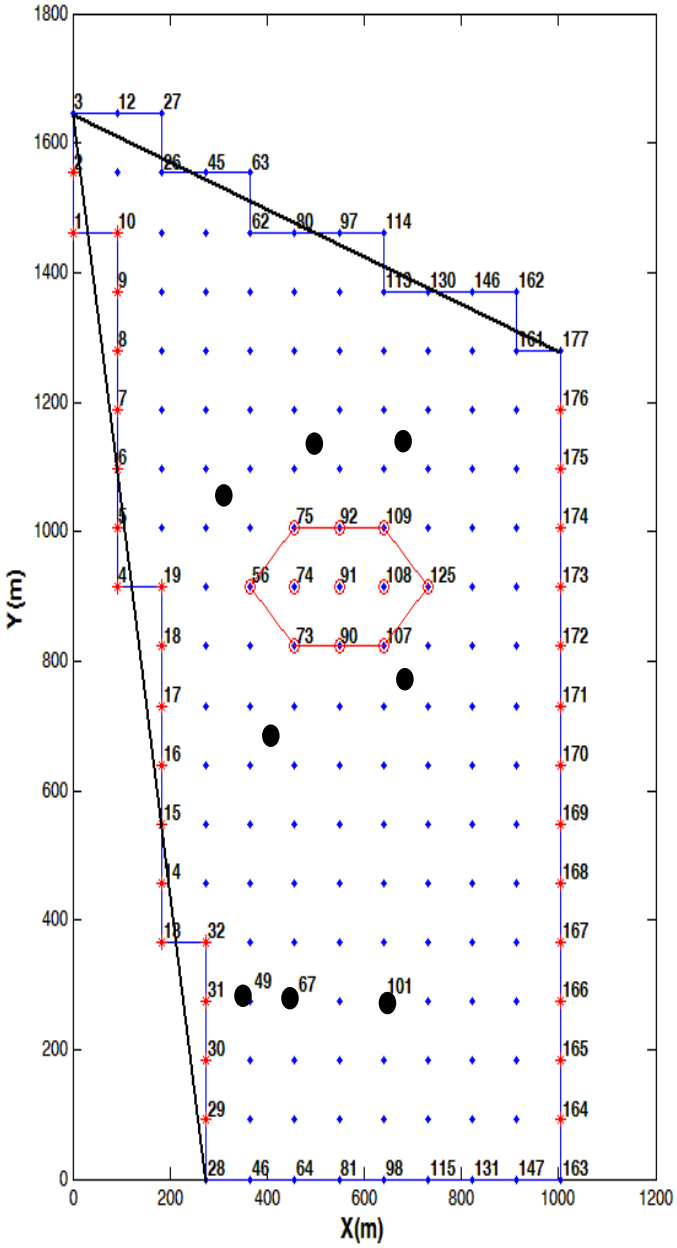

Figure 5.9 Nodes used in the meshfree RPCM transport simulation

$$S = \sum_{i=1}^{NO}\sum_{j=1}^{NT}\left(C_{i,j}^{Pred} - C_{i,j}^{Obs}\right)^2 \tag{5.14}$$

where, NO = no. of observation bore wells, NT = no. of time steps, $C_{i,j}^{Pred}$ =Predicted concentration at i^{th} observation point at the j^{th} time step, $C_{i,j}^{Obs}$ =Observed/measured concentration at i^{th} observation point at j^{th} time step.

Further, the following two error metrics are defined for measuring the accuracy of the predictions from the source identification model:

Root mean square error in concentration predictions :

$$RMS\_Concn = \sqrt{\frac{\sum_{i=1}^{NO}\sum_{j=1}^{NT}\left(C_{i,j}^{Pred} - C_{i,j}^{Obs}\right)^2}{N}} \quad (5.15)$$

Root mean square error in source strength predictions:

$$RMS\_source = \sqrt{\frac{\sum_{i=1}^{NS}\sum_{t=1}^{NR}\left(S_{i,t}^{Pred} - S_{i,t}^{Actual}\right)^2}{N}} \quad (5.16)$$

where, $NS =$ no of sources or injection wells, $NR =$ no. of release years, $S_{i,t}^{Pred} =$ Predicted concentration of the i^{th} source in the t^{th} release year, $S_{i,t}^{Actual} =$ Actual source concentration of the i^{th} source in the t^{th} release year. The first of the error metric RMS_Concn is a measure of the effectiveness of the PSO optimization algorithm while the second error metric RMS_source is a measure of performance of the source identification model as a whole. It may be noted that the primary objective of the optimization algorithm is to minimize the difference between the measured and predicted concentrations only. It does not directly minimize the differences between the predicted and the actual source strengths. Therefore both the metrics have been defined to gauge the performance of the model.

The number of objective (fitness) function evaluations (iterations) is an important factor which directly controls the convergence of the PSO and is a measure of efficiency of the optimizer. More iterations produce better results but at the cost of more computation time. A convergence study with respect to the number of iterations has been conducted for this case study. Table 5.4 shows the results of this convergence analysis. It is observed that the *RMS_Concn* values are very low even with only 10^3 iterations while the *RMS_Source* has much slower rate of convergence. This implies that the optimizer is very effective in minimizing the fitness function. The slower convergence rate in identifying the disposal fluxes despite very close matching of predicted and observed concentrations, as inferred from the low values of *RMS_Concn*, is due to the non-uniqueness of the source identification problem (Atmadja and Bagtzoglou, 2001b). Several sets of source strengths (disposal fluxes) may lead to nearly the same spatial and temporal concentration distribution.

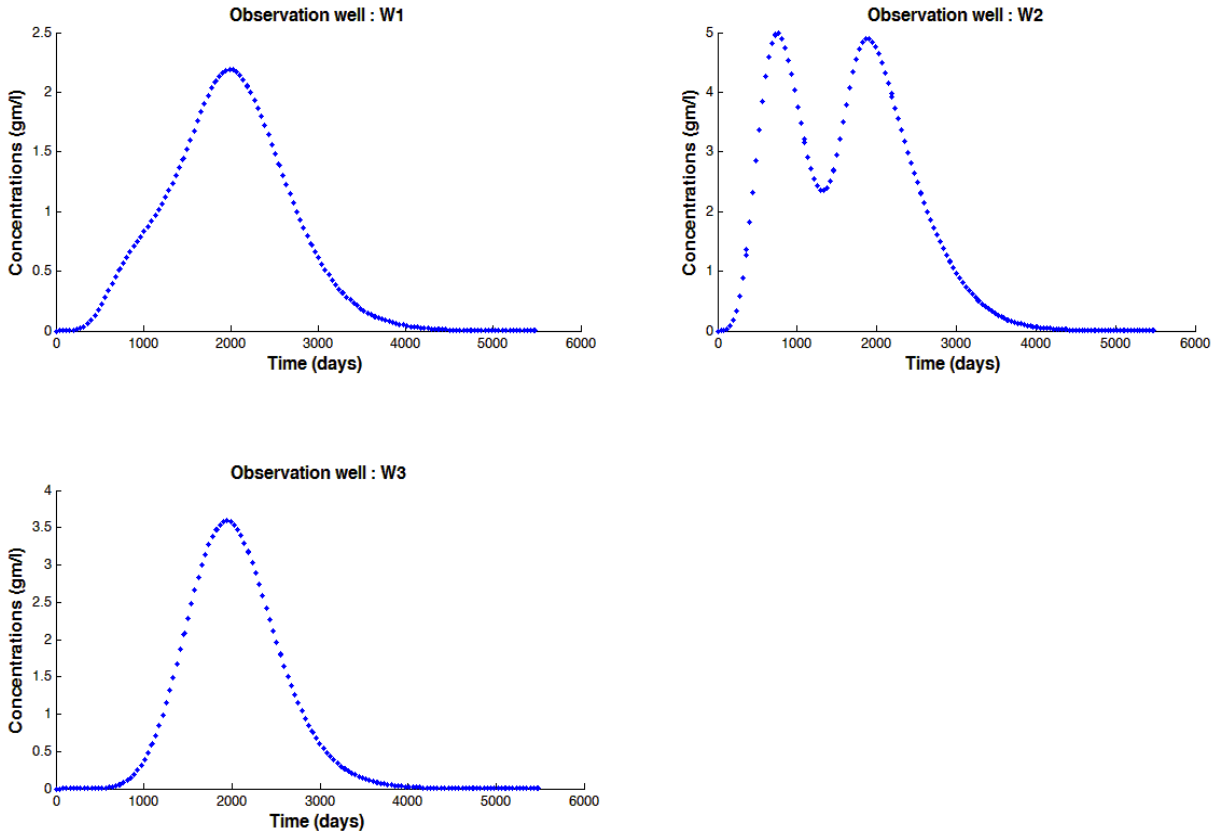

Figure 5.10 Breakthrough curves at the observation wells

Table 5.4: Convergence with respect to iterations

No. of iterations	***RMS_Source***	***RMS_Concn***
10^3	9.574	0.0035
$5x\ 10^3$	5.033	5.867×10^{-4}
$10\ x10^3$	3.593	4.514×10^{-4}
50×10^3	3.366	3.768×10^{-4}
10^5	1.645	2.575×10^{-4}

Table 5.5 shows the comparison of the source predictions of the PSO based source identification model with 10^5 iterations to those predicted by linear programming and stepwise regression used by Gorelick et al.(1983). It can be seen that the source identification model with PSO optimizer yields better results in comparison to the model values of Gorelick et al.(1983) which uses linear programming and stepwise regression as the optimizer. This may be readily inferred from the smaller value of *RMS_Source* for the

PSO based SO model. In fact, looking at Table 5.4 and Table 5.5 shows that the PSO based model already yields better results than the linear programming model of Gorelick et. al (1983) when the number of iterations touches 5 x 10^4. Most of the disposal fluxes were correctly identified to within 10% of their value except for a point where the error was around 30%. It may also be observed that a few erroneous or spurious sources are also predicted by the SO model. However their magnitudes are very small and can be safely ignored.

Table 5.5: Comparison of PSO based SO model source release rate predictions with conventional optimization approaches

Disposal Site	Year	Actual release rates (gm/s)	SO model with PSO optimizer (10^5 iterations) (gm/s)	Prediction by SO model of Gorelick et al.,(1983)	
				Linear Programming	Stepwise regression (20 variable)
1	1	51	51	51	51
	2	0	0	0	-0.04
	3	0	0	0	-0.08
	4	24	24	21	22
2	1	15	15	15	14
	2	9	9	9	10
	3	11	11	11	11
	4	0	0	0	-0.08
3	1	47	44	62	55
	2	44	46	39	40
	3	8	7	8	7
	4	0	0	0	0.4
4	1	27	24	26	29
	2	35	34	37	37
	3	0	1	0	-1
	4	0	0	0	0.3
5	1	0	0	0	-0.02
	2	0	3	0	-0.03
	3	12	16	11	11
	4	16	17	11	12
RMS Source			**1.645**	**3.8079**	**2.3798**

5.6 Sensitivity study of PSO parameters

To understand the impact of the PSO parameters, a sensitivity study is conducted for these parameters. The steady state case of contaminated effluent leakage from an underground pipe, discussed in section 5.5.2, is re-examined here.

The convergence of the PSO optimizer is heavily influenced by the values of the two parameters namely –size of the swarm population and the values of the acceleration coefficients. There are no fixed criteria for choosing the optimal values of these parameters. Clerc and Kennedy (2002) and Trelea (2003) have provided empirical values of these parameters. In the absence of any criteria to find the optimal values of the parameters, a sensitivity study is conducted to obtain the optimal values of these parameters. In this section, the contaminant leak magnitudes predicted by the PSO based SO model is studied for various parameter values of the PSO.

The following two (root mean square (RMS) quantities or error metrics are defined to study the convergence behavior of the source identification model:

$$RMS^{source} = \sqrt{\frac{\sum_{i=1}^{NS}\left(S_i^{Predicted} - S_i^{actual}\right)^2}{N}} \tag{5.17}$$

$$RMS^{conc} = \sqrt{\frac{\sum_{i=1}^{NO}\left(C_i^{Predicted} - C_i^{actual}\right)^2}{N}} \tag{5.18}$$

where,

S_i^{actual} = Actual Source flux of the ith potential source

$S_i^{Predicted}$=Predicted Source flux of the ith potential source

C_i^{actual} = Measured Concentration of the contaminant at the ith observation point

$C_i^{Predicted}$ = Predicted Concentration of the contaminant at the ith observation point

NS = Total number of potential sources

NO = Total number of measurement /observation points for the contaminant

RMS^{source} is the root mean square error in the prediction of the source fluxes while RMS^{conc} is the root mean square error of the contaminant concentration prediction by the SO model.

5.6.1 Swarm population size sensitivity

The results of the sensitivity study with respect to the size of the swarm used in the optimization are summarized in the Table 5.6. The source strength predictions from these population size studies are shown in Table 5.7. It can be seen that a swarm size of 190 particles gives the best predictions of the source strengths.

It can be seen from the Table 5.6 and Table 5.7 above that the swarm size does affect the final outcome but in a limited manner. Though a swarm size of 190 yields the best estimate of the source strength predictions, a swarm size of 100 and above yields nearly the same results –the variations are negligible. A

larger swarm size leads to more computational time. Therefore a swarm size of 100 may be a good balance between accuracy and computational cost.

Table 5.6 : Swarm population size sensitivity study

Population Size	RMS (source strength)	RMS (Concentration)	Mean fitness (25 runs)	Total time taken (hrs.)
30	15.8066	0.1477	2.20E-08	1.9186
40	15.4236	0.1441	2.02E-08	2.2512
50	14.6535	0.1369	2.07E-08	2.6636
75	12.1509	0.1135	1.37E-08	3.5945
100	11.219	0.1048	1.24E-08	4.5952
125	10.0134	0.0934	9.76E-09	5.5421
150	12.2016	0.1138	1.34E-08	6.737
160	9.8637	0.0921	9.42E-09	7.0776
170	9.6576	0.0902	8.96E-09	7.446
175	10.7321	0.1003	1.22E-08	7.6448
180	10.5751	0.0988	1.01E-08	7.8158
185	12.4234	0.116	1.30E-08	8.1277
190	**9.1197**	**0.0844**	**8.98E-09**	**8.354**
195	11.713	0.1094	1.25E-08	8.4806
200	11.0438	0.1032	1.08E-08	8.7552
210	12.7987	0.1195	1.43E-08	9.2336
225	9.3608	0.0872	8.98E-09	9.9299
250	11.5115	0.1075	1.13E-08	10.9005

Table 5.7: Source strength predictions for various sizes of the swarm population

Actual Source Strength	Source strength predictions for various population sizes														
	Population Size (λ)														
	40	**50**	**75**	**100**	**125**	**150**	**160**	**170**	**180**	**190**	**195**	**200**	**210**	**225**	**250**
0	0.0	0.0	0.0	0.0	0.0	0.0	0.0	0.0	0.0	0.0	0.0	0.0	0.0	0.0	0.0
0	0.0	0.0	0.0	0.0	0.0	0.0	0.0	0.0	0.0	0.0	0.0	0.0	0.0	0.0	0.0
518.4	516.2	516.3	516.6	516.8	516.9	516.6	517.0	517.0	516.9	517.1	516.7	516.8	516.5	517.0	516.7
0	3.1	2.9	2.4	2.2	2.0	2.4	2.0	1.9	2.1	1.8	2.3	2.2	2.5	1.9	2.3
350	348.9	348.9	349.1	349.2	349.3	349.1	349.3	349.3	349.2	349.3	349.1	349.2	349.1	349.3	349.2
0	0.0	0.0	0.0	0.0	0.0	0.0	0.0	0.0	0.0	0.0	0.0	0.0	0.0	0.0	0.0
0	26.5	25.1	20.8	19.2	17.2	20.9	16.9	16.6	18.1	15.6	20.1	18.9	22.0	16.1	19.7
259.20	223.8	225.5	231.3	233.4	236.2	231.2	236.5	237.0	234.9	238.2	232.3	233.8	229.8	237.7	232.7
0	13.0	12.4	10.2	9.5	8.4	10.3	8.3	8.1	8.9	7.7	9.9	9.3	10.8	7.9	9.7

5.6.2 Acceleration coefficients sensitivity study

The acceleration coefficients namely ϕ_1 and ϕ_2 play a very vital role in the overall convergence of the particle swarm optimizer. These parameters control the trade-off between exploitation and extrapolation aspects of the PSO optimizer. The results of the sensitivity study with respect to the various values of these parameters are summarized in the tables Table 5.8 and Table 5.9.

Table 5.8: Sensitivity study with respect to the acceleration coefficients

ϕ_1	$\phi_2 = 4.1 - \phi_1$	RMS (Source Strength)	RMS (Concentration)	Mean Fitness	Total time taken (Hrs.)#
1.85	2.25	9.76	0.09	8.66E-09	8.4885
1.9	2.2	10.26	0.09	1.02E-08	8.4991
1.95	2.15	10.89	0.10	1.11E-08	8.4682
2	2.1	11.71	0.11	1.18E-08	8.4656
2.05	2.05	10.73	0.10	1.07E-08	8.2733
2.1	2	10.60	0.10	1.12E-08	8.5265
2.15	1.95	13.21	0.12	1.51E-08	8.511
2.2	1.9	11.93	0.11	1.39E-08	8.3608
2.25	1.85	14.08	0.13	1.84E-08	8.3812
2.3	1.8	14.67	0.14	2.03E-08	8.4142
2.35	1.75	14.26	0.13	1.95E-08	8.3039

Table 5.9: Sensitivity study with respect to the acceleration coefficient (below ϕ=1.8)

ϕ_1	RMS (Source Strength)	RMS (Concentration)	Mean Fitness	Total time taken (Hrs.)
1.8	8.84	0.08	7.09E-09	17.5349
1.75	7.02	0.07	5.40E-09	17.3838
1.7	7.53	0.07	5.19E-09	17.5729
1.65	7.89	0.07	5.85E-09	17.511
1.6	7.08	0.07	5.21E-09	17.7042
1.55	5.07	0.05	2.56E-09	17.5879
1.5	5.64	0.05	3.26E-09	17.3843
1.45	5.16	0.05	2.65E-09	17.5497
1.4	5.28	0.05	2.64E-09	17.546

In this study the sum of the acceleration coefficients ϕ_1 and ϕ_2 have been kept constant to 4.1 as recommended by Clerc and Kennedy (2002). The swarm size has been kept at 190 which is the best value of swarm size found from the sensitivity analysis in the previous section. It is seen that from the table above that the optimum value of ϕ_1 is 1.55 which yields the minimum value of the RMS error in source strength and concentrations predictions.

Table 5.10 and Table 5.11 shows the source strength predictions corresponding to the different values of the acceleration parameters used in the Table 5.8 and Table 5.9. Figure 5.11 shows the change in the values of fitness function, root mean square (RMS) error in source strength and concentrations predictions with changing values of the acceleration coefficient.

It may be observed, from the results presented in tables 6.8 – 6.11, that though the best source strength estimates were obtained at $\phi_1 = 1.55$, the impact of the acceleration coefficients are limited. The changes in the final outcome of the source strength predictions changes minimally with respect to the values of acceleration coefficients. Therefore the acceleration coefficient can be set arbitrarily within the range of 1.4 to 2.1 without significant loss of accuracy

It may be observed from the Figure 5.11 that the results of the particle swarm optimization improve in general with decreasing values of the acceleration coefficient ϕ_1. However as the figure shows there are erratic behavior of this trend at higher values.

Table 5.10 : Source strength predictions for values of acceleration coefficients in the range of 1.8 to 2.3

Actual Source Strength	Source strength predictions for various values of ϕ_1 ($\phi_2 = \phi - \phi_1$; $\lambda = 190$)										
	$\phi_1 = 1.8$	$\phi_1 = 1.85$	$\phi_1 = 1.90$	$\phi_1 = 1.95$	$\phi_1 = 2.0$	$\phi_1 = 2.05$	$\phi_1 = 2.1$	$\phi_1 = 2.15$	$\phi_1 = 2.2$	$\phi_1 = 2.25$	$\phi_1 = 2.3$
0	0.0	0.0	0.0	0.0	0.0	0.0	0.0	0.0	0.0	0.0	0.0
0	0.0	0.0	0.0	0.0	0.0	0.0	0.0	0.0	0.0	0.0	0.0
518.4	517.4	517.0	516.8	516.8	516.7	516.8	516.9	516.5	516.7	516.4	516.3
0	1.3	1.9	2.1	2.2	2.3	2.2	2.1	2.6	2.4	2.8	2.9
350	349.5	349.3	349.2	349.2	349.1	349.2	349.2	349.0	349.1	349.0	348.9
0	0.0	0.0	0.0	0.0	0.0	0.0	0.0	0.0	0.0	0.0	0.0
0	11.4	16.7	17.6	18.7	20.1	18.4	18.2	22.7	20.5	24.2	25.2
259.2	244.0	236.8	235.6	234.2	232.3	234.5	234.8	228.8	231.8	226.8	225.5
0	5.6	8.2	8.6	9.2	9.9	9.0	8.9	11.1	10.1	11.9	12.4

Table 5.11: Source strength predictions for values of acceleration coefficients in the range of 1.4 to 1.75

Actual Source Strength	Source strength predictions for various values of ϕ_1 ($\phi_2 = \phi - \phi_1$; $\lambda = 190$)							
	$\phi_1 = 1.75$	$\phi_1 = 1.70$	$\phi_1 = 1.65$	$\phi_1 = 1.60$	$\phi_1 = 1.55$	$\phi_1 = 1.50$	$\phi_1 = 1.45$	$\phi_1 = 1.40$
0	0.0	0.0	0.0	0.0	0.0	0.0	0.0	0.0
0	0.0	0.0	0.0	0.0	0.0	0.0	0.0	0.0
518.4	517.4	517.3	517.2	517.4	517.7	517.6	517.6	517.6
0	1.4	1.5	1.6	1.4	1.0	1.1	1.0	1.1
350	349.5	349.5	349.4	349.5	349.6	349.6	349.6	349.6
0	0.0	0.0	0.0	0.0	0.0	0.0	0.0	0.0
0	12.0	12.9	13.5	12.1	8.7	9.7	8.9	9.1
259.2	243.1	241.9	241.1	242.9	247.5	246.2	247.3	247.1
0	5.9	6.3	6.7	6.0	4.3	4.8	4.3	4.5

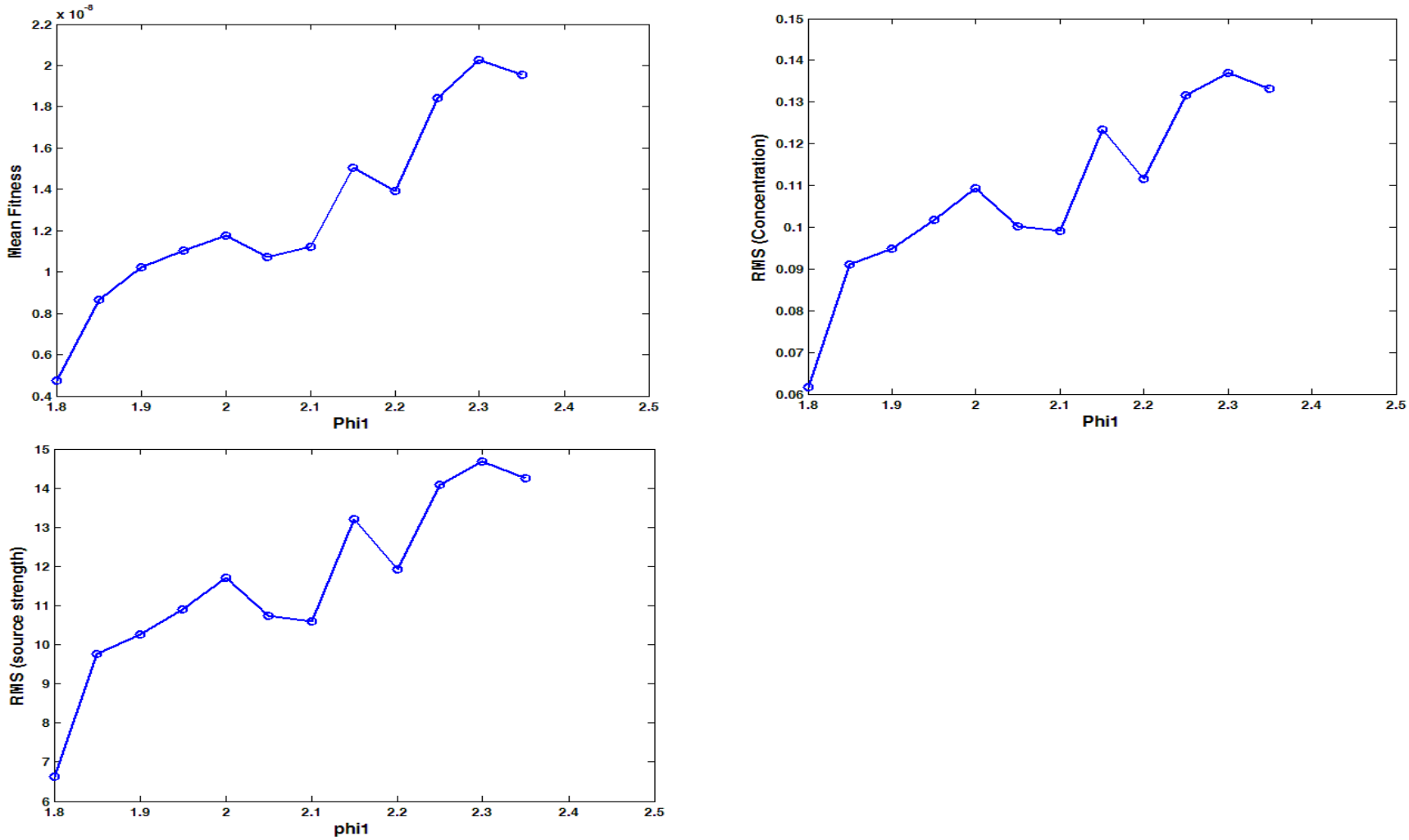

Figure 5.11 : Sensitivity study with respect to the acceleration coefficients in the range of 1.8 to 2.3

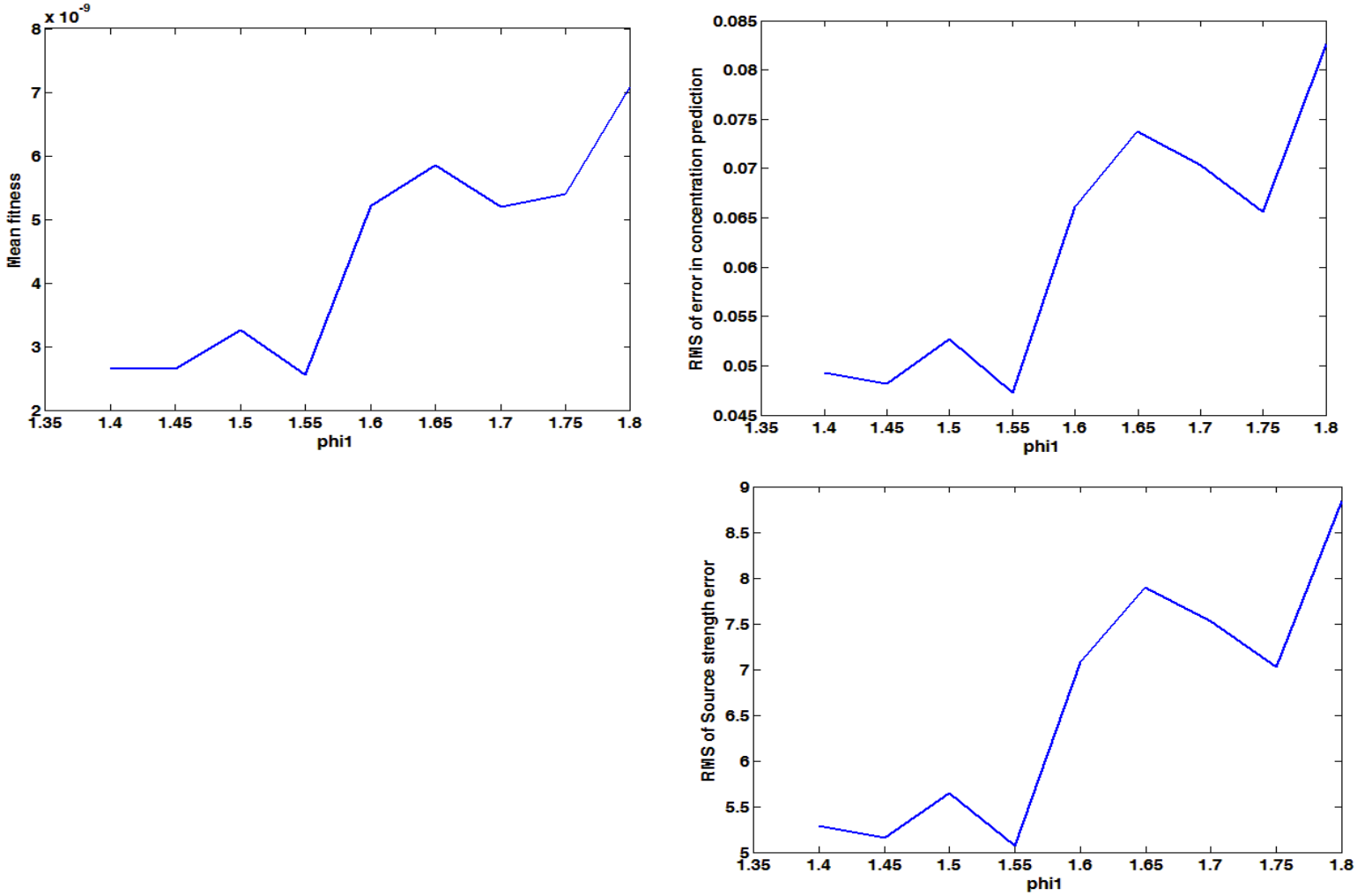

Figure 5.12: Sensitivity study with respect to the acceleration coefficients in the range of 1.4 to 1.8

5.6.3 Sensitivity study w.r.t. sum of constriction coefficient

In this final sensitivity study, the effect of changing the value of the sum of constriction coefficients, ϕ on the source strength predictions is studied. The swarm size has been fixed at 190 and the acceleration coefficient $\phi_1$has been set at 1.55. Both these values are found from the previous sections as the optimum values of the said parameters. Table 5.12 shows the performance of the PSO optimizer where the changes in the error metrics are tabulated with respect to the changing values of the sum of the constriction coefficients. Table 5.13 shows the source strength predictions corresponding to the various values of the sum of the constriction coefficients used in Table 5.12. From these tables, it can be seen that the optimal values of the constriction coefficient is at $\phi = 4.2$. However, it may be observed from the tables that sum of constriction coefficients in the range of 4.1 to 4.3 yields identical results but beyond a value of 4.4 and above the errors quickly grows.

Figure 5.13 shows graphically the outcomes of the sensitivity studies with respect to the values of the sum of constriction coefficients.

Table 5.12 : Sensitivity study of the sum of constriction coefficients
($\boldsymbol{\phi_1 = 1.55}$; $\boldsymbol{\phi_2 = \phi - \phi_1}$; $\boldsymbol{\lambda = 190}$)

$\boldsymbol{\phi}$	**RMS (Source Strength)**	**RMS (Concentration)**	**Mean Fitness**	**Total time taken (Hrs.)**
4.1	6.29	0.06	3.88E-09	17.6502
4.2	0.09	0.00	1.02E-12	17.6088
4.3	3.49	0.04	1.31E-08	18.9474
4.4	70.76	0.77	1.25E-06	20.3984
4.5	98.18	4.61	5.95E-05	17.3611
4.6	115.81	5.82	1.20E-04	17.3067
4.7	140.38	11.55	3.80E-04	17.4244
4.8	129.62	10.53	5.59E-04	17.2875

Table 5.13: Source strength predictions from sensitivity study w.r.t. sum of constriction coefficients

Actual Source Strength	Source strength predictions for various values of ϕ ($\phi_1 = 1.55$ and $\phi = \phi_1 + \phi_2$; $\lambda = 190$)							
	$\phi = 4.1$	$\phi = 4.2$	$\phi = 4.3$	$\phi = 4.4$	$\phi = 4.5$	$\phi = 4.6$	$\phi = 4.7$	$\phi = 4.8$
0	0.0	0.0	0.0	0.0	0.0	0.1	2.2	3.7
0	0.0	0.0	0.0	0.0	0.0	0.2	2.4	0.4
518.4	517.5	518.4	517.6	507.6	430.5	415.4	378.7	407.5
0	1.3	0.0	1.1	16.7	153.3	182.9	233.2	195.7
350	349.5	350.0	349.6	339.2	219.0	186.3	136.6	148.7
0	0.0	0.0	0.0	4.5	55.0	72.1	111.0	119.8
0	10.8	0.2	6.0	121.1	110.5	126.7	119.4	119.4
259.2	244.7	259.0	251.2	96.9	116.4	99.9	93.9	92.8
0	5.3	0.1	2.9	59.4	52.5	56.8	63.1	61.8

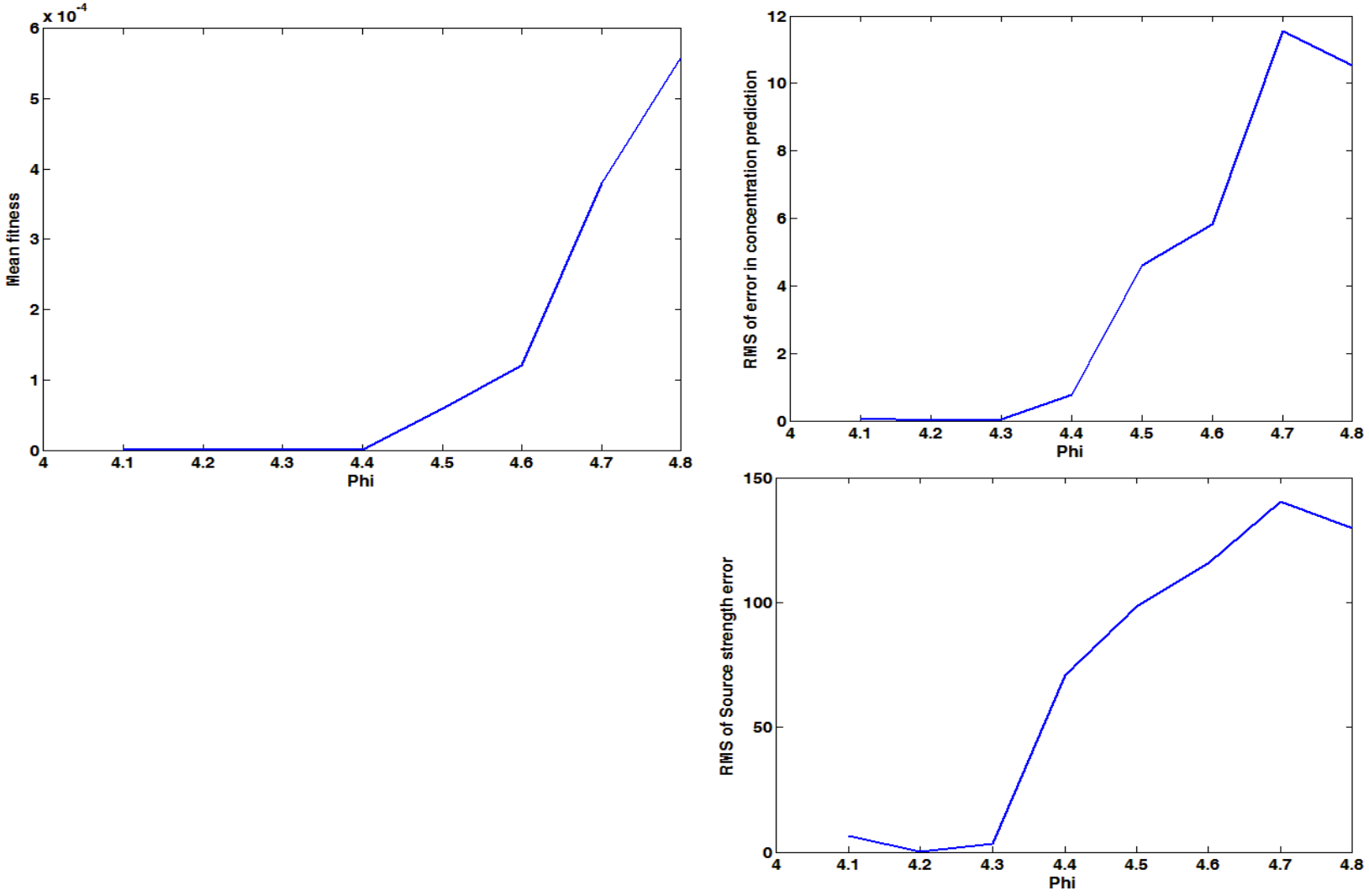

Figure 5.13 :Sensitivity w.r.t. sum of constriction coefficients

In summary, the sensitivity studies with respect to the parameters of the PSO optimizer yields the following optimal values:

Population Size (λ) = 190

Acceleration parameter (cognitive), $\phi_1 = 1.55$

Constriction coefficient, $\phi = 4.2$

Inertia weight (χ) corresponding to the optimal value of the constriction coefficient $\phi = 4.2$ is given by:

$$\chi = \frac{2}{\phi - 2 + \sqrt{\phi^2 - 4\phi}} = 0.6417$$

The source strength predictions corresponding to the above optimal values of the PSO parameters are given in the Table 5.14 below:

Table 5.14: Comparison of actual and predicted source strength with optimal parameters

Actual source strength (l/day)	Predicted Source Strength (l/day)
0	0
0	0
518.4	518.4
0	0.02
350	350.0
0	0
0	0.2
259.2	259.0
0	0.1

It can be seen that the source strength predictions with the optimal values of the parameters is nearly indistinguishable from the true values.

5.7 Closure

Simulation-optimization approach is a very powerful tool for groundwater source identification. It also provides flexibility in that there are several ways for performing the simulation and optimization. In the present study, a simulation-optimization model RPCM-PSO-SO has been developed for groundwater source identification. This model uses the meshfree RPCM model as the simulator and PSO as the optimizer. The meshfree model does away with the requirement to create a mesh unlike conventional methods such as FDM, FEM etc. which are grid based methods. This avoids the computationally cost step of mesh creation. PSO is a swarm intelligence based optimization technique. It is very simple to implement and can be easily integrated with any simulation model. The RPCM-PSO-SO model takes advantage of the benefits of both the meshfree and PSO techniques. The developed SO model have been verified by applying to test problems available in the literature and found to perform satisfactorily. In the

next chapter, this model is applied to a hypothetical problem and a field case problem. The practical issues that may be encountered in a real field situation such as lack of data, irregular or intermittent concentration data, uncertainties in the field data, random location of the surveillance borewells etc. have been considered to test the robustness of the developed SO model.

Chapter 6
Simulation-Optimization models –Results and Discussions

6.1 Introduction

This chapter presents different case studies and scenarios to demonstrate the groundwater source identification using RPCM-PSO based Simulation-Optimization approach. The first case presented is a modified version of the steady state contaminated effluent leakage problem discussed in section 5.5.2. Instead of the two leak sources in that problem, various scenarios are examined where effluents leakage takes place from more points of leakage. A transient field case study of contamination in an unconfined aquifer is considered in section 6.3. The model attempts to reconstruct the release histories of two disposal sites from the concentration measurements over a period of time.

The source identification model is applied to a real aquifer with hypothetical sources in section 6.4. To test the robustness of the proposed approach, additional scenarios which simulates limited amount of concentration data, missing concentration data, intermittent or irregular data collection etc. have been studied. In these studies the observation borewells were placed along the path of the contaminant plume and hence each of them receives significant contaminants over the simulation period. To study the effect of the location of the observation borewells with respect to the sources, an additional case study was taken up in the next section wherein the observation borewells were placed randomly and not necessarily in the contaminant plume path. The ability of the model to identify the sources, where all the sources are located in a small region of the domain and maximum interference of the releases from each source over the simulation period is expected, is being examined in the next section.

Since errors are unavoidable in measuring the solute concentration, any source identification model must take into consideration errors in the concentration data which is used as the input data to the model. Section 6.7 explores ways to deal with uncertain concentration data. Smoothing of the input data, applying constraints from field information, using weighting to reduce the contribution of the erroneous data etc. have been considered in this section.

6.2 Steady state problem –multiple releases scenario

In this section, the simulation-optimization approach demonstrated in chapter 5 is further investigated for its robustness. While the steady state problem studied by Gorelick et al.,(1983) and discussed in section 5.5.2 consists of two sources of leak, in this section the number of leaks or sources is increased and the capability of the PSO base source identification to identify the sources is examined.

Different case scenarios are studied where the number of actual sources of leaks is increased from 2 to the case where all the potential sources are leaking. The same problem of effluent leakage through an underground pipe (Gorelick et al., 1983) is being reinvestigated but here it is assumed that there are seven potential points of leakage instead of nine as was the case earlier (Figure 6.1). It is assumed that the effluent (pollutant) has been flowing continuously within the pipe and contains high concentrations of the non-reactive pollutants –chloride and tritium. Several observation or surveillance borewells are located within the modeling region which is used for detecting and measuring the concentration of the pollutant found in the groundwater.

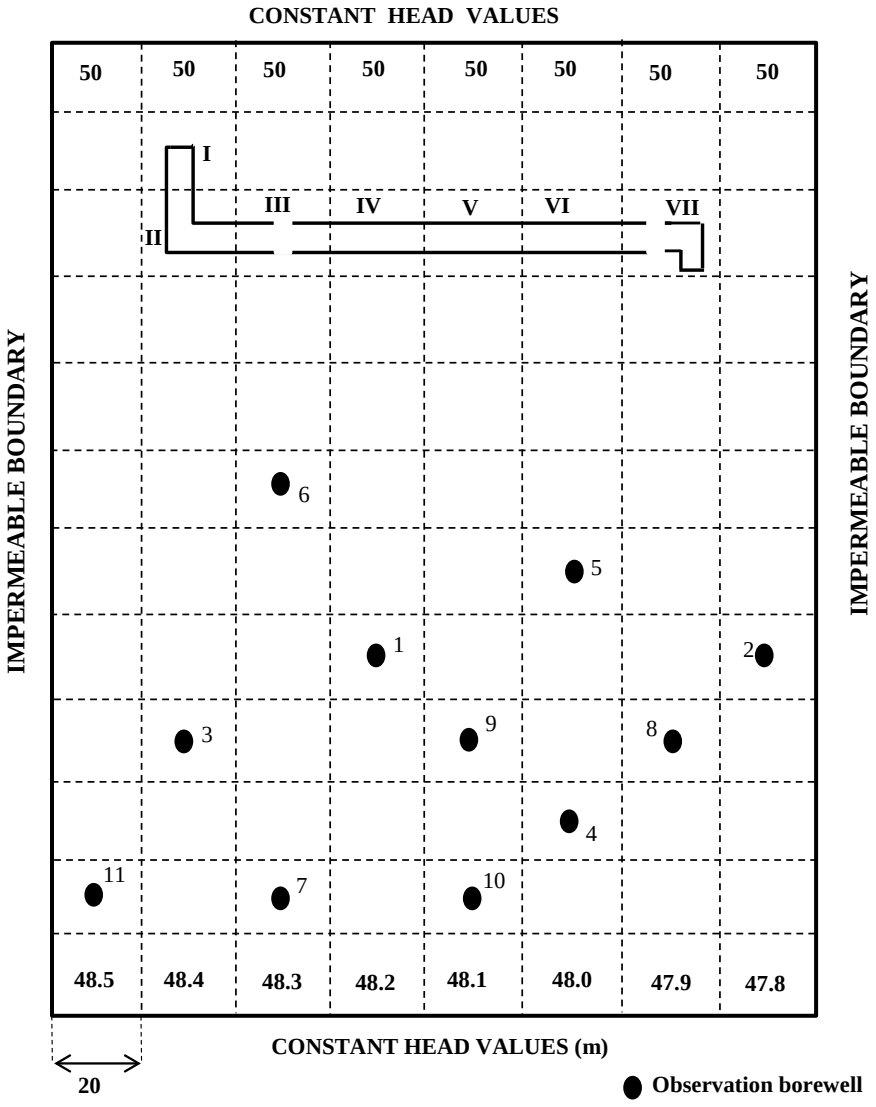

Figure 6.1: Hypothetical Aquifer system for steady state pollutant source identification. Potential leak locations are marked by I through VII

Given this concentration data and the location of all the potential sources, the optimization model seeks to find a set of simulated sources (i.e. source strength vector) which yields closest match to the concentration data. The following 3 types of objective functions are defined to measure the matching between predicted and observed concentrations:

(i) Sum of squared residuals, $R = \sum_{i=1}^{N} \left(C_i^{predicted} - C_i^{observed}\right)^2$ (6.1)

(ii) Sum of squared normalized residuals, $R = \sum_{i=1}^{N} \left(\frac{C_i^{predicted} - C_i^{observed}}{C^*}\right)^2$ (6.2)

(iii) Sum of absolute residuals, $R = \sum_{i=1}^{N} \left|C_i^{predicted} - C_i^{observed}\right|$ (6.3)

where,

$$N = number\ of\ observation\ points$$

$$C^* = C^{observed} \text{ or some smoothed value of } C^{observed}$$

The optimization model seeks to minimize the value of *R* with respect to various sets of the source strength vector in order to determine the pipe leak locations and leak magnitudes. Since PSO is being used for optimization in this work, the sets of source strength vectors acts as the particles of the swarm. Several particles are generated randomly to start the search process. Each particle moves around (i.e. is perturbed) in the search space trying to find the lowest value of the objective function (referred to as fitness function in this context) till all the particles converge to the global minima. Additional constraints are applied to stop the particles from crossing the search boundary. In the present case, the constraint on the source strength is that it cannot be negative but the upper limit is unbounded.

The results of the source identification using PSO optimization is shown in Table 6.1. It tabulates the source fluxes from the 7 potential sources as predicted by the simulation-optimization model alongside the true leak magnitudes i.e. source fluxes in l/d. It can be seen that the SO model using PSO as the optimizer is able to predict the source locations III and VII and their leak magnitudes very accurately. For the rest of the potential leak points, it has predicted a leak magnitude of zero which means no leakage is taking place from these points. All the 3 objective function types in equations 6.1, 6.2 and 6.3 lead to the same results. Therefore any of them can be used for the source identification problem.

The PSO parameters used in the simulation are (Clerc and Kennedy, 2002):

Population or Swarm size : 40

Acceleration Coefficients:

ϕ_1 = 2.05 ;

ϕ_2 = 2.05

$$\chi = \frac{2}{\phi - 2 + \sqrt{\phi^2 - 4\phi}} = 0.7298 \quad where\ \phi = \phi_1 + \phi_2 > 4$$

Table 6.1: Prediction of Leak locations and magnitude by PSO model

Potential Source Location	True Leak Magnitudes (l/d)	PSO Predicted Leak Magnitudes (l/d)	Difference
I	0	0	0
II	0	0.3	-0.3
III	518.4	518.3	0.1
IV	0	1.1	-1.1
V	0	0.5	-0.5
VI	0	0.7	-0.7
VII	259.2	259.6	-0.4

Table 6.3 shows the computational performance of the PSO optimizer using the objective function type in equation (6.3) i.e. sum of squared normalized residuals while Table 6.4 compares the concentrations at the observation points as predicted by the PSO model against the observed concentrations. The source fluxes as shown in Table 6.1 is average of source fluxes predicted by 25 independent runs of the PSO model. As seen from Table 6.3, the convergence in each run was achieved by using less than 2000 fitness function evaluations only which is quite impressive for a PSO based optimization problem. The variations among the independent runs of the model are also very small, which shows that the PSO model is very stable. It can also be seen from Table 6.4 that the predicted and observed concentrations match exactly.

To test the robustness of the source identification model, some variations of the above problem are considered. Let the number of leak sources be increased one by one at other locations in addition to the existing sources.

Table 6.2 shows four variations of the original problem with increasing number of leak sources:

Table 6.2: Additional cases with changing number of leak sources

Cases	Leak sources and their magnitudes/fluxes (l/d)						
	I	II	III	IV	V	VI	VII
Case 1 : 3 Leak sources			518.4		350		259.2
Case 2: 4 Leak sources	200		518.4		350		259.2
Case3: 5 Leak sources	200		518.4		350	150	259.2
Case 4 : 6 Leak sources	200		518.4	100	350	150	259.2

Table 6.3: Performance of the PSO

Run	Time taken (sec)	Number of Function Evaluations	Fitness value (sum of normalized squared residual)
1	0.55	1721	9.24E-16
2	0.54	1594	9.47E-16
3	0.57	1756	6.65E-16
4	0.42	1225	9.97E-16
5	0.6	1911	9.43E-16
6	0.61	1812	9.27E-16
7	0.51	1575	9.41E-16
8	0.37	1068	9.55E-16
9	0.56	1760	9.62E-16
10	0.50	1483	9.60E-16
11	0.61	1883	9.60E-16
12	0.55	1623	9.99E-16
13	0.5	1584	7.09E-16
14	0.63	1916	9.34E-16
15	0.54	1628	7.01E-16
16	0.59	1642	9.91E-16
17	0.52	1571	9.98E-16
18	0.55	1604	8.53E-16
19	0.55	1600	9.43E-16
20	0.36	1111	9.33E-16
21	0.48	1504	9.95E-16
22	0.62	1832	8.63E-16
23	0.61	1791	6.46E-16
24	0.41	1270	9.75E-16
25	0.55	1722	9.81E-16
Avg.	**0.532**	**1607**	**9.08E-16**

Table 6.4: Comparison of the predicted and observed concentrations

Observation Point	Predicted Concentration (mg/l)	Observed Concentration (mg/l)	Difference
1	2805.0	2805.0	0
2	2922.4	2922.4	0
3	2440.6	2440.6	0
4	2568.5	2568.5	0
5	2868.2	2868.2	0
6	3054.0	3054.0	0
7	2095.2	2095.2	0
8	2776.0	2776.0	0
9	2700.1	2700.1	0
10	2238.8	2238.8	0
11	1340.3	1340.3	0

For each of the cases listed in table 9 the source identification model is re-run to identify the leak sources. The predictions of the PSO source identification model are shown in Table 6.5 through Table 6.8.

Table 6.5: 3 Leak Sources at locations III, V and VII

Potential Source Location	True Leak Magnitudes (l/d)	PSO Predicted Leak Magnitudes (l/d)	Diff.
I	0	1.2	-1.2
II	0	0.6	-0.6
III	518.4	518.4	0
IV	0	0.6	-0.6
V	350	350	0
VI	0	1.3	-1.3
VII	259.2	257.6	1.6

Table 6.6: 4 leak sources at locations I, III, V and VII

Potential Source Location	True Leak Magnitudes (l/d)	PSO Predicted Leak Magnitudes	Diff.
I	200	199.79	0.21
II	0	0	0
III	518.4	516.8	1.6
IV	0	3.6	-3.6
V	350	346.3	3.7
VI	0	1. 7	-1.7
VII	259.2	259.3	-0.1

Table 6.7: 5 Leak sources at locations I, III, V, VI and VII

Potential Source Location	True Leak Magnitudes (l/d)	PSO Predicted Leak Magnitude (l/d)s	Diff.
I	200	199.9	0.1
II	0	0	0
III	518.4	517.5	0.9
IV	0	2.1	-2.1
V	350	347.9	2.1
VI	150	151.0	-1.0
VII	259.2	259.3	-0.1

Table 6.8: 6 Leak Sources at locations I, III, IV, V, VI and VII

Potential Source Location	True Leak Magnitudes (l/d)	PSO Predicted Leak Magnitudes	Diff.
I	200	199.8	0.2
II	0	0.2	-0.2
III	518.4	519.3	-0.9
IV	100	97.9	2.1
V	350	352.1	-2.1
VI	150	149.1	0.9
VII	259.2	259.1	0.1

It is seen that noises or errors start appearing in identification of the leak sources (Table 6.5 through Table 6.8), even though they are quite small. For example, in Table 6.5 there are actually 3 leak sources viz, I,

III, V and VII. The PSO model has identified these major sources but also has predicted very small (noises) leakages from other locations as well. Referring to Table 6.9, it is seen that the number of function evaluation required by the PSO model has increased drastically e.g. for the case 1 (3 leak sources) the average number of function evaluations required for convergence has gone up to more than 75,000 as compared to less than 2000 function evaluation for the case with 2 leak sources (Table 6.1). For the cases with more than 3 leak sources present in the aquifer, the number of fitness function evaluations required for convergence is upwards of one million. This shows that the limitations/weakness of the PSO optimizer.

The two RMS error metrics defined in equation (5.17) and (5.18) being used here to study the convergence behavior of the source identification model. RMS^{source} is the root mean square error in the prediction of the source fluxes while RMS^{conc} is the root mean square error of the contaminant concentration prediction by the SO model. Since the exact source strengths and contaminant concentration distribution are assumed to be known exactly, these quantities can be calculated. Table 6.9 shows the values of these error metrics for different cases and for various number of function evaluations used in the PSO optimization:

Table 6.9: Convergence analysis of the Source identification model

No of sources	**RMS error in source flux prediction for various numbers of function evaluations of the PSO**						**RMS error in contaminant concentration prediction for various numbers of function evaluations of the PSO**					
	No of PSO Function Evaluations						**No of PSO Function Evaluations**					
	10^3	**$5x10^3$**	**10^4**	**$5x10^4$**	**10^5**	**10^6**	**10^3**	**$5x10^3$**	**10^4**	**$5x10^4$**	**10^5**	**10^6**
2	0.04	0	0	0	0	0	0.02	0	0	0	0	0
3	117.37	46.21	23.92	0.06	0.0	0.0	7.66	2.89	1.51	0.00	0	0
4	146.02	142.42	116.1	102.5	87.69	2.10	3.06	2.30	1.87	1.65	1.42	0.03
5	115.07	107.72	85.38	78.43	58.61	1.22	4.53	1.97	1.39	1.27	0.95	0.02
6	78.90	89.05	115.7	56.66	45.21	1.18	3.42	1.76	1.89	1.05	0.83	0.02
7	111.58	106.80	94.35	95.03	105.3	70.3	1.56	0.85	0.58	0.55	0.60	0.40

It can be seen that the source identification model generally improves with increasing the number of PSO function evaluations. For the case with only two sources, it requires very small number of function evaluations to correctly predict the unknown sources. But for the cases with more number of sources, the number of function evaluation i.e. iterations of the PSO has to be significantly increased in order to be able to predict the source fluxes to acceptable error. For the case with 7 sources, the model is unable to

predict the source fluxes correctly even with 10^6 iterations. But looking at the concentration prediction errors, it is seen that the models is able to predict the concentration very accurately even when it is unable to predict the source fluxes acceptably. This may be due to the non-uniqueness of source identification problems. The PSO optimization is able to minimize the objective function i.e. the difference between predicted and measured contaminant concentrations, which it is supposed to minimize. The convergence of the PSO with the number of function evaluations can be seen from the Figure 6.2. It can be seen that with increasing number of iterations of the PSO, the source prediction improves. But this improvement comes at the cost of increasing computational time.

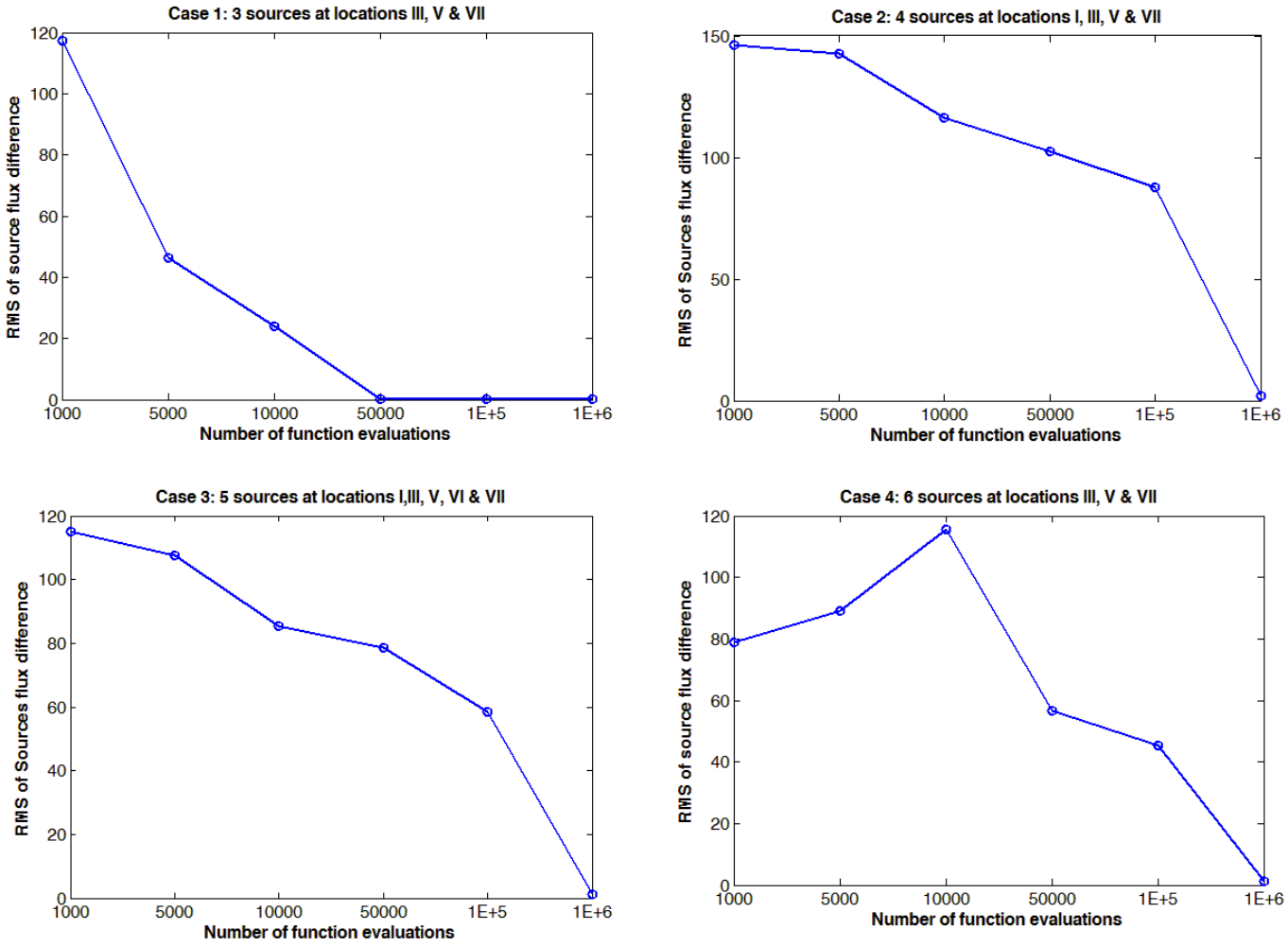

Figure 6.2: Convergence of Source identification model w.r.t. PSO function evaluations

6.3 Transient source identification – unconfined aquifer case

Consider the unconfined aquifer of size 900 m by 540 m shown in Figure 6.3. It is bounded by impermeable boundaries on the two sides (Figure 6.3). The other two boundaries are constant head boundaries with head values of 100m and 88m respectively. Two contaminant disposal sources S_1 and S_2 are releasing contaminants over a period of 5 years with source fluxes as per the schedule given in Table 6.10. Of the two disposal sources only S1 is assumed to be operational over the disposal period of 5 years. Three observation borewells namely, O_1, O_2 and O_3 located downstream, measures the contaminant concentration over a simulation period of 10 years. The aquifer parameters values are: $k_{xx} = 0.0001$ m/s , $k_{yy} = 0.0001$ m/s , porosity (θ) = 0.20, longitudinal dispersivity (α_L) = 30.5 m, transverse dispersivity (α_T) = 12.2. The thickness of the aquifer is 30.5 m. The locations of the sources and the observation borewells are given Table 6.11.

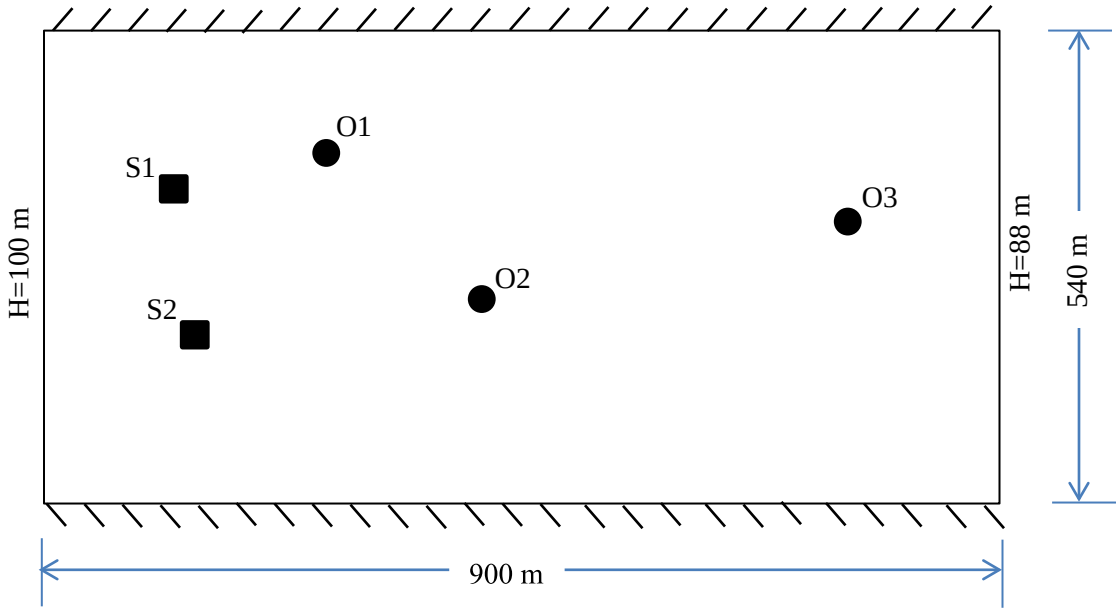

Figure 6.3: Hypothetical unconfined aquifer

A coupled meshfree RPCM flow and solute transport model as formulated in chapter 4 was constructed. The flow equation for an unconfined aquifer is non-linear. Newton-Raphson iteration method has been applied to find the solution iteratively. The breakthrough curves at the borewells resulting from the source disposals are shown in the Figure 6.4. The time step size used in the simulation was 30 days (monthly). The breakthrough curves shown in the Figure 6.4 serve as the measured concentration for the source identification model. From this input concentration data, the source identification model seeks to construct the release histories of the sources (Table 6.10).

Table 6.10: Source flux from the contaminant sources

Year of release	Source flux (gm/sec)	
	S_1	S_2
1	48.8	0
2	0.0	0
3	10.0	0
4	42.0	0
5	36.0	0

Table 6.11: Locations (coordinates) of the sources and wells

Source / observation well	(x,y) locations (m)
S1	(100, 343)
S2	(123, 203)
O1	(254, 365)
O2	(340, 247)
O3	(615, 288)

A concentration response matrix as described in section 5.4 is created. The PSO optimization model uses this concentration matrix to evaluate the predicted concentrations from different trial sets of source fluxes.

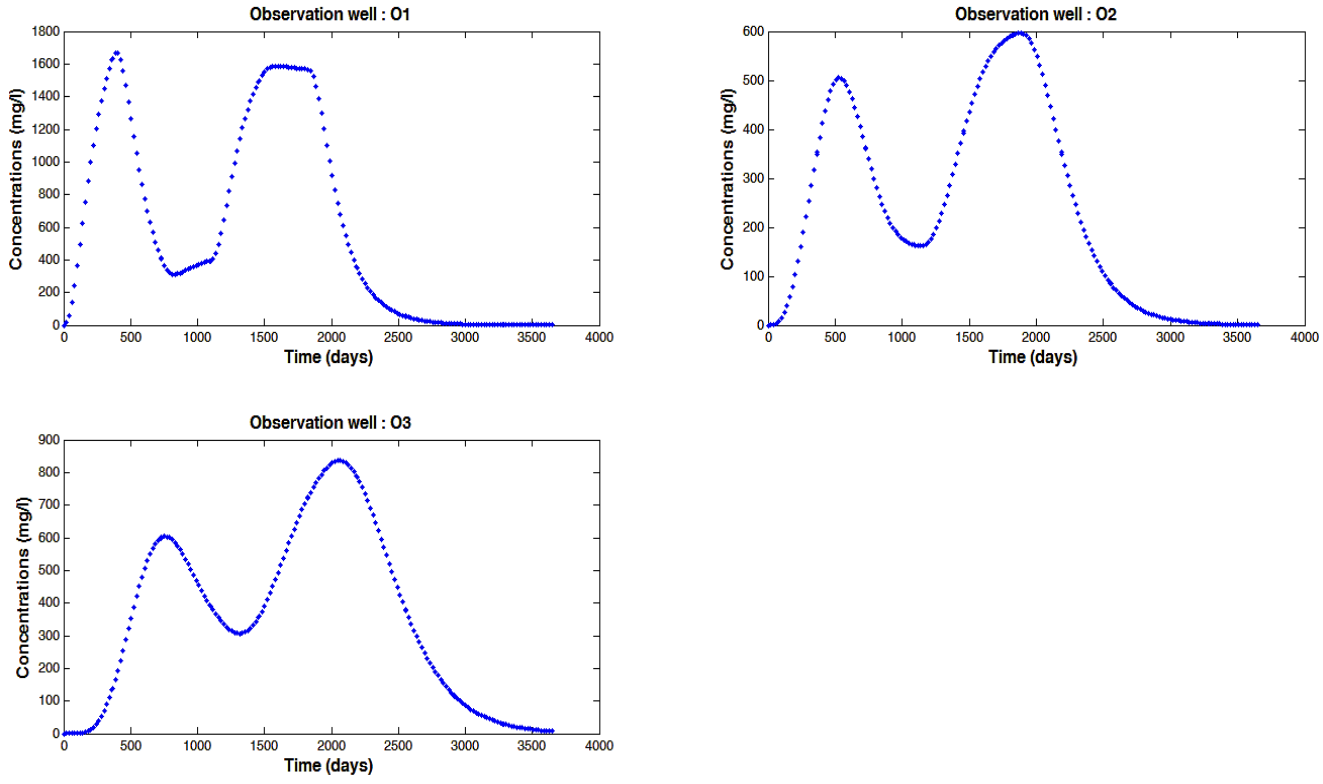

Figure 6.4: Breakthrough curves at the observation borewells

A swarm size of 50 particles was used in the PSO. The acceleration coefficients have been kept as: $\phi_1 = 2.05$ and $\phi_2 = 2.05$. The source predictions from the RPCM-PSO-SO model are as shown in

Table 6.12. The source predictions are indistinguishable from the actual releases. This may be expected since the model uses rather a very long series of concentration data (10 years) from the three observation wells and the no uncertainty is present in the concentration data. This drastically reduces the chances of non-uniqueness in the solutions and consequently the PSO optimization model will be able to quickly converge on the true solutions. Table 6.13 which shows the computational performance of the RPCM-PSO-SO model confirms this observation. The model convergence happens in less than a 1000 iterations of the PSO. It may be mentioned that the source predictions are averaged over 25 independent runs of the PSO to remove any statistical randomness present.

Table 6.12: Source predictions from the SO model

Source	Year of release	Actual Source flux (gm/sec)	RPCM-PSO-SO model predicted source flux (gm/sec)
S_1	1	48.8	48.80
	2	0.0	0.1
	3	10.0	10.02
	4	42.0	42.1
	5	36.0	36.03
S_2	1	0.0	0.0
	2	0.0	0.1
	3	0.0	0.2
	4	0.0	0.0
	5	0.0	0.1

Table 6.13: Computational performance of the SO model

Run	Time taken (sec)	No. of iterations	Value of fitness function
1	1.36	814	7.34E-16
2	1.48	813	8.86E-16
3	1.29	788	9.51E-16
4	1.85	796	8.98E-16
5	1.4	819	7.98E-16
6	1.43	765	2.94E-16
7	1.31	770	8.39E-16
8	1.34	735	8.50E-16
9	1.26	752	6.97E-16
10	1.39	779	9.13E-16
11	1.46	819	9.72E-16
12	1.48	774	9.91E-16
13	1.33	783	9.04E-16
14	1.36	750	7.26E-16
15	1.51	809	9.64E-16
16	1.36	750	8.92E-16
17	1.41	769	9.54E-16
18	1.48	806	7.12E-16
19	1.43	805	6.63E-16
20	1.35	811	8.03E-16
21	1.37	798	8.82E-16
22	1.14	687	8.88E-16
23	1.3	761	9.65E-16
24	1.25	741	9.05E-16
25	1.33	782	8.51E-16

6.4 Field case study - time-dependent sources

Here we consider the field case study given in chapter 4 in section 4.12 to study the source identification problem. This case study investigates the leaching of contaminants from storage sites or tanks which has been occurring intermittently over a period of time. Consider the aquifer as shown in Figure 6.5 (refer to section 4.12). As shown in section 4.12, the study area is bounded by a lake on the north, north-east, west and south-west boundaries. There are no water bodies on the rest of the boundary. The area to be modeled is approximately 4.5 km^2. The water level in the lake is used as the constant head value at the boundaries bounded by the lake. The flux boundary value is estimated and adjusted during calibration of the model (Guneshwor et al., 2016). Six hypothetical sources located at S_1, S_2, S_3, S_4, S_5 and S_6 are releasing TDS (Total Dissolved Solids) as a contaminant through leaching over a period of four years according to the concentration data given in Table 6.14. It is assumed that after the 4 years of release, the sites stop releasing any contaminants. Four observation wells viz. *OB-1*, *OB-2*, *OB-3* and *OB-4* records the contaminant (solute) concentrations due to the releases from the sources over a period of 10 years (simulation period).

This case study has been taken from Guneshwor et al.,(2016). Six potential hypothetical sources located at S_1, S_2, S_3, S_4, S_5 and S_6 are releasing contaminant over a period of four years according to the release schedule given in Table 6.14 . It is assumed that after the 4 years of release, the sites stop releasing any solutes/contaminants to the aquifer. Five surveillance (observation) bore wells viz, O_1, O_2, O_3, O_4 and O_5 located in the study area records the contaminant (solute) concentrations due to the releases from the sources over a period of 10 years (simulation period).

Table 6.14 : Release schedule of the sources

Release Year	Source Releases (in ppm)					
	S1	**S2**	**S3**	**S4**	**S5**	**S6**
1st year	1000	1500	890	0	0	500
2nd year	0	1200	1000	0	0	700
3rd year	900	500	0	1000	850	0
4th year	0	0	800	1300	1100	0

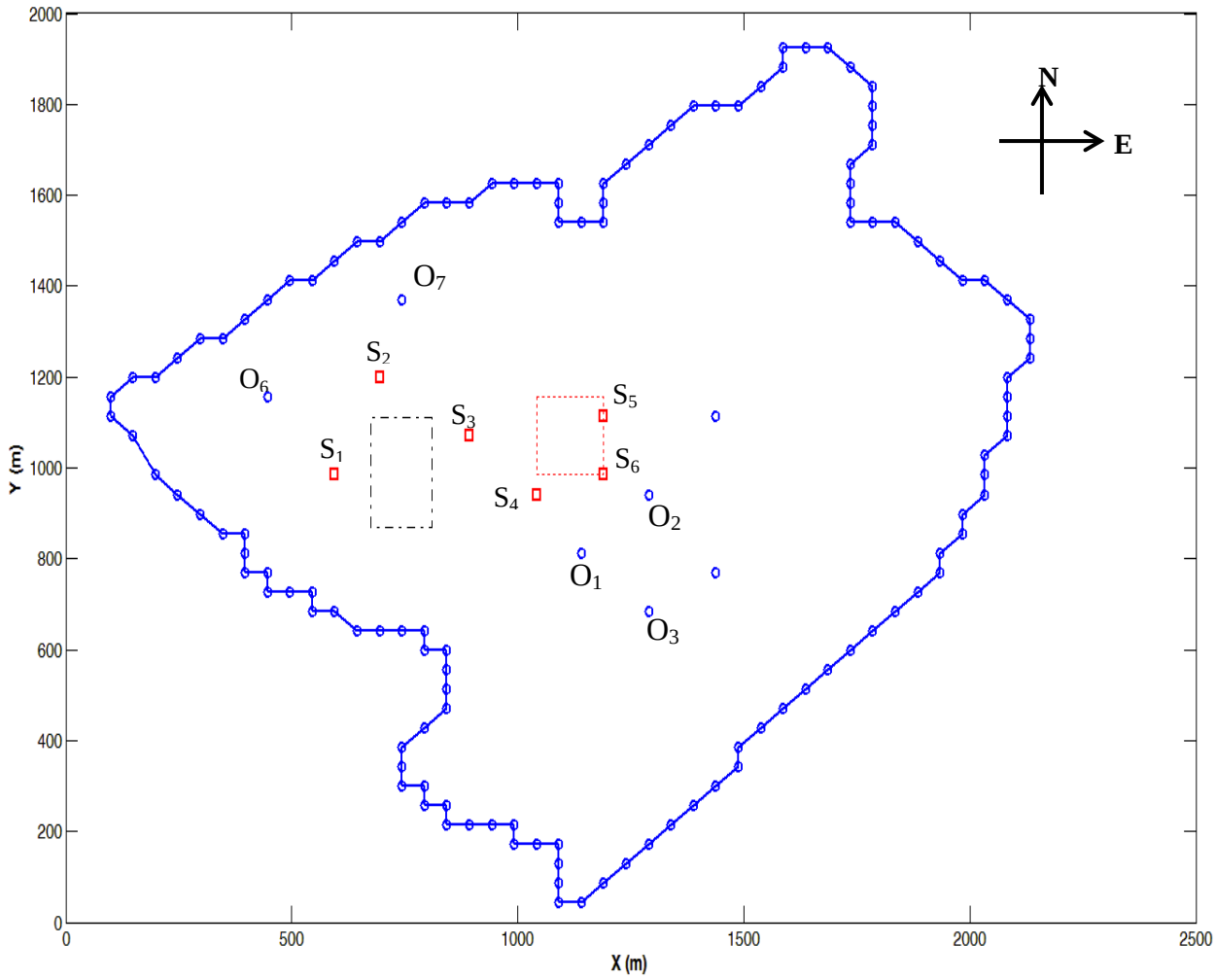

Figure 6.5: Model area with the sources and observation bore wells (reduced number of bore wells)

The model area was divided into a regular grid of 1008 nodal points corresponding to $\Delta x = 49.6\, m\,, \Delta y = 42.8\, m$ (Guneshwor et al.,2016). The flow and transport modeling was carried out using radial point collocation method as outlined in section 4.12. Figure 6.6 shows the contour of hydraulic head distribution in the study area. There is a recharge zone in the area and the groundwater flow directions radiate out from this zone in all the directions (Guneshwor et al., 2016). The main flow direction is in the south-east directions. The sources S_4, S_5 and S_6 are located downstream along this direction while the sources S_1 and S_2 are located along the north-western flow path.

The transport model tracks the migration of the contaminants for a period of 10 years (3650 days) including the 4 years during which the release took place. The time step size used in the transport model is $\Delta t = 10\, days$. The concentration values at the observation bore wells are recorded for every 30 days (monthly) to construct the breakthrough curves at the wells. Each breakthrough curves therefore contains 123 concentration data (3650/30 plus the initial and the last time steps).

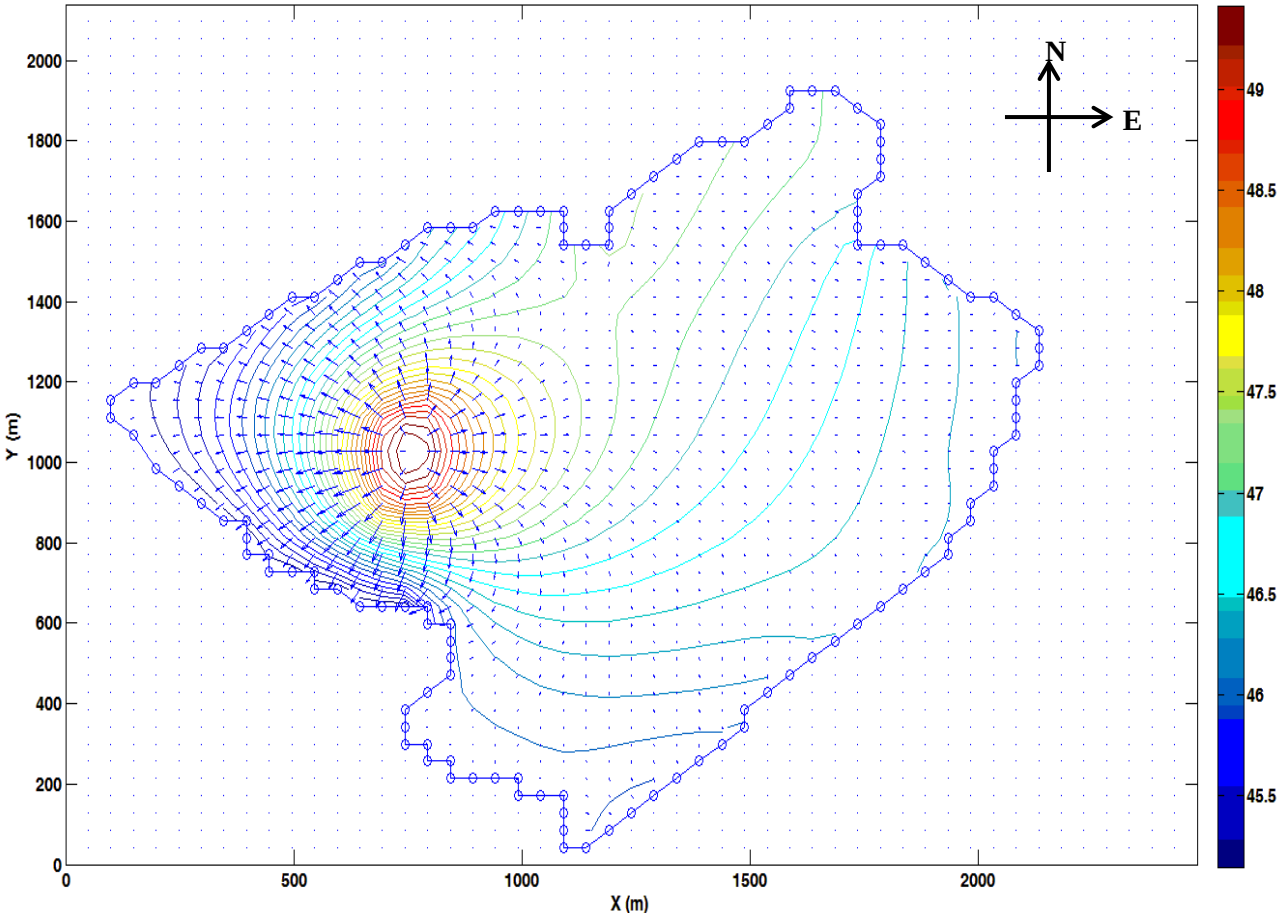

Figure 6.6 : Head distribution in the aquifer and groundwater flow directions

The breakthrough curves at the 5 observation bore wells serve as the measured concentration data and used as input to the source identification model. The goal of the source identification model is to reconstruct the release history of the sources from this given concentrations data. The use of breakthrough curves is justified since generally in any field scenario, concentrations are measured through water sample collection only at a few surveillance (observation) borewells at a set time interval of sample collection e.g. weekly, monthly, bi-monthly etc. over a period of time, normally few years.

A concentration response matrix was constructed similar to the case for steady state effluent flow through an underground pipeline as mentioned in section 5.5.2. Each column of this matrix stores the breakthrough curves at the five observation borewells resulting from unit release from each of the sources in a particular release year. For example, the first column stores the concentrations at every recorded time steps for the observation borewells due to a unit release from the first source in the first year. The second column corresponds to the unit release from the 2nd source in the first year of release; the third column corresponds to unit release from the 3rd source and so on. When the columns (block) for all the sources in

the first year of release are completed, the columns (block) for the second of year of release are populated. This is followed by the data for the 3rd and 4th year of the releases. Thus the concentration response matrix will have a size of : (5*123) x (6*4) i.e. 615 x 24

For this transient case, the following two objective functions are used for minimization:

(i) Sum of squared differences between predicted and observed concentrations:

$$S = \sum_{i=1}^{NO}\sum_{j=1}^{NT}\left(C_{i,j}^{Pred} - C_{i,j}^{Obs}\right)^2 \quad (6.4)$$

(ii) Sum of absolute values of the differences between predicted and observed concentration:

$$S = \sum_{i=1}^{NO}\sum_{j=1}^{NT}\left|C_{i,j}^{Pred} - C_{i,j}^{Obs}\right| \quad (6.5)$$

where,

NO = no. of observation bore wells

NT = no. of time steps

$C_{i,j}^{Pred}$ = Predicted concentration at i^{th} observation point at j^{th} time step

$C_{i,j}^{Obs}$ = Observed/measured concentration at i^{th} observation point at j^{th} time step

As for the steady case, the following two error metrics are defined for measuring the accuracy of the predictions from the source identification model:

Root mean square error in concentrati predictions :

$$RMS\_Concn = \sqrt{\frac{\sum_{i=1}^{NO}\sum_{j=1}^{NT}\left(C_{i,j}^{Pred} - C_{i,j}^{Obs}\right)^2}{N}} \quad (6.6)$$

Root mean square error in source strength predictions:

$$RMS\_source = \sqrt{\frac{\sum_{i=1}^{NS}\sum_{t=1}^{NR}\left(S_{i,t}^{Pred} - S_{i,t}^{Actual}\right)^2}{N}} \quad (6.7)$$

where, NS = no. of sources or injection wells., NR = No of release years ,$S_{i,t}^{Pred}$ =Predicted concentration of the i^{th} in the t^{th} year , $S_{i,t}^{Actual}$ = Actual source concnetrtaion of the ith source in tth release year

6.4.1 Case A: Extended period of concentration data

6.4.1.1 Results and discussion

The results from the source identification model for this transient field case study are given in Table 6.15 while Figure 6.7 shows the comparison of the measured and predicted breakthrough curves at the observation bore wells. The PSO optimization model used a population size of 100.

Table 6.15 : Source strength prediction comparison for different objective type functions

Source	Year of release	Actual Source (ppm)	Predicted Source strength (ppm) for different types of the objective function used		
			Objective type 1: sum of squared residuals	Objective type 2: sum of normalized squared residuals	Objective type 3: sum of absolute residuals
1	1	1000	1000	1027	1000
	2	1500	1500	756	1500
	3	890	890	830	890
	4	0	0	1072	0
2	1	0	0	1091	0
	2	500	500	1138	500
	3	0	0	939	0
	4	1200	1200	921	1200
3	1	1000	1000	833	1000
	2	0	0	1040	0
	3	0	0	906	0
	4	700	700	887	700
4	1	900	900	1193	900
	2	500	500	924	500
	3	0	0	857	0
	4	1000	1000	918	1000
5	1	850	850	998	850
	2	0	0	1157	0
	3	0	0	884	0
	4	0	0	1080	0
6	1	800	800	1129	800
	2	1300	1300	1139	1300
	3	1100	1100	1066	1100
	4	0	0	1042	0
RMS (Source strength)			0	700.1302	0.0048
RMS (concentration)			0	296.4406	0
Mean fitness			9.94E-16	Does not converged	2.03E-03

The convergence criteria set for the PSO optimization is that either the maximum number of fitness function evaluations is 10^5 or the fitness function value is smaller than 10^{-15}. The criteria on the value of the fitness function is set very low in order to allow the PSO optimization to reach maximum number of function evaluations set i.e. emphasis has been given to the number of function evaluation. Usually the performance of any PSO optimization is measured in terms of number of function evaluation needed to achieve convergence.

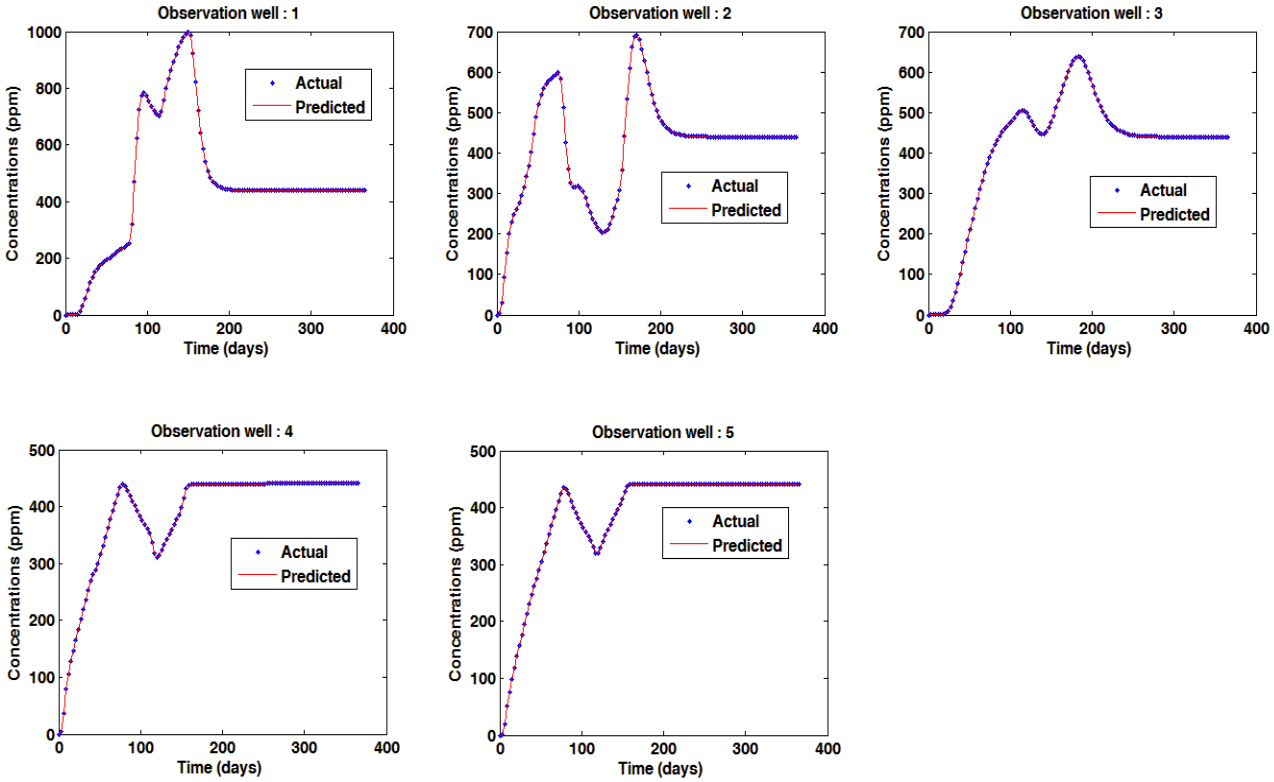

Figure 6.7 : Comparison of measured and predicted breakthrough curves at the 5 observation bore wells

It is observed from Table 6.15 that the source identification model could exactly construct the release histories of the sources for this case study. The computational performance of the optimization model can be seen in Table 6.16. This table also compares the computational performance of the optimization model for both types of the objective or fitness function defined in equations (6.7) and (6.8). While Table 6.15 indicates that employing both the types of objective function in the optimization yields nearly the same results when it comes to source prediction, Table 6.16 shows that the model that uses sum of squared residuals as the objective function is computationally very efficient requiring less than 10,000 fitness function evaluations to achieve the preset convergence criteria. The simulation was carried out in MATLAB on a HP Z800 workstation.

Table 6.16: Computational Performance of the optimization model

Iteration/run	Objective function: sum of absolute residuals			Objective function: sum of squared residuals		
	Time taken(s)	No. of function evaluations	Fitness function value	Time taken(s)	No. of function evaluations	Fitness function value
1	165.23	100000	3.98E-03	13.14	7963	1.00E-15
2	165.88	100000	3.59E-05	13.21	7851	9.99E-16
3	165.33	100000	1.56E-09	15.56	8996	9.99E-16
4	166.33	100000	6.37E-03	13.54	7935	9.96E-16
5	174.92	100000	1.86E-08	15.24	9275	9.78E-16
6	188.31	100000	7.52E-03	12.97	7808	9.98E-16
7	171.57	100000	4.71E-03	11.35	6809	9.94E-16
8	166.75	100000	8.05E-04	9.55	5693	1.00E-15
9	206.03	100000	6.12E-06	9.74	5962	9.96E-16
10	170.1	100000	3.41E-03	13.75	8241	9.96E-16
11	168.37	100000	5.96E-06	12.81	7749	9.86E-16
12	210.56	100000	1.12E-03	8.62	5132	9.93E-16
13	170.36	100000	2.23E-03	8.56	5169	9.97E-16
14	169.63	100000	2.01E-05	8.55	5063	9.89E-16
15	161.89	100000	1.00E-09	14.17	8584	9.92E-16
16	197.04	100000	2.32E-09	12.45	7417	9.99E-16
17	164.66	100000	2.60E-03	14.67	8853	9.89E-16
18	168.37	100000	5.25E-04	16.55	7934	9.97E-16
19	163.5	100000	6.37E-03	12.89	7679	9.89E-16
20	164.13	100000	1.28E-03	14.42	8734	9.98E-16
21	163.52	100000	2.71E-03	13.75	8361	9.72E-16
22	165.03	100000	6.33E-03	12.16	7427	9.98E-16
23	166.22	100000	9.59E-06	13.48	8091	9.92E-16
24	163.32	100000	2.73E-04	13.38	8134	9.97E-16
25	158.3	100000	4.15E-04	14.22	8587	9.96E-16

6.4.2 Case B: Limited amount of data

The previous case considers that the concentration data is available for an extended period of time and assumes no missing data over the entire period. This may be divergent from the actual field situation where regular monitoring may start only after detecting solute concentrations that exceed a particular regulatory limit and may continue only for a limited period or number of years. In such cases, the concentration data will be limited. Figure 6.8 shows how a typical concentration data for such cases might look like. Monitoring starts when the solute concentration in the surveillance borewells crosses 200 ppm or more. These monitoring period have been chosen arbitrarily to represent a typical field condition.

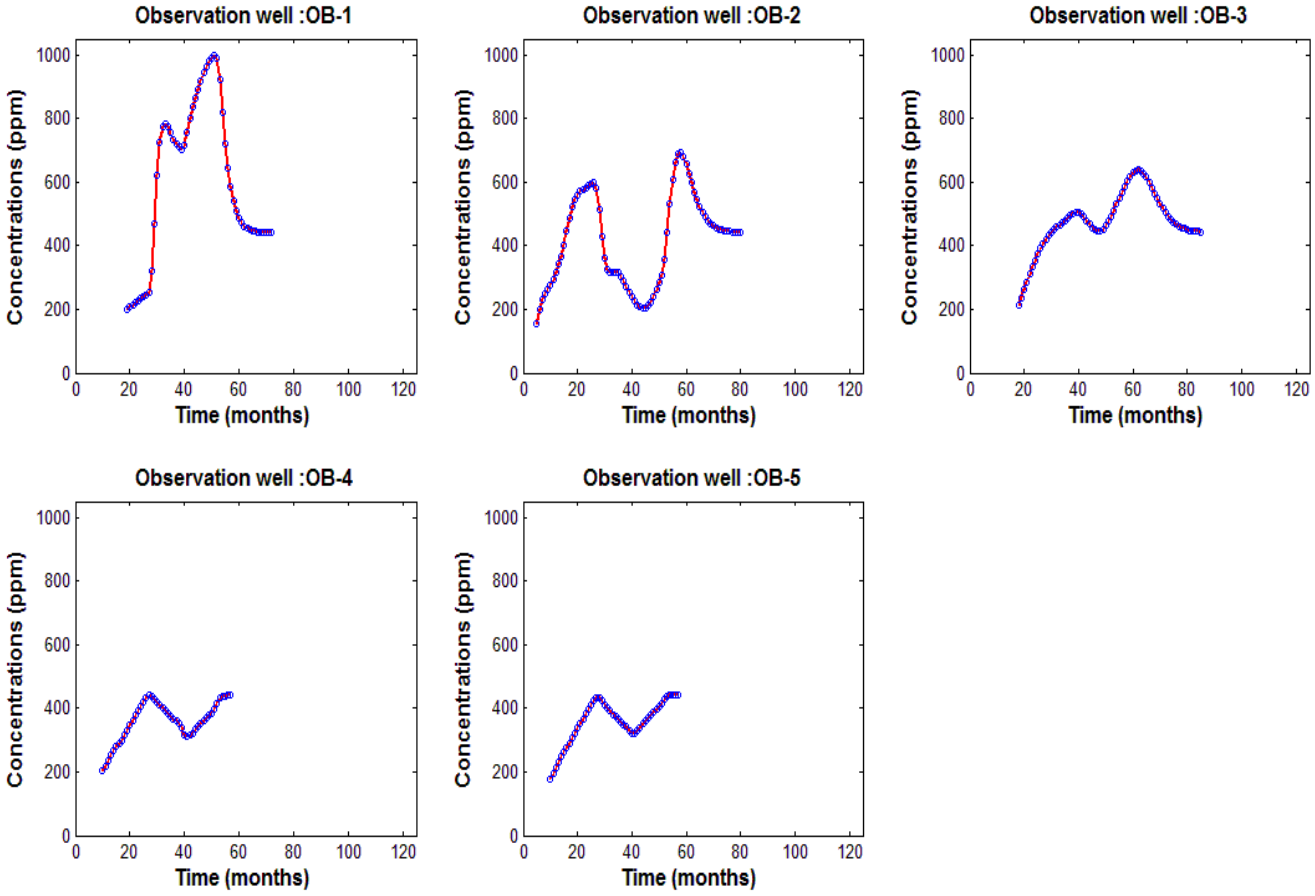

Figure 6.8 Concentration measurement starts after it crosses a certain level

Table 6.17 below shows the results of the source predictions for this case study. It is observed that with 5000 iterations only convergence was achieved. This may be expected since even though the data has been reduced, still it represents an abundance concentration data. Further the data is assumed to be free from uncertainties. These means that the non-uniqueness of the solution is significantly less. It may be noted that longer the data series the lesser the problem of non-uniqueness. . The PSO optimizer will be able to find this global minimum sufficiently close. When we further reduce the concentration data series, it is expected the PSO optimizer may take more iterations to converge. As the Table 6.17 shows there are some spurious source predictions. However their magnitudes are relatively less and hence may ne neglected.

Figure 6.9 presents another case where the concentration data was even more limited. The measurement period was limited to only a few years typically 3 to 4 years and represents the peak period of the concentration profile in each borewell. The result of the source identification model for this case is presented in the Table 6.18 below. As expected the model took more number of PSO iterations to converge.

Table 6.17: Results of source identification with limited observation data

Source	Year of release	Actual source (ppm)	Predicted source (ppm)	Percentage error
1	1	1000	1179	-17.9
	2	1500	1496	0.3
	3	890	885	0.6
	4	0	3	
2	1	0	4	
	2	500	500	0.1
	3	0	41	
	4	1200	1195	0.4
3	1	1000	998	0.2
	2	0	1	
	3	0	0	
	4	700	701	-0.2
4	1	900	873	3.0
	2	500	500	0.0
	3	0	0	
	4	1000	1000	0.0
5	1	850	849	0.1
	2	0	1	
	3	0	6	
	4	0	1	
6	1	800	800	0.0
	2	1300	1300	0.0
	3	1100	1100	0.0
	4	0	0	
RMS_Source		**37.9**		
RMS_Concn		**0.19**		

With 5000 iterations, the source predictions were having high errors along with significant spurious source predictions. As the number of iterations is increased to 10,000, the source predictions have become very close to the actual source releases. This case study shows that the RPCM-PSO-SO model is effective in field situation with limited available concentration data.

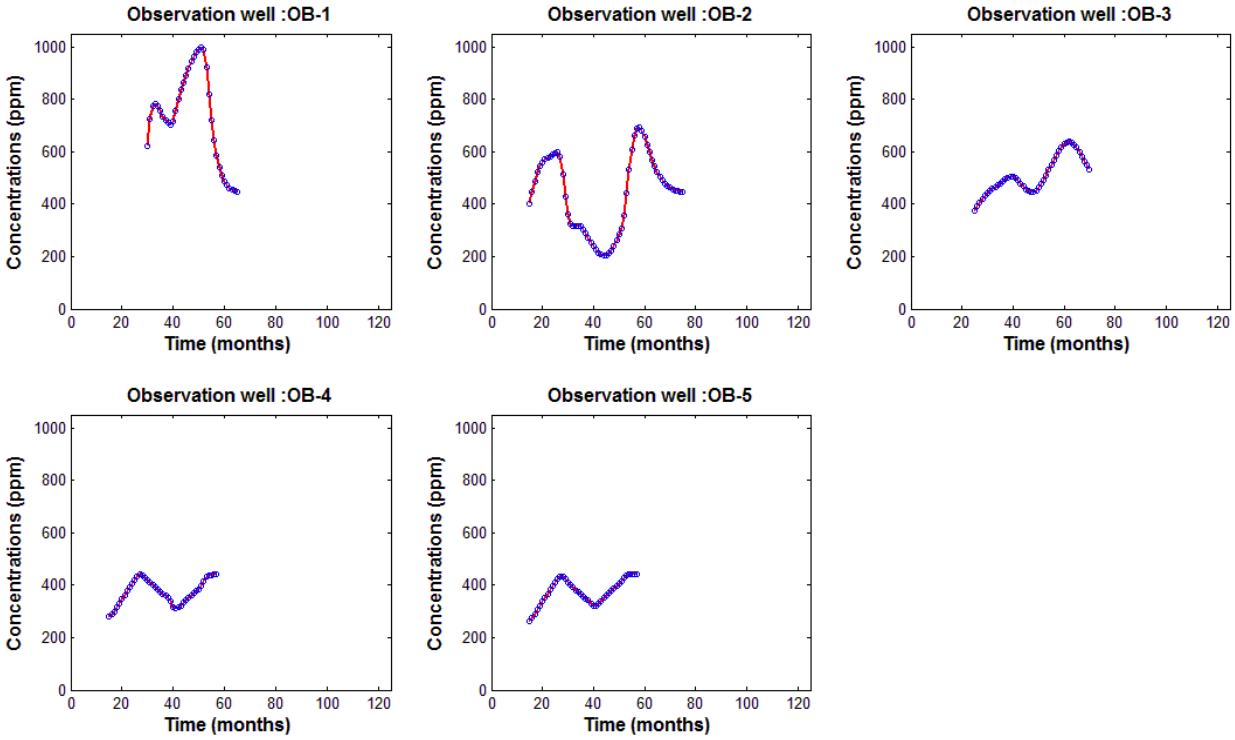

Figure 6.9: Limited amount of concentration data

Table 6.18: Source identification with a few years of concentration measurements

Source	Year of release	Actual source (ppm)	Predicted source (ppm)			
			5000 iterations	Percent error	10,000 iterations	Percent error
1	1	1000	1384	-38.4	1006	-0.6
	2	1500	1472	1.8	1499	0.0
	3	890	879	1.2	890	0.0
	4	0	12		0	
2	1	0	26		0	
	2	500	494	1.3	500	0.0
	3	0	168		4	
	4	1200	1184	1.3	1200	0.0
3	1	1000	993	0.7	1000	0.0
	2	0	7		0	
	3	0	15		0	
	4	700	698	0.3	700	0.0
4	1	900	829	7.9	898	0.2
	2	500	497	0.7	500	0.0
	3	0	0		0	
	4	1000	1000	0.0	1000	0.0

5	1 2 3 4	850 0 0 0	851 0 4 1	-0.1	850 0 0 0	0.0
6	1 2 3 4	800 1300 1100 0	800 1300 1099 0	0.0 0.0 0.1	800 1300 1100 0	0.0 0.0 0.0
RMS_Source		**87.36**			**1.46**	
RMS_Concn		**0.93**			**0.02**	

6.4.3 Case C: Missing data in concentration measurement

It is possible that there are missing data or gaps in concentration data measurement over a prolonged period of time. The simulation-optimization model should take into account such solute concentration data. Figure 6.10 shows a typical example of concentration data with missing data in between.

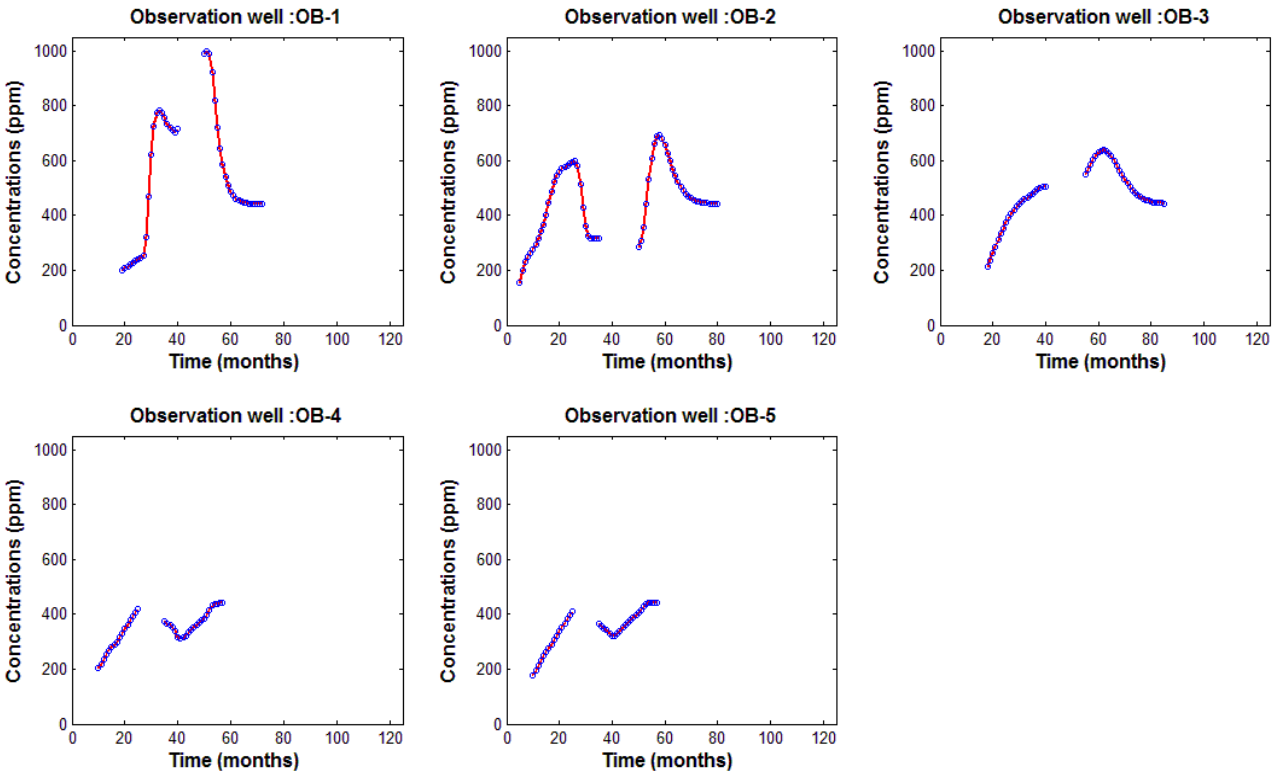

Figure 6.10 : Concentration data with missing or data gaps

The results of the source identification model for this case are presented in the Table 6.19 below. The number of iterations used for the results presented in the table is 30,000 iterations of the PSO. This is significantly higher than in the preceding cases. Further the errors are also substantial in two release

events. One significant spurious source is also predicted but as compared to the magnitude of the release events it is still very small. However, the model correctly predicted most of the release events with sufficient accuracies.

Table 6.19: Source identification with missing observed concentration data

Source	Year of release	Actual source (ppm)	Predicted source (ppm)	Percentage differences
1	1	1000	1352	-35.2
	2	1500	1488	0.8
	3	890	881	1.0
	4	0	5	
2	1	0	6	
	2	500	500	0.1
	3	0	144	
	4	1200	1180	1.7
3	1	1000	995	0.5
	2	0	1	
	3	0	0	
	4	700	702	-0.3
4	1	900	792	12.0
	2	500	496	0.8
	3	0	0	
	4	1000	1000	0.0
5	1	850	847	0.3
	2	0	2	
	3	0	9	
	4	0	1	
6	1	800	800	0.0
	2	1300	1300	0.0
	3	1100	1100	0.0
	4	0	0	
RMS_Source		**80.88**		
RMS_Concn		**0.33**		

6.4.4 Case D: Intermittent solute concentration data

To simulate irregular or intermittent concentration data measurements, let us consider the data presented in the Figure 6.11. It represents serious missing data and misses some of the important periods in the breakthrough curves at the wells. This can happen where water samplings are done very irregularly and

leading to a very poorly monitored system. It is expected that the source identification model will have difficulties in reconstructing the release events.

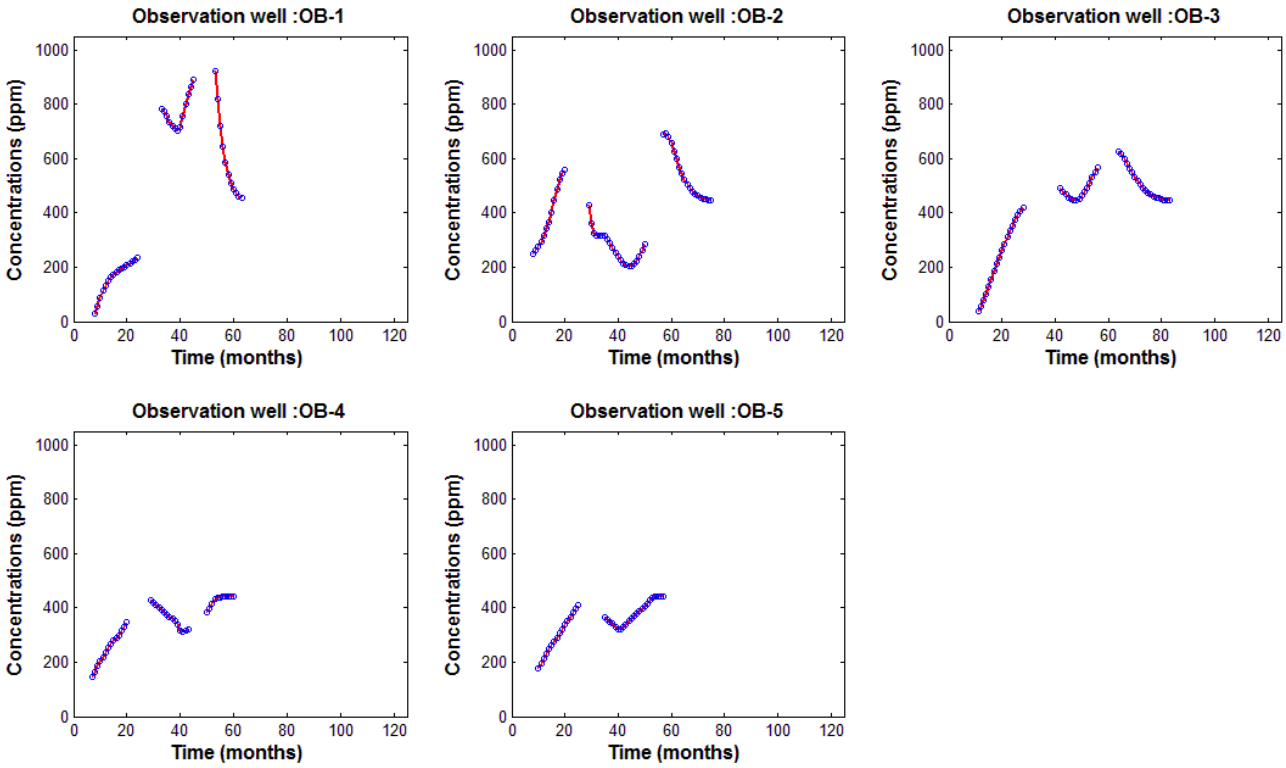

Figure 6.11: Intermittent or irregular concentration data

The source identification model is run with the above intermittent concentration profiles. The source predictions of the source identification model are presented in Table 6.20. However, the number of iterations required to achieve the convergence is now 10^5 iterations. It is observed that the source identification model was able to predict the sources accurately despite the missing data. The spurious sources are also small. Referring to Figure 6.11 it is observed that the missing periods are not very prolonged. Also it has been assumed that the concentration data has no uncertainties thereby reducing the problem of non-uniqueness significantly. This case study demonstrates that the source identification model is effective in handling intermittent or irregularly sampled concentration data.

Table 6.20: Source identification with intermittent concentration data

Source	Year of release	Actual source (ppm)	Predicted source (ppm)	Percentage error
1	1	1000	944	5.6
	2	1500	1505	-0.4
	3	890	890	0.0
	4	0	0	
2	1	0	0	
	2	500	500	0.0
	3	0	31	
	4	1200	1205	-0.4
3	1	1000	999	0.1
	2	0	0	
	3	0	0	
	4	700	700	0.0
4	1	900	851	5.4
	2	500	507	-1.5
	3	0	0	
	4	1000	1000	0.0
5	1	850	850	0.0
	2	0	0	
	3	0	47	
	4	0	4	
6	1	800	800	0.0
	2	1300	1300	0.0
	3	1100	1100	0.0
	4	0	0	
RMS_Source		**19.16**		
RMS_Concn		**0.06**		

6.5 Effect of location of the observation wells

6.5.1 Random placement of wells

It may be mentioned here that the borewells used in the preceding case study were all placed along the major flow path of the groundwater so that very significant concentration values of the solute are recorded by the borewells. To understand the effect of the borewell locations on the source identification model, the same problem is studied but with a different locations or distribution of the observation borewells. Figure 6.12 shows the locations of the borewells for this case study.

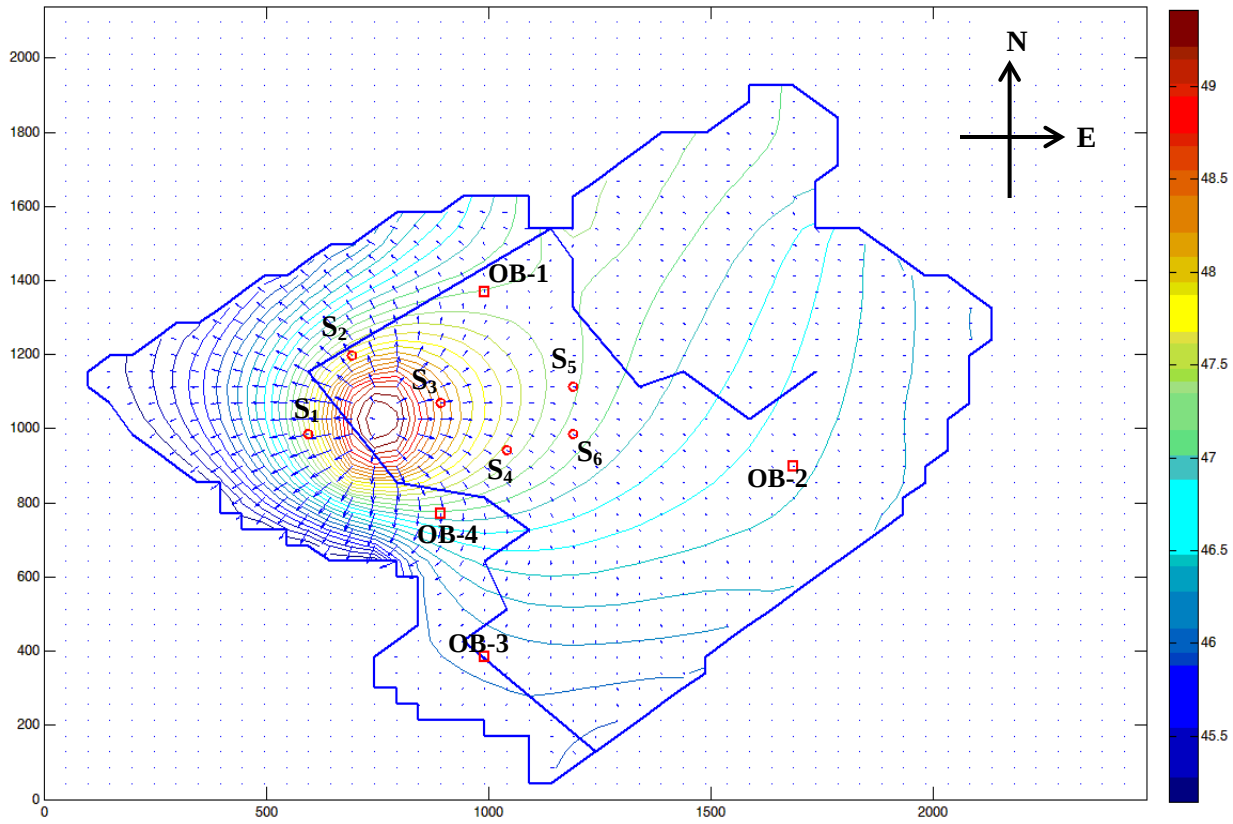

Figure 6.12: Model area with the sources and observation bore wells at different locations

The grid structure used is the same as in the preceding study. The transport model tracks the migration of the contaminants for a period of 10 years (3650 days) including the 4 years during which the release took place. The time step size used in the transport model is $\Delta t = 10\ days$ and the time-stepping scheme used is the Crank-Nicholson method. The concentration values at the observation bore wells are recorded for every 30 days (monthly) to construct the breakthrough curves at the wells. Figure 6.13 shows the breakthrough curves of the four observation borewells. The breakthrough curves at the four observation bore wells serve as the measured concentration data and used as input to the source identification model. The goal of the source identification model is to reconstruct the release history of the sources (Table 6.21) from this given concentrations data. The use of breakthrough curves is justified since generally in any field scenario concentrations are measured through water sample collection only at a few surveillance (observation) bore wells at a set time interval of sample collection e.g. weekly, monthly, bi-monthly etc. over a period of time, normally few years.

Table 6.21: Strength of the sources during the leaching period

Release Year	Source strength (in ppm)					
	S1	**S2**	**S3**	**S4**	**S5**	**S6**
1st year	1000	1500	890	0	0	500
2nd year	0	1200	1000	0	0	700
3rd year	900	500	0	1000	850	0
4th year	0	0	800	1300	1100	0

A concentration response matrix is constructed as described in section 5.2. Each column of this matrix stores the breakthrough curves at the four observation bore wells resulting from unit release from each of the sources in a particular release year.

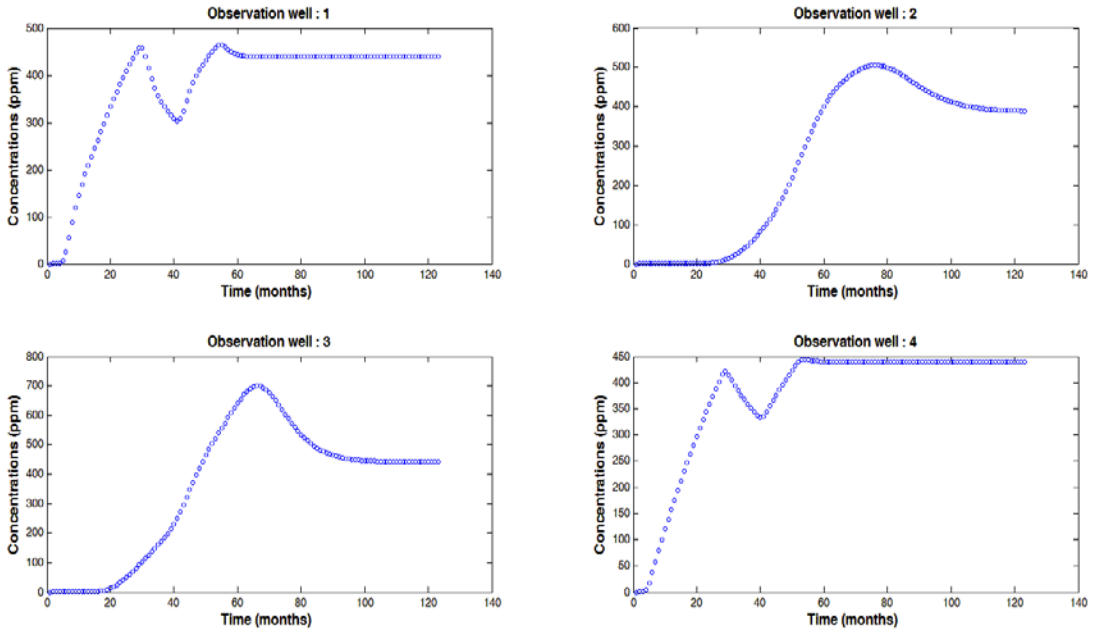

Figure 6.13 Breakthrough curves at the observation borewells

The results of the convergence study of the source identification model are presented in Table 6.22 and Fig.6.14 where the variation of error metrics viz., *RMS_Source* and *RMS_Concn* with the number of iterations is shown. It may be observed that acceptable values of *RMS_Source* are obtained when the number of iterations crosses 30 x 10^3. As observed in the previous case study, the *RMS_Concn* values are much smaller even with just 10^3 iterations. This implies that the optimization algorithm is very effective in matching the observed and model predicted concentrations (minimizing the objective function) but due to non-uniqueness of source identification problem, the source strength predictions are not accurate when

the number of iteration are low. Table 6.23 presents the comparison of the actual source strengths with those predicted by the PSO based SO model. The source strength predictions are presented for $3x10^3$ and $5x10^3$ iterations of the particle swarm optimizer. With $3x10^3$ iterations, though the source predictions are accurate to within 15% of the actual values, many erroneous sources are also predicted. When the number of iterations touches $5x10^3$, the magnitude of these spurious source predictions has been reduced to levels which can be safely ignored. It is observed from Table 6.23 that the source identification model could construct the release histories of the sources with high accuracy i.e. within 8% error. The very low value of the RMS_Concn suggest that the PSO algorithm was very effective in minimizing the difference between simulated and measured concentration values

Table 6.22: Convergence w.r.t. number of iterations

No. of iterations	***RMS_Source***	***RMS_Concn***
10^3	719.79	0.423
5×10^3	251.21	0.149
10×10^3	180.5	0.093
20×10^3	105.27	0.046
30×10^3	53.024	0.024
50×10^3	20.34	0.008

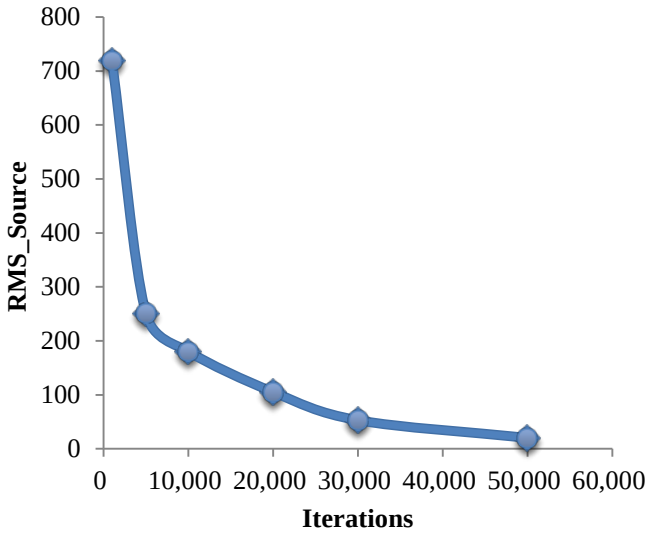

Fig.6.14 Convergence of source predictions with iterations

Table 6.23 : Source strength predictions from the PSO based source identification model

Source	Year of release	Actual Source strength (ppm)	Source Strength predictions from the PSO based SO model (ppm)	
			30 x 10^3 iteration	50 x 10^3 iteration
1	1	1000	1054	1031
	2	1500	1585	1552
	3	890	888	889
	4	0	1	0
2	1	0	5	1
	2	500	469	491
	3	0	77	27
	4	1200	1360	1257
3	1	1000	997	999
	2	0	2	1
	3	0	4	1
	4	700	661	691
4	1	900	827	878
	2	500	373	462
	3	0	3	1
	4	1000	1000	1000
5	1	850	848	850
	2	0	29	9
	3	0	10	3
	4	0	19	6
6	1	800	800	800
	2	1300	1299	1300
	3	1100	1099	1100
	4	0	16	4
RMS_source			53.024	20.34
RMS_concn			0.024	0.0082

6.5.2 Analysis with Limited Data

The previous case considers that the concentration data is available for an extended period of time and assumes no missing data over the entire period. This may not be always true in actual field situation where regular monitoring may start only after detecting solute concentrations that exceed a particular regulatory limit and may continue only for a limited period or number of years. In such cases, the concentration data will be limited. Fig.6.15 shows how a typical concentration data for such cases might

look like. Monitoring starts when the solute concentration in the surveillance borewells crosses 200 ppm or more. These monitoring period have been chosen arbitrarily to represent a typical field condition.

Except for borewell OB-4, whose monitoring period is two and half years, the rest of the borewells has a monitoring period between 3 to 5 years. Due to the reduction in the concentration data, more number of iterations might be required to achieve convergence. Alternatively if more information from the field is available, it can be incorporated into the model to fasten the convergence. One such commonly available information in industrial waste disposal facilities is the information on the level of contamination of the waste being handled by the facility. Such information can then be incorporated as constraints in the model. For example, if the maximum concentration (level) of the contaminant that a disposal facility handles is available, it may be used as a global constraint on all the potential sources in the optimization model. It is common in industrial practice, such as in nuclear industry, to classify wastes according to the concentration level of the contaminant being handled. Further in certain cases, within a disposal facility there may be many disposal sites and each disposal site is designated to handle a specified (or pre-classified) level of waste. In such cases, individual constraints (local constraints) can be imposed on each disposal sites (sources) in the optimization model.

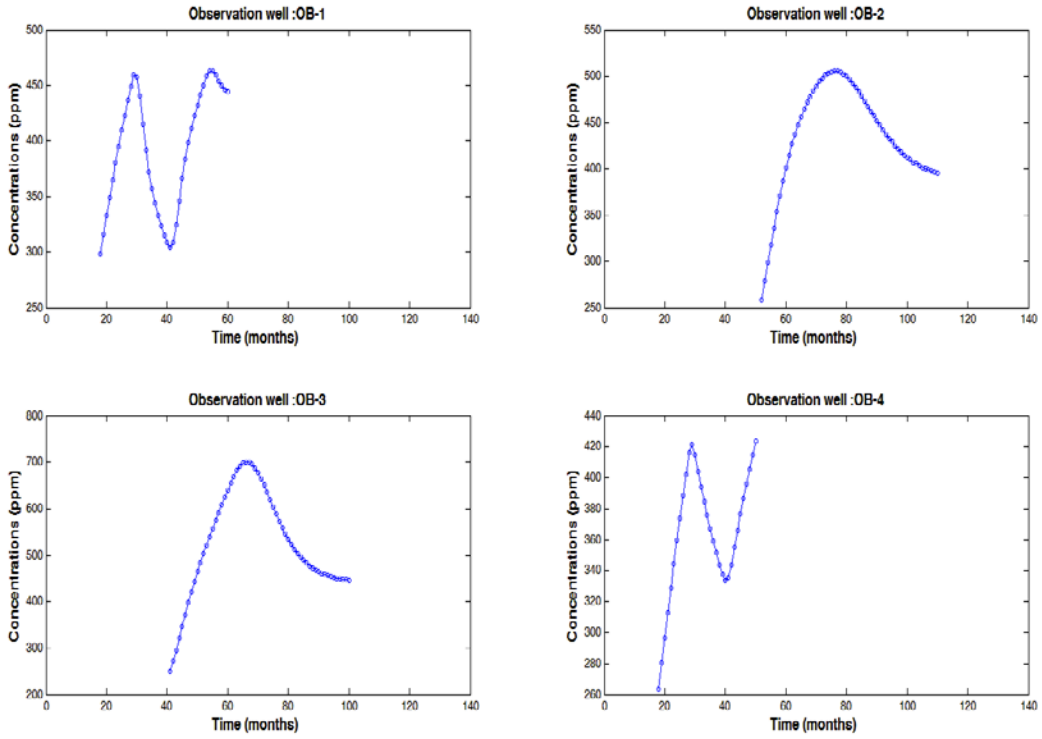

Fig.6.15 Water quality monitoring for a limited period of time.

Both the above cases of source strength constraining have been illustrated in the present study and compared to the case where no constraints are placed on the sources. In the first case, maximum source strength of 2000 ppm (global constraint) is imposed on all the disposal sites. Referring to Table 6.21, it is approximately 30% more than the highest release concentration of all the sources during the 4 year release period and has been chosen arbitrarily for illustration. It will demonstrate that only a rough estimate of constraint on the concentration is needed for the source identification model. For the case where individual constraints are to be imposed on each disposal site, the upper limit on the concentration for each site may be obtained from the maximum release concentration of each site during the 4 year release period (by referring to Table 6.21). Table 6.24 shows the caps on the concentration level of the contaminants handled by each disposal site as used in the source identification model.

Table 6.24: Concentration level of waste (contaminant) handled by individual disposal sites

Constraints on the individual disposal sites – maximum allowable concentration (level) of contaminant (waste) handled by each disposal site (in ppm)					
Site 1	Site 2	Site 3	Site 4	Site 5	Site 6
1500	2000	1500	2000	1500	1000

It may be observed, as in the first case, that these values are set to a value higher than the maximum release concentration of each site during the 4 year release period (see Table 6.21) to demonstrate that only a rough estimate is required. These limits were set arbitrarily.

The source identification model is run with and without the constraints as discussed above. Table 6.25 shows the results of convergence study with respect to the number of iterations of the particle swarm optimizer for different scenarios discussed above. In Table 6.27, the actual source predictions by the SO model after $50x10^3$ iterations are shown for the different scenarios. It is observed that (i) when there is no constraint on the solute concentration of the sites, most of the disposal events have been identified to within 20% of the actual value except for two disposal events where the errors were relatively larger at 39% and 54%. Also a few erroneous sources were predicted but their magnitudes are very small and may be ignored; (ii) the source predictions are improved when constraints are placed on the maximum concentration level of the contaminant. The best prediction was observed when individual upper limits (local constraints) are placed on the concentration of the releases for each disposal sites followed by the case where a facility wide upper limit (global constraint) was placed on the concentration of the releases from the disposal sites. In the former case, most of the disposal events were predicted within 5% of the true value except for two disposal events where the errors were 13% and 36%. The magnitude of the spurious sources predicted by the model has also reduced drastically.

It may be observed (Table 6.26) that the RPCM-SO model has slower convergence when no constraint is placed on the magnitude of the releases. This is inferred from the relatively high values of the *RMS_Source*. However, the predictions are improved by placing constraints on the source releases. This is because the solution search space has been drastically reduced by placing constraints. When local constraints are placed on individual sites, the search space is the lowest. Consequently the impact of non-uniqueness issue associated source identification will be mitigated to a large extent as a result of the reduced search space. Imposing the constraints calls for more information from the field. But such informations are generally available. In case this information is not directly available, a rough estimate can be made from the type of waste being disposed.

Other information from the field, if available, can be incorporated into the SO model to improve the convergence and also accuracy of the predictions. The only way to mitigate the effect of non-uniqueness of groundwater source identification problem is to provide more information to the inverse model. Incorporating more field information can drastically reduce the solution search space and hence improve convergence. Field information can also be used to rule out any significant erroneous sources predicted by the model. Increasing the length of the borewell monitoring period will also improve the model predictions as the case studies presented in this study shows.

Table 6.25: Convergence w.r.t. iterations for different scenarios

No. of iterations	**No upper limit placed on the concentration of source releases**		**2000 ppm upper limit concentration placed on the releases from the sources**		**Separate upper limit on the concentration of source releases for each disposal site**	
	RMS_Source	*RMS_Concn*	*RMS_Source*	*RMS_Concn*	*RMS_Source*	*RMS_Concn*
1000	1780.00	0.95	197.31	0.24	169.46	0.15
5000	1630.00	0.32	143.38	0.06	133.58	0.05
10000	1440.00	0.19	133.26	0.037	126.39	0.029
20000	278.50	0.09	125.57	0.017	106.17	0.015
30000	129.02	0.06	107.09	0.013	96.70	0.011
50000	107.17	0.02	74.76	0.008	46.29	0.006

In this study, it is implicitly assumed that the potential sources of leak are known a priori and also that the aquifer parameters are known exactly. The first assumption is not very restrictive since in any real groundwater contamination situation, the suspected sources or facilities are always known. For example, if a chloride contamination is found in the groundwater, then all the facilities and underground pipes

which handle chloride are the potential sources. The second assumption of no uncertainty in aquifer parameters does not represent the actual field conditions since aquifer parameters are known to have significant measurement errors. However, if calibrated aquifer parameters are available then they can be readily used in the model presented in this study.

Table 6.26: Source strength predictions from the SO model

Source	**Year of release**	**Actual Source strength (ppm)**	**Source Strength predictions of the SO model for 50 x 10^3 iteration (in ppm)**		
			No constraint placed on the releases	Global constraint on maximum release concentration	Local constraint on maximum concentration imposed on individual disposal sites
1	1	1000	1135	924	1029
	2	1500	1782	1327	1562
	3	890	884	893	889
	4	0	3	5	7
2	1	0	66	46	34
	2	500	230	260	320
	3	0	54	22	20
	4	1200	1335	1253	1252
3	1	1000	998	999	999
	2	0	17	11	8
	3	0	10	4	2
	4	700	421	513	603
4	1	900	889	896	891
	2	500	491	498	488
	3	0	0	0	0
	4	1000	1002	1002	1001
5	1	850	849	848	849
	2	0	33	14	17
	3	0	1	1	1
	4	0	3	4	3
6	1	800	800	800	800
	2	1300	1299	1300	1300
	3	1100	1100	1100	1100
	4	0	6	5	4
RMS_source			107.17	74.76	46.29
RMS_concn			0.02	0.008	0.006

The number of borewells used has also been reduced to examine the capability of the model when there is lesser input concentration data. Table 6.27 below shows the results of this study.

Table 6.27:Output of the source identification model (random location of the borewells)

Source	Year of release	Actual Source (ppm)	Predicted Source strength (ppm) **objective function :** sum of squared residuals	
			Predicted source strength	**Error**
1	1	1000	1016	-15.89
	2	1500	1525	-25.25
	3	890	889	0.58
	4	0	0	-0.11
2	1	0	0	-0.44
	2	500	497	2.83
	3	0	18	-18.4
	4	1200	1235	-35.18
3	1	1000	999	0.78
	2	0	0	-0.24
	3	0	0	-0.49
	4	700	698	1.99
4	1	900	898	1.92
	2	500	499	1.06
	3	0	0	-0.03
	4	1000	1000	0.01
5	1	850	850	-0.2
	2	0	4	-3.84
	3	0	0	-0.07
	4	0	0	-0.46
6	1	800	800	-0.01
	2	1300	1300	0.1
	3	1100	1100	-0.13
	4	0	1	-1.08
RMS (Source strength)			10.21	

It is observed that errors start appearing in the source identification model predictions. This means that the locations or distributions of the borewells have some effect on the model predictions.

6.6 Transient field case study –case when all potential sources are confined in a zone

Figure 6.16 shows a case where all the contaminant sources are located in a small zone within the model area. In this case it is expected that there will be maximum interference in the contaminant contributions

from the sources. The ability of the SO model to predict the sources by resolving these complex interferences is being studied in this section. The location of the observation borewells have also been kept at randomly located points (as in the preceding case, section 6.5), not necessarily in the direction of the contaminant plume.

Table 6.28: Concentration of the leaked contaminants

Concentration of the leaked contaminant from the sources (ppm)				
S_1	S_2	S_3	S_4	S_5
1300	750	1200	950	800

The sources in this case are assumed to be continuously leaking (leaching) for the entire simulation period. The concentrations of the releases from the sources are given in Table 6.28 above. The breakthrough curves at the observation borewells corresponding to the releases from the sources is shown in the Figure 6.17. The grid structure and other parameters are the same as in the preceding cases.

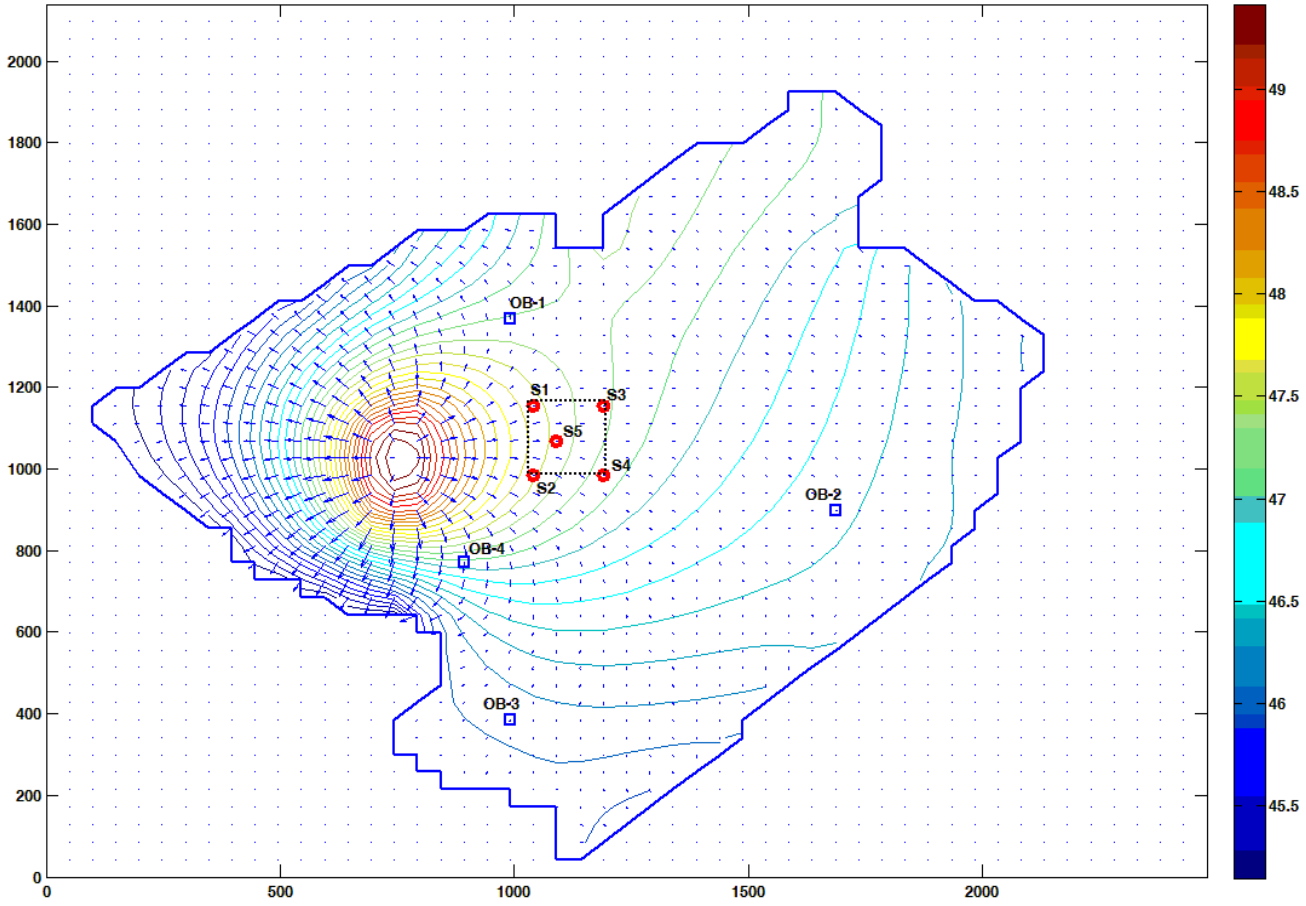

Figure 6.16: Case study with when all the sources are located in a small zone

The results of the source identification model are shown in the Table 6.29. The objective function used in this case is the sum of square of the residual between the predicted and observed concentrations. The number of PSO iterations used is 50 x 10^3. The source concentrations are predicted within 10% of their true values. Thus it may be concluded that the RPCM-PSO-SO model is able to resolve the inherent complexities due to interferences of the source contributions.

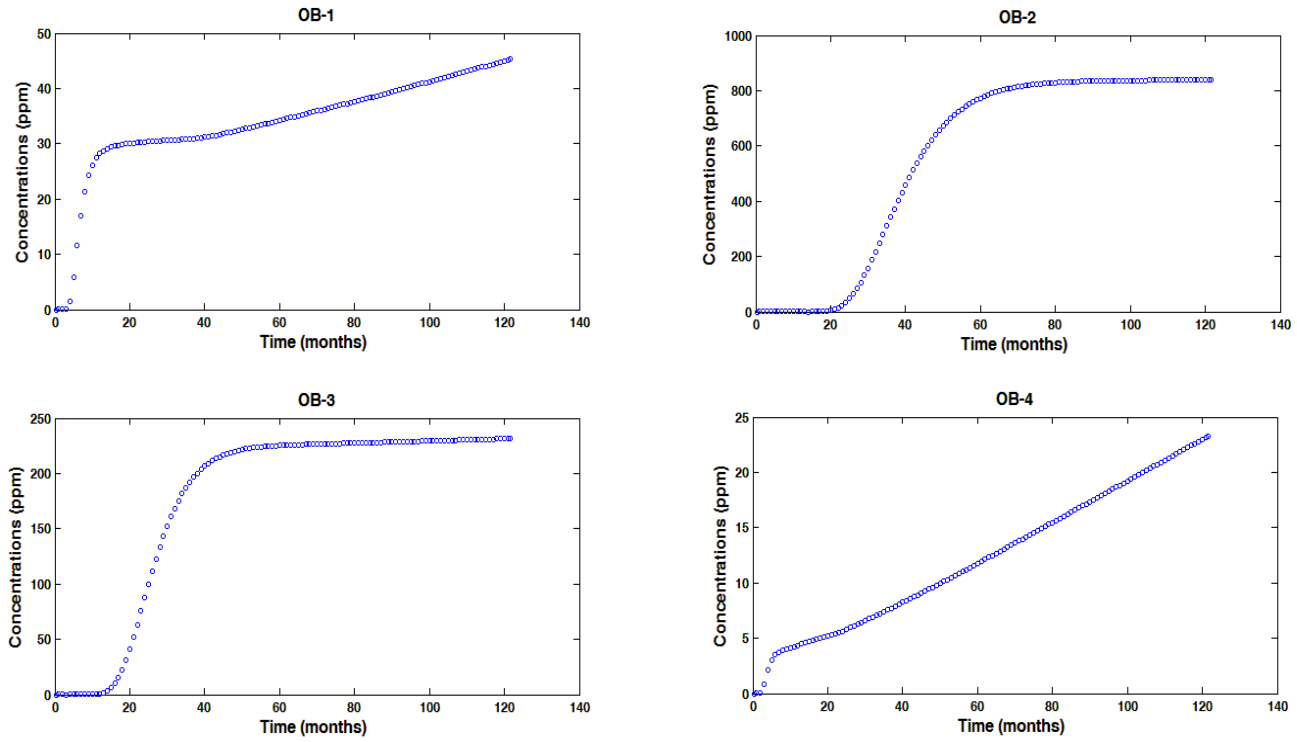

Figure 6.17: Breakthrough curves at the observation wells (all sources are confined in a small zone)

Table 6.29: SO model predictions of the source concentration

Source	Actual Source concentration (ppm)	RPCM-PSO-SO model predictions		
		Predicted source concentration (ppm)	Error	Percentage error
1	1300	1375	75	5.8
2	750	797	47	6.3
3	1200	1164	-36	-3.0
4	950	870	-80	-8.4
5	800	823	23	2.9
RMS (Source strength)		56.7		

6.7 Source identification with measurement errors in the concentration data

In the case studies presented above, it has been implicitly assumed that the observed concentration data has no uncertainty or error. This assumption may not hold in actual field conditions as uncertainties are unavoidable in any measurement. In this section, we discuss the various ways of dealing with erroneous concentration data.

6.7.1 Simulating measurement errors

To simulate uncertainty or errors in the measured concentration data, the true/observed concentration data (as predicted by the forward run of the groundwater flow and transport model) is perturbed by adding a random noise. Each perturbed datum was assumed to be sampled from a normal distribution having the exact datum as its means. This is achieved by adding normal random deviates as below:

$$C_n^{meas} = C_n^{meas} + \delta . \xi_n . C_n^{meas} \tag{6.8}$$

Where C_n^{meas} is the n^{th} measured data, δ is a scale factor which determines the magnitude of the noise/perturbation and ξ_n is the n^{th} normal random deviate. In this study, two values of $\delta = 0.05$ and $\delta = 0.1$ are used to represent moderate and high noise levels. The field case source identification model as described in section 6.2 is being re-considered here for uncertainty analysis with the perturbed concentration data.

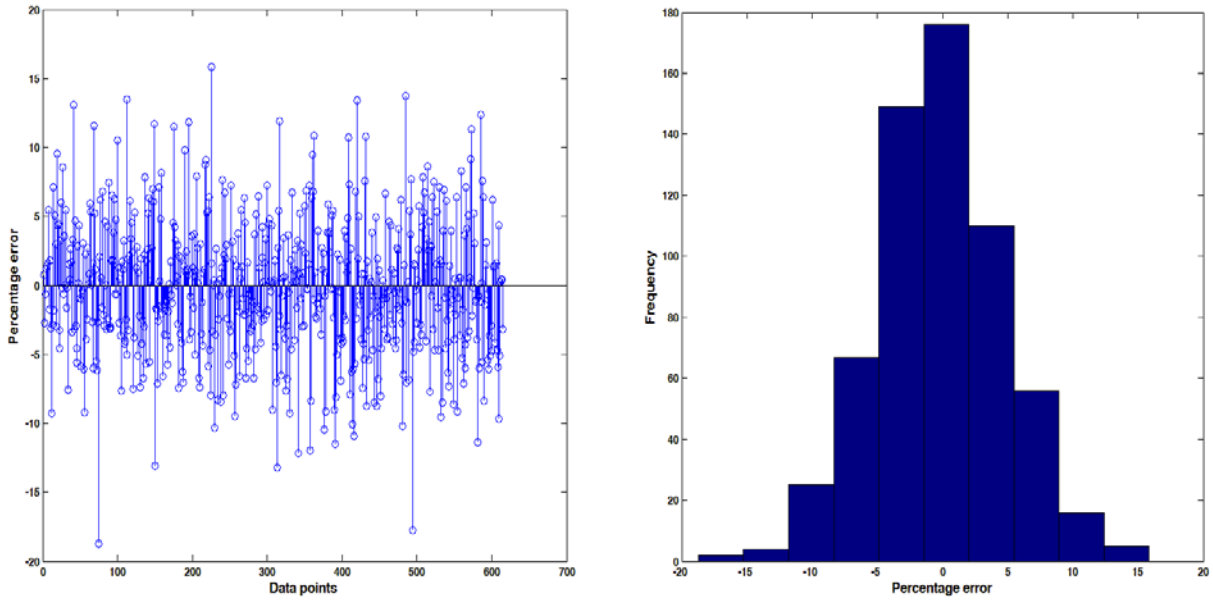

Figure 6.18: Perturbations corresponding to scaling factor $\delta = 0.05$

Figure 6.18 shows the errors or noise corresponding to application of a scaling factor $\delta = 0.05$. It is seen that the errors are as high as 17% of their true value. This represents a moderate level of measurement error in the solute concentration. It can also be seen from the histogram in the figure that the errors are normally distributed within this range. To simulate higher levels of errors, a scaling factor of $\delta = 0.1$ is applied.

Figure 6.19 shows the errors or noise corresponding to application of a scaling factor of $\delta = 0.1$. It can be seen that the errors go as high as 37% of their true value which is fairly high level of error.

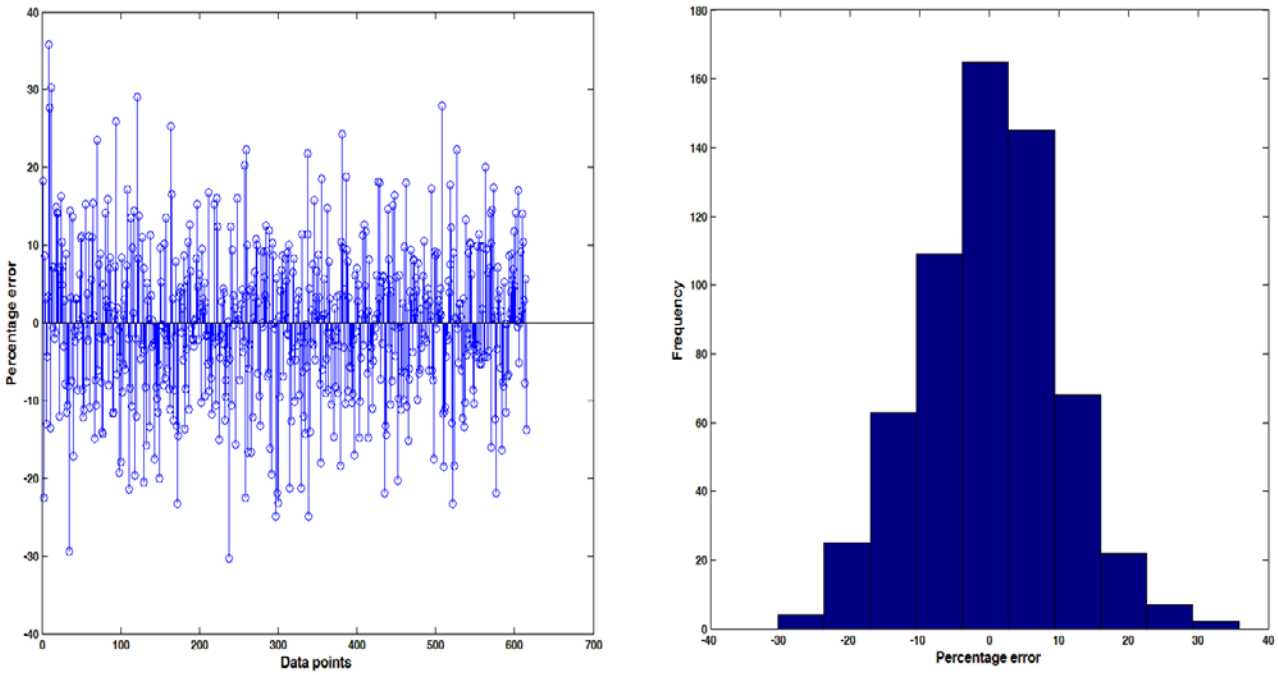

Figure 6.19: Errors corresponding to scaling factor $\delta = 0.1$

6.7.2 Dealing with erroneous concentration data

Since the groundwater source identification problem is an ill-posed problem (Atmadja and Bagtzoglou, 2001b), it is very sensitive to errors in the input data. The non-uniqueness of the source identification can lead to significant errors while using optimization models. The only way to overcome the non-uniqueness issue is to incorporate more field information into the model. As discussed in section 6.5, one such commonly available information in industrial waste disposal practices is the approximate level of contamination of the waste being handled by the facility or by the individual disposal sites within a disposal facility. This information may be used to impose constraints (global or local) on the potential sources thereby reducing the feasible search space and also reducing chances of unrealistic predictions. Other informations from the design and operation of the waste disposal facility, if available, may be used

to rule out spurious predictions or improve the quality of the predictions. Another way to deal with measurement errors in the concentration data is to use smoothing of the data which has been discussed in the next section.

6.7.3 Data smoothing

It is a common practice to smoothen experimentally measured data to extract the underlying relationship between the dependent and independent variables and reduce the experimental noises. In this study, a simple moving average smoothing of the perturbed concentration data is performed. A moving average filter smooth data by replacing each data point with the average of the neighboring data points defined within a span. The smoothing is done by using the following difference equation,

$$y_s(i) = \frac{1}{2N+1}(y_{i+N} + y_{i+N-1} + \cdots + y_{i-N}) \tag{6.9}$$

where $y_s(i)$ is the smoothed value for the i^{th} data point, *N* is the number of neighboring data points on the either side of $y_s(i)$ and *2N+1* is the span. For example, let us smooth a given data series using a moving average filter with a span of 5. The first four elements of the smoothed data y_s are given by,

$$\begin{aligned} y_s(1) &= y_1 \\ y_s(2) &= \frac{y_1 + y_2 + y_3}{3} \\ y_s(3) &= \frac{y_1 + y_2 + y_3 + y_4 + y_5}{5} \\ y_s(3) &= \frac{y_2 + y_3 + y_4 + y_5 + y_6}{5} \end{aligned} \tag{6.10}$$

In this study, a single run of the moving average smoothing with a span of 7, chosen arbitrarily, has been performed on the perturbed concentration data to demonstrate the technique. This smoothing has been applied to smoothen the perturbed concentration data (Figure 6.18 and Figure 6.19) of the field case study described in 6.2. Since the exact concentration data is known, an RMS error can be used to quantify the amount of error and measure the performance or effectiveness of the smoothing operation of the concentration profile for each of the 5 borewells. Table 6.30 shows the performance of the smoothing operation. It may be observed that the smoothing has significantly brought down the average error (RMS error) for most of the borewells. This shows that the smoothing operation is able to recover some of the underlying relationship between the concentration and time which has been lost by the perturbation of the concentrations. However this smoothing has varying effect on the borewells since the concentration profile vary widely from borewell to borewell. In usual practice of exploratory data analysis, it is not

uncommon to perform several smoothing operations (passes) on the measurement data using different spans. But in this study, a single pass or operation has been performed to illustrate the technique.

Table 6.30: Performance of the moving average smoothing

Borewell Number	Scaling factor $\delta = 0.05$		Scaling factor $\delta = 0.1$	
	RMS error without smoothing	RMS error with smoothing	RMS error without smoothing	RMS error with smoothing
1	25.923	25.233	53.798	31.905
2	21.322	15.571	38.638	24.905
3	21.947	7.492	42.674	14.708
4	21.277	8.320	34.313	14.491
5	20.254	7.759	37.308	15.966

The effectiveness of the smoothing can be seen graphically also. Figure 6.20 and Figure 6.21 shows the plot of the exact , perturbed and smoothed concentration profiles for two selected observation borewells viz, borewell no.1 and 3, for the case study described in section 6.2. These correspond to the case of moderate amount of error/noise as depicted in Figure 6.18. The smoothing is able to capture the trend of the concentration profile to a large extent.

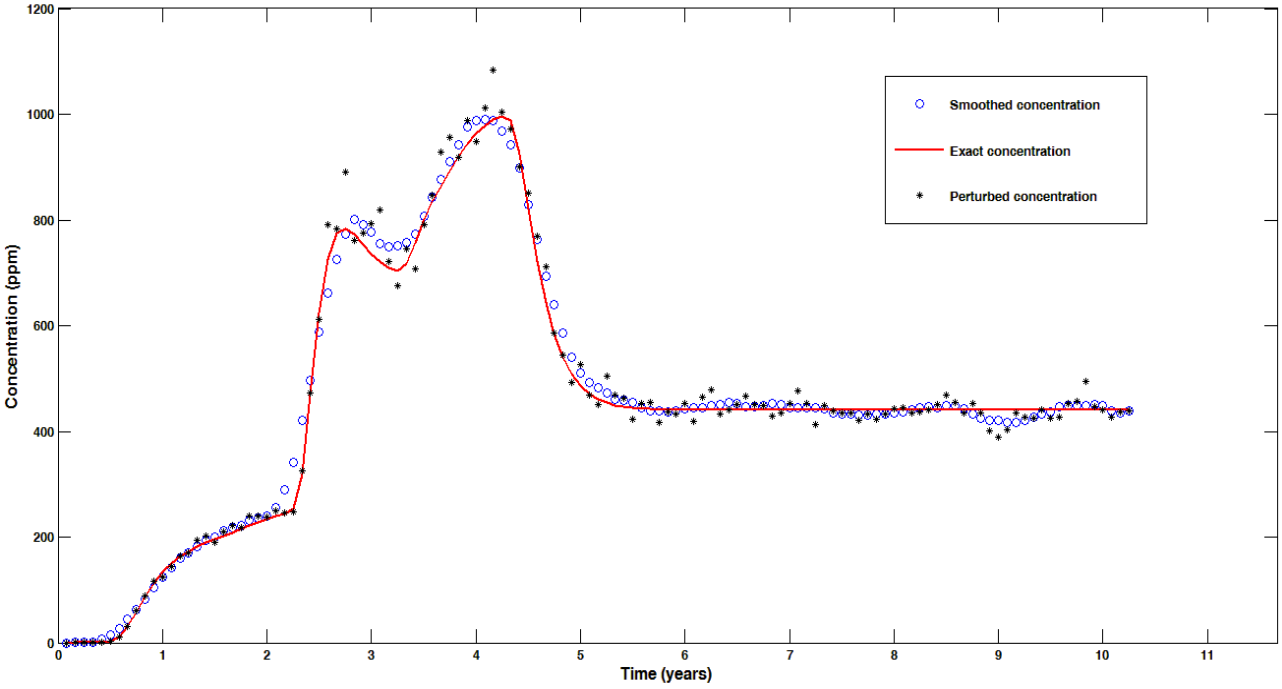

Figure 6.20: Perturbation ($\delta = 0.05$) and smoothing of concentration profile for borewell no.1

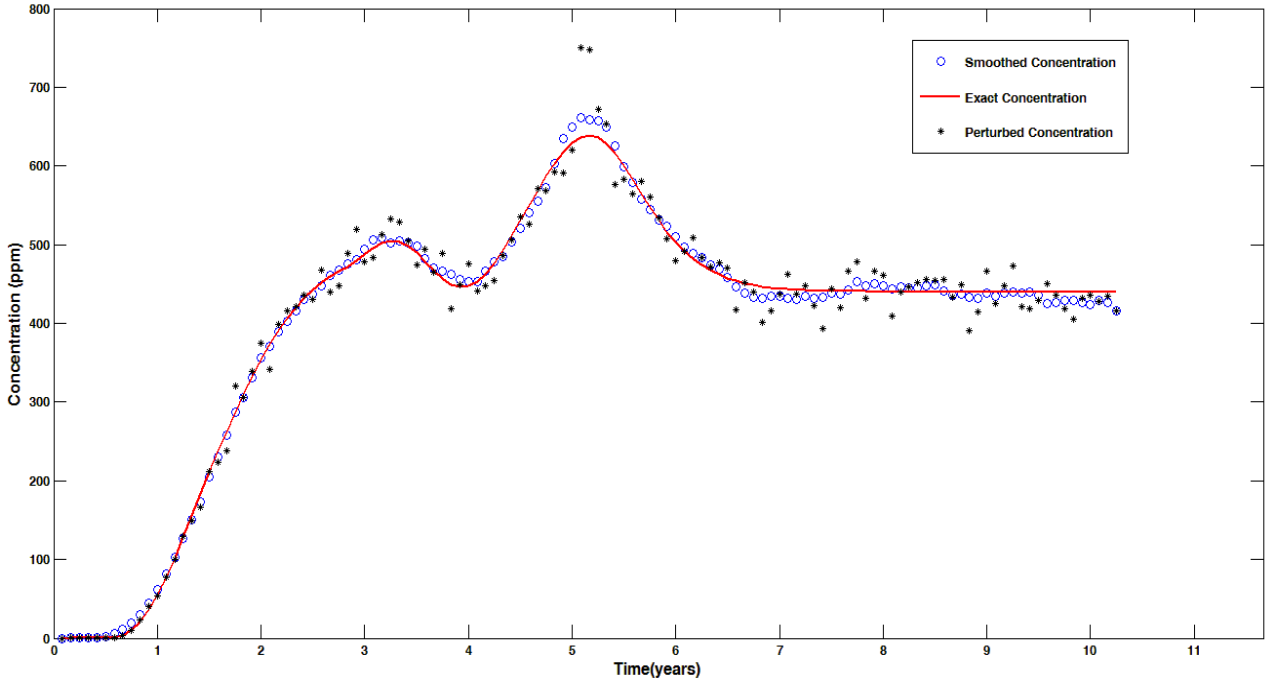

Figure 6.21: Perturbation ($\delta = 0.05$) and smoothing of the concentration profile of borewell no. 3

For the case of high errors corresponding to scaling factor of $\delta = 0.1$ (as depicted in Figure 6.19), Figure 6.22 and Figure 6.23 shows the same plot of the exact, perturbed and smoothed concentration profiles for the two selected observation borewells. It may be observed the trend of the data has been more or less captured by the smoothing operation.

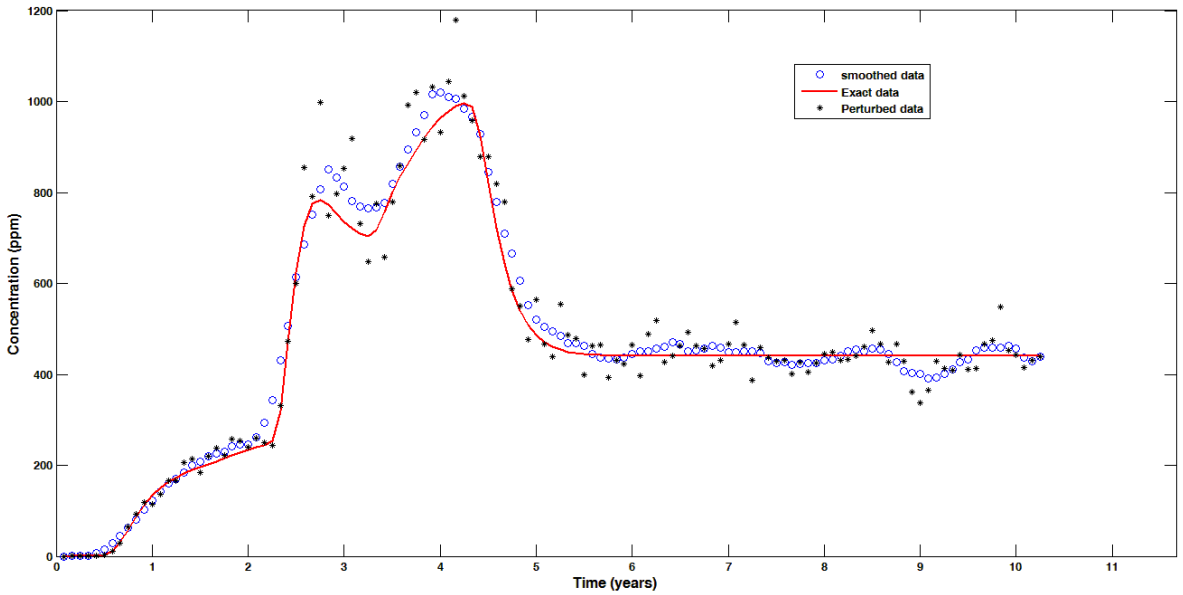

Figure 6.22:Perturbation ($\delta = 0.1$) and smoothing of concentration profile for borewell no.1

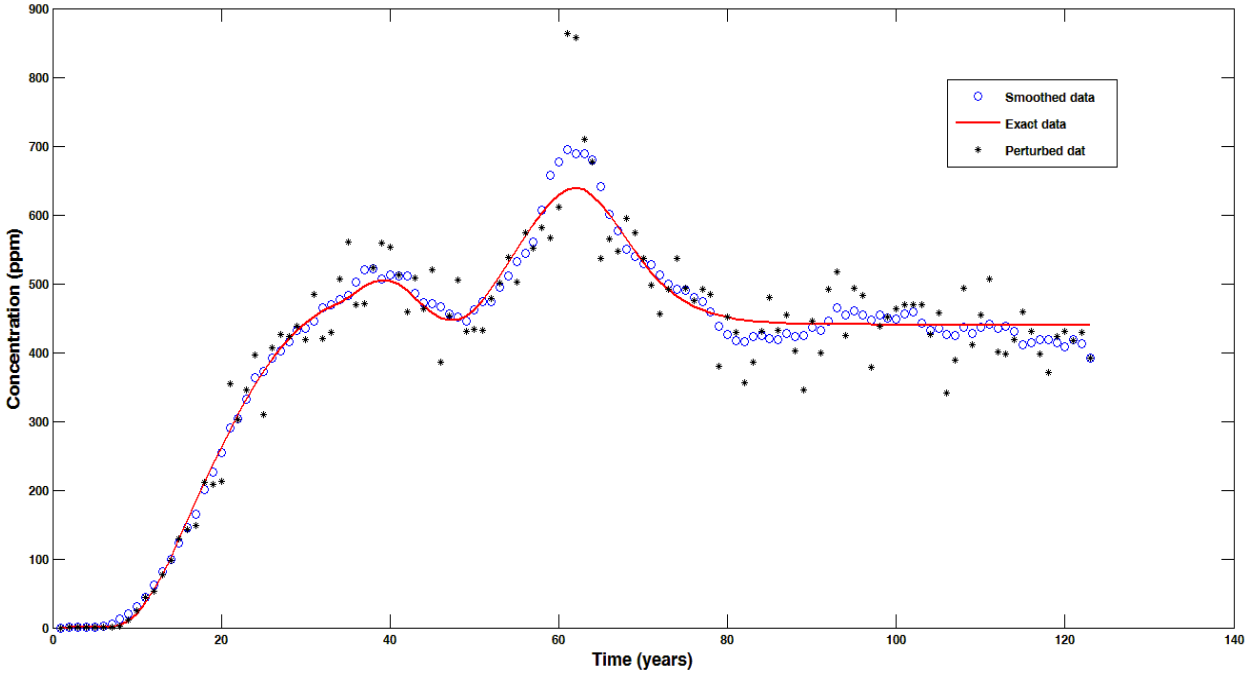

Figure 6.23: Perturbation ($\delta = 0.1$) and smoothing of the concentration profile of borewell no. 3

6.7.4 Transient field case with uncertain concentration data

The field case study discussed in section 6.2 are re-run with perturbed concentration data to simulate measurement errors. As mentioned in previous discussion, two levels of perturbation or errors are applied

(i) Moderate level of error with maximum errors as high as 17% of the true concentration value

(ii) High levels of error with maximum errors as high as 37% of the true concentration value

These perturbed data are then smoothed with a one pass of moving average smoothing with a span of 7. The smoothed data is then inputted to the source identification model. Table 6.31 shows the predicted sources from the Simulation-Optimization model. The number of iterations used in the PSO optimization is $50x10^3$. It may be observed that the source identification model was able to identify all the major disposal events with acceptable accuracy. However, the error was around 49% for one disposal event even though the model could identify this release event. In this context, it is desirable to get more information from the field to deal with such predictions. It may also be observed that a few spurious (noise) source predictions were made however their magnitudes are small and may safely be ignored. Additional field knowledge may also be used to rule out or reject such noises.

Table 6.31: Source prediction with erroneous concentration data (moderate level of errors)

Source	Year of release	Actual source (ppm)	Predicted source (ppm)	Percentage error
1	1	1000	800	20.0
	2	1500	1481	1.3
	3	890	888	0.2
	4	0	0	
2	1	0	150	
	2	500	464	7.2
	3	0	0	
	4	1200	1323	-10.3
3	1	1000	962	3.8
	2	0	0	
	3	0	76	
	4	700	621	11.3
4	1	900	630	30.0
	2	500	747	-49.4
	3	0	0	
	4	1000	1003	-0.3
5	1	850	779	8.4
	2	0	35	
	3	0	0	
	4	0	14	
6	1	800	807	-0.9
	2	1300	1235	5.0
	3	1100	833	24.3
	4	0	69	
RMS_Source		**188.9**		
RMS_Concn		**8.3**		

Table 6.32 shows the results for the second case characterized by high levels of measurement errors in the concentration. The measurement errors are as high as 37% of their true values. The number of iteration used in the PSO optimization is $50x10^3$. As seen from this table, the source identification model was able to identify all the major disposal events with acceptable accuracy. However for two disposal events the errors were above 40% of the true value. Also the overall error in the predictions were a little higher compared to the preceding case with moderate level of measurement errors in the concentration data as indicated by the higher value of *RMS_Source*. The spurious errors are also more prominent even though they are small enough to be treated as noises.

Table 6.32: Source prediction with erroneous concentration data (high level of errors)

Source	Year of release	Actual source (ppm)	Predicted source (ppm)	Percentage error
1	1	1000	1104	-10.4
	2	1500	1563	-4.2
	3	890	848	4.7
	4	0	7	
2	1	0	120	
	2	500	475	5.1
	3	0	0	
	4	1200	1515	-26.3
3	1	1000	891	10.9
	2	0	93	
	3	0	150	
	4	700	629	10.1
4	1	900	540	40.0
	2	500	712	-42.4
	3	0	0	
	4	1000	1079	-7.9
5	1	850	744	12.4
	2	0	35	
	3	0	0	
	4	0	144	
6	1	800	832	-4.0
	2	1300	1330	-2.3
	3	1100	725	34.1
	4	0	67	
RMS_Source		**235.4**		
RMS_Concn		**11.0**		

6.7.5 Handling uncertainties using weighting

In this section, the effect of giving weightage to the uncertain measured data is being explored. Giving weightage to each measured data can be highly subjective to the extent of being unrealistic in actual field practice. However when such information is conceivable, it may be used directly in the model to deal with the uncertainties. Applying weighting to the uncertain measured data can reduce their impact or importance on the objective function. When weighting is applied, the objective function is modified as,

$$S = \sum_{i=1}^{NO} \sum_{j=1}^{NT} w_{ij} \left(C_{i,j}^{Pred} - C_{i,j}^{Obs} \right)^2 \quad (6.11)$$

Where,

$NO = no.of\ observation\ bore\ wells$

$NT = no.of\ time\ steps$

$C_{i,j}^{Pred} = Predicted\ concentration\ at\ i^{th}\ observation\ point\ at\ j^{th}\ time\ step$

$C_{i,j}^{Obs} = Observed\ /measured\ concentration\ at\ i^{th}\ observation\ point\ at\ j^{th}\ time\ step$

$w_{ij} = weighting\ value\ applied\ to\ the\ i^{th}\ observation\ point\ at\ j^{th}\ time\ step$

To study the effect of uncertainty or errors in the measured concentration data, the true/observed concentration data (as predicted by the forward run of the groundwater flow and transport model) is perturbed by adding a random noise. This is achieved by adding random numbers within a specified limit i.e. spread around the true value. For example to add a 10% spread of random error or noise around the true value, the true concentration value is perturbed as below:

$$Perturbed\_conc = true\_conc + (1.1 - 0.9) * random(0,1) * true\_conc \quad (6.12)$$

where $random(0,1)$ is a uniformly distributed random number in [0,1]. Different scenarios are considered here to analyze the impact of uncertainties on the concentration data. Following parameters are changed to study the ability of the model to handle uncertainties:

1. The amount of uncertainty in the data i.e. the spread of the noise are varied viz. 10%, 20% and 30%
2. Number of concentration data points with uncertainties is varied viz. 300, 400, 500 and 600 concentration data points are perturbed and their effects examined.

The weighting factor is a subjective quantity which should be decided by the modeler based on the reliability of the field data collected. It can be any complex function. But in this study we have given the weighting factor to be a quantity between 0 and 1. Smaller the weight lesser its contribution to the objective function and hence lesser the influence of the corresponding data points on the source identification model.

Table 6.33 and Table 6.34 show the results from uncertainty analysis of the source identification problem. The uncertainty in the input data is simulated by adding perturbations of varying amounts to randomly selected measured concentration data. The tables show the cases when 300, 400, 500 and 600 concentration data are perturbed out of a total of 615 measured concentration data. The amounts of

perturbations or error used are 10%, 20% and 30%. A uniform weighting of 0.1 is given to all the perturbed data.

Table 6.33: Results of Uncertainty analysis

Source	Year of release	Actual Source (ppm)	Number of perturbed data: 300						Number of perturbed data: 400					
			Amount of perturbation: 10%		Amount of perturbation: 20%		Amount of perturbation: 30%		Amount of perturbation: 10%		Amount of perturbation: 20%		Amount of perturbation: 30%	
			Predicted	Diff	Predicted	Diff	Predicted	Diff	Predicted	Diff	Predicted	Diff	Predicted	Diff
1	1	1000	1000	0	1001	-1	1000	0	1000	0	1000	0	1000	0
	2	1500	1500	0	1500	0	1500	0	1500	0	1500	0	1500	0
	3	890	890	0	890	0	890	0	890	0	890	0	890	0
	4	0	0	0	0	0	0	0	0	0	0	0	0	0
2	1	0	0	0	0	0	0	0	0	0	0	0	0	0
	2	500	500	0	500	0	500	0	500	0	500	0	500	0
	3	0	0	0	1	-1	0	0	5	-5	0	0	0	0
	4	1200	1200	0	1200	0	1200	0	1200	0	1200	0	1200	0
3	1	1000	1000	0	1000	0	1000	0	1000	0	1000	0	1000	0
	2	0	0	0	0	0	0	0	0	0	0	0	0	0
	3	0	0	0	0	0	0	0	0	0	0	0	0	0
	4	700	700	0	700	0	700	0	700	0	700	0	700	0
4	1	900	900	0	899	1	900	0	897	3	900	0	900	0
	2	500	500	0	500	0	500	0	500	0	500	0	500	0
	3	0	0	0	0	0	0	0	0	0	0	0	0	0
	4	1000	1000	0	1000	0	1000	0	1000	0	1000	0	1000	0
5	1	850	850	0	850	0	850	0	850	0	850	0	850	0
	2	0	0	0	0	0	0	0	0	0	0	0	0	0
	3	0	0	0	0	0	0	0	1	-1	0	0	0	0
	4	0	0	0	0	0	0	0	0	0	0	0	0	0
6	1	800	800	0	800	0	800	0	800	0	800	0	800	0
	2	1300	1300	0	1300	0	1300	0	1300	0	1300	0	1300	0
	3	1100	1100	0	1100	0	1100	0	1100	0	1100	0	1100	0
	4	0	0	0	0	0	0	0	0	0	0	0	0	0
RMS (Source strength)			**3.83E-06**		**0.4**		**0.05**		**1.27**		**0.12**		**0.06**	
RMS (Concentration)			**17.94**		**35.26**		**54.69**		**19.93**		**41.07**		**60.79**	

Table 6.34 : Results of Uncertainty analysis

Source	Year of release	Actual Source (ppm)	Number of perturbed data: 500						Number of perturbed data: 600					
			Amount of perturbation: 10%		Amount of perturbation: 20%		Amount of perturbation: 30%		Amount of perturbation: 10%		Amount of perturbation: 20%		Amount of perturbation: 30%	
			Predicted	Diff	Predicted	Diff	Predicted	Diff	Predicted	Diff	Predicted	Diff	Predicted	Diff
1	1	1000	1492	-492	1258	-258	1325	**-325**	1148	**-148**	1388	**-388**	1381	**-381**
	2	1500	1476	24	1479	21	1481	19	1455	45	1588	-88	1521	-21
	3	890	878	12	886	4	884	6	893	-3	861	29	859	31
	4	0	2	-2	1	-1	0	0	1	-1	1	-1	0	0
2	1	0	9	-9	1	-1	0	0	30	-30	0	0	0	0
	2	500	500	0	500	0	500	0	500	0	500	0	460	40
	3	0	269	-269	245	-245	610	-610	0	0	696	**-696**	0	0
	4	1200	1171	29	1169	31	1149	51	1463	**-263**	1256	-56	919	**281**
3	1	1000	983	17	989	11	969	31	941	59	924	76	1062	-62
	2	0	4	-4	1	-1	8	-8	14	-14	55	**-55**	21	-21
	3	0	12	-12	0	0	0	0	0	0	36	-36	9	-9
	4	700	702	-2	704	-4	704	-4	698	2	700	0	656	44
4	1	900	666	234	810	90	621	279	183	**717**	238	**662**	0	**900**
	2	500	522	-22	495	5	523	-23	597	**-97**	778	**-278**	859	**-359**
	3	0	1	-1	0	0	6	-6	27	-27	27	-27	0	0
	4	1000	1003	-3	1000	0	998	2	942	58	998	2	939	61
5	1	850	851	-1	846	4	807	43	571	**279**	658	**192**	187	**663**
	2	0	4	-4	4	-4	17	-17	83	-83	40	-40	116	**-116**
	3	0	158	-158	12	-12	99	**-99**	458	**-458**	732	**-732**	0	0
	4	0	14	-14	2	-2	10	-10	30	-30	0	0	4	-4
6	1	800	800	0	800	0	801	-1	811	-11	802	-2	798	2
	2	1300	1300	0	1300	0	1299	1	1246	54	1280	20	1141	**159**
	3	1100	1101	-1	1102	-2	1097	3	1058	42	1330	**-230**	808	**292**
	4	0	0	0	0	0	1	-1	55	**-55**	11	-11	183	**-183**
RMS (Source strength)			**128.57**		**75.32**		**154.33**		**196.65**		**273.95**		**271.81**	
RMS (Concentration)			**22.43**		**45.86**		**71.86**		**24.92**		**47.72**		**73.12**	

6.8 Model application – merits and limitations

The developed RPCM-PSO-SO model for groundwater source identification offers a number of advantages over other existing techniques. It also has a few limitations and some assumptions are made implicitly. However, as discussed in the sections below, the limitations are not very serious in nature and will not pose a hindrance to the application of the model. It may be mentioned that the structure of the SO model is very simple and it is potentially applicable to a wide range of source identification problems.

6.8.1 Merits

As demonstrated in this chapter, the RPCM-PSO-SO model is applicable in field scale problems of any complexity. It is able to handle most of the practical problems that may arise in any field situation. Most of the proposed methods for groundwater source identification are applicable only to a limited number of problems and have serious other limitations that potentially prevent them from being applied in real field cases. Simulation-optimization models in general are more widely applicable than other methods and also avoid the mathematical complexities associated with other inversion models.

The developed RPCM-PSO-SO model also offers a number of computational advantages apart from being applicable in real field problems. The meshfree RPCM simulation model does away with the requirement to create a mesh unlike conventional methods such as FDM, FEM etc. which are grid based methods. This avoids the computationally cost step of mesh creation and facilitates other applications such as adaptive analysis. The PSO optimization model is very simple to implement and can be easily integrated with any simulation model.

6.8.2 Limitations

However the developed model has also some limitations. Being a recently developed method, the meshfree RPCM simulation model has a few technical issues yet to be addressed (Guneshwor et al., 2016) such as the optimal choice of shape parameters, size and shape of the local support domain etc. The shape parameter, in particular, has a profound impact on the accuracy and stability of the RPCM method. The choice of these parameters is subjective. However it does not pose any serious hindrance to the application of the method since a simple sensitivity or parametric study may be conducted to determine these parameters. The PSO optimization model used in the source identification model also has a few issues to be addressed, most pertaining to the optimal choice of parameters, and can also be computationally intensive if the convergence is slow.

The RPCM-PSO-SO model implicitly assumes that calibrated aquifer parameters are used. It does not take into account the uncertainties in hydro-geological parameters. The use of breakthrough curves apparently requires extended period of concentration data collection. The later issue, however, is not as

serious as it may appear. As demonstrated through the case studies, the source identification model is able to handle limited and intermittent concentration data. Uncertainty in the concentration data pose a problem for any simulation-optimization based source identification model. However, as discussed in this chapter, there various ways in which uncertain concentration data may be tackled.

6.9 Closure

Groundwater source identification is vital aspect to effective remediation of contamination. This chapter has explored the applicability of the developed RPCM-PSO-SO source identification model to various problems. It also has examined the ability of the model to handle various problems that may arise in real field situations. It has been observed that the model is able to handle source identification problems of varying complexities. The model can handle practical levels of uncertainties in the concentration data. The source predictions are very good to satisfactory in all the cases. The developed RPCM-PSO-SO model thus may be used as an effective practical tool for groundwater source identification.

Chapter 7
Summary and Conclusions

7.1 Summary

Groundwater flow and transport models are widely used for planning and remediation of groundwater resources. The objective of the present study is to determine or backtrack the sources of pollution in an aquifer from the given field measurements of concentration distributions. The approach used in this work is to run forward simulations of the transport model and check the solutions with the field measured data. Owing to the non-uniqueness of the solution and the infinite number of plausible combinations, one needs to follow an optimization method to obtain the best fitted solution. Such a model where forward simulation is linked to an optimization model is generally known as simulation-optimization (SO) model.

In this study a new SO model is developed for source identification. The forward modeling is performed using meshfree radial point collocation method. Though grid based methods such as finite difference and finite element are the dominant methods currently used for groundwater modeling, these methods have many shortcomings due to the use of a fixed grid or mesh. The creation of mesh is a major component being computationally expensive and also difficult to solve field problems. Moreover, because of the need to create mesh, adaptive analysis of a problem is also difficult to carry out as several re-meshing or re-zoning are required. Meshfree methods, on the other hand, do not suffer from the above shortcomings and is increasingly becoming popular. In this study, a collocation based meshfree method known as Radial Point Collocation Method (RPCM) has been developed for application in groundwater modeling. In this method, the basis function used for interpolation of the state variable is a class of functions called the Radial Basis Function (RBF). Two of the most widely used RBFs viz, Multi-Quadrics RBF (MQ-RBF) and Exponential EBF (EXP-RBF) have been examined in this work. The applicability of the RPCM method has been validated through several numerical examples for both the one and two-dimensional problems and also for transient cases. Several issues that arise in application of the RPCM has been examined and addressed. Some of the major issues that have been examined in this study are:

- determination of the optimal values of the shape parameter of the RBF function
- handling derivative boundary conditions,
- regularization of singular sources or sinks
- handling high-Peclet number transport problem
- use of sub-domain approach for handling problems with material heterogeneity

Groundwater flow and transport modeling using meshfree RPCM method forms the forward modeling part of the source identification model. For optimization, the particle swarm optimization (PSO) has been utilized in this study. It is a nature-inspired swarm intelligence algorithm that relies on interactions of simple processing units (also known in artificial intelligence as agents). It offers many advantages over other optimizers in that the implementation is very simple and straight forward and that there are relatively fewer parameters which has to be adjusted. In this study, the canonical PSO with Clerc's constriction coefficients is implemented.

The basic goal of an optimization based model for source characterization is to identify source characteristics (location, disposal duration, and solute mass flux or volume disposal rates). The objective is to search for a feasible set of source characteristics which minimize some function of the deviations between the observed and the simulated values of concentrations and hydraulic heads. This can be achieved by minimizing the weighted sum of the squared deviations (or absolute deviations) between observed values of spatially and temporally varying hydraulic head and/or concentration, and the corresponding simulated values of hydraulic head and concentration.

Initially, the source identification in groundwater has been demonstrated through a hypothetical aquifer where leaks of effluents or contaminants are assumed to occur at selected points. Case studies for both the steady state and transient contaminant releases have been studied. A field case study has been also studied in this work. The concentration distribution data (which form the observed/field measured concentration data) is generated by a forward run of the groundwater flow and transport model (RPCM) by assuming leaks at certain points with specified solute fluxes. From this baseline concentration data, the SO model tries to locate and quantify the leaks by minimizing the difference between the observed and predicted concentrations. A concentration response matrix (section 5.3.4) has been defined in the SO model which drastically improves the efficiency of the model.

Uncertainty in the field data namely concentration measurement has been simulated through randomly introduced perturbations to the input data. The amount of error or perturbations introduced has been varied to examine the tolerance of the model to input data. Since groundwater source identification problem is inherently ill-posed, it is therefore very sensitive to errors in the input data. The only way to deal with the non-uniqueness issue of groundwater source identification is to incorporate more field information into the model. Various methods were examined to deal with uncertain concentration data. Smoothing of the input data, applying constraints from field information, using weighting to reduce the contribution of the erroneous data etc. are some of the techniques that have been examined in this study.

In this study, the developed RPCM-PSO based simulation-optimization model has been found to be effective in groundwater pollution source identification.

The simulation-optimization model developed in this study can be used in environmental forensics to address questions related to release histories and sources of contamination in the environment. Environmental forensics generally involves the reconstruction of past environmental events, such as the timing, types and amounts, and sources of chemical or contaminant releases to the environment. Questions requiring environmental forensic applications usually relate to understanding the extent, duration, and responsibility for environmental contamination sites in a regulatory and/or legal context. These approaches are also integral to environmental due diligence remediation cost recovery. The model developed in this study will be able to resolve these questions pertaining to environmental forensics especially when it comes to groundwater contamination. As shown in this study, the model was able to reconstruct the operational histories of disposal sites with acceptable accuracy.

7.2 Conclusions

Following are the conclusions from this study:

a) Meshfree Radial point collocation method(RPCM)

- The developed RPCM model has been applied to one and two dimensional problems. The output from the model is compared to the output obtained by analytical and FEM models and found to be in very good agreement.
- A few issues in the application of the meshfree methods are yet to be addressed such as choosing the optimal value of shape parameters, size and shape of the local support domain etc. In particular, the value of shape parameter was found to have a profound impact on the accuracy.
- It was demonstrated that the above issues do not pose any significant hurdle in application of the method. With a simple numerical sensitivity or parametric analysis, these parameters can be determined.
- The meshfree RPCM method does away with the need to construct a grid or mesh, is relatively easy to implement and offers good accuracy.
- As shown in this study, both the MQ-RBF and EXP-RBF gave almost equal accuracy and either of them can be used for the interpolation without concerning about losing accuracy, provided the proper shape parameter values are used.
- It has also been demonstrated that the proposed method can easily handle the numerical instability associated with high Peclet transport problems.

- Another issue of the RPCM method is the inability to capture heterogeneity of the problem due to smooth nature of the RBF functions used in interpolation. These problems are alleviated by using the subdomain collocation approach.
- Though several issues arises in application of the meshfree RPCM method, as demonstrated in this study, they can be easily handled and does not pose any serious hindrance.

Considering the significant advantages offered by the meshfree RPCM model, it can be concluded that the RPCM can serve as a good alternative to the finite difference and finite element methods.

b) PSO as optimization model

- For optimization, the canonical particle swarm optimization with Clerc's constriction coefficient has been implemented.
- As compared to other non-linear optimization algorithms, PSO offers many advantages in that it is very simple to implement and there are relatively fewer parameters to adjust.
- On the downside, there are issues of convergence and stagnation which need special care in selecting the parameters such as swarm size, acceleration coefficients etc.
- The choices of these parameters are subjective and based on hit and trial runs. In this study, it was determined by sensitivity study that the optimal values of the PSO parameters are: swarm size in the range of 100 to 200, acceleration coefficient in the range of 1.4 to 2.1 and the sum of the constriction coefficients in the range of 4.1 to 4.3.
- Despite these minor issues, as demonstrated in this study *PSO can be applied effectively in groundwater inverse modeling.*

c) Source identification using simulation-optimization model

- In this study, groundwater pollutant source identification has been performed through the use of Simulation-Optimization (SO) model.
- A major advantage of this approach is that the SO model is free from the complex mathematical formulations associated with other inverse modeling techniques.
- The application of the SO model has been demonstrated through various case studies with known leakage sources. Both the steady state and transient contaminant release cases studies has been studied.

- The source identification approach has been compared to an existing linear programming and regression based source identification approach. It was found that the PSO based model gave comparable accuracies.
- The use of the concentration response matrix has drastically improved the efficiency of the SO model.
- It is found that the SO model proposed in this work is able to locate and quantify the main leak sources within acceptable accuracy. However, it also produces some noise or identified a spurious minor source which has to be isolated or ruled out.

d) Application to field problem

- The developed RPCM-PSO-SO model has been applied to a case of confined aquifer field problem of 4.5 sq. km for source identification and has been found to be very effective
- The model attempts to reconstruct the release histories of several disposal sites from the concentration measurements over a period of time. The model was able to predict the sources within 5% of their true value.
- Robustness of the proposed approach examined by considering additional scenarios which simulates limited amount of concentration data, missing concentration data, intermittent or irregular data collection etc. have been studied. The model was able to predict most of the sources within 20% of their true value
    - Effect of the location of the observation borewells with respect to the sources examined by placing the wells randomly and not necessarily in the contaminant plume path. The model predicted most of the sources within 5% of their true value.
    - A case study was taken up where all the potential sources are located within a small zone in the domain. The model was able to predict the sources within 9% of their true value.

e) Handling concentration data with measurement errors

- Being ill-posed problem, groundwater source identification problem is very sensitive to input errors. Only way to deal with non-uniqueness is incorporating more field information into the model.
- Case studies taken up which simulates measurement errors in the concentration data.
- Measurement uncertainties simulated by perturbing the concentration data with random error. Both moderate and high levels of measurement errors were simulated with maximum errors as high as 17% and 37% of the true values respectively

- Various ways of dealing with erroneous concentration data were examined namely,
  - Smoothing of the input data to recover the underlying relationship
  - Imposing global and local constraints on the sources from field information
  - Incorporating field information to rule out spurious predictions
  - Giving weights when such information is conceivable or available
- The RPCM-PSO-SO model was able to deal with all these issues effectively
- Proposed model was able to cope with the uncertain input data but the prediction accuracies are reduced along with spurious sources or noises. More field information needed to improve the accuracies and rule out the spurious sources.

7.3 Research contributions

Following are the important research contributions from the present study:

- Simulation models based on meshfree RPCM are developed for both groundwater flow and solute transport through groundwater. The two models are coupled (CFTM-RPCM) so that it can be used for complete modeling of the flow and transport process in aquifers.
- An optimization model based on PSO has been developed which uses regrouping of particle swarms to deal with stagnation problem. This model also incorporates velocity clamping and confinement of particles.
- For groundwater source identification, a simulation-optimization model (RPCM-PSO-SO) has been developed by using a meshfree RPCM simulator and PSO as the optimizer.
- Application of the RPCM-PSO-SO model to hypothetical and field case studies for groundwater source identification were carried out. Developed model was applied to various field situations such as missing or incomplete data, irregular or intermittent data etc. Effect of the location of observed borewells were also studied.
- Application of the RPCM-PSO-SO model to cases with uncertain concentration data was carried out and the model has been found to be effective in dealing with the uncertainties..

7.4 Scope for Future works

Following are the further scope in this research area:

Forward modeling using meshfree RPCM:

1. Method to objectively identify the optimal value of the shape parameters of the radial basis functions used in interpolation. So far hit and trial or sensitivity study is the dominant means to determine this parameter
2. More works need to be done for heterogeneous problems. Though subdomain collocation approach can handle heterogeneous problems, too many subdomains will need to be created in case of highly heterogeneous problems and the method can become very inefficient.

Simulation optimization model using PSO:

1. There are a multitude of variants or types of PSO each with incremental improvements in certain aspects of swarm optimization. The choice of a PSO variant can be quite confusing. A single standard may be developed for PSO.
2. The source identification model used in the study requires more number of observation bore wells or measurement points than the possible potential numbers of sources for convergence to occur for the steady state case. In the transient case, this was not an issue since there is an abundance of the input concentration data Improvements in the optimization algorithm are required to alleviate this shortcoming.
3. The capability of the SO model to handle uncertainty in the input concentration data needs to be improved. While use of weighting could improve its error tolerance, it could not alleviate this issue.
4. More field case studies involving different contaminant release scenarios may need to be modeled to test the robustness of the proposed source identification model.
5. Further development of the SO model to cater to the requirements of environmental forensics applications pertaining to groundwater contamination.

REFERENCES

Ajmera, T., & Rastogi, A. (2008). Artificial Neural Network Application on Estimation of Aquifer Transmissivity. *Journal of Spatial Hydrology, 8*(2), 15-31.

Ala, N., & Domenico, P. (1992). Inverse analytical techniques applied to coincident contaminant distributions at Otis Air Force Base, Massachussets. *Ground water, 32*, pp. 212-218.

Alapati, S., & Kabala, Z. (2000). Recovering the release history of a groundwater contaminant using a non-linear least squares method. *Hydrological Processes, 14*(6), 1003-1016.

Alhuri, Y., Ouazar, D., & Taik, A. (2011). Comparison between local and global Mesh-free methods for Ground-Water modeling. *IJCSI International Journal of Computer Science Issues, 8*(2), 337-342.

Alice, T. ,Eldho, T.I. and Rastogi,A. (2014) A comparative study of point collocation based MeshFree and finite element methods for groundwater flow simulation, *ISH Journal of Hydraulic Engineering*, 20(1), 65-74

Anderson, M. P. (1984) Movement of contaminants in groundwater: groundwater transport--advection and dispersion, *Groundwater Contamination*, 37-45, National Academic Press Washington, DC

Anderson, M., & Woessner, W. (2002). *Applied Groundwater Modeling: Simulation of flow and advective transport.* New York: Academic Press.

Armando, D., & Oden, J. (1995). Hp clouds-a meshless method to solve boundary value problem. *TICAM Report*, 95-105. Austin: University of Texas.

Ashyraliyev, M., Blom, J., & Verwer, J. (2008). On the numerical solution of diffusion-reaction equations with singular source terms. *Journal of Computational and Applied Mathematics, 216*(1), 20-38.

Atluri, S., & Zhu, T. (1998). A new Meshless Local Petrov-Galerkin (MLPG) approach in computational mechanics. *Comput. Mech., 22*, 117-127.

Atmadja, J., & Bagtzoglou, A. (2001a). Pollution Source Identification in heterogeneous media. *Water Resources Research, 37*(8), 2113-2125.

Atmadja, J., & Bagtzoglou, A. (2001b). State of the art report on Mathematical Methods for Groundwater Pollution Source Identification. *Environmental Forensics, 2*, 205-214.

Bagtzoglou, A., Dougherty, D., & Tompson, A. (1992). Application of Particle Methods to Reliable Identification of Groundwater Pollution Sources. *Water Resources Management, 6*, 15-23.

Bear, J. (1979). *Hydraulics of Groundwater*. New York: McGraw Hill Publishing.

Belytschko, T., Krongauz, Y., Organ, D., Fleming, M., & Krysl, P. (1996). Meshless methods: An overview and recent developments. *Comput. Methods Appl. Mech. Engg., 139*, 3-47.

Belytschko, T., Lu, Y., & Gu, L. (1994). Element-free Galerkin methods. *Int. J. Numer. Methods Eng., 37*, 229-256.

Bernal, F., Guitierrez, G., & Kindelan, M. (2009). Use of singularity capturing functions in the solution of problems with discontinuous boundary conditions. *Engineering Analysis with Boundary Elements, 33*, 200-208.

Birchwood, R. (1999). Identifying the location and release characteristics of a groundwater pollution source using spectral analysis. *Proceedings of the 19th Annual American Geophysical Union Hydrology Days Conference* (pp. 37-50). Fort Collins, Colorado: Colorado State University.

Bonet, J., & Kulasegaram, S. (2000). Correction and stabilization of smooth particle hydrodynamics methods with application in metal forming simulation. *Int. J. Numer. Methods Eng., 47*(6), 1189-1214.

Butcher, J., & Gauthier, T. (1994). Estimation of residual dense NAPL mass by inverse modelling. *Ground Water, 32*, pp. 71-78.

Carasso, A. (1972). The Backward beam equation: Two A-stable schemes for parabolic problems. *SIAM Journal of Numerical Analysis, 9*(3), 406-434.

Carrera, J., & Neuman, S. (1986). Estimation of Aquifer Parameters Under Transient and Steady State Conditions: 1. Maximum Likelihood Method Incorporating Prior Information. *Water Resources Research, 22*(2), 199-210.

Chadalavada, S., Datta, B., & Naidau, R. (2012). Optimal identification of groundwater pollution sources using feedback monitoring information: a case study. *Environmental Forensics, 13*(2), 140-153.

Chandhini, G., & Sanyasiraju, Y. (2007). Local RBF-FD solutions for steady convection-diffusion problems. *International Journal of Numerical Methods in Engineering, 72*, 352-378.

Chen, J.-S., Wang, L., Hu, H.-Y., & Chi, S.-W. (2009). Subdomain radial basis collocation method for heterogeneous media. *International Journal for Numerical Methods in Engineering, 80*, 163-190.

Cifti, E., Avci, C., Borekci, O., & Sahin, A. (2012). Assessment of advective–dispersive contaminant transport in heterogeneous aquifers using a meshless method. *Environ Earth Sci, 67*, 2399-2409.

Clayton, M. (2005). Groundwater Contaminant Source Identification Using Hybrid Optimization Methods. *EWRI 2005: Impacts of Global Climate Change* (pp. 1-7). Anchorage, Alaska: ASCE.

Clerc, M. (2006). *Stagnation analysis in particle swarm optimization or what happens when nothing happens.* Technical Report CSM-460, University of Essex, Department of Computer Science.

Clerc, M., & Kennedy, J. (2002). The particle swarm - explosion, stability,and convergence in a multidimensional complex space. *IEEE Transactions on Evolutionary Computation, 6*(1), 58-73.

Cooley, R. L. (1977). A method of estimating parameters and assessing reliability for models of steady state groundwater flow: 1. Theory and numerical properties. *Water Resour. Research, 13*(2), 318-324.

Datta, B., Chakrabarty, D., & Dhar, A. (2009). Simultaneous identification of unknown groundwater pollution sources and Estimation of aquifer parameters. *Journal of Hydrology, 376*, 48-57.

Delleur, J. (2007). *The Handbook of Groundwater Engineering* (2nd ed.). Boca Raton: CRC Press.

Desai, Y., Eldho, T., & Shah, A. (2011). *Finite Element Method with Applications in Engineering.* New Delhi: Pearson.

Donea, J., & Huerta, A. (2003). *Finite Element Methods for Flow Problems.* West Sussex(England): Wiley.

Driscoll, T., & Fornberg, B. (2002). Interpolation in the limit of increasingly flat radial basis functions. *Computers and Mathematics with Applications, 43*(3-5), 413-422.

Emsellem, Y., & Marsily, G. (1971). An Automatic Solution for the Inverse Problem. *Water Resources Research, 7*(5), 1264–1283.

Evers, G., & Ghalia, M. (2009). Regrouping Particle Swarm Optimization: A new Global Optimization Algorithm with improved performance consistency across benchmarks. *Proceedings of the 2009 IEEE International Conference on Systems, Man, and Cybernetics*, pp. 3901-3908 San Antonio,Texas.

Fedoseyev, A., Friedman, M., & Kansa, E. (2002). Improved multiquadrics method for elliptic partial differential equation via PDE collocation on the boundary. *Comput. Math. Appl., 43*, 439-455.

Fornberg, B., & Wright, G. (2004). Stable Computation of multiquadric interpolants for all values of the shape parameter. *Comput. Math. Appl., 47*, 497-523.

Franke, C., & Schaback, R. (1997). Solving Partial Differential Equations by Collocation using Radial Basis Functions. *Applied Mathematics and Computation, 93*, pp. 73-82.

Freeze, R., & Cherry, J. (1979). *Groundwater.* Englewood Cliffs,New York: Prentice Hall.

Gingold, R., & Monaghan, J. (1977). Smoothed particle hydrodynamics: theory and applications to non-spherical starts. *Monthly Notices R. Astron. Soc., 181*, 375-389.

Goldberg, M., Chen, C., & Bowman, H. (1999). Some recent results and proposals for the use of radial basis functions in the BEM. *Engineering Analysis with Boundary Elements, 23*, pp. 285-296.

Gorelick, S., Evans, B., & Remson, I. (1983). Identifying Sources of Groundwater pollution: An optimization approach. *Water Resources Research, 19*(3), 779-790.

Guneshwor L., S., Eldho, T., & Vinod Kumar, A. (2016). Coupled groundwater flow and contaminant transport simulation in a confined aquifer using meshfree radial point collocation method(RPCM). *Engineering Analysis with Boundary Elements, 66*, pp. 20-33.

Gurarslan, G., K. (2015) Solving inverse problems of groundwater-pollution-source identification using a differential evolution algorithm, *Hydrogeology Journal, 23(6),* 1109-1119

Gutierrez, G., & Florez, W. (2008). Issues of the local radial basis collocation method implementation for solving second order partial differential equation. *Mecanica Computacional I, XXVI*, pp. 2241-2252.

Gzyla,G., Zaninib, A.,Fraczekc, R. & Kuraa, K.(2014) Contaminant source and release history identification in groundwater: A multi-step approach, *Journal of Contaminant Hydrology, 157*, 59-72

Harbaugh, A., & McDonald, M. (1996). *MODFLOW: A modular thre-dimensional finite-difference groundwater flow models.* USGS.

Hardy, R. L. (1971). Multiquadric equations of topography and other irregular surfaces. *J. Geophys. Res., 76*, pp. 1905-1915.

REFERENCES

Hester, R.E. and Harrison, R. M. (2008) Environmental Forensics, Royal Society of Chemistry, Springer

Huang, C., Li, J., & Kim, S. (2008). An inverse problem in estimating the strength of contaminant source for groundwater systems. *Applied Mathematical Modeling, 32*, 417-431.

Huyakorn, P. S., & Pinder, G. F. (1983). *Computational Methods in Subsurface Flow*. San Diego: Academic Press.

Jha, M., & Datta, B. (2013). Three-Dimensional Groundwater Contamination Source Identification Using Adaptive Simulated Annealing. *Journal of Hydrologic Engineering, 18*(3), 307-317.

Jung, J.-H. (2009). A Note on the Spectral Collocation Approximation of Some Differential Equations with Singular Source Terms. *Journal of Scientific Computation, 39*, 49-66.

Kansa, E. (1990). Multiquadrics - a scattered data approximation scheme with applications to comptational fluid-dynamics-II: Solutions to parabolic, hyperbolic and elliptic partial differential equations. *Comput. Math. Appl.,, 19*, 147-161.

Kansa, E., & Carlson, R. (1992). Improved accuracy of multiquadric interpolation using variable shape parameters. *Comput. Math. Appl, 24*, 99-120.

Kansa, E., & Hon, Y. (2000). Circumventing the Ill-Conditioning Problem with Multiquadric Radial Basis Functions. *Computers and Mathematics with Applications, 39*, 123-137.

Kennedy, J., & Eberhart, R. (1995). Particle Swarm Optimization. *Proc of IEEE International Conference on Neural Networks*, pp. 1942-1948, Piscataway, IEEE Press.

Kennedy, J., & Mendes, R. (2002). Population structure and particle swarm performance. *Proceedings ofthe IEEE congress on evolutionary computation (CEC)* (pp. 1671–1676). Honolulu, HI. Piscataway: IEEE Press.

Larsson, E., & Fornberg, B. (2005). Theoretical and computational aspects of multivariate interpolation with increasingly flat radial basis functions. *Comput. Math. Appl., 49*, 103-130.

Lee, C., Liu, X., & Fan, S. (2003). Local multiquadric approximation for solving boundary value problems. *Computational Mechanics, 30*, pp. 396-409.

Leichombam,S.and Bhattacharjya ,R.K.(2016) Identification of Unknown Groundwater Pollution Sources and Determination of Optimal Well Locations Using ANN - GA Based Simulation - Optimization Model, *Journal of Water Resource and Protection, 8*, 411-424

Li, J., Chen, Y., & Pepper, D. (2003). Radial basis function method for 1-D and 2-D groundwater contaminant transport modeling. *Computational Mechanics, 32*(1-2), 10-15.

Libersky, L., Petscheck, A., Carney, T., Hipp, J., & Allahdadi, F. (1993). High strain Lagrangian hydrodynamics. *J. Comput. Phys., 109*, 67-75.

Ligget, J. (1987). Advances in the boundary integral equation method in subsurface flow. *Water Resources Bull., 23*(4), 637-651.

Liu , W., Jun, S., & Zhang, Y. (1995). Reproducing Kernel Particle Method. *Int. J. Numer. Methods Eng., 20*, 1081-1106.

Liu, G., & Gu, Y. (1999). A point interpolation method. *Proceedings of 4th Asia-Pacific Conference on Computational Mechanics*, (pp. 1009-1014). Singapore.

Liu, G., & Gu, Y. (2005). *An Introduction to Meshfree Methods and Their Programming.* New York: Springer.

Lucy, L. (1977). A numerical approach to the testing of the fission hypothesis. *Astron. J., 82*, 1013-1024.

Madych, W., & Nelson, S. (1990). Multivariable interpolation and conditionally positive definite functions II. *Math. Comp., 54*, pp. 211-230.

Mahar, P., & Datta, B. (2000). Identification of Pollution Sources in Transient Groundwater Systems. *Water Resources Management, 14*, 209-227.

Mahar, P., & Datta, B. (2001). Optimal Identification of Ground-Water Pollution Sources and Parameter Estimation. *Journal of Water Resources Planning and Management, 127*(1), 20–29.

Medina, A., & Carrera, J. (1996). Coupled estimation of flow and solute transport parameters. *Water Resour. Research, 32*(10), 3063-3076.

Meenal, M., & Eldho, T. (2011). Simulation of groundwater flow in an unconfined aquifer using meshfree point collocation method. *Engineering Analysis with Boundary Elements, 35*, 700-707.

Meenal, M., & Eldho, T. (2012a). Simulation-optimization model for groundwater contamination remediation using meshfree point collocation method and particle swarm optmization. *Sadhana, 37*(3), 351-369.

Meenal, M., & Eldho, T. (2012b). Two-dimensional contaminant transport modeling using meshfree point collocation method (PCM). *Engineering Analysis with boundary Elements, 36*, 551-561.

Melensk, J., & Babuska, I. (1996). The Partition of Unity Finite Element Method: Basic Theory and Applications. *Computer Methods in Applied Mechanics and Engineering, 139*, 289-314.

Mhatre, A., Guneshwor, L., & Sharma, V. (2010). *Report on Groundwater modeling of KAPS site.* BARC, Mumbai: Unpublished.

Michalak, A., & Kitanidis, P. (2004). Estimation of historical groundwater contaminant distribution using the adjoint state method applied to geostatistical inverse modeling. *Water Resources Research, 40*, W08302, doi:10.1029/2004WR003214.

Milnes, E., & Perrochet, P. (2007). Simultaneous identification of a single pollution point-source location and contamination time under known flow field conditions. *Advances in Water Resources, 30*(12), 2439-2446.

Monaghan, J. (1982). Why particle methods works. *SIAM J. Sci. Stat. Comput., 3*(3), 422-433.

Monaghan, J. (1988). An introduction to SPH. *Comput. Phys. Commun., 48*(1), 89-96.

Napoles, G., Grau, I., & Bello, R. (2012). Constricted particle swarm optimization based algorithm for global optimization. *Polibits, 46*, 5-11.

Neupauer, R., & Wilson, J. (1999). Adjoint method for obtaining backward-in-time location and travel time probabilities of a conservative groundwater contaminant. *Water Resources Research, 35*(11), pp. 3389-3398.

Nguyen, V., Rabczuk, T., Bordas, S., & Duflot, M. (2008). Meshless methods: A review and computer implementation aspects. *Mathematics and Computers in Simulation, 79*, 763-813.

Ogata, A., & Banks, R. (1961). *A Solution of the Differential Equation of Longitudinal Dispersion in Porous Media*. Washington, DC: U.S. Geological Survey,U.S. Government Printing Office.

Onate, E. (1998). Derivation of stabilized equations for numerical solution of advective-diffusive transport and fluid flow problems. *Comput. Methods Appl. Mech. Engg. , 151* , 233-265.

Ortega, J., & Rheinboldt, W. (1970). *Iterative Solution of Nonlinear Equations in Several Variables.* Philadelphia: SIAM.

Pepper, D., & Heinrich, J. (1992). *The Finite Element method: Basic Concepts and Applications.* Taylor & Francis.

Pinder, G. F. (1973). A Galerkin-finite element simulation of groundwater contamination on long Island, New York. *Water Resource Research, 9*(6), 1657-1669.

Prasad, K., & Rastogi, A. (2001). Estimating net aquifer recharge and zonal hydraulic conductivity values for Mahi Right Bank Canal project area,India by genetic algorithm. *Journal of Hydrology, 243*, 149-161.

Praveen Kumar, R., & Dodagoudar, G. (2008). Two-dimensional modelling of contaminant transport through saturated porous media using the radial point interpolation method (RPIM). *Journal of Hydrogeology, 16*, 1497–1505.

Rastogi, A. (2007). *Numerical Groundwater Hydrology*. Mumbai: Penram International Publishing (India).

Richtmyer, R., & Morton, K. (1967). *Difference Methods for Initial Value Problems.* New York: John Wiley & Sons.

Rippa, S. (1999). An Algorithm for selecting a good value for the parameter c in radial basis function interpolation. *Advances in Comput. Math., 11*, pp. 193-210.

Rude, U., Kostler, H., & Mohr, M. (2003). *Accurate multigrid techniques for computing singular solutions of elliptic problems.* 11th Copper Mountain Conference on Multigrid Methods.

Sampat, P. (2000). Groundwater Shock: The Polluting of the World's Major Freshwater Stores. *World Watch Magazine, 13*(1) : www.worldwatch.org/node/481.

Sampat, P. (2000, January/February). Groundwater Shock: The Polluting of the World's Major Freshwater Stores. *World Watch Magazine, 13*(1).

Schaback, R., & Wendland, H. (2000). Adaptive greedy techniques for approximate solution of large RBF systems. *Numer. Algorithms, 24*, pp. 239-254.

Segerlind, L. J. (1984). *Applied Finite Element Analysis.* New York: John Wiley and Sons.

Sharan, M., Kansa, E., & Gupta, S. (1997). Application of the Multiquadric Method for Numerical Solution of Elliptic Partial Differential Equations. *Applied Mathematics and Computations, 84*, pp. 275-302.

REFERENCES

Shi, Y., & Eberhart, R. (1998). A modified particle swarm optimizer. Proceedings of the IEEE International Conference on Evolutionary Computation, *10.1109/ICEC.1998.699146*, pp. 69–73.

Sidauruk, P., Cheng, A.-D., & Ouazar, D. (1998). Ground Water Contaminant Source and Transport Parameter Identification by Correlation Coefficient Optimization. *Groundwater, 36*(2), 208–214.

Singh, R., & Datta, B. (2004). Groundwater Pollution Source Identification and Simultaneous Parameter Estimation Using Pattern Matching by Artificial Neural Network. *Environmental Forensics, 5*(3), 143-153.

Singh, R., & Datta, B. (2006). Identification of Groundwater Pollution Sources using GA-basec linked Simulation Optimisation Model. *Journal of Hydrologic Engineering, 11*(2), 101–109.

Singh, V., & Sarma, M. (2009). Groundwater Data generation at KAPS. *Technical Report No. NGRI-2009-GW-673*. Hyderabad (India): National Geophysical Research Institute.

Skaggs, T. H., & Kabala, Z. J. (1994). Recovering the release history of a groundwater contaminant. *Water Resources Research, 30*(1), 71-79.

Skaggs, T., & Kabala, Z. (1995). Recovering the history of a groundwater contaminant plume: Method of quasi-reversibility. *Water Resources Research, 31*(11), 2669-2673.

Snodgrass, M., & Kitanidis, P. (1997). A geostatisticaal pproacht o contaminants ourcei dentification. *Water Resources Research, 33*(4), 537-546.

Srivastava D. & Singh, R.M. (2014) Breakthrough Curves Characterization and Identification of an Unknown Pollution Source in Groundwater System Using an Artificial Neural Network (ANN), *Environmental Forensics, 15(1)*, 2014

Stallman, R. (1956). Numerical analysis of regional water levels to define aquifer hydrology. *Transactions American Geophysical Union, 37*(4), 451-460.

Strack, O., & Haitjema, H. (1981). Modeling double aquifer flow using a comprehensive potential and distributed singularities 1. Solution for homogeneous permeabilities. *Water Resour.Res., 17*(5), 1535-1549.

Sun, A., Painter, S., & Wittmeyer, G. (2006). A constrained robust least squares approach for contaminant source release hsirtory identification. *Water Resources Research, 42*(4), W04414, doi:10.1029/2005WR004312.

Swathi, B., & Eldho, T. (2013). Groundwater flow simulation in confined aquifers using Meshless Local Petrov-Galerkin (MLPG) method. *ISH Journal of Hydraulic Engineering, 19*(3), 335-348.

Tornberg, A., & Engquist, B. (2004). Numerical approximation of singular source terms in differential equations. *Journal of Computational Physics, 200*, 462-488.

Trelea, I. C. (2003). The particle swarm optimization algorithm: convergence analysis and parameter selection. *Information Processing Letters, 85*, 317-325.

Wagner, B. J. (1992). Simultaneous parameter estimation and contaminant source characterization for coupled groundwater flow and contaminant transport modelling. *Journal of Hydrology, 135*(1-4), 275-303.

Wang, H., & Anderson, M. (1982). *Introduction to Groundwater Modeling with Finite Difference and Finite Elelment Methods.* New York: W.H. Freeman and Company.

Wang, J., & Liu, G. (2002). A Point Interpolation meshless method based on radial basis functions. *International Journal for Numerical Methods in Engineering, 54*, 1623-1648.

Wilson, J., & Liu, J. (1994). Backward Tracking to the source of pollution. In *Waste Management from Risk to Remediation* (Vol. 1, pp. 181-199). Albuquerque: ECM.

Wilson, J., & Miller, P. (1978). 2D Plume in uniform groundwater flow. *Journal of Hydraulic Division, ASCE, 4*, pp. 503-514.

Woodbury, A., Sudicky, E., Ulrych, T., & Ludwig, R. (1998). Three-dimensional plume source reconstruction using minimum relative entropy inversion. *Journal of Contaminant Hydrology, 32*, 131-158.

Worasucheep, C. (2008). A particle swarm optimization with stagnation detection and dispersion. *IEEE congress on Evolutionary Computation (CEC 2008)*, pp. 424-429.

Wright, G. B. (2003). Radial Basis Function Interpolation: Numerical and Analytical Developments. University of Colorado (Boulder).

Wright, G., & Fornberg, B. (2006). Scattered node compact finite difference type formulas generated from radial basis functions. *Journal of Computational Physics, 212*(1), 99-123.

Xin, L. (2006). Radial Point Collocation method for solving convection-diffusion problems. *Journal of Zhejiang University SCIENCE A, 7*(6), 1061-1067.

Zhang J.,Zeng L., Chen C., Chen D. & Wu L. (2015). Efficient Bayesian experimental design for contaminant source identification, *Water Resources Research, 51(1)*, 576-598

Zheng, C., & Bennet, G. (2002). *Applied Contaminant Transport Modeling* (2nd ed.). New York: Wiley-Interscience.

Zheng, C., & Wang, P. (1998). *MT3DMS: A Modular Three-Dimensional Multispecies Transport Model for Simulation of Advection , Dispersion and Chemical Reactions of Contaminants in Groundwater Systems.* University of Alabama.

Zi, L., & Mao, X. (2011). Global multiquadric collocation method for groundwater contaminant source identification. *Environmental Modeling and Software, 26*, 1611-1621.

Zienkiewicz, O., & Taylor, R. (2000). *The Finite Element Method.* Oxford, UK: Butterworth Heinemann.

Zuppa, C., & Cardona, A. (2003). A collocation meshless method based on local optimal point interpolation. *International Journal for Numerical Methods in Engineering, 57*, 509-536.

INDEX